Ondersteuning van de netfrequentieregeling door windturbines

Support of Grid Frequency Control by Wind Turbines

Jan Van de Vyver

Promotoren: prof. dr. ir. L. Vandevelde, dr. ir. B. Meersman
Proefschrift ingediend tot het behalen van de graad van
Doctor in de ingenieurswetenschappen: werktuigkunde-elektrotechniek

UNIVERSITEIT
GENT

Vakgroep Elektrische Energie, Systemen en Automatisering
Voorzitter: prof. dr. ir. L. Dupré
Faculteit Ingenieurswetenschappen en Architectuur
Academiejaar 2016 - 2017

ISBN 978-90-8578-937-6
NUR 961, 959
Wettelijk depot: D/2016/10.500/69

UNIVERSITEIT
GENT

Ghent University
Faculty of Engineering and Architecture (FEA)
Department of Electrical Energy,
Systems and Automation (EESA)
Electrical Energy Laboratory (EELAB)

Ondersteuning van de netfrequentieregeling door windturbines

Support of Grid Frequency Control by Wind Turbines

Jan Van de Vyver

Promoters
Prof. dr. ir. Lieven Vandevelde (UGent - EESA)
dr. ir. Bart Meersman (UGent - EESA)

Chairman
Prof. dr. ir. Hendrik Van Landeghem (UGent)

Exam Commission
Prof. dr. ir. Guillaume Crevecoeur (UGent - EESA)
Prof. dr. ir. Herbert De Smet (UGent - ELIS)
Prof. dr. ir. Johan Gyselinck (ULB)
Prof. dr. ir. Han Slootweg (TU Eindhoven)
Prof. dr. ir. Dirk Van Hertem (KU Leuven - ESAT)
dr. ir. Tine Vandoorn (UGent - EESA)

Dankwoord

't Is gebeurd. Na vier jaar universiteit zijn er heel wat mensen om te bedanken. Ik ga er ongetwijfeld vergeten, maar ik doe toch een verdienstelijke poging. Er zijn vier mensen die ik in het bijzonder wil bedanken, want zonder hen was er van dit boek(je) geen sprake geweest: Bart, Jeroen, Lieven en Tine.

Laat ik maar beginnen bij het begin. In 2012 overtuigde Jeroen me tijdens mijn masterthesis om aan een doctoraat te beginnen. Het vervolg is gekend. Vooral de leuke samenwerking en de vele grappige momenten zullen me bijblijven. Bedankt daarvoor! Lieven, als promotor heb jij me de kans gegeven om dit doctoraat tot een goed einde te brengen. Jij bent degene die me als student heeft ingewijd in de wereld van de elektrische netten. Toen professor Vandevelde werd ingeruild voor Lieven, stond jij ondanks je drukke agenda steeds rustig klaar om mij bij te staan met goede raad. Ook de vele treinritten van en naar Brussel vlogen voorbij als je honderduit begon te vertellen. Merci voor alles. Bart, jou wil ik graag bedanken voor de kritische opmerkingen en gerichte feedback. Jouw positieve ingesteldheid overtuigde me om toch door te zetten als het wat minder ging. En dan was jij er nog, Tine. Ook toen je al bij Eandis werkte, kwam je nog regelmatig langs om met mij samen te zitten. Onze brainstormsessies hebben mij goed vooruit geholpen. Ik had me geen betere begeleider kunnen wensen!

Daarnaast zijn er nog de vele bureaugenoten. Mede door de verhuis naar Zwijnaarde is dit een indrukwekkende lijst geworden: Bart M., Bart W., Brecht, Christof, Dominique, Giustino, Jeroen, Joachim, Joannes, Kristof, Louis, Nils, Samie, Sophie, Thomas en Tine. Jullie zorgden voor een goeie sfeer en maakten het leuk om naar het werk te komen. Ook de andere collega's wil ik graag bedanken voor de leuke gesprekken tijdens de middagpauze en de aangename samenwerking. Hier ga ik me alvast niet aan een opsomming wagen.

Omdat er niet altijd gewerkt moet worden, wil ik ook alle vrienden en vriendinnen bedanken die de voorbije jaren altijd klaar stonden om voor de nodige ontspanning te zorgen. De wekelijkse zwempartijen en de jaarlijkse skireizen waren meer dan welkom. In het bijzonder wil ik Roel bedanken voor de wekelijkse lasles en lunch op vrijdag. Hopelijk kunnen we die traditie in de toekomst verderzetten!

Tot slot wil ik mijn ouders en broer bedanken. Zij stonden altijd klaar, ook als ik eens wat minder goed gezind was. Bedankt daarvoor!

Voor zij die zich geroepen voelen om nog verder te lezen: veel plezier!

September 2016
Jan Van de Vyver

The research of Jan Van de Vyver was partly funded by the SBO Project OptiWind: Serviceability Optimisation of the Next Generation Offshore Wind Turbines.

Table of Contents

Summary

In the past decades, wind energy has become one of the most popular renewable energy sources. Especially for large wind turbines, the technology is already quite mature which results in a high efficiency and a good reliability. Furthermore, the maximum rated power of the wind turbines is continuously increasing and the offshore wind farms are gaining interest. Therefore, it is very likely that wind turbines will provide an important share of the future renewable energy in the electrical power system.

In the current power system, renewable energy sources such as wind turbines have priority access to the grid. This means that they can always inject the maximum available power into the network. Consequently, conventional (controllable) generators should make sure that the balance between produced power and consumed power is always guaranteed. Balancing of load and production at any point in time is achieved by an important ancillary service, known as frequency control. At this moment, the participation of wind turbines in this service is very limited and often non-existing.

Besides frequency control, other ancillary services such as voltage control and congestion management are needed to ensure a reliable operation of the electrical power system. Again, the majority of these services is still provided by conventional power plants. In a power system with an increasing penetration of renewable energy sources, this becomes an unsustainable situation. On one hand, the need for ancillary services such as balancing and voltage control is likely to increase in the future due to the volatile nature of the renewable energy sources. On the other hand, when renewable energy starts to replace conventional generation, less power plants are available to provide ancillary services.

However, the modern variable-speed wind turbine are perfectly suited to assist in the provision of a variety of ancillary services. Due to the power-electronic converter that is used in these wind turbines, it is possible to control the active and reactive power output of the wind turbine. This makes it possible to assist in frequency control, voltage control, etc.

In this dissertation, the focus is on the provision of frequency control

with wind turbines. In the power system, the production and consumption have to be balanced at any point in time. The grid frequency is used as a measure for this balance. In normal operation, the frequency is very close to the nominal value of 50 Hz. If the frequency increases above 50 Hz, it means that too much power is produced, if the frequency decreases below 50 Hz, too much power is consumed. Consequently, when the power production or consumption suddenly changes, for example due to a failure in a power plant, the grid frequency starts to deviate from the nominal value. In order to avoid a large deviation of the grid frequency, several power plants are equipped with an automatic primary frequency controller, which adapts the power output depending on the frequency deviation. If the frequency is too high, less power is injected and vice versa. This frequency control ensures a proper operation of the power system.

The speed at which the frequency changes in case of a disturbance is determined by the rotating inertia of all the synchronously-coupled generators and motors. The higher the system inertia is, the slower the frequency changes in case of a disturbance and the more time the primary control has to increase or decrease the power output. Consequently, sufficient inertia is necessary to ensure the proper functioning of the power system. However, when converter-coupled generators, such as variable-speed wind turbines, start to replace conventional generation, this results in a decrease of the system inertia. For increasing wind power penetrations this could complicate the frequency control of the network.

Fortunately, wind turbines still have a rotating inertia in their rotor that could be used to virtually increase the system inertia. By adding an additional control loop to the wind turbine converter, the power output of the wind turbine can be altered to mimic the inertial response behavior of a conventional synchronous generator. The virtual inertia is obtained by injecting or absorbing active power in the wind turbine inertia in case of a disturbance, similar to the behavior of synchronous machines. In literature, different control strategies are available and it is shown that the available inertia of the wind turbine blades is large enough to obtain a similar amount of system inertia with wind turbines as with conventional generators when these control loops are added to the wind turbine control.

From the system perspective, it is not the maximum amount of kinetic energy that can be stored in or released from the wind turbine inertia that matters, but the impact it has on the frequency behavior immediately after a disturbance. Therefore, in this work, the influence of the system composition, i.e., the type of generators, on the optimal parameter selection of the emulated inertial response strategies is investigated. It is shown that the correct parameter selection is important to obtain the desired inertial

response. If too much power is injected immediately after a frequency dip, it might result in a slower primary control action of the conventional power plants, which results in a lower frequency nadir after the disturbance. It might also result in a second, deeper, frequency dip which is undesired. When the different emulated inertial response strategies are compared, it can be concluded that the synthetic inertia strategy is the most promising strategy as it is the most stable strategy with the lowest parameter sensitivity.

When the emulated inertial response strategies are used in wind turbines to support the grid, also some negative side-effects can be observed. First, additional energy yield losses arise due to the suboptimal operation of the wind turbines during the inertial response. However, in this work it is shown that these energy yield losses are very limited for the inertial response strategies. This is due to the small variations in the rotational speed that are needed to optimally support the grid. Second, additional torque variations are caused by the emulated inertial response strategies. These variations cause an additional loading of the wind turbine drive-train which might affect the lifetime of the wind turbines equipped with emulated inertial response. In order to limit the impact of the emulated inertial response on the drive-train dynamics, the DC-bus voltage modulation strategy is developed in this work. By using this control strategy, the energy buffer of the DC-bus is used to limit the torque variations that are caused by the inertial response strategies. As the negative side-effects are quite limited (energy yield losses) or can be effectively mitigated by using an appropriate control strategy (torque variations), it is clear that the emulated inertial response strategies can be used to enhance the integration of wind turbines in the power system.

Besides the provision of emulated inertial response, wind turbines can also be used to assist in the primary frequency control. As wind turbines are usually operated in the maximum power point to capture as much renewable energy as possible, the provision primary control in case of frequency dips is not straightforward. In order to achieve this, wind turbines should be operated continuously below the maximum power point. Therefore, different deloading strategies are compared in this dissertation. This shows that the provision of power reserves is possible with a variety of control strategies, but some strategies are clearly better suited. When the wind turbines are aggregated in wind farms, the differences between these strategies become smaller due to the smoothing effect of the wind farm. Finally, the adaptive droop control strategy is developed to achieve equal power sharing between remote wind turbines under different wind speed conditions.

Samenvatting

Gedurende de laatste decennia is windenergie één van de meest populaire hernieuwbare energiebronnen geworden. Vooral voor grote windturbines is de technologie reeds behoorlijk volwassen, wat voor een hoge efficiëntie en grote betrouwbaarheid zorgt. Bovendien neemt het nominaal vermogen van de windturbines continu toe en winnen ook windturbines op zee aan populariteit. Het is bijgevolg zeer waarschijnlijk dat windturbines in de toekomst voor een belangrijk deel van de hernieuwbare elektriciteitsproductie zullen zorgen.

In het huidige elektrische net hebben hernieuwbare energiebronnen zoals windturbines voorrang om in het net te injecteren. Dit betekent dat ze op elk moment het maximaal beschikbare vermogen aan het net mogen leveren. Bijgevolg moeten conventionele (regelbare) generatoren er voor zorgen dat de balans tussen geproduceerd en geconsumeerd vermogen altijd in evenwicht blijft. Het op elk moment balanceren van de last en de productie wordt verwezenlijkt door een belangrijke netondersteunende dienst, zijnde frequentieregeling. Op dit moment is de bijdrage van windturbines in deze dienst zeer beperkt en vaak zelfs onbestaande.

Naast frequentieregeling zijn er nog andere netondersteunende diensten zoals spanningsregeling en congestiemanagement nodig om de goede werking van het elektriciteitsnet te verzekeren. Opnieuw wordt het merendeel van deze diensten door conventionele centrales geleverd. In een elektrisch net met een toenemend aandeel hernieuwbare energiebronnen wordt dit een onhoudbare situatie. Enerzijds is het zeer waarschijnlijk dat de nood aan netondersteunende diensten zoals frequentie- en spanningsregeling in de toekomst zal toenemen door het volatiele karakter van de hernieuwbare energiebronnen. Anderzijds zijn er minder conventionele generatoren beschikbaar om de netondersteunende diensten te leveren wanneer ze vervangen worden door windturbines.

De moderne variabele-snelheid windturbines zijn echter perfect geschikt om deel te nemen aan het leveren van netondersteunende diensten. Door de vermogenselektronische omvormer die in dit type van windturbines gebruikt

wordt, is het mogelijk om zowel het geproduceerde actieve als reactieve vermogen te regelen. Dit laat toe om deel te nemen aan frequentieregeling, spanningsregeling, enz.

In dit proefschrift ligt de nadruk op het leveren van frequentieregeling met windturbines. In het elektriciteitsnetwerk moet het geproduceerde en geconsumeerde vermogen op elk ogenblik in evenwicht zijn. De netfrequentie wordt gebruikt als een maatstaf voor dit evenwicht. Gedurende normale werking ligt de netfrequentie zeer dicht in de buurt van de nominale waarde van 50 Hz. Wanneer de frequentie groter wordt dan 50 Hz, betekent dit dat er teveel vermogen geproduceerd wordt. Daalt de frequentie onder de 50 Hz, dan wijst dit op een te grote afname van elektrisch vermogen. Als de productie of consumptie nu plots wijzigt, bijvoorbeeld ten gevolge van een storing in een elektriciteitscentrale, begint de frequentie af te wijken van haar nominale waarde. Om te voorkomen dat de netfrequentie te sterk zou afwijken zijn verschillende elektriciteitscentrales uitgerust met een automatische primaire frequentieregeling. Als de netfrequentie te laag is, wordt er extra vermogen geïnjecteerd en omgekeerd. Op deze manier verzekert frequentieregeling de goede werking van het systeem.

De snelheid waarmee de frequentie verandert in het geval van een storing wordt bepaald door de draaiende traagheid of inertie van al de synchroongekoppelde generatoren en motoren. Hoe hoger de systeeminertie is, hoe trager de frequentie verandert in het geval van een storing en hoe meer tijd de primaire regeling heeft om het vermogen te verhogen of te verlagen. Er moet dus voldoende inertie in het net aanwezig zijn om de goede werking ervan te verzekeren. Wanneer convertorgekoppelde generatoren, zoals variabele-snelheid windturbines, conventionele generatoren beginnen te vervangen, zorgt dit voor een daling van de systeeminertie. Voor een toenemend aandeel van windturbines kan dit de frequentieregeling van het netwerk bemoeilijken.

Gelukkig beschikken windturbines wel over een roterende inertie in de turbinerotor die kan aangewend worden om de systeeminertie virtueel te verhogen. Door het toevoegen van een extra controlekring aan de convertor kan het uitgangsvermogen van de windturbine aangepast worden om het inertieresponsgedrag van een conventionele synchrone generator na te bootsen. De virtuele inertie wordt verkregen door vermogen uit de windturbine-inertie te injecteren of te absorberen, gelijkaardig aan het gedrag van synchrone machines. In de literatuur zijn verschillende controlestrategieën beschikbaar om inertie na te bootsen. Bovendien is er aangetoond dat de beschikbare inertie in de windturbinebladen groot genoeg is om een gelijkaardige hoeveelheid systeeminertie te verkrijgen als met conventionele generatoren wanneer windturbines uitgerust zijn met een bijkomende controlelus.

Vanuit het oogpunt van het netwerk is het niet de maximale hoeveelheid kinetische energie die in de inertie kan opgeslagen worden of eruit kan worden gehaald die van belang is, maar de impact die deze extra energie heeft op het frequentiegedrag onmiddellijk na de storing. Daarom wordt in dit werk de invloed van de netwerksamenstelling, d.i. het type van de generatoren, op de optimale parameterselectie van de geëmuleerde inertiesponsstrategieën onderzocht. Er wordt aangetoond dat correcte parameters van belang zijn om de gewenste inertierespons te bekomen. Als er teveel vermogen in het net wordt geïnjecteerd onmiddellijk na een frequentiedip kan dit een tragere primaire regelactie van de conventionele generatoren veroorzaken, wat leidt tot een diepere frequentieval na de storing. Bovendien kan het een ook leiden tot een tweede, diepere frequentiedip, wat uiteraard ongewenst is. Wanneer de verschillende geëmuleerde inertiesponsstrategieën met elkaar vergeleken worden, is het duidelijk dat de synthetische inertie de meest veelbelovende strategie is aangezien ze het stabielst is en de kleinste parametersensitiviteit vertoont.

Wanneer de geëmuleerde inertiesponsstrategieën in windturbines gebruikt worden om het net te ondersteunen, brengen ze ook enkele neveneffecten met zich mee. Om te beginnen ontstaan er opbrengstverliezen door de suboptimale werking van de windturbines gedurende de inertierespons. In dit werk wordt er echter aangetoond dat deze extra opbrengstverliezen zeer beperkt zijn voor de inertiesponsstrategieën. Dit is het gevolg van de kleine variaties in de draaisnelheid van de windturbines die nodig zijn om het net op een optimale manier te ondersteunen. Daarnaast veroorzaakt de geëmuleerde inertierespons ook nog bijkomende koppelvariaties. Deze variaties zorgen voor een extra belasting van de aandrijflijn van de windturbine, wat een impact kan hebben op de levensduur van windturbines die uitgerust zijn met een inertiesponsstrategie. Om de invloed van de geëmuleerde inertierespons op de dynamica van de aandrijflijn te beperken, wordt in dit werk de DC-bus spanningsmodulatiestrategie ontwikkeld. Door deze controlestrategie te gebruiken, wordt de buffercapaciteit van de DC-bus aangewend om de koppelveranderingen veroorzaakt door de geëmuleerde inertierespons te beperken. Aangezien de neveneffecten ofwel beperkt zijn (opbrengstverliezen) ofwel doeltreffend voorkomen kunnen worden door een geschikte controlestrategie te gebruiken (koppelvariaties), is het duidelijk dat de geëmuleerde inertiesponsstrategieën gebruikt kunnen worden om de integratie van windturbines in het elektriciteitsnet te bevorderen.

Naast het leveren van inertierespons, kunnen windturbines ook gebruikt worden om deel te nemen aan de primaire frequentieregeling. Aangezien windturbines meestal in het maximale vermogenspunt worden uitgebaat om zoveel mogelijk hernieuwbare energie op te vangen, is het leveren van pri-

maire frequentieregeling in het geval van frequentiedips niet voor de hand liggend. Om dit te verwezenlijken, moeten windturbines continu onder het maximale vermogenspunt uitgebaat worden. Daarom worden in dit proefschrift verschillende ontlastingsstrategieën met elkaar vergeleken. Dit toont aan dat het aanbieden van primaire reserve met windturbines mogelijk is met een uiteenlopend aanbod aan controlestrategieën, maar dat sommige strategieën toch duidelijk beter geschikt zijn. Wanneer de windturbines gegroepeerd worden in windmolenparken worden de verschillen tussen de verschillende strategieën steeds kleiner door het uitmiddelende effect van het park. Tenslotte wordt ook de adaptieve proportionele controlestrategie ontwikkeld om een gelijke vermogensverdeling tussen verafgelegen windturbines met sterk verschillende windcondities mogelijk te maken.

List of Figures

List of Tables

Abbreviations

AC	alternating current
BRP	balancing responsible party
CCGT	combined cycle gas turbine
DC	direct current
DFIG	doubly-fed induction generator
DG	distributed generator
FACTS	flexible alternating current transmission system
FCP	frequency containment process
FCR	frequency containment reserves
FRP	frequency restoration process
FRR	frequency restoration reserves
FSC	full-scale converter
FSIG	fixed-speed induction generator
HV	high-voltage
HVDC	high-voltage direct current
LIDAR	laser imaging detection and ranging
LV	low-voltage
MPP	maximum power point
MPPT	maximum power point tracker
MV	medium-voltage
OLTC	on-load tap changer
PLL	phase locked loop
PMSG	permanent magnet synchronous generator
PS	power surge
PV	photovoltaic
PWM	pulse-width modulation
ROCOF	rate of change of frequency
RR	replacement reserves
RRP	reserve replacement process
SG	synchronous generator
SI	synthetic inertia

STATCOM	static synchronous compensator
SVC	static var compensator
THD	total harmonic distortion
TSO	transmission system operator
TSR	tip-speed ratio
UPS	uninterrupted power supply
UTC	coordinated universal time
VSC	voltage source converter
WT	wind turbine

1 Introduction

In this chapter, the context and goal of this research is briefly discussed. Furthermore, an overview of the work is given.

1.1 Wind turbines and ancillary services

In the last decades, climate change due to human activities has become an important topic. Several industrial activities, transportation, agriculture, etc. have led to an increased emission of greenhouse gasses such as carbon dioxide and methane, which have an important impact on global warming. Recently, on the 2015 United Nations Climate Change Conference (COP21) 195 countries decided to decrease their carbon output and keep the global warming well below 2°C. In order to do so, a variety of measures will have to be taken in different fields. In this dissertation, the focus is on the transition towards a more sustainable electricity production.

These environmental concerns have already led to an increased use of renewable energy in the electricity production. Wind turbines, photovoltaic panels, wave energy, geothermal energy and biomass are examples of renewable energy sources that can be used in the future energy mix. Wind turbines already play an important role in the current renewable energy production. At the end of 2015, the global installed wind power capacity was almost 433 GW, with 63 GW of installations in the last year [1]. Considering 140 GW of renewable power installations in 2015, wind power accounts for more than 40 % of the newly installed renewable power capacity. This

makes wind turbines, together with photovoltaic panels, one of the more mature renewable energy sources.

However, large-scale integration of renewable energy sources in the existing electrical power system causes numerous challenges. The connection of distributed generation units, such as PV panels or wind turbines, to the distribution grids might result in current congestion and voltage problems as these systems were not designed to cope with large amounts of generation [2]. Furthermore, also the intermittent behavior of the wind causes some challenges. Due to varying wind conditions, fluctuations in the output power of wind turbines arise. To maintain the balance in the power system, the thermal base-load units have to be more flexible: they need to operate at part-load levels more often or are even shut down for some time, which results in a reduced life cycle and increased costs [3].

In order to obtain a secure and reliable operation of the power system, ancillary services are needed. For example, the power production and consumption have to be balanced at all times to ensure a stable operation of the grid at 50 Hz. This is achieved by means of a service called frequency control. Also the voltage at the different voltage levels is maintained within certain limits by means of voltage control systems. Besides these two important services, there are also other services such as congestion management, black start capability, etc. which are needed to ensure the proper functioning of the power system. In the current power system, the majority of these ancillary services is still provided by conventional power plants. Also flexible AC transmission systems (FACTS), high-voltage direct current systems (HVDC), loads and capacitor banks provide part of the services. On the one hand, when wind turbines start to replace the conventional units, it is likely that more ancillary services will be needed. As explained, decentralization might lead to more voltage problems, whereas the variable power production and decreasing system inertia may impede the frequency control. On the other hand, with an increasing wind power penetration, less conventional units are available to provide these services.

Consequently, in the future, difficulties with the provision of ancillary services may arise with an increasing penetration of wind turbines in the power system. However, the participation of wind turbines in the provision of ancillary services seems a promising option. The variable-speed wind turbines that are used today are perfectly suited to provide different kinds of services. As these wind turbines are connected to the grid by means of a power-electronic converter, it is possible to (partly) control their active and reactive power output. In this way, wind turbines can assist in a broad variety of ancillary services such as voltage control and frequency control.

This research mainly focuses on the provision of inertial response and

primary frequency control with variable-speed wind turbines. The main contributions of this work are the optimization of the emulated inertial response strategies and power reserve strategies to provide primary control. For the emulated inertial response strategies, the optimal parameters to obtain a similar inertial response for power systems with either a low or high penetration of wind turbines are derived. Also, a strategy to decrease the impact of the inertial response on the wind turbine drive-train dynamics is presented. For the primary control, different reserve strategies are compared to find the optimal one. The adaptive droop control method to obtain equal power sharing between remote wind turbines is developed. The principles developed in this work, might help to expedite the large-scale integration of wind turbines in the power system.

1.2 Overview

This dissertation is organized as follows:

Chapter 2 gives an overview of ancillary services with wind turbines. First, the different ancillary services that are needed in the power system are listed. Then, the different types of wind turbines are considered, together with an overview of the wind turbine model that is used in the remainder of this work. Finally, the possibilities to provide ancillary services with wind turbines are discussed.

Optimal emulated inertial response with wind turbines is one of the important topics of this research. In chapter 3, the need for inertial response in the power system is explained. The natural inertial response behavior of variable-speed wind turbines is discussed and two possible emulation strategies are presented: synthetic inertia and temporary power surge. Here the importance of a correct parameter selection for both strategies is elaborated.

In chapter 4, the possible side-effects of emulated inertial response are discussed. During the inertial response, the wind turbines are operating in a suboptimal operating point, which causes energy yield losses. Furthermore, the sudden increase of active power that is needed for the emulation strategies has an impact on the drive-train dynamics. Therefore, a control strategy that minimizes this impact is presented in this chapter.

Chapter 5 gives an overview of the provision of primary frequency control with wind turbines. Different control strategies to provide active power reserves are discussed. The adaptive droop control method is presented as an alternative for the fixed droop control, which results in an equal power sharing between wind turbines under different wind speed conditions.

In chapter 6, the main conclusions of this dissertation are summarized. Furthermore, some possible topics for further research are presented.

2

Ancillary services with wind turbines

In this chapter, firstly, a short introduction on the different ancillary services that are needed in the electric power system is given. Secondly, variable-speed wind turbines are discussed. Finally, the ability to provide ancillary services with wind turbines (WTs) is presented.

2.1 Overview of ancillary services

2.1.1 Definition

Ancillary services are defined by Eurelectric as [4]:
"All services required by the transmission or distribution system operator to enable them to maintain the integrity and stability of the transmission or distribution system as well as the power quality".

Ancillary services are procured by the system operators and are provided by the grid users, such as generators or consumers.

Of course, many different services can be regarded as ancillary services, so different authors/organizations list different services. Here, only ancillary services that can be provided by generating units are considered as the topic of this work is the provision of ancillary services with wind turbines [4–7]:

- Frequency control

- Voltage control
- Congestion management
- Improvement of power quality
- Compensation of active power losses
- Black start

In the next paragraph, a short overview of the different services is given.

2.1.2 Frequency control

As electricity cannot be stored easily in large quantities, the production always equals the system load (which includes the line losses). This balance guarantees a stable operation of the electricity grid at a constant frequency of 50 Hz [1]. When there is a sudden change in the production or consumption, frequency deviations occur. In order to maintain and/or to restore the frequency, the output of the generators must be rapidly increased or decreased.

In the European synchronous electricity grid, the frequency regulation is achieved in three stages: primary, secondary and tertiary control [5, 8–10]. These different stages are discussed next.

2.1.2.1 Primary frequency control

Primary control maintains the balance between power generation and consumption when a deviation occurs. Its main task is to limit the frequency deviation Δf from the nominal value f_{nom} and stabilize the grid frequency after a disturbance. It is a local and automated control and within seconds ($\sim$ 15 s - 30 s) the active power output of the participating generators can be increased or decreased. The change in active power output due to the functioning of the primary control, ΔP_{prim}, is proportional to the deviation of the grid frequency:

$$\Delta P_{\text{prim}} = K_{\text{prim}} \left(f_{\text{nom}} - f \right) \tag{2.1}$$

where f is the actual grid frequency, f_{nom} is the nominal grid frequency (50 Hz) and K_{prim} is determined by the slope of the droop characteristic, shown in Fig. 2.1. In order to achieve this change in active power output, primary or frequency containment reserves have to be maintained at any

[1] In a large part of the world, including Europe, 50 Hz is the nominal frequency. In some countries (e.g., USA, Canada, parts of Japan, etc.), 60 Hz is used instead of 50 Hz. However, this has no impact on the operation of the frequency control.

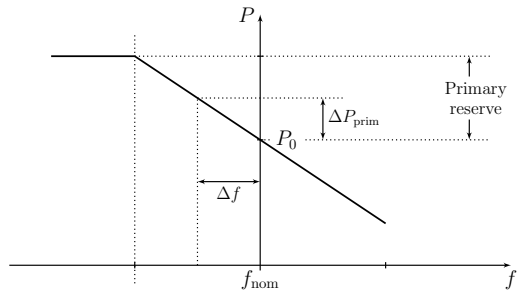

Figure 2.1: Frequency control: P/f droop function.

time. After the activation of these reserves, the power balance is restored at a frequency deviating from the nominal value.

2.1.2.2 Secondary frequency control

Secondary control is used to restore the grid frequency to the nominal frequency. Furthermore, the desired energy exchange between the different control areas is maintained by this control. A control area is a part of the network that is controlled by a transmission system operator (TSO). Secondary control is only activated in the control area where a power deficit exists and is activated automatically. It starts after a few seconds and is usually completed after 15 min. In this case, secondary or frequency restoration reserves are needed. An automatic PI-control function that is applied at the transmission system operator control center activates the secondary reserves. After about 15 min, secondary control has finished and the secondary reserve are replaced by the tertiary control.

2.1.2.3 Tertiary frequency control

The main function of the tertiary control is to restore the required level of operating reserves (primary and secondary reserves). Tertiary or replacement reserves are maintained at any time and are activated manually by the TSO about 15 min after the initial deviation. Tertiary control copes with persistent control deviations after production outages or long-lasting load changes. The tertiary reserves can be situated in the control area where the power deficit exists or in other areas of the synchronous area.

2.1.2.4 Operational reserves

Operational reserves are active power reserves located in the generation units or loads to maintain balance between generation and demand and

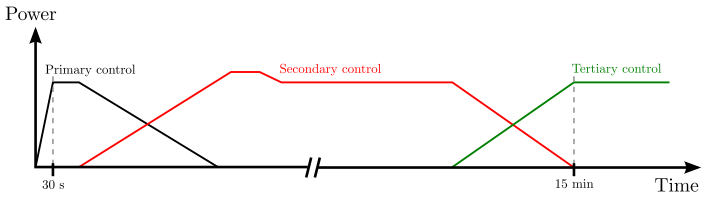

Figure 2.2: Activation of power reserves (based on [10]).

restore the frequency to its set point value in the synchronous system. As already stated, operational reserves are classified as frequency containment reserves, frequency restoration reserves and replacement reserves [11]. Sometimes, a distinction is made between spinning reserves and standing reserves [4, 6, 12]:

- *spinning reserves:* increase or decrease in generation that can be provided at short notice, carried out by partially-loaded generating units that are synchronized to the grid.
- *standing reserves:* increase or decrease in generation that can be provided by those generating units that are not synchronously online.

In Fig. 2.2, the timing of the activation of the different power reserves is shown. First the primary reserves are deployed, which have to be completely available after 30 s. Then, the secondary reserves start to take over to free the primary reserves and to restore the frequency to the nominal value. After about 15 min, tertiary reserves are manually activated.

2.1.2.5 Time control

If the mean system frequency in the synchronous zone deviates from the nominal frequency of 50 Hz, this results in a discrepancy between the synchronous time and the universal coordinated time (UTC). Therefore, the synchronous time is calculated and its correction is organized centrally. Correction involves the setting of the set-point frequency for secondary control at 49.99 Hz or 50.01 Hz, depending upon the direction of correction, for full periods of one day.

The different functions of primary, secondary, tertiary and time control are summarized in Fig. 2.3.

2.1.2.6 New terminology

In recent grid codes, new terminology is introduced concerning frequency control [13, 14]. However, the operating principle remains the same. The new control structure is as follows:

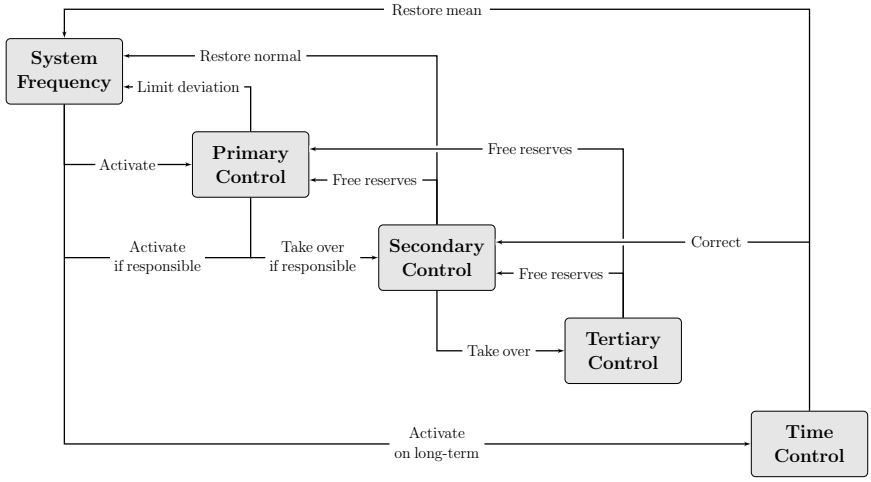

Figure 2.3: Overview of frequency control (based on [10]).

- **Frequency containment process (FCP):** stabilizes the grid frequency to a steady state value after a disturbance by activation of frequency containment reserves (FCR). This process corresponds to the primary frequency control.
- **Frequency restoration process (FRP):** restores the frequency to the nominal frequency (50 Hz) by activating frequency restoration reserves (FRR). Some of the frequency restoration reserves are automatically activated, which corresponds to the secondary control reserves. The reserves that are activated manually activated are part of the tertiary control reserves.
- **Reserve replacement process (RRP):** replaces the FRR by activation of replacement reserves (RR). This is part of the tertiary frequency control.

Furthermore, the imbalance netting process is added to reduce the amount of simultaneous counteracting FRR activation of different control areas.

In the remainder of this work, the 'old' terminology is used, as it is well known and still widely used.

2.1.3 Voltage control

Besides the frequency f, the voltage V is an important parameter in the electric power system. Excessive deviation from the nominal voltage should

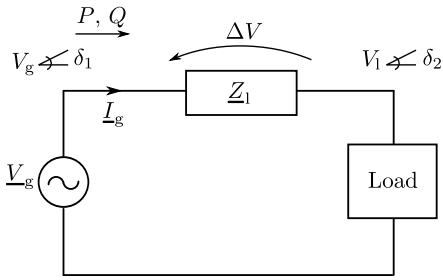

Figure 2.4: Single phase equivalent of the simple system to study the power flow equations.

be avoided since loads are designed to operate at their nominal voltage level. According to the EN 50160 standard, only ±10 % voltage deviation is allowed in the low and medium voltage grid [15]. Consequently, it is important to properly control the voltage within the operational limits. The way to achieve this, is by means of voltage control. Voltage control depends strongly on the voltage level of the considered network, which is elaborated in the next paragraphs.

2.1.3.1 Load flow equations

In an AC power system, the voltage and current are usually not in phase. Hence, reactive power will flow. Reactive power is absorbed by inductive components (e.g., transformers, overhead lines, induction machines, ...) and generated by capacitive components (e.g., over-excited synchronous machines, capacitors, ...).

The active and reactive power flows in the network cause voltage drops over the network impedances. These voltage drops can be compensated by supplying active and/or reactive power. To study the influence of the active and reactive power on the voltage, the simplified system of Fig. 2.4 is considered.

The complex power $\underline{S}$ injected by the three phase power source is given by:

$$\underline{S} = 3\underline{V}_g \underline{I}_g^* \tag{2.2}$$

with $\underline{V}_g$ the voltage of the power source: $\underline{V}_g = V_g e^{j\delta_1}$ in the complex notation, $\underline{I}_g$ the line current and $\underline{I}_g^*$ the complex conjugate of $\underline{I}_g$. This power source is connected to a load with voltage $\underline{V}_l = V_l e^{j\delta_2}$ through a line impedance $\underline{Z}_l = R_l + jX_l$:

$$\underline{I}_g = \frac{\underline{V}_g - \underline{V}_l}{R_l + jX_l} \tag{2.3}$$

The load's phase angle δ_2 can be chosen as zero as voltage angles are relative quantities, therefore, $\underline{V}_\mathrm{l} = V_\mathrm{l}$. The active and reactive power generated by the power source can be written as:

$$P = \frac{V_\mathrm{g}}{Z_\mathrm{l}^2}\left[R_\mathrm{l}(V_\mathrm{g} - V_\mathrm{l}\cos\delta_1) + X_\mathrm{l}V_\mathrm{l}\sin\delta_1\right] \tag{2.4}$$

$$Q = \frac{V_\mathrm{g}}{Z_\mathrm{l}^2}\left[-R_\mathrm{l}V_\mathrm{l}\sin\delta_1 + X_\mathrm{l}(V_\mathrm{g} - V_\mathrm{l}\cos\delta_1)\right] \tag{2.5}$$

Generally, the phase angle variations in the network are limited, hence $\delta_1 \approx \delta_2$, $\sin\delta_1 \approx \delta_1$ and $\cos\delta_1 \approx 1$, where $\delta_1 = 0$ is chosen as the reference angle. By using these approximations, P and Q can be expressed as:

$$P \approx \frac{V_\mathrm{g}}{Z_\mathrm{l}^2}\left[R_\mathrm{l}(V_\mathrm{g} - V_\mathrm{l}) + X_\mathrm{l}V_\mathrm{l}\delta_1\right] \tag{2.6}$$

$$Q \approx \frac{V_\mathrm{g}}{Z_\mathrm{l}^2}\left[-R_\mathrm{l}V_\mathrm{l}\delta_1 + X_\mathrm{l}(V_\mathrm{g} - V_\mathrm{l})\right] \tag{2.7}$$

According to (2.6) and (2.7), both active and reactive power have an influence on the grid voltage. However, three different cases can be considered: high-voltage, medium-voltage and low-voltage networks. As the medium-voltage grid has characteristics of both the high- and low-voltage grid, these are first considered.

The high-voltage (HV) transmission grids are mainly inductive of nature, hence R_l is low compared to X_l. Therefore, in inductive networks, the expressions for the active power P and reactive power Q reduce to:

$$P \approx \frac{V_\mathrm{g}V_\mathrm{l}}{X_\mathrm{l}}\delta_1 \tag{2.8}$$

$$Q \approx \frac{V_\mathrm{g}}{X_\mathrm{l}}(V_\mathrm{g} - V_\mathrm{l}) \tag{2.9}$$

A decoupling of P and Q is achieved. The active power P is predominantly dependent on the phase difference (and thus dynamically dependent on the frequency), whereas the reactive power Q is determined mainly by the voltage difference over the line. This leads to the well-known P/δ and Q/V linkage in high-voltage networks. Consequently, in high-voltage grids, reactive power is used to control the voltage amplitude.

Low-voltage (LV) networks, on the other hand, are mainly resistive. The active and reactive power flows in the network are then given by:

$$P \approx \frac{V_\mathrm{g}}{R_\mathrm{l}}(V_\mathrm{g} - V_\mathrm{l}) \tag{2.10}$$

$$Q \approx \frac{-V_\mathrm{g}V_\mathrm{l}}{R_\mathrm{l}}\delta_1 \tag{2.11}$$

Again, a decoupling between P and Q is achieved. Here, P is mainly determined by the voltage difference over the line, so in low-voltage networks, there is a P/V linkage instead of a Q/V linkage. Therefore, in low-voltage grids, using active power to control the voltage is more effective than using reactive power. Furthermore, reactive power injection or absorption in low-voltage grids may lead to increased line losses and reactive power fines due to a bad power factor $\cos\phi = \frac{P}{S}$.

In medium-voltage (MV) grids, voltage control is less straightforward. In the conventional power system, the voltage level in the distribution network is controlled by means of on-load tap changers (OLTCs). If distributed generators are connected to the medium-voltage network, they should control the voltage by injecting or absorbing active and reactive power, since the R/X-value of these networks is usually around one. Therefore, P and Q are no longer decoupled.

Similar to the frequency control, voltage control can be divided into primary, secondary and tertiary control. These types are discussed for the case of high-voltage grids.

2.1.3.2 Primary voltage control

In HV grids, primary voltage control is an automated control that adjusts the injection of reactive power when the terminal voltage deviates from the nominal value. Generally, droop functions as shown in Fig. 2.5 are used to stabilize the voltage at the terminal of the unit by injecting or absorbing reactive power. This reactive power control influences the voltage within seconds or even faster. The reactive power set-point of the generator is adjusted by ΔQ_{prim} that is calculated as:

$$\Delta Q_{\mathrm{prim}} = K_{\mathrm{Q}} \left(V_{\mathrm{nom}} - V_{\mathrm{m}} \right) \tag{2.12}$$

where V_{m} is the terminal voltage, V_{nom} is the nominal voltage and K_{Q} is determined by the slope of the droop function.

2.1.3.3 Secondary voltage control

To achieve secondary voltage control, the network operator performs measurements of the voltage in some critical buses that are representative for a certain area. If the voltages are out of range, the voltage reference values for the generators are adjusted to recover a voltage profile in the normalized interval. The time response of the secondary voltage control goes up to one minute and less than several minutes. Similar to secondary frequency control, secondary voltage control is activated automatically in the control center of the network operator where the new voltage reference values are determined. Then, these are sent to the different generators.

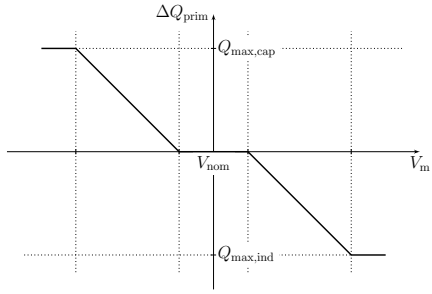

Figure 2.5: Voltage control: Q/V droop function.

2.1.3.4 Tertiary voltage control

Tertiary voltage control is manually activated by the network operator. It is used to optimize the voltage profile and achieve an optimal power flow by adjusting the reference values for the secondary voltage control. The tertiary control acts on a time-scale of about 10 to 30 minutes.

It should be noted that secondary and tertiary voltage control are not commonplace within Europe [16]. It is used in some countries (e.g., France, Italy), but the implementation can differ [16].

2.1.4 Congestion management

In an electric power system, the power flows are restricted by technical limitations of the network (i.e., voltage, thermal or stability limits). When the power flow is constrained by these limitations, it is sometimes referred to as congestion.

Usually, least-cost dispatch of the generation units is used to produce electricity. Renewable energy sources, such as wind turbines, have priority to inject power into the grid. The lowest-cost or renewable production may come from remote power plants whose energy must be imported into the load center over long-distance transmission lines. If the transmission system is composed out of a few high-capacity lines, loss of one of these lines may limit the import capacity. Moreover, when additional (renewable) generation capacity is connected to the existing network, congestion problems may arise as well.

A possible solution for congestion problems is to build additional lines to increase the transmission capacity. However, the planning and building of these lines often takes a long time. Furthermore, if the additional capacity is only needed for a limited number of hours per year, this might not be the most economic option to solve congestion problems. Therefore, another

option to solve congestion problems is that the TSO or balancing responsible party (BRP) re-dispatches the production if possible. In this way, the congestion problem is relieved without extensive investments in the grid infrastructure. Consequently, the system stability can be maintained.

2.1.5 Improvement of power quality

2.1.5.1 Definitions concerning power quality

It is hard to find a general definition of power quality as various sources give different and sometimes conflicting definitions of power quality [17]. The following consistent set of definitions is used in this work [17, 18]:

- **Voltage quality** is concerned with deviations of the voltage from the ideal case. The ideal voltage is a single-frequency sine wave of constant amplitude and frequency.
- **Current quality** is the complementary term to voltage quality: it is concerned with the deviation of the current from the ideal case. The ideal current is again a single-frequency sine wave of constant amplitude and frequency, with the additional requirement that the current sine wave is in phase with the voltage sine wave.
- For **three-phase systems**, symmetry of the current and voltage in the three phases is an additional property of the ideal case. However, most literature about power quality does not mention the three-phase phenomena. The only phenomenon that is treated in a three-phase sense is **voltage unbalance**.
- **Power quality** is the combination of voltage quality and current quality.

Consequently, any deviation of voltage or current from the ideal waveform is a power quality disturbance. The disturbance can be a voltage disturbance or a current disturbance, but it is often not possible to distinguish between the two because any change in current gives a change in voltage and the other way around. This difficulty of distinguishing between voltage and current disturbances is one of the reasons the term power quality is generally used. The term voltage quality is reserved for cases where only the voltage at a certain location is considered. The term current quality is sometimes used to describe the performance of power-electronic converters connected to the power network.

The above definition considers every disturbance as a power quality issue. A commonly used alternative is to distinguish between continuity (reliability) and quality. Continuity includes interruptions, whereas quality

covers all other disturbances. Short interruptions are sometimes seen as part of continuity, sometimes as part of quality.

Sometimes the term quality of services in electricity supply is used, which considers three dimensions:

- **Commercial quality** concerns the relationship between the network company and the customer.
- **Continuity of supply** concerns long and short interruptions.
- **Voltage quality**, as defined above.

2.1.5.2 Variations and events

Power quality disturbances can be divided in two types: variations and events [17, 18].

- **Variations** are small deviations of voltage or current characteristics from its nominal or ideal value, e.g., the variation of the voltage root-mean-square (rms) value and frequency from their nominal values, or the harmonic distortion of voltage and current. Variations are disturbances that are measured at any moment in time. A typical example of a power quality variation is the variation of the power system frequency. Its nominal value is 50 Hz, but the actual frequency f is continuously fluctuating around this value.
- **Events** are larger deviations that only occur occasionally, e.g., voltage interruptions or load switching currents. Events are disturbances that start and end with a threshold crossing. A typical example of a power quality event is an interruption. During an interruption, the voltage at the customers interface or at the measurement location is zero.

The difference between variations and events is not always obvious, and related to the way in which the disturbance is measured. The best way of distinguishing between the two is as follows: variations can be measured at any moment in time, whereas events require waiting for a voltage or current to exceed a predefined threshold (a trigger). As the setting of a threshold is always somewhat arbitrary, there is no strict border between variations and events.

The definitions of power quality events and variations result in a very wide interpretation of power quality. Usually, a power quality disturbance is only seen as an issue when it causes problems, either for the customer or for the network operator. For example, voltage dips and harmonics are usually considered as a power quality issue, whereas voltage and frequency

variations are not. This is because voltage and frequency control were incorporated in the design of the power system many years ago.

2.1.5.3 Power quality issues

In this section, different power quality issues are shortly discussed [17–22]. In Fig. 2.6 an overview of several power quality issues is given.

- **Voltage dip:** A voltage dip or voltage sag is a sudden reduction (between 10 % and 90 %) of the rms voltage for periods ranging from a half cycle to a minute (Fig. 2.6a). Voltage dips are usually caused by the flow of heavy currents due to the starting of large motors or the flow of fault currents.

- **Voltage swell:** Voltage swells are defined as an increase of the rms voltage between 110 % and 180 % for periods ranging from a half cycle to a minute (Fig. 2.6b). Voltage swells often appear on the unfaulted phases of a three-phase circuit that has developed a single-phase short circuit.

- **Interruption:** An interruption occurs when the supply voltage decreases to less than 10 % of the rms voltage (Fig. 2.6c). Interruptions can be caused by faults, blown fuses, breaker opening, control malfunctions or equipment failures.

- **Voltage impulse:** An impulsive transient is a sudden change in the steady-state condition of the voltage or current, or both, which is unidirectional in polarity, either positive or negative (Fig. 2.6d). Impulsive transients are normally characterized by their rise and decay times. The most common causes of impulsive transients are lightning and insulation breakdown.

- **Oscillatory transient:** In Fig. 2.6e, an oscillatory transient is shown. It consists of a voltage or current whose instantaneous value changes polarity rapidly and is usually described by its spectral content. Oscillatory transients are caused by switching disturbances, either directly or as a result of resonating circuits associated with switching devices. An example is capacitor switching, which can cause resonant oscillations.

- **Unbalance:** Voltage unbalance describes a situation in which either the voltages of a three-phase system are not identical in magnitude (Fig. 2.6f) or the phase differences between them are not 120 electrical degrees (Fig. 2.6g) or a combination of both. The main causes of

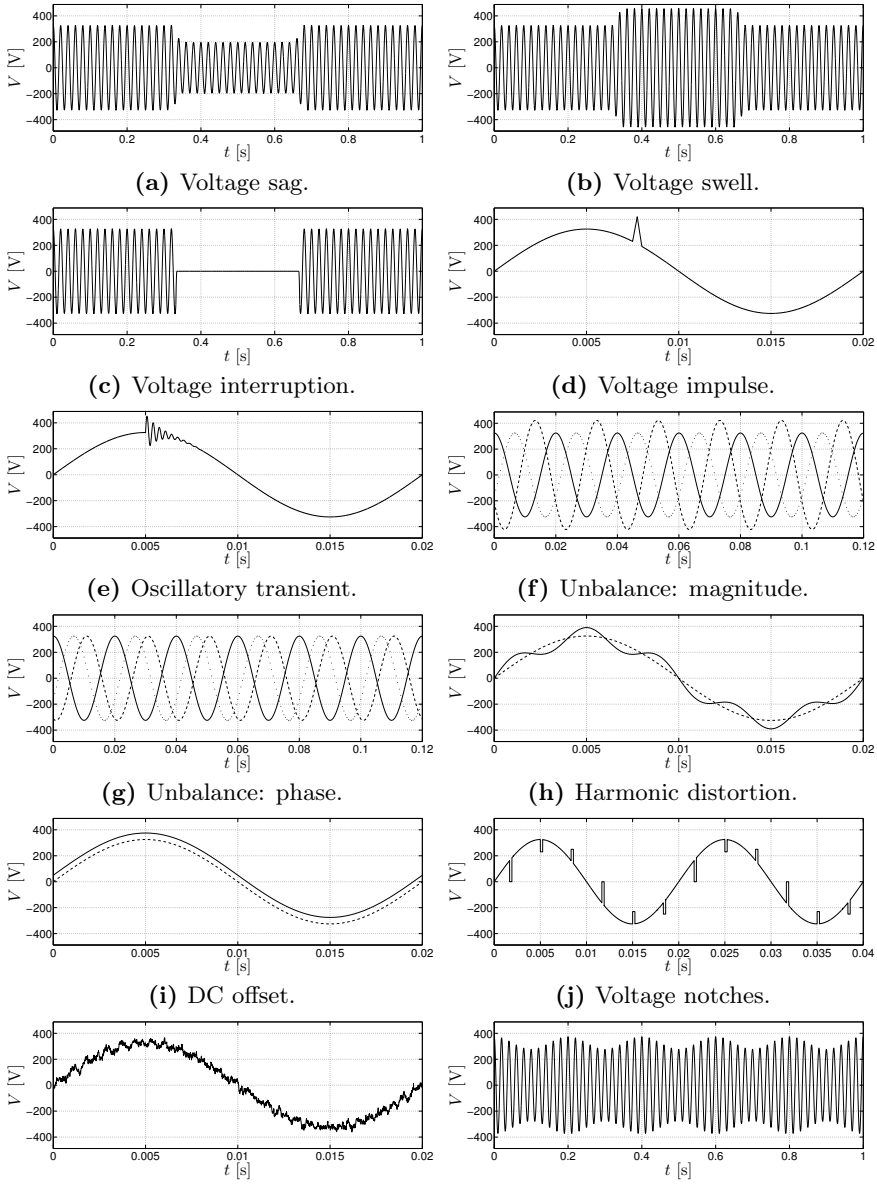

(a) Voltage sag.

(b) Voltage swell.

(c) Voltage interruption.

(d) Voltage impulse.

(e) Oscillatory transient.

(f) Unbalance: magnitude.

(g) Unbalance: phase.

(h) Harmonic distortion.

(i) DC offset.

(j) Voltage notches.

(k) Noise.

(l) Flicker.

Figure 2.6: Power quality issues (based on [23]).

unbalance are single-phase loads and distributed generators. Also unequal impedances in transformers and untransposed (long) overhead transmission lines may cause unbalance.

- **Harmonic distortion:** For a power system operating at 50 Hz, any non-sinusoidal voltage or current can be decomposed into a fundamental (50 Hz) component plus a number of harmonic components with frequencies that are a multiple integer of 50 Hz. The latter are called harmonic components. In Fig. 2.6h, the 250 Hz component is shown and is referred to as the fifth harmonic. Therefore, harmonic distortion is distortion where the waveform is non-sinusoidal, but periodic with a period equal to the fundamental period $T_0 = 1/f_0$ of the power system. Harmonic distortion is caused by nonlinear elements in the system (either in the network or in the loads). The main distortion is due to power-electronic loads like computers, televisions, energy-saving lamps, etc.

- **DC offset:** The presence of a DC component in the voltage or current in an AC power system is called DC offset. It can be seen as a special case of harmonic distortion, but is often treated separately due to its specific consequences. An example is showed in Fig. 2.6i. This phenomenon is often caused by half-wave rectification, which is sometimes used in light dimmer circuits and TV power supplies.

- **Voltage notches:** Three-phase converters that convert AC to DC require commutation of the alternating current from one phase to another. During this period, there is a momentary short circuit between the two phases. This causes a periodic voltage disturbance, which is called notching. The frequency components associated with notching can be quite high due to the sharp edges created by the switching instants. In Fig. 2.6j, an example of notching in a six-pulse converter is shown.

- **Noise:** Noise are all the non-periodic frequency components in the voltage or current (see Fig. 2.6k). These unwanted electrical signals cause problems with sensitive electronic equipment and are caused by power electronic devices, switching power supplies, arcing equipment, etc.

- **Flicker:** Fluctuations in the voltage amplitude can cause perceptible (low frequency) light flicker depending on the magnitude and frequency of the variation. Flicker or voltage flicker is in fact a special case of interharmonic distortion. Even very small fluctuations in

the rms voltage with frequencies between 1 and 15 Hz lead to light-intensity variation, for which our eyes are very sensitive. In Fig. 2.6l, a simple case of flicker is illustrated, where the AC voltage is amplitude modified by a sine wave seen as the envelope of the voltage waveform. The main causes of flicker are loads that draw large and highly variable currents. Arc furnaces, the starting of electric motors and motors that require an irregular torque. Also, wind turbines can cause flicker due to variations in the wind speed and, more importantly, tower shadow and wind shear [24, 25]. Tower shadow and wind shear cause periodic dips in the power output of the wind turbine which are called 3p-pulsations, as they appear three times per rotation of the turbine. Especially the (early) fixed-speed wind turbines cause flicker, whereas modern variable-speed wind turbines have less impact [24]. Moreover, aggregation of wind turbines in wind farms results in further reduced flicker levels [26].

2.1.5.4 Mitigation of power quality issues

Some of the aforementioned power quality problems can be mitigated by installing the appropriate devices or using the correct control methods.

The negative effects of voltage dips, swells and interruptions can be avoided by placing uninterrupted power supplies (UPS) or power conditioners at sensitive installations. Furthermore, voltage variations can be actively mitigated by injecting reactive (and/or active) power into the grid with smart control strategies.

The same applies to unbalance mitigation: by injecting the appropriate currents in the different phases, unbalance can be (partly) counteracted. Distributed generators (DG) that are connected to the grid by means of a power-electronic converter are ideally suited to mitigate unbalance.

Harmonics are usually mitigated by placing filters in the network. Passive filters consist of passive network elements such as capacitors (C) and inductors (L). The passive filter consists of a series of LC-filters tuned for specific harmonics. They provide low impedance paths for current harmonics, so they flow into the filters instead of back to the utility grid. The main disadvantage of passive filters is that the filter characteristics depend strongly on the system impedance. This may cause unwanted resonances between the filter and the system and may cause overload of the filter. Active filters, on the other hand, consist of a controllable voltage source behind a reactance to act as a current source. The voltage source converter (VSC) based active filter is the most common active filter. It consists of a DC-link capacitor, controllable switches and filter inductors, which connect the filter to the grid. When using an active filter, it is possible to choose the current

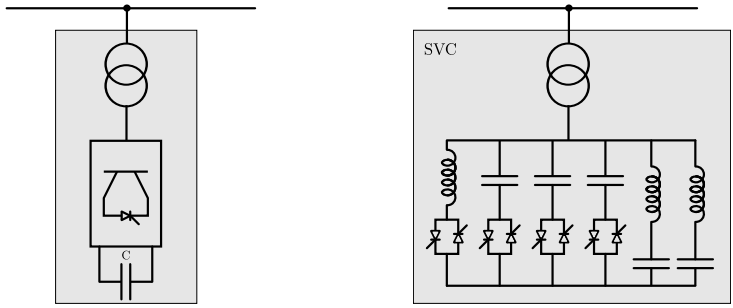

(a) Statcom. **(b)** SVC.

Figure 2.7: Statcom and SVC (based on [27]).

harmonics that have to be filtered and the degree of the attenuation. Again, power-electronically interfaced DG units are suited to act as an active filter.

As flicker is a (slow) variation of the voltage amplitude, it is usually mitigated by means of reactive power control. Often, a static synchronous compensator (Statcom) is used to inject or absorb reactive power. A Statcom consists of a voltage source converter (VSC) with pulse-with modulation (PWM) connected to a DC-source, which is usually a capacitor or a battery (see Fig. 2.7a) [27]. Due to its fast controllability, a Statcom is suited to mitigate flicker. For slowly-varying flicker, e.g., due to electric arc furnaces, sometimes static var compensators (SVCs) are used. The slower speed of response of a SVC makes it less suited for faster variations [27,28]. Power-electronic converters of DG units can also be used to inject the needed amount of reactive power, if properly controlled.

2.1.6 Compensation of active power losses

Active power losses are the differences between the generated active power and the active power delivered to the customers. The transmission of power from the generators to the consumers always results in losses due to the resistance of each element in the network. The losses depend on the network configuration and the location and power output/use of the generators and the loads. For a typical power system, the losses average from 2 to 3 % of the system load for the transmission system and another 3 - 5 % for the distribution system [6]. However, the losses vary greatly as the conditions in the network change. In particular, at times of system peak demands, losses are often much higher than under average loading conditions.

It is often difficult to assign the losses unambiguously to particular transactions in the power system. Therefore, the losses are usually calculated

with load-flow models to allocate them.

Either way, the losses have to be compensated by generators. The TSO contracts generators to deliver additional power for which they receive a remuneration.

2.1.7 Black start

After a system blackout, the system has to be restored again. To do this, black start enabled power stations ensure the restoration after a major incident. Special operational sequences and procedures are applied to coordinate this restoration. Therefore, a certain number of appropriately equipped power stations with auxiliary installations are needed in the power system. These power plants are able to switch themselves on to the grid on request of the TSO. A power plant is capable of black start if it can go from idle to operation without requiring the electricity grid. Technically, this means that the power plant is able to control both the frequency and the voltage and power its auxiliaries.

2.1.8 Conclusion

In order to obtain a reliable operation of the electric power system, many ancillary services are needed, as is shown in this overview. In the next sections, an overview of variable-speed wind turbines and their ability to participate in the provision of ancillary services is given.

2.2 Variable-speed wind turbines

In this section, an overview of different types of wind turbine systems is given. For large wind turbines, almost solely three-bladed horizontal axis wind turbines are used, so this is the only type that is considered further in this work. Furthermore, a mathematical model of the wind turbine system that is used in this thesis is presented.

2.2.1 Wind turbine types

Wind turbines can be divided in two major groups:

- fixed-speed wind turbines
- variable-speed wind turbines

Considering variable-speed wind turbines, only the two most common topologies will be described: wind turbines with a doubly-fed induction generator and these with a full-scale converter.

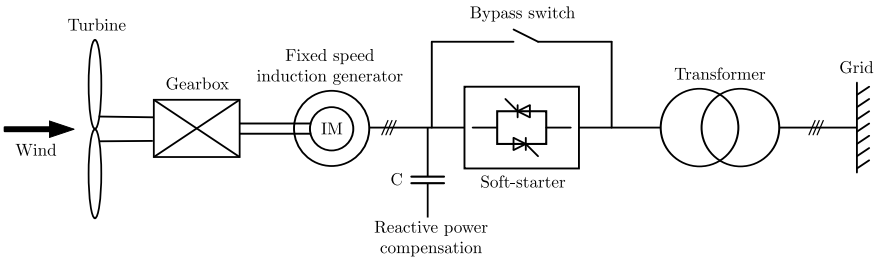

Figure 2.8: Fixed-speed induction generator wind turbine (based on [29]).

2.2.1.1 Fixed-speed wind turbines

In the early days of wind turbine systems, fixed-speed wind turbines were commonly used. They consist of a fixed-speed induction generator (FSIG) which is directly connected to the grid, also known as the 'Danish concept' [29], see Fig. 2.8. Soft-starters are often used to reduce the high inrush currents of the induction generator. Capacitor banks can be installed to provide the reactive power that is needed. The main advantages are the lower cost due to the absence of a power converter and the simple construction. As the rotational speed of the wind turbine is quasi constant, the turbine rarely operates in the maximum power point, which reduces the energy yield. Furthermore, the electric power output cannot be changed rapidly, as the only power control options are active stall or pitch control. Finally, these turbines require a stiff power grid to enable a stable operation. Because of these disadvantages, this type is almost not used anymore for large wind turbines [30].

2.2.1.2 Doubly-fed induction generator wind turbines

The doubly-fed induction generator (DFIG) is often used in wind turbines [29]. The stator of a DFIG is connected to the grid directly, whereas the rotor is connected to the grid by power electronic converters through slip rings, as shown in Fig. 2.9. By changing the power flow through the power electronic circuit, the slip s of the induction generator can be varied. In this way, the generator can deliver power to the grid at both supersynchronous and subsynchronous speeds. Thus, by controlling the active power of the converter, it is possible to vary the rotational speed of the generator and consequently the speed of the wind turbine. The variable speed operation is the main advantage of a DFIG wind turbine, which results in a higher energy yield as the turbine can operate more often in the maximum power point. Another advantage is that only part of the power production is fed through the power electronic converter, so a smaller converter can be used

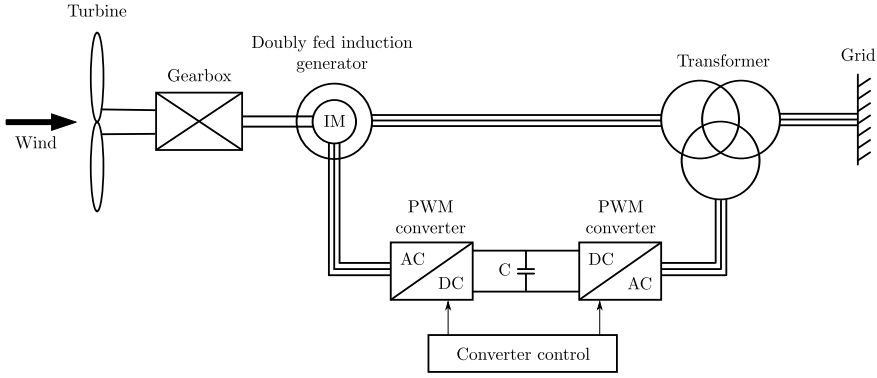

Figure 2.9: Doubly-fed induction generator wind turbine (based on [29]).

to obtain variable speed operation. In general, using a converter rated at 25 % of the nominal wind turbine power results in a speed range of about ± 33 % around the synchronous rotor speed [31]. Furthermore, power factor control can be implemented on DFIG systems to control the reactive power consumption/production of the wind turbine [31]. The presence of slip rings and carbon brushes is a disadvantage as they require maintenance.

2.2.1.3 Wind turbines with a full-scale converter

Induction generators and synchronous generators in wind turbines may be integrated into the power system by means of a full-scale converter (FSC) [29]. The generator is connected to the grid via a power converter. Usually, a back-to-back voltage source converter (VSC) with DC-link is used in order to achieve a full control of the active and reactive power. Diode rectifiers are sometimes used in combination with synchronous generators. Since, in this system, the generator is completely decoupled from the grid, the wind turbine can operate at the maximum power point for a broad range of turbine speeds. In this way, the energy yield is maximized. Furthermore, active and reactive power can be controlled independently, so the power factor can be controlled to a desired value without the need for compensation. The converter has to be rated for the maximum power output of the turbine, making it more expensive than the one used in a DFIG. In Fig. 2.10, four possible topologies with a full-scale converter are shown. The configurations (a) and (b) are characterized by having a gearbox. Configuration (a) uses a squirrel cage induction generator with a full-scale converter. The synchronous generator of (b) needs a small power electronic converter for field excitation. Since gearboxes are expensive and difficult to replace in case of a failure, this component is often omitted in new wind turbines.

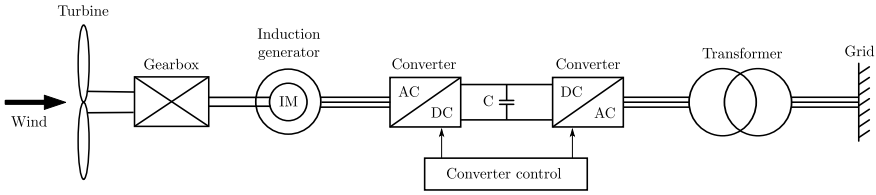

(a) Induction generator with gearbox.

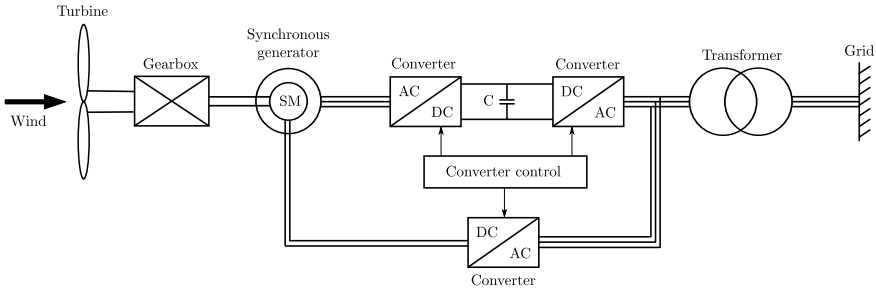

(b) Synchronous generator with gearbox.

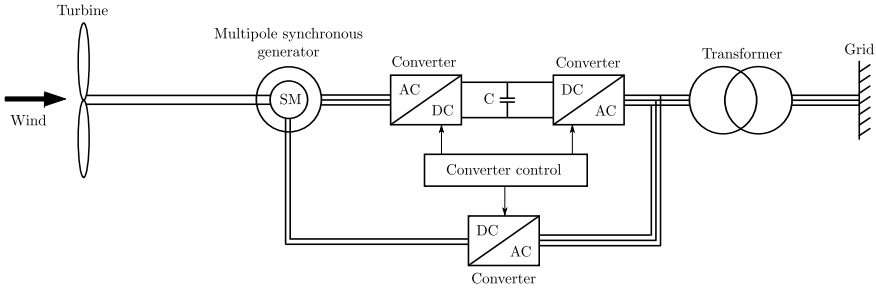

(c) Multipole synchronous generator.

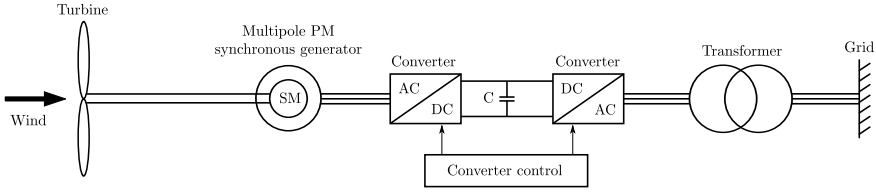

(d) Multipole permanent magnet synchronous generator.

Figure 2.10: Full-scale converter wind turbines (based on [29]).

Therefore, multi-pole synchronous generators are used in configuration (c) and (d). Permanent magnets in (d) can replace the field excitation.

2.2.2 Wind turbine model

2.2.2.1 Wind turbine

The wind turbine rotor converts the kinetic energy in the wind to mechanical energy on a rotating shaft. The mechanical turbine power P_t is given by [32–36]:

$$P_\mathrm{t} = \frac{1}{2}\rho\pi r^2 v^3 \cdot C_\mathrm{p}(\lambda, \beta) \tag{2.13}$$

where ρ is the air density, r is the blade radius, v is the wind speed, C_p is the power coefficient, β is the blade pitch angle and λ is the tip-speed ratio (TSR) which is given by:

$$\lambda = \frac{r\Omega}{v} \tag{2.14}$$

with Ω the rotational speed of the turbine. The TSR is a dimensionless representation of the rotational speed of the wind turbine. The power coefficient C_p reflects the aerodynamic performance of the wind turbine. It depends on the pitch angle β and the tip-speed ratio λ and is determined by the shape of the blade. The power coefficient can either be measured in a wind tunnel, calculated with computational fluid dynamics (CFD) software or determined theoretically.

There exist several expressions for the power coefficient C_p, but in this work a general approximation obtained by curve-fitting on manufacturer data is used [32, 36–38]:

$$C_\mathrm{p}(\lambda, \beta) = 0.73\left(\frac{151}{\lambda_i} - 0.58\beta - 0.002\beta^{2.14} - 13.2\right)e^{\left(-\frac{18.4}{\lambda_i}\right)} \tag{2.15}$$

$$\lambda_i = \frac{1}{\frac{1}{\lambda - 0.02\beta} - \frac{0.003}{\beta^3 + 1}} \tag{2.16}$$

The C_p curve (2.15) is an approximation as it depends on the blade design, blade size, etc. of the considered wind turbine. However, this has no negative impact on the validity of the results of this research.

The power coefficient can be visualized as a surface in function of the parameters λ and β. However, as long as the wind turbine is operating below the rated power and no deloaded operation for primary control is considered, the power output does not need to be limited by pitching the blades. Then, the pitch angle β can be considered zero and (2.15) reduces to:

$$C_\mathrm{p} = 0.73\left(\frac{151}{\lambda} - 13.653\right)e^{\left(-\frac{18.4}{\lambda} + 0.0552\right)} \tag{2.17}$$

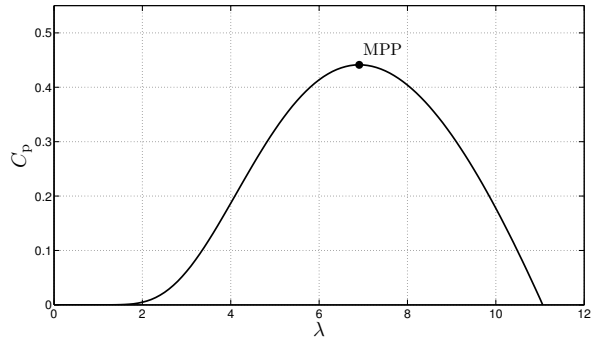

Figure 2.11: Power coefficient with maximum power point.

Fig. 2.11 shows the power coefficient as a function of λ when β is zero. It can be noted that C_p has a maximum, which is called the maximum power point (MPP), which equals 0.44 in this case. The theoretical maximum power coefficient is given by the Betz limit, which equals 0.593 for every type of wind turbine. The maximum power point is reached for the optimal tip-speed ratio λ_opt ($\lambda_\mathrm{opt} = 6.91$ for this curve). Consequently, for any given wind speed v, an optimal shaft speed Ω_opt can be found such that λ remains λ_opt. Variable-speed wind turbines are equipped with a power-electronic converter with a maximum power point tracker (MPPT) which regulates the turbine to the optimal tip-speed ratio, as is explained further. In this way, the energy yield from the wind turbine can be maximized.

In this work, the inertia J_t of the wind turbine rotor is needed to model the dynamic behavior of the wind turbine correctly. It can be calculated as follows [39]:

$$J_\mathrm{t} = \frac{1}{3} M_\mathrm{b} r^2 \tag{2.18}$$

where M_b is the mass of one blade of a three-bladed wind turbine. This equation is valid under the assumption that the center of mass of each blade is located at $1/3$ of the rotor radius r, which is a good approximation for a three-bladed horizontal wind turbine. If more information about the geometry and the weight distribution of the rotor is known, a more accurate estimation of the inertia can be made by using the following expression [39]:

$$J_\mathrm{t} = \sum_i m_i r_i^2 \tag{2.19}$$

where r_i is the radial distance from the inertia axis to the representative particle of mass m_i and where the summation is taken over all particles of the turbine rotor.

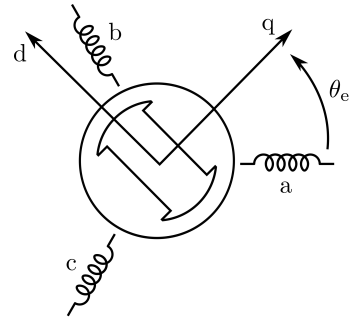

Figure 2.12: Definition of the reference axes in a PMSG.

2.2.2.2 Generator

As already discussed in § 2.2.1, different types of generators are used in variable-speed wind turbines. For doubly-fed induction generator wind turbines (DFIGs), slip-ring induction generators are used in combination with a gearbox. For full-scale converter wind turbines (FSCs), multi-pole wound-rotor and permanent magnet synchronous generators are gaining popularity as they allow a direct-drive system. In this way, the gearbox can be omitted.

In the next paragraph, the model of a permanent magnet synchronous generator (PMSG) is presented as this type of generator is used in this work. However, most of the results in this thesis remain valid for other types of generators as well.

A synchronous reference system is used for the electrical equations of the permanent magnet synchronous generator. This reference system is fixed with respect to the rotor and consists of a direct (d) and quadrature (q) axis, lagging 90 electrical degrees behind the direct axis (see Fig. 2.12). The zero-sequence component is automatically zero as only wye-connected machines without neutral wire are considered. To describe the phase variables (a,b,c) in a dq-reference frame, first the Clarke transformation is used to transform the variables to an equivalent two phase (α,β) system in a fixed stator reference frame:

$$V_\alpha = \frac{2}{3}(V_\mathrm{a} - \frac{1}{2}V_\mathrm{b} - \frac{1}{2}V_\mathrm{c}) \tag{2.20}$$

$$V_\beta = \frac{1}{\sqrt{3}}(V_\mathrm{b} - V_\mathrm{c}) \tag{2.21}$$

Then, the stator reference frame is converted into the synchronous reference system by means of the Park transformation. A rotation over the

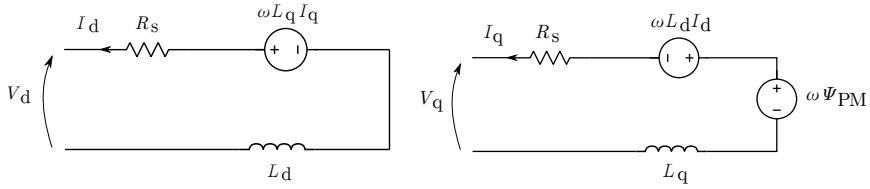

(a) d-axis **(b)** q-axis

Figure 2.13: Equivalent schemes of a PMSG.

electrical angle $\theta_e = N_p \theta_m$ is performed:

$$V_q = V_\alpha \cos\theta_e + V_\beta \sin\theta_e \tag{2.22}$$

$$V_d = -V_\alpha \sin\theta_e + V_\beta \cos\theta_e \tag{2.23}$$

with θ_m the mechanical rotor angle and N_p the number of pole pairs

The electrical stator voltage equations of a PMSG in the synchronous reference system are [40]:

$$V_q = -R_s I_q - L_q \frac{dI_q}{dt} + \omega \Psi_{PM} - \omega L_d I_d \tag{2.24}$$

$$V_d = -R_s I_d - L_d \frac{dI_d}{dt} + \omega L_q I_q \tag{2.25}$$

were R_s is the stator resistance, Ψ_{PM} the permanent magnet flux linkage, ω the electric angular speed given by:

$$\omega = d\theta_e / dt \tag{2.26}$$

and L_d and L_q are the stator inductances along the d- and q-axis. The equivalent schemes of (2.24) and (2.25) are shown in Fig. 2.13.

The electric power P_e produced by the generator can be calculated from the voltages and currents:

$$P_e = \frac{3}{2}(V_q I_q + V_d I_d) \tag{2.27}$$

or, after substituting the voltage equations:

$$P_e = \frac{3}{2} R_s (I_q^2 + I_d^2) + \frac{3}{2}\left(\frac{d}{dt}\left(\frac{L_q I_q^2}{2}\right) + \frac{d}{dt}\left(\frac{L_d I_d^2}{2}\right)\right) + \frac{3}{2}(\omega \Psi_{PM} I_q + \omega (L_d - L_q) I_d I_q) \tag{2.28}$$

The first term in this equation represents the Joule losses in the stator, the second term is the change in energy conserved in the magnetic field and the electromagnetic power P_g is given by the third term:

$$P_g = \frac{3}{2}(\omega\Psi_{PM}I_q + \omega(L_d - L_q)I_dI_q) \tag{2.29}$$

Consequently, the generator torque T_g can be calculated:

$$T_g = \frac{P_g}{\Omega} = \frac{3}{2}N_p(\Psi_{PM}I_q + \omega(L_d - L_q)I_dI_q) \tag{2.30}$$

with Ω the mechanical angular speed ($\omega = N_p\Omega$).

The dynamic behavior of the wind turbine is determined by the equation of motion:

$$J_{wt}\frac{d\Omega}{dt} = T_t - T_g - F\Omega \tag{2.31}$$

with J_{wt} the total inertia of generator (J_g) and turbine (J_t), F the viscous friction and T_t the torque produced by the wind turbine:

$$T_t = \frac{P_t}{\Omega} \tag{2.32}$$

2.2.2.3 Generator-side converter

In order to maximize the energy yield of a wind turbine, variable-speed wind turbines operate at a varying rotational speed Ω. In this way, the power coefficient C_p can be controlled in the MPP for a wide range of wind speeds. Consequently, the voltages and currents that are produced by the generator have a varying amplitude and frequency. This is called 'wild AC', which cannot be injected directly into the electric grid. Therefore, the generator-side converter rectifies the 'wild AC' into DC, which can then be converted to AC currents and voltages with a frequency of 50 Hz by the grid-side converter. Besides converting AC to DC, another important task of the generator-side converter is to control the rotational speed Ω of the wind turbine in order to perform maximum power point tracking.

There exist many different topologies for the generator-side converter. Two common topologies are the passive diode rectifier with a boost chopper and the full active rectifier (see Fig. 2.14).

- The diode rectifier with boost chopper (Fig. 2.14a) consists of a passive diode rectifier which is connected to the three-phase terminals of the generator. The DC-side of the passive rectifier is connected to a capacitor to smooth the rectified voltage. This voltage serves as an input for the boost chopper which consists of a choke inductor, a

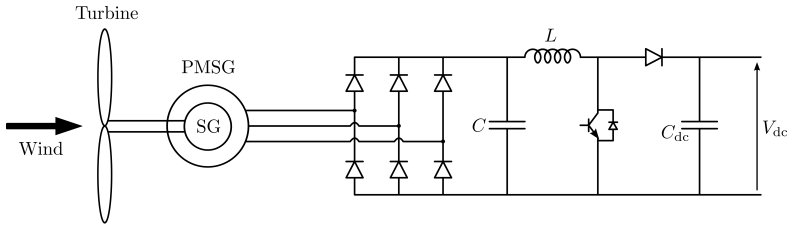

(a) Passive diode rectifier with boost chopper.

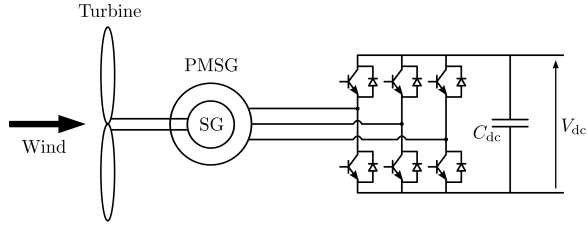

(b) Full active rectifier.

Figure 2.14: Common generator-side converter topologies.

switch (IGBT or MOSFET) and a diode. The boost chopper increases the rectified voltage to the constant DC-bus voltage V_{dc}. The DC-bus consists of a capacitor and the DC-bus voltage is kept constant by the grid-side converter (see § 2.2.2.4).
The only way to control this type of rectifier is by controlling the PWM-controlled switch in the boost chopper. By changing the duty ratio of the switch, the input voltage of the boost chopper can be controlled. This affects the generator currents. For example, when the duty ratio of the boost chopper is increased, the input voltage increases. This results in a smaller voltage drop over the generator impedance and consequently, a lower generator current. A lower generator current also means a lower generator torque and vice versa (see (2.30)). As the generator torque can be controlled, the acceleration or deceleration of the wind turbine can be changed according to (2.31). In this way, the wind turbine can be brought to the MPP, just by changing the duty ratio of the boost chopper.

- The full active rectifier (Fig. 2.14b) consists of six PWM-controlled switches witch convert the three-phase AC to DC. The AC-side is connected directly to the generator terminals, whereas the DC-side is again connected to the DC-bus which has a constant DC-bus voltage V_{dc}. Again, the generator currents can be controlled by properly controlling the switching actions of the active rectifier. A common way

of controlling a full active rectifier is by using field-oriented control. Usually, the current is controlled in the dq-frame by two current controllers. When the current in the d-axis is controlled to zero while the current in the q-axis is controlled to a desired set value, the torque of the generator can be controlled. The desired torque set-point is then obtained from the MPPT algorithm. In order to be able to perform field-oriented control, the mechanical angle θ_{m} should be known. An encoder, resolver or hall-sensor can be used to measure this angle. Also, different estimation techniques exist to estimate this angle. Using a full active rectifier instead of a passive diode rectifier with boost chopper has several advantages, such as a more sinusoidal current, which affects the losses, and the possibility to drive the wind turbine if needed (e.g., to capture wind gusts [41] or start wind turbines with a low starting torque). The higher complexity of the control and higher cost can be mentioned as disadvantages.

By either controlling the duty ratio of the boost chopper switch or the duty ratios of the six switches of the full active rectifier, the generator torque can be controlled. This allows to bring the wind turbine to the maximum power point (MPP). There exist different maximum power point strategies, which try to maximize the energy yield of the wind turbine. In literature, three basic types can be found: tip-speed ratio control, perturb and observe and power control [29]. These types can also be combined to obtain a better performance. The three basic types are discussed below:

- **Tip-speed ratio control (TSR control):** In Fig. 2.11 it can be seen that the maximum power point is obtained for a fixed TSR-value: λ_{opt}. By measuring the rotational speed Ω (e.g., with an encoder, or calculated from the frequency of the generator currents) and the wind speed v, the actual TSR λ can be calculated. The actual TSR is then compared to the optimal one. Both signals are fed into a PI-controller which determines the set-point of the rectifier. This is a simple and effective MPPT algorithm. The main disadvantage is the need for a wind speed measurement, which is often unreliable or inaccurate.

- **Perturb and observe (P&O):** For the perturb and observe method, a step change in the rotor speed is applied by the rotor speed controller. Then, after the transients have died out, the power output of the wind turbine (usually the DC power) is measured and compared with the previous value. If the power output has increased, the next step in the rotor speed will be in the same direction as this means that the wind turbine is going to the MPP. If the power output has decreased, the next step in the rotor speed will be in the opposite

direction. After different steps in the rotor speed, the wind turbine will oscillate around the MPP. The main disadvantage of the P&O algorithm is that it is quite slow as the system has to reach a new steady state after each speed step. Furthermore, the operating point oscillates around the MPP, which is undesired. A smaller speed step size will decrease the oscillations, but also make the control strategy slower.

- **Power control:** A commonly-used MPPT strategy is power control. For every wind speed, the maximum available power is determined by changing the control variable (e.g., the rotor speed Ω or the duty ratio). This maximum power together with the control variable is tabulated as an empiric curve which shows the relationship between the control variable and the maximum power. For example: the maximum power output of a wind turbine in function of the rotational speed can usually be approximated by a cubic curve:

$$P_{\text{mppt}} = K_{\text{mppt}}\Omega^3 \tag{2.33}$$

  By measuring the control variable (in this case the rotational speed Ω) and calculating the corresponding maximum available power, this can be used as a power set point for the wind turbine. In this way, the MPP can be reached.

In conclusion, by connecting the generator to a rectifier, the power output of the wind turbine can be controlled. In normal operation, the wind turbine is controlled into the MPP. However, it is also possible to control the wind turbine in another operating point, for example to provide ancillary services such as frequency control to the power system. This will be explained later.

2.2.2.4 Grid-side converter

In Fig. 2.15, an example of the grid-side inverter is shown. Different topologies are available, but here a PWM-switched inverter with six switches is used. The DC-side of the grid-side converter is connected to the DC-bus. The AC-side is connected to the three-phase grid by means of a filter to mitigate the harmonics caused by the PWM-switching.

In order to be able to inject sinusoidal currents synchronized with the grid voltage, a phase locked loop (PLL) is used. The PLL extracts the fundamental component of the grid voltage and is then scaled with the appropriate set-point value for the current. In this way, a current that is in phase with the grid voltage is injected and only active power is injected by

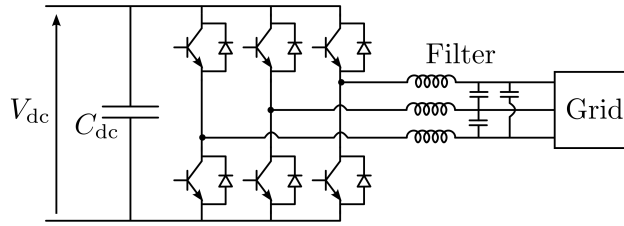

Figure 2.15: Grid-side converter.

the wind turbine. Reactive power can also be injected or consumed by the grid-side converter by injecting current with a certain phase shift compared to the fundamental grid voltage. By controlling the grid-side converter in the *dq* frame, the active and reactive power can be separately controlled by changing the set points for the *d*-axis and *q*-axis currents.

The set point for the current amplitude is determined by the DC-bus voltage controller. The active power that is injected into the DC-bus by the generator-side converter should equal (minus the losses) the power that is injected into the grid. This active power balance is maintained by using the DC-bus voltage V_{dc} as a measure. The DC-bus consists of electrolytic capacitors. When more power is injected in the DC-bus than there is injected in the grid, V_{dc} increases. The grid-side converter is equipped with the DC-bus voltage controller that controls V_{dc} to a certain set value. When the DC-bus voltage start to increase, the set point of the grid current is increased to balance the DC-bus. The opposite holds for a decreasing DC-bus voltage.

In conclusion, the grid-side converter is used to inject the power generated by the wind turbine into the grid. The active power set point of the wind turbine is controlled by the generator-side converter, whereas the grid-side converter injects the appropriate active power into the grid by controlling the DC-bus voltage. By changing the phase shift of the injected currents, reactive power can be injected or consumed by the wind turbine.

2.3 Ancillary services with wind turbines

In the conventional power system, most of the ancillary services are provided by the large, centralized power plants. With increasing penetration of renewable energy sources, however, more ancillary services will have to be provided by distributed generators such as wind turbines and loads. As variable-speed wind turbines have a power-electronic converter to inject the generated power in the grid, they are able to provide different ancillary ser-

vices such as frequency control, voltage control, enhancement of the power quality and even black start. In the next paragraphs, the opportunities to provide several ancillary services with wind turbines are discussed.

2.3.1 Frequency control with wind turbines

In this section, the ability of wind turbines to provide frequency control is discussed.

2.3.1.1 Emulated inertial response with wind turbines

An important difference between frequency control in directly-coupled synchronous generators and variable-speed wind turbines is the inertial response after a frequency disturbance. For directly-coupled synchronous generators, kinetic energy from the rotor inertia is automatically injected into the grid in case of a frequency dip as the rotational speed Ω decreases proportional to the grid frequency f. In case of a frequency rise, all the generators speed up and absorb kinetic energy in their rotor inertia. For variable-speed wind turbines, the rotational speed Ω is decoupled from the grid frequency f. Consequently, variable-speed wind turbines have no automatic stabilizing impact on the grid frequency, unless they are programmed to do so. This is called emulated inertial response. As the emulated inertial response with wind turbines is the main topic of this work, a complete overview is given in Chapter 3. Side-effects of the emulated inertial response are discussed in Chapter 4.

2.3.1.2 Primary frequency control

Primary control with wind turbines is achieved by adding an additional control loop to the wind turbine controller. Similar to the primary controller in a conventional power plant, a droop controller is used in the wind turbines. The reference power for the wind turbine converter is given by [42]:

$$P_{\mathrm{ref}} = P_{\mathrm{ref},0} + K_{\mathrm{prim}} \left(f - f_{\mathrm{nom}} \right) \tag{2.34}$$

When the frequency exceeds the nominal frequency f_{nom}, the power output of the wind turbine is decreased. When the frequency is lower than the nominal frequency f_{nom}, the power output is increased. Decreasing the power output of a wind turbine is always possible. Increasing the power output is much more difficult, as wind turbines are usually operated in their maximum power point. In order to be able to increase the power output of a wind turbine, the turbine has to maintain power reserves at any point in time, so the turbine has to be operated in deloaded mode. This results in a

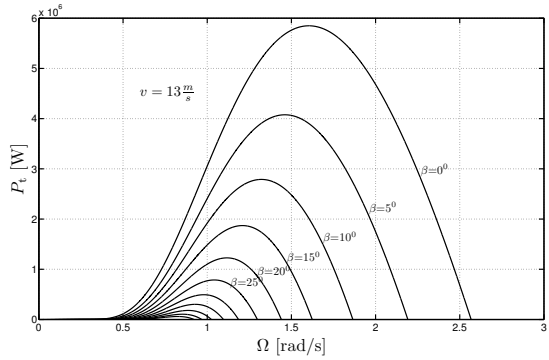

(a) Pitch control.

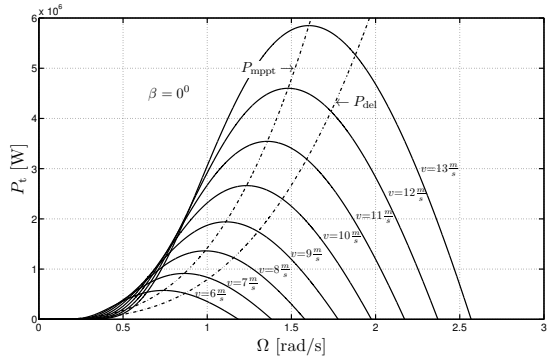

(b) Speed control.

Figure 2.16: Deloaded operation of wind turbines.

lower energy yield, as the turbine is not operating in the maximum power point. Consequently, $P_{\mathrm{ref},0}$ is determined by the MPPT for operation in the MPP or by a deloaded function to provide active power reserves (see Chapter 5). Another option is to add storage to the wind turbine/farm. Two strategies exist to operate a wind turbine in deloaded mode, which will be presented briefly [5, 43].

- **Pitch control:** This control strategy uses the pitch mechanism in wind turbines. Usually, the pitch mechanism is only used to limit the power output of the wind turbine for wind speeds above the rated wind speed. However, pitch control can also be used to obtain a power reserve for the provision of primary control. During normal operation, an increased pitch angle is used to achieve deloaded operation. In this way, the power output of the wind turbine is limited to a value lower than the maximum power output for the given wind speed, see

Fig. 2.16a. The resulting power reserve can be delivered by decreasing the pitch angle so that the turbine can extract more power from the wind in case of a frequency dip.

- **Speed control:** Another way to deload a wind turbine is by means of speed control. From Fig. 2.16b, it is clear that there exists an optimal rotational speed Ω_{opt} for every wind speed. This optimal rotational speed results in the maximum power output for the given speed v. However, if the turbine operates at a lower or higher rotational speed, the power coefficient C_{p} decreases and the power output is lower. The rotational speed Ω of the wind turbine is controlled by means of a power-electronic converter. By using a deloaded reference curve P_{del} for the converter, deloading of the wind turbine is achieved.

2.3.1.3 Secondary and tertiary frequency control

Secondary control could be provided by wind turbines, but accurate predictions of the wind speed are needed. Furthermore, a large amount of energy has to be curtailed to provide upwards power reserves. Contracted tertiary control with wind turbines is less likely, as the time scale of this service is too long to obtain reliable wind speed predictions [44].

2.3.2 Voltage control with wind turbines

Here, voltage control with wind turbines is discussed. First, the reactive power delivery capability of wind turbines is presented. Then, primary and secondary voltage control are summarized. It is important to note that, opposed to frequency control, voltage control is a local issue, so wind turbines could be very effective to tackle voltage issues.

2.3.2.1 Reactive power delivery capability

Especially in medium- and high-voltage grids, reactive capability is an important aspect of voltage control. Fig. 2.17 shows an example of the wind turbine capability for providing reactive power support (the actual values differ for different wind turbines) [45–48]. It can be observed that even in case of zero ($P = 0$ %) or full ($P = 100$ %) power output, the wind turbine is still capable to deliver or absorb reactive power Q. Furthermore, over a large range of active power outputs, the turbine is able to deliver maximum reactive power. It can be concluded that variable-speed wind turbines have a sufficient ability to provide reactive power support. However, although wind turbines have the ability to provide reactive power, the option to provide voltage support is not always activated in the wind turbine control. It

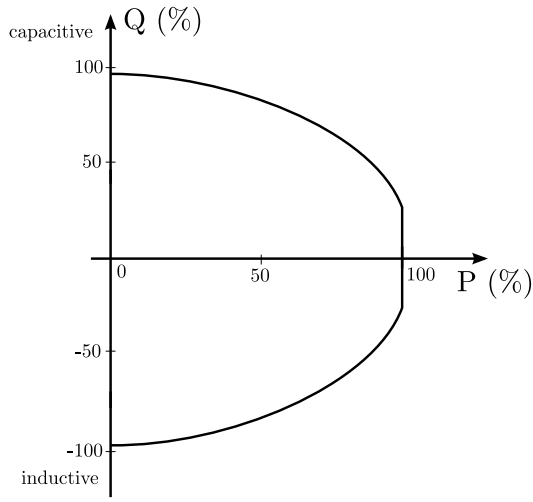

Figure 2.17: Example of wind turbine capability for providing reactive power support (based on [46–48]).

might also be restricted by certain grid code requirements (e.g., constant P/Q, constant V, etc.).

2.3.2.2 Primary voltage control

As already mentioned, primary voltage control is usually achieved by means of a local (droop) controller. Due to the differences between low-, medium- en high-voltage networks, they are discussed separately. Again, high- and low-voltage networks are considered first due to their specific characteristics.

HV networks

Voltage control with wind turbines in HV grids is equal to voltage control with conventional generators. The wind turbines measure the terminal voltage V_{m} and change their reactive power output accordingly. The controller is automatically and fast. The reactive power output is then given by:

$$Q = Q_0 + K_{\mathrm{Q}} \left(V_{\mathrm{nom}} - V_{\mathrm{m}} \right) \tag{2.35}$$

where Q_0 is the nominal reactive output and K_{Q} is determined by the slope of the Q/V characteristic, which depends on the characteristics of the wind turbine (i.e., the reactive power delivery capability). As long as the total output current does not exceed the rated current, the wind turbines are able to provide reactive power and thus voltage support. So voltage control can be regarded as a "free" service. Only if the active power output of the

wind turbines has to be lowered to allow reactive power injection (when the current limits are exceeded), the service is not "free" anymore.

LV networks

Connection of distributed generators (e.g., small wind turbines) to the low-voltage network, will usually result in an increased voltage as active power is injected by these generators. The strong linkage between active power and voltage in resistive networks can lead to voltage problems. To solve the voltage issues, three common strategies are used: network reinforcements, hard curtailment and soft curtailment.

The historical approach to deal with voltage problems is by grid upgrades. However, this is costly and often has a long lead time. A second option is hard curtailment. When the voltage exceeds a certain level, the distributed generator is disconnected from the grid, which is known as on-off control. This leads to a significant loss of revenue, since it is usually not necessary to disconnect the complete unit to solve the voltage problem. Furthermore, it can lead to on-off oscillations, which are detrimental for the power system. The third option is soft curtailment, by means of a P/V droop controller. When the voltage exceeds a certain threshold, the power output of the wind turbine is decreased by either speed or pitch control. If the wind turbine is operating in deloaded mode, it could also assist in voltage control in case of a decreased voltage.

MV networks

Voltage control in MV networks can be considered as a combination of the previous control strategies, since both P and Q injection have an influence on the terminal voltage of the wind turbine. Usually, at first instance, reactive power is controlled to solve the voltage problem. Only if this is not sufficient, the wind turbines are curtailed. Both hard curtailment and soft curtailment (P/V droops) can be used.

A more advanced method is to use a combination of both P/V and Q/V droops to control the voltage [49, 50]. When using both droop controllers, it is key how to coordinate these controllers to avoid unnecessary loss of renewable energy injection, reactive power fines and overly large grid losses.

2.3.2.3 Secondary and tertiary voltage control

Also secondary control is possible with wind turbines, but it is less important. In secondary control, the set points of the Q/V (or P/V) droops of the generators in one zone are changed in order to control the voltage of one pilot node in this zone to a reference value. This is completely analogous to the secondary voltage control in conventional generators. Another option is

to send directly new set points for P and Q to the wind turbines, but this leads to communication delays and decreased robustness of the system [45]. Tertiary control is completely equivalent to the conventional case.

2.3.3 Enhancement of power quality with wind turbines

Different power quality issues can be mitigated by wind turbines, as is summarized in the following.

2.3.3.1 Unbalance mitigation

Wind turbines have the ability to actively mitigate unbalance by using an appropriate control strategy in the power-electronic converter. Instead of injecting a perfectly balanced current into the three-phase system, an unbalanced current is injected to mitigate unbalance [20, 51, 52]. As the injected currents are unbalanced, the power that is injected in the three phases is also unbalanced. At high power outputs, the injected power in one or more phases may exceed the allowed power injection since it is not evenly spread over the three phases. In order to be able to inject the rated power and mitigate unbalance at the same time, the converter should be (slightly) over-dimensioned. This may result in a more expensive converter. However, mitigation of unbalance does not affect the active power generation and can therefore be seen as a 'free' service. The service is only available for sufficient wind speed.

2.3.3.2 Mitigation of waveform distortion

To mitigate waveform distortion, the converter of wind turbines can behave as an active filter (see Fig. 2.18). Instead of injecting perfect sinusoidal currents in the grid, (slightly) distorted current waveforms can be injected to mitigate the harmonics in the grid [53].

2.3.3.3 Flicker mitigation

As flicker is a slow variation of the voltage amplitude, it is usually mitigated by means of reactive power. By controlling the reactive power output of the wind turbines with an additional control loop, flicker in the grid can be mitigated [54, 55]. However, wind turbines are often causing flicker due to the periodical dip in the output power caused by wind shear and tower shadow. To reduce the flicker emission of wind turbines, an additional control loop can be added to the power converter which reduces the variation in the power output by temporarily storing energy in the DC-link [56].

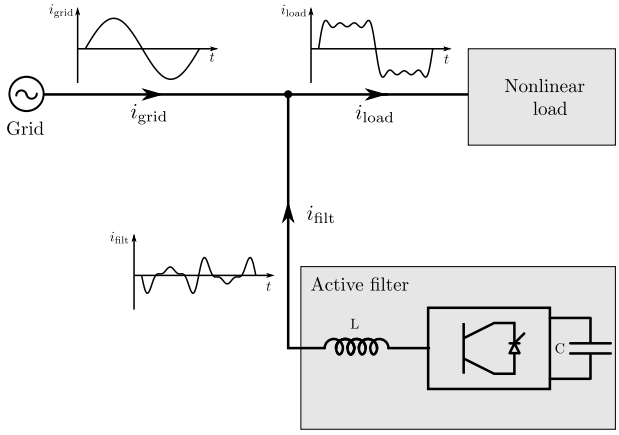

Figure 2.18: Active filter (based on [27]).

2.3.3.4 Mitigation of voltage dips and swells

Considering mitigation of voltage dips and voltage swells, a distinction should be made between quite small voltage variations (both dips and swells) and severe voltage dips. For small voltage variations, converter-connected wind turbines can behave as a Statcom, so they are able to mitigate voltage dips and swells by injection or absorption of reactive power [57, 58]. Both FSC and DFIG wind turbines can inject reactive power, dependent on their ratings [47, 48].

For low voltage ride through, full-scale converter wind turbines are still able to inject reactive power during the fault. Doubly-fed induction generators, on the other hand, are directly connected to the grid via the stator. Severe voltage dips result in large stator and rotor currents which may damage the power converter. Therefore, DFIGs are equipped with a crowbar to protect the power-electronics [29, 59–62]. As a result, usually reactive power is consumed by the wind turbine generator. Proper control strategies, however, may allow a limited injection of reactive power during faults [59–61, 63, 64].

2.3.4 Black start with wind turbines

In order to be able to provide black start capability, the following requirements must be met [5, 65, 66]:

- Need for an independent power source
- Ability to directly control the voltage to a certain set point

- Ability to directly control the frequency to the nominal value

In theory, wind turbines could meet these requirements, as they have an independent power source, which is the wind. Furthermore, they are able to directly control both the voltage level and the frequency by means of their power-electronic converter.

However, there are several problems. Firstly, the black start capability of wind turbines is only guaranteed as long as there is wind. Secondly, a small power source (e.g., battery) is needed to power the converter. Furthermore, wind farms should be considered as the power output of a single wind turbine is too low. Consequently, it is unlikely that wind turbines will provide black start for the complete grid, but they might be part of the start-up sequence. For small, islanded power systems, black start with wind turbines is more likely, but still far from trivial.

2.4 Conclusion

In this chapter, an overview of the different ancillary services that are needed in the power system was presented. It is clear that several ancillary services have to be available to obtain a reliable operation of the electric power system.

Then, a short overview of variable-speed wind turbines was given. The different topologies were discussed and models of the most important parts of a wind turbine were presented.

Finally, the possibilities to provide ancillary services with wind turbines were summarized. In a power system with increasing penetrations of renewable energy sources, participation of these units in the ancillary service market will be needed. Due to the power-electronic interface of the wind turbines, they are perfectly suited to provide a variety of services. In the next chapters, the focus will be on the support of the frequency control with wind turbines, as this is an important service to ensure the safe and reliable operation of the electric power system. First, emulated inertial response with wind turbines is discussed in Chapter 3 and 4. Second, primary frequency control with wind turbines is elaborated in Chapter 5.

3

Optimal emulated inertial response with wind turbines

In this chapter, the provision of inertial response with wind turbines is considered. First, an overview of inertial response in the conventional power system is given. Second, the natural inertial response behavior of different wind turbine types is investigated. Then, methods to emulate inertial response with variable-speed wind turbines are considered. Finally, the optimal parameter selection for the emulation strategies is investigated. In this PhD, a new approach is developed where the influence of the power system composition is considered.

3.1 Inertial response in a conventional power system

3.1.1 Power balance

When the electrical power system is operating in steady state, the total power generation P_{gen} equals the total system load P_{load}:

$$P_{\text{gen}} = P_{\text{load}} \tag{3.1}$$

An unexpected failure of a power plant or a sudden increase or decrease in electrical consumption results in a power imbalance ΔP. This power imbalance is redressed by a change in the kinetic energy E_{kin} of the system:

$$\Delta P = \frac{dE_{\text{kin}}}{dt} = P_{\text{gen}} - P_{\text{load}} \tag{3.2}$$

This kinetic energy E_{kin} is contained in the rotating masses of the generators and motors which are connected to the grid. The total kinetic energy in these rotating masses is given by:

$$E_{\text{kin}} = \frac{1}{2} J \Omega^2 \tag{3.3}$$

where J is the total system inertia and Ω is the speed of the generators. In a conventional power system, most of the generators are synchronous generators (SG) which are directly coupled to the grid. The rotor speed Ω of these generators is strongly linked with the grid frequency f, i.e., f is proportional to Ω:

$$\omega = N_{\text{p}} \Omega \tag{3.4}$$

$$f = \frac{\omega}{2\pi} = \frac{N_{\text{p}} \Omega}{2\pi} \tag{3.5}$$

with N_{p} the pole pair number of the generator and ω the grid pulsation. In this way, eq. (3.2) can be rewritten as:

$$\frac{J 4\pi^2}{N_{\text{p}}^2} f \frac{df}{dt} = P_{\text{gen}} - P_{\text{load}} \tag{3.6}$$

The frequency changes are assumed small relative to the nominal frequency f_{nom}, i.e., $f \approx f_{\text{nom}}$, so the following equation is obtained:

$$J' f_{\text{nom}} \frac{df}{dt} = P_{\text{gen}} - P_{\text{load}} \tag{3.7}$$

Eq. (3.7) implies that a difference between the generated and consumed power results in a change of the rotational speed of the generators and, thus, in a change of the grid frequency f. An electrical frequency change (df/dt) is a measure of a power imbalance in the system.

In electrical power engineering, often the so-called inertia constant H is used instead of the inertia J for a single generator [39, 67]:

$$H = \frac{E_{\text{kin}}}{S} = \frac{J \Omega_{\text{nom}}^2}{2S} \tag{3.8}$$

where S is the nominal apparent power of the generator and Ω_{nom} is the nominal rotational speed of the generator. The inertia constant H has the

dimension of time and is a measure of the time that a rotating generator can provide rated power by only using its kinetic energy. Typical inertia constants for the generators of large power plants are in the range 2-9 s [68]. This results in:

$$\frac{2SH}{\Omega_{\text{nom}}}\frac{d\Omega}{dt} = P_{\text{gen}} - P_{\text{load}} \tag{3.9}$$

The inertia constant of a system comprising generators with different inertia constants H and apparent power S can be calculated easily. Eq.(3.9) may then represent an equivalent of the power system with several synchronously connected machines where the equivalent inertia constant H is calculated as [69]:

$$H = \frac{\sum_{i=1}^{n} S_i H_i}{\sum_{i=1}^{n} S_i} \tag{3.10}$$

where S_n and H_n are the rated apparent power and inertia constant of generator n.

3.1.2 Inertial response and frequency control after a disturbance

In this section, the frequency response in a conventional power system (consisting of directly-coupled synchronous generators) is briefly discussed. As already mentioned, kinetic energy is stored in the rotating masses of all synchronously coupled machines in the power system. If the load in the system suddenly exceeds the generation, a mismatch ΔP arises (with $\Delta P < 0$). This results in a release of the kinetic energy that is transferred as electric energy to the power system. Since the power input of the generators cannot be increased immediately (e.g., due to the slow thermodynamic behavior of the steam turbines), the initial power increase is solely determined by the release of kinetic energy. This is called inertial response. During this process, the generator speed Ω decreases and so does the frequency f. Some seconds after the disturbance, the primary frequency control increases the power input of the generators to limit the frequency deviation Δf from the nominal frequency f_{nom}. An example of the frequency behavior following the loss of 3 GW of generation ($\Delta P < 0$) for a total system load of 93 GW is shown in Fig. 3.1. Immediately after the tripping of 3 GW of generation capacity at $t = 0$ s, the remaining generators naturally increase their power output by releasing the kinetic energy stored in their rotors. The electrical power output is higher than the input power, which forces the generators to slow down. This is between 0 and 6 s in Fig. 3.1. After a short time, the primary control increases the power input of the generators. When the generator power P_{gen} equals the load power P_{load}, the minimum frequency f_{min} is reached (around 6 s in Fig. 3.1). After this point, the generated power

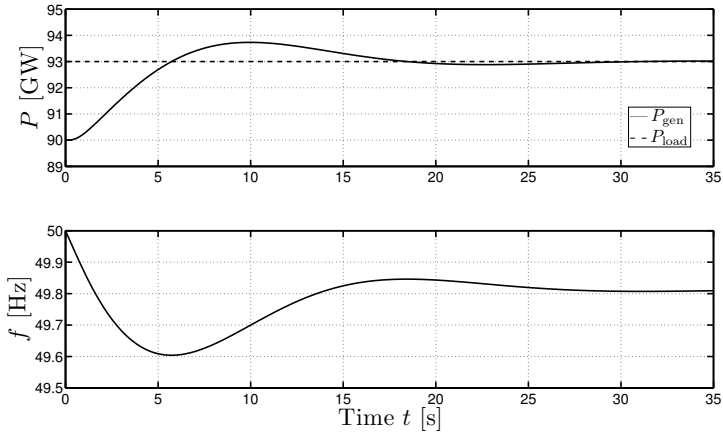

Figure 3.1: Simulation of a loss of generation in a system with frequency control from steam-based generation units.

P_{gen} is higher than the load power P_{load} and part of the kinetic energy in the rotor is restored. Finally, the frequency stabilizes when the generated and consumed power are equal. A stationary frequency error remains (0.2 Hz in this case), which is removed by the secondary control by increasing the set points of the generators. As is explained in § 3.6.1, the exact primary response depends strongly on the type of power plant.

3.1.3 Characterization of the frequency response

In order to compare the frequency response of power systems with different generator compositions, varying wind power penetrations, etc., two metrics are commonly used: the frequency nadir f_{min} and the rate of change of frequency (ROCOF) df/dt.

1. **Frequency nadir:** The frequency nadir is the minimum frequency which is reached after a disturbance. It should be high enough as loads disconnect at low frequencies due to under-frequency load-shedding. The threshold for load-shedding is usually around 49 Hz [10]. When the frequency decreases even further, also generation units disconnect automatically [10].

2. **Rate of change of frequency (ROCOF):** The initial ROCOF determines how fast the frequency changes after a disturbance. It should be low enough to avoid a disconnection of certain generation units or loads.

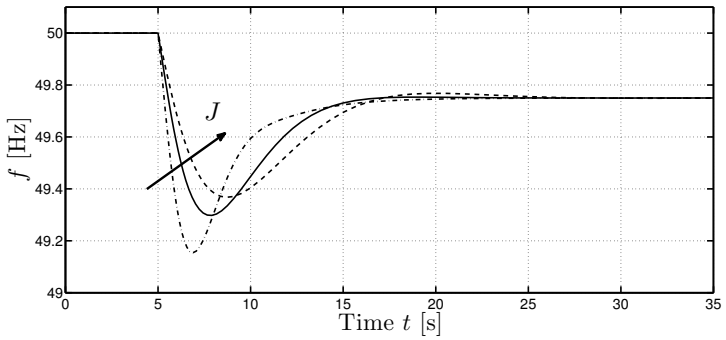

Figure 3.2: Frequency behavior after a loss of generation capacity for different values of the system inertia.

Besides the minimum permissible frequency after an event, there also is a maximum permissible frequency. However, as only under-frequency events are considered in this chapter, this is not needed for the characterization of the frequency response [10]. For the reference incident in the European synchronous area, which is a power deviation of 3 GW, a maximum frequency deviation of 800 mHz is allowed. This results in a minimum instantaneous frequency of 49.2 Hz and a maximum instantaneous frequency of 50.8 Hz. In emergency conditions, the critical negative limit of the system frequency is 47.5 Hz, whereas the critical positive limit equals 52.5 Hz [10].

3.1.4 Influence of the system inertia on the inertial response

In the previous section, it was shown that the initial frequency response after a disturbance is determined mainly by the amount of stored kinetic energy E_{kin} in directly coupled machines. As E_{kin} is given by $\frac{1}{2}J\Omega^2$, the amount of kinetic energy is determined by the total system inertia J for a given grid frequency. In Fig. 3.2, the frequency behavior following a loss of generation is shown for different system inertia values. Higher inertia results in a lower rate of change of frequency (ROCOF) and a higher frequency nadir f_{min}. Due to the improved inertial response at higher inertia, the turbine governors have more time to act and restore the frequency. It can be concluded that the system inertia has to be high enough to ensure a reliable operation of the electrical power system. Therefore, the grid frequency is controlled within certain limits. If the system inertia is too low, the frequency could rapidly fall below this critical limit resulting in the disconnection of certain generation units. This aggravates the already low frequency and would

eventually, in the worst case, result in a blackout. Furthermore, automatic load shedding relays could be triggered if the ROCOF is too high, which results in disconnection of consumers [70]. Therefore, care should be taken to ensure a minimum system inertia at all time.

3.2 Natural inertial response of wind turbines

In this section, the natural inertial response behavior of the different wind turbines types is discussed.

3.2.1 Inertial response behavior of fixed-speed wind turbines

The fixed-speed wind turbines use a squirrel-cage induction generator to generate electricity. Contrary to synchronous generators, induction generators do not rotate at the synchronous speed of the grid, but at a slightly higher rotational speed. The slip s of an induction machine is defined as:

$$s = \frac{\Omega_\mathrm{s} - \Omega_\mathrm{r}}{\Omega_\mathrm{s}} \tag{3.11}$$

where Ω_s is the speed of the stator field, which is the speed of the grid and Ω_r is the speed of the rotor. From (3.11), it can be concluded that the slip s is negative for generators. Due to the slip, the inertial response of induction generators differs from the one obtained with synchronous generators. A simplified induction generator model [71] yields the following relation between slip s and electrical torque T_e (see Fig. 3.3):

$$T_\mathrm{e} = 3N_\mathrm{p}\left(\frac{R_\mathrm{r}}{s\Omega_\mathrm{s}}\right)\frac{V_\mathrm{e}^2}{\left(R_\mathrm{e}+\frac{R_\mathrm{r}}{s}\right)^2 + \left(X_\mathrm{e}+X_\mathrm{r}\right)^2} \tag{3.12}$$

where N_p is the number of pole pairs, V_e, X_e and R_e are the equivalent stator voltage, reactance and resistance and X_r and R_r are the rotor reactance and resistance referred to the stator side. Eq. (3.11) and (3.12) can be used to determine the inertial behavior of a FSIG. During a frequency drop, the frequency f decreases which results in a decreasing speed of the stator field Ω_s. Consequently, the slip s will increase and as a result, the electrical torque T_e will increase according to (3.12). Initially, the turbine torque T_t remains constant, so an increasing electrical torque T_e will cause the rotor speed Ω_r to decrease. Eventually, a new equilibrium ($T_\mathrm{t} = T_\mathrm{e}$) will be reached at a lower rotor speed. This shows that the FSIG exhibits an inertial response as the rotor speed Ω_r follows the grid speed Ω_s while temporarily delivering more electrical power to the grid.

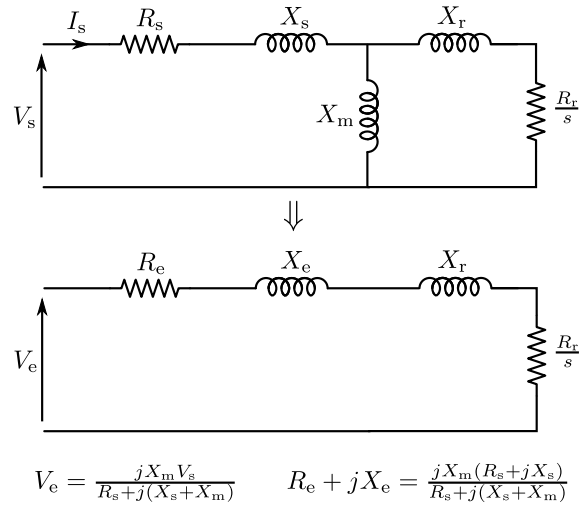

Figure 3.3: Scheme of an induction machine.

The inertial response of fixed-speed induction generators is well-known in literature [72–76]. In [72], field measurements of a wind farm consisting of FSIG turbines show an increase in turbine output during a frequency drop until the protection relays automatically disconnect the wind turbines when the frequency deviation gets too large. The inertial contribution provided by FSIG-based wind farms is revealed to be comparable to that of larger synchronous machines.

In [74], a fifth-order model is used to simulate the inertial response of a FSIG and compare it with the response of a synchronous generator. The synchronous generator produces the maximum inertial response in the shortest period of time. The inertial response of the fixed-speed induction generator wind turbine is lower and slower than the response of a synchronous generator, due to the reduced coupling of the induction generator rotor speed and system speed. Furthermore, a lower inertia constant was used to simulate the FSIG wind turbine, which reduces the maximum power output.

3.2.2 Inertial response behavior of doubly-fed induction generators

When the converter controllers of the DFIG are assumed ideal (infinitely fast), the grid frequency and turbine rotational speed are effectively decoupled. Hence, a change in the grid frequency will not result in a changing rotational speed and a change in the power output of the wind turbine. Consequently, no inertial response is obtained from a DFIG wind turbine.

However, as the current controllers of the converters are not infinitely fast and the stator of the DFIG is directly connected to the grid, a very small inertial response from DFIG wind turbines can usually be noted [73, 74].

In [75], the influence of the current controller on the inertial response of a DFIG system is investigated. A simple PI-controller is used as current controller for the rotor current of the DFIG. This current controller enables the regulation of the electrical torque T_e of the DFIG. The time constant τ of the current control loop can be changed by adjusting the PI-gains. With a time constant τ of 0.1 s (fast controller), almost no change in rotational speed or electrical torque can be noted, showing negligible inertial response of the DFIG. However, a time constant of 5 s (slow controller) results in a change in rotational speed Ω and electrical torque T_e, i.e, an inertial response. However, usually a fast current controller with a high bandwidth is used to obtain good current control capability during normal operation. Very high time constants might even affect the MPPT, which is undesired. Furthermore, compared to an equivalent directly coupled induction generator, the inertial response is significantly lower and slower. Therefore, using a slow controller to achieve an inertial response with a DFIG wind turbine is not the optimal solution.

In [77], it is shown that the control strategy of the DFIG has an influence on the inertial response behavior of the wind turbine. If the stator power P_{st} of the DFIG is controlled, the DFIG is not completely inertialess but provides an inertial response through changes in the rotor power P_{rot}. Consequently, the total power $P_{tot} = P_{st} + P_{rot}$ changes and shows an inertial response to frequency disturbances. On the other hand, when the electrical torque T_e of the DFIG is regulated (under the assumption of constant wind speed: $T_e = T_t = \text{cst}$), the rotor speed Ω_r remains constant. As the total power P_{tot} is given by:

$$P_{tot} = T_e \cdot \Omega_r \tag{3.13}$$

the total power remains constant. Accordingly, no inertial response is obtained when the electrical power T_e is perfectly controlled.

3.2.3 Inertial response behavior of wind turbines with a full-scale converter

Due to the back-to-back converter, the rotational speed of the generator is completely decoupled from the grid frequency. The decoupling is achieved by the separate control of the converters and the buffering effect of the DC-link capacitor. As a consequence of the complete decoupling, no inertial response is obtained with full-scale converter wind turbines [74, 75, 78–80].

Generator type	Inertial response behavior
Conventional synchronous generator	++
Fixed-speed induction generator	+
Doubly-fed induction generator	−
Full-scale converter	− −

Table 3.1: Overview of natural inertial response.

3.2.4 Conclusion

In Table 3.1, an overview of the natural inertial response of a conventional synchronous generator and the different wind turbine technologies is presented. The fixed-speed induction generator shows the best inertial response. An inertial response can be obtained with a DFIG (without adding an additional control loop) by using a very slow current controller. However, in most cases, almost no response can be noted as the current controllers are fast to ensure a correct tracking of the desired reference torque. Full-scale converter wind turbines do not provide any inertial response as rotor speed and grid frequency are completely decoupled.

It can be concluded that the addition of wind turbines to the grid will affect the global inertial response of the power system. As fixed-speed wind turbines are rarely built these days, variable-speed wind turbines with little or no natural inertial response are increasingly being connected to the grid. As long as no conventional power plants are disconnected from the grid, the global inertial response to a disturbance remains the same (same amount of synchronously coupled inertia). However, when conventional power plants are replaced by wind turbines, the global inertial response deteriorates as the amount of synchronously coupled inertia decreases and the conventional wind turbines exhibit no inertial response. This results in a higher rate of change of frequency (ROCOF) df/dt and a lower frequency nadir $f_{\min}$ following a low-frequency event [77,81]. Furthermore, the high ROCOF may induce the tripping of the anti-islanding protection of the wind turbines, which aggravates the problem [74, 82].

3.3 Inertial response enhancement

3.3.1 Capability of wind turbines to enhance the inertial response

Despite the very weak (or sometimes even non-existing) natural inertial response of variable-speed wind turbines, they have a huge potential to

Param.	Value	Unit	Param.	Value	Unit
$P_{\mathrm{t,nom}}$	3.0	MW	r	56	m
M_{b}	11900	kg	Ω_{nom}	1.4451	rad/s

Table 3.2: Wind turbine data for calculation of inertia constant H.

enhance the global inertial response of the power system. As they are grid-connected via a power electronic converter, additional control loops can enhance the inertial response of wind turbines. It may even be possible to obtain a better performance than with conventional directly-coupled synchronous generators. Some of the characteristics of variable-speed wind turbines are listed below to show their huge potential to provide additional inertial response.

3.3.1.1 Inertia constant H of wind turbines

In conventional power plants, the inertial response is solely determined by the rotating inertia of the turbine and generator. The inertia constant H is a measure for the time that a generator can provide rated power by only using the kinetic energy stored in the rotating inertia. Therefore, H can be used to compare the inertial response of directly-coupled generators with a different rotational speed Ω and/or rated power. For conventional generators of large power plants, H is in the range of 2-9 s [67,68]. Typical values for wind turbines have roughly the same value: $H \approx 2-6$ s [39,67,83]. For the wind turbine considered in this work, some parameters are listed in Table 3.2. This gives the following results:

$$J_{\mathrm{t}} = \frac{1}{3} M_{\mathrm{b}} r^2 = 1.24 \cdot 10^7 \text{ kgm}^2$$

$$H = \frac{J_{\mathrm{t}} \Omega_{\mathrm{nom}}^2}{2 P_{\mathrm{t,nom}}} = 4.33 \text{ s}$$

This implies that the total amount of kinetic energy in the system does not necessarily decrease when variable-speed wind turbines are connected to the system. Only an appropriate control loop should be added which is responsible for releasing the stored kinetic energy, since this does not happen naturally.

3.3.1.2 Release of kinetic energy

The release of kinetic energy ΔE_{kin} by the rotating mass of a synchronous generator for a proportional change in grid frequency from f_0 to f_1 is given

by [73, 84]:

$$\Delta E_{\text{kin}} = E_{\text{kin0}} \left(1 - \frac{\Omega_1^2}{\Omega_0^2}\right) = E_{\text{kin0}} \left(1 - \frac{f_1^2}{f_0^2}\right) \tag{3.14}$$

$$E_{\text{kin0}} = \frac{1}{2} J \Omega_0^2 \tag{3.15}$$

From (3.14) is clear that the amount of kinetic energy that is released by a conventional generator is determined by:

1. the total amount of stored kinetic energy E_{kin0} before the disturbance
2. the difference Δf between the pre-disturbance frequency f_0 and the post-disturbance frequency f_1

As conventional generators are directly coupled to the grid, their release of kinetic energy is solely determined by the change in grid frequency Δf, which is very small as the grid frequency is controlled in a very narrow band. So the amount of released kinetic energy cannot be controlled for conventional generators. The rotational speed of variable-speed wind turbines, on the other hand, is completely decoupled from the grid frequency. As the inertia constant H for wind turbines and conventional generators is very similar, the relative amount of stored kinetic energy E_{kin0} is more or less the same for both technologies. However, the change of rotational speed $\Delta\Omega = \Omega_0 - \Omega_1$ can be controlled by the power electronic converter. Consequently, for a broad range of operating points, $\Delta\Omega$ can be regulated to be larger than for conventional generators, which results in a higher release of kinetic energy by the wind turbine (relative to the rated power of the wind turbine) [80, 81]. However, as is explained later, it is important to inject the right amount of kinetic energy rather than as much as possible. Injecting too much energy might lead to a fast depletion of the kinetic energy in the rotor of the wind turbine and an even worse inertial response than without the emulated inertia as is shown in § 3.6 and § 3.7.

3.3.1.3 Fast power control

As variable-speed wind turbines use a power electronic converter, the power output can be increased or decreased almost immediately, whereas the power control of conventional units is much slower. The fast control of the power output makes it possible to emulate the inertial response of a conventional generator or to provide an even faster response. Furthermore, the power output can be controlled to almost any given value (at least within the converter and mechanical limits and for a limited period of time). This enables the improvement of the global inertial response.

3.3.1.4 Conclusion

It can be concluded that wind turbines have huge potential to provide inertial response. To obtain the desired inertial response, an additional control loop has to be added to the existing wind turbine controller. In this way, a similar or even better performance could be obtained with wind turbines.

3.3.2 Introduction to synthetic inertia and temporary power surge

In the following sections, a distinction is made between synthetic inertia and temporary power surges. Synthetic inertia is the general term for all strategies that emulate the inertial behavior of a directly coupled synchronous generator. The main characteristic of this strategy is that the initial frequency response is altered as a synthetic or emulated inertia is added to the power system. Especially the ROCOF is enhanced by this control strategy. The name temporary power surge is used for all other strategies that try to enhance the frequency response on a short time, but without mimicking the behavior of a synchronous generator. These strategies usually tend to improve the frequency nadir, while the improvement of the ROCOF depends strongly on the strategy of interest.

Both strategies are temporarily, i.e, they tend to improve the initial frequency response after a disturbance (e.g. ≈ 30 s). Thereafter, the wind turbines resume normal operation. Frequency response on larger time scales, such as primary, secondary or even tertiary control are not considered in this chapter.

3.4 Synthetic inertia

3.4.1 Overview of the control strategy

3.4.1.1 Inertial control loop

The synthetic inertia (SI) strategy mimics the natural inertial response behavior of a directly-coupled synchronous generator [39,67,69,73,77]. In case of a frequency disturbance, kinetic energy is extracted from (or absorbed in) the rotor of the synchronous generator:

$$P_{\text{in,SG}} = \frac{dE_{\text{kin}}}{dt} = J\Omega_{\text{SG}}\frac{d\Omega_{\text{SG}}}{dt} \tag{3.16}$$

with Ω_{SG} the rotational speed of the synchronous machine, which is proportional to the grid frequency f. Eq. (3.16) clearly shows the natural increase in output power of a synchronous generator following a frequency

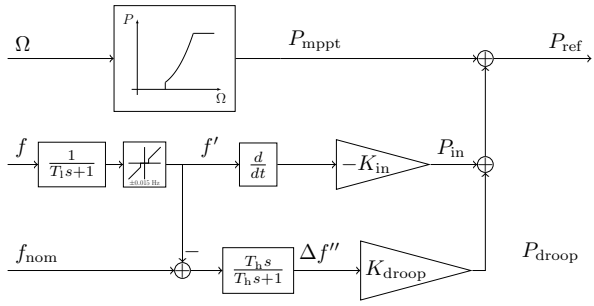

Figure 3.4: Control loop of the synthetic inertia strategy.

dip. The additional power output is extracted from the rotating inertia of the generator.

A similar response can be obtained from wind turbines by adding an extra control loop to the wind turbine controller. The complete control scheme is presented in Fig. 3.4. In normal operation, the power reference P_{ref} for the power converter is determined by the maximum power point tracker (MPPT), which is given by P_{mppt}. This ensures that the wind turbine is operating close to its maximum power point to increase the energy yield. During a frequency disturbance, an inertial response value P_{in} is added to P_{mppt} and is given by:

$$P_{\mathrm{in}} = -K_{\mathrm{in}} \frac{df'}{dt} \tag{3.17}$$

According to (3.17), when the frequency decreases, the reference power P_{ref} of the turbine is increased with P_{in}, slowing down the turbine and extracting kinetic energy from the rotor. In this way, the power output of the turbine is temporarily increased and an inertial response from the wind turbine is obtained.

In order to calculate P_{in}, the grid frequency f has to be measured and filtered by means of a low-pass filter to reject measurement noise. As the derivative of the frequency is used to calculate P_{in}, adequate filtering is needed. Differentiation of a noisy signal may lead to large variations in the value of P_{in}, which is undesired as it may cause heavy torque pulsations in the drive-train of the wind turbine. Therefore, a low-pass filter is added to filter the measured frequency f [39, 69, 73, 80, 85]:

$$f' = \frac{1}{T_{\mathrm{l}}s + 1} f \tag{3.18}$$

Here, a first-order low-pass filter with time constant T_{l} is used. The cut-off frequency of the filter can be adjusted by changing T_{l} to obtain the desired

amount of filtering. Due to the filter, a delay arises between the measured frequency and the filtered frequency [39]. A high cut-off frequency results in less filtering and less delay and vice versa. The filter delay results in a slower reaction of the inertial controller, so the ROCOF will be higher. Heavy filtering (low cut-off frequency and high T_l) results in higher delays and a higher ROCOF. A proper tuning of the filter is important to avoid deterioration of the emulated inertial response. Using higher order filters may reduce the delay and therefore enhance the inertial response.

The major advantage of the addition of a filter is the reduction of oscillations in the set-point, which enhances the stability and reliability of the wind turbine. Also, excessive wear caused by these oscillations is avoided.

Furthermore, a small dead band (± 0.015 Hz) is used to avoid the reaction of the synthetic inertia strategy on very small frequency variations during normal operation of the power system.

3.4.1.2 Droop control loop

When the inertial control loop is added to the wind turbine, interaction with the maximum power point tracker arises during a frequency event [69, 78]. If the frequency drops, the inertial control loop increases the reference value with P_{in}, resulting in a decreasing rotor speed. The MPPT, however, tries to maintain operation at the MPP by decreasing its reference value P_{mppt}. This behavior of the MPPT counteracts the desired increase in output power. This results in a lower inertial response of the wind turbine than expected.

Two solutions are available [39, 67, 69, 86]:

1. the reference value P_{mppt} is kept constant during inertial response
2. a droop controller is added to allow suboptimal operation

The first possibility is to hold the value from the maximum power point tracker constant when a frequency disturbance is detected. As the MPPT is deactivated, the inertial response will be larger. When the disturbance is over or when the wind turbine has reached its minimum speed limit Ω_{min}, the operation point of the wind turbine has to be gradually shifted back to the normal operation, where the operation point is determined by the MPPT. Care should be taken when reactivating the maximum power point tracker to avoid stability problems [86]. Therefore, this control method is not used in this work.

In the second option, the maximum power point tracker is kept active during a frequency event. This is beneficial, as it stabilizes the operation of the wind turbine by reducing the deceleration of the rotor. In this way, stalling of the turbine is prevented [77, 78] and stability problems are

avoided. However, to improve the inertial response, a droop controller is often added [39, 67]. The droop term P_{droop}, which is proportional to the frequency deviation $\Delta f''$ from its nominal value f_{nom}, is added to the reference value:

$$P_{\text{droop}} = K_{\text{droop}} \Delta f'' = K_{\text{droop}} \left(\frac{T_{\text{h}} s}{T_{\text{h}} s + 1} \left(f_{\text{nom}} - f' \right) \right) \tag{3.19}$$

where T_{h} is the time constant of the high-pass filter that prevents a steady state contribution of the droop controller (see further). This droop controller has two functions:

1. To counteract the control action of the MPPT, which tries to bring the wind turbine back in its maximum power point (MPP). This would decrease the inertial response in case of a disturbance.

2. To limit the frequency deviation by increasing the power output of the wind turbine proportional to the frequency deviation.

After the inertial response, the wind turbine should recover to the pre-disturbance operating point. Consequently, the overproduction period during the inertial response should be followed by an underproduction or recovery period. To allow a recovery of the wind turbine, a high-pass filter, which prevents a contribution of the droop controller in steady state, is added:

$$\lim_{t \to \infty} P_{\text{droop}}(t) = \lim_{s \to 0} s P_{\text{droop}}(s) = \lim_{s \to 0} s \frac{T_{\text{h}} s \cdot \Delta F(s)}{T_{\text{h}} s + 1} = 0 \tag{3.20}$$

where $P_{\text{droop}}(s)$ and $\Delta F(s)$ are the Laplace transforms of $P_{\text{droop}}(t)$ and Δf respectively. The time constant T_{h} of the high-pass filter should be tuned properly in order to obtain the desired result: ignoring the steady-state frequency deviation after the inertial response while passing the rapid frequency variations during the first seconds of the inertial response. Two things should be taken into account when tuning the time constant T_{h}:

1. T_{h} should not be too low, to avoid elimination of the rapid frequency variations during the first seconds after the disturbance by the high-pass filter. This would seriously reduce the emulated inertial response of the wind turbine. The simulations show that values above 20 s for T_{h} do not filter out the fast frequency variations.

2. T_{h} should not be too high either, as this would result in an overly-long recovery period. This causes undesired energy yield losses as the wind turbine operates too long below the maximum power point.

3.4.1.3 Complete control loop

The complete reference power P_{ref} is therefore given by [87]:

$$P_{\text{ref}} = P_{\text{mppt}} - K_{\text{in}} \frac{df'}{dt} + K_{\text{droop}} \Delta f'' \tag{3.21}$$

This reference power is tracked very fast by the power-electronic converter, hence, no pitch control actions are needed. The pitch controller is too slow to track the fast power set-point variations of the synthetic inertia strategy.

3.4.2 Operating conditions of the synthetic inertia strategy

Until now, it was assumed that the wind turbines are able to follow the desired set-point. However, the ability to provide inertial response with the synthetic inertia strategy depends on the type of disturbance, the control strategy of the wind turbine, the operating point and the parameter selection, as is discussed in the next paragraphs.

3.4.2.1 Influence of the frequency disturbance

Considering the frequency f, there are mainly two distinct types of disturbances:

1. **over-frequency:** f exceeds the nominal frequency f_{nom}
2. **under-frequency:** f is lower than the nominal frequency f_{nom}

As discussed in § 2.3.1, decreasing the power output of a wind turbine in case of an over-frequency event is relatively easy by either pitching the blades or controlling the rotational speed Ω (see Fig. 2.16). For the inertial response, usually speed control is used as the pitching mechanism is too slow. Furthermore, for speed control, kinetic energy is automatically stored in the rotor inertia J_{t} of the wind turbine. From Fig. 3.5, it is clear that the power output can be lowered easily by means of speed control. A lower reference power P_{ref} is applied to the converter. As the power input from the wind P_{t} is then higher than the power output determined by P_{ref}, the rotor speed Ω increases. This causes a decrease in power input P_{t} until a stable operating point is reached. Due to the increased rotational speed Ω, kinetic energy E_{kin} is indeed stored in the rotor inertia J_{t}. Consequently, inertial response (and primary frequency control) in case of over-frequency events can be provided easily by wind turbines.

Under-frequency events, however, require an increase of the power output of the wind turbine. This is much more difficult as wind turbines are

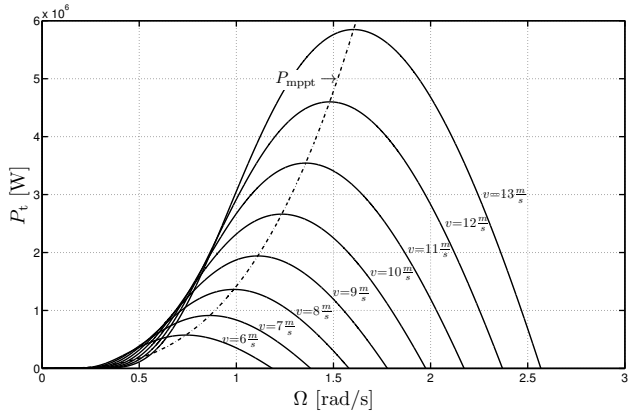

Figure 3.5: Operation in the maximum power point.

usually already injecting the maximum available power. Unlike conventional generators, they cannot increase their power input by changing the fuel consumption, as wind is their primary energy source. Therefore, in the remainder of this chapter, only under-frequency events are discussed as these are the challenging events concerning the inertial response with wind turbines.

3.4.2.2 Influence of the control strategy

The control strategy of the wind turbine, which determines the reference value P_{ref} under normal operating conditions, has an influence on the inertial response behavior. In general, two distinct control methodologies can be used in wind turbines under normal operating conditions:

1. operation in the maximum power point: $P_{\mathrm{ref}} = P_{\mathrm{mppt}}$
2. operation in deloaded mode: $P_{\mathrm{ref}} = P_{\mathrm{del}}$

First, operation in the maximum power point is discussed. This strategy is used in most wind turbines to maximize the energy yield. From Fig. 3.5, it is clear that there exists an optimal rotor speed where the power input from the wind is maximal. In variable-speed wind turbines, the converter controls the current of the generator to enable operation in the maximum power point (MPP).

However, when an additional control loop is added to emulate inertia, the power output should increase in case of a frequency dip. Since the wind turbine is operating in the maximum power point, the power input from the wind cannot further increase. To obtain an increase in the power output,

kinetic energy is extracted from the rotor, which causes the turbine to slow down. Furthermore, as the rotor speed is decreasing, the wind turbine leaves the maximum power point, which results in a lower power input from the wind. When the turbine has finished the inertial support, it is operating in a suboptimal operating point at a lower speed. In order to resume normal operation, the wind turbine needs to reduce its power output for some time to allow for the acceleration of the rotor.

In Fig. 3.6, the inertial behavior is shown. From 0 to 5 s, the wind turbine is operating in the maximum power point. Suddenly, at 5 s, another power plant is disconnected from the system, which results in a lower power output from the generators P_{gen} and consequently a frequency drop. The inertial control loop from the wind turbine increases the power output from the wind turbine above the available wind power by extracting kinetic energy from the rotor from 5 to 8 s. Since the power output is higher than the available wind power, the turbine slows down from 5 to 8 s. After 8 s, the power output from the turbine decreases below the maximum available wind power, hence, the recovery period has started. The wind turbine accelerates to resume normal operation. During the inertial response, it can be seen that the wind power P_{t} slightly decreases due to the suboptimal operation during the inertial response.

With the addition of the inertia controller, the inertial response is almost the same as if no conventional generators were replaced by wind turbines. The period of reduced power output to allow the acceleration of the rotor is clearly visible. This recovery period where less power is injected in the grid is the only difference with the inertial response of conventional generators. These generators omit this period by increasing the power input of their steam or gas turbines.

Second, the operation in deloaded mode is presented. Instead of operating in the maximum power point to maximize the energy yield, wind turbines could also be operated in deloaded mode. In deloaded mode, the wind turbines operate in a suboptimal operating point to maintain a power reserve at any point in time. This power reserve can be used to participate in frequency control and inertial response [88–90]. As a consequence, the energy yield of the wind turbine is reduced, since the wind turbine is continuously operating at a lower power point [82, 86]. It is a design decision to chose for operation in the maximum power point without power reserves or to operate at a lower power point with power reserves.

In Fig. 2.16, the two control strategies to obtain deloaded operation were already presented: speed control and pitch control [5]. For speed control, the reduced power output is obtained by operating the turbine at a higher rotational speed than the optimal speed. The greatest advantage of speed

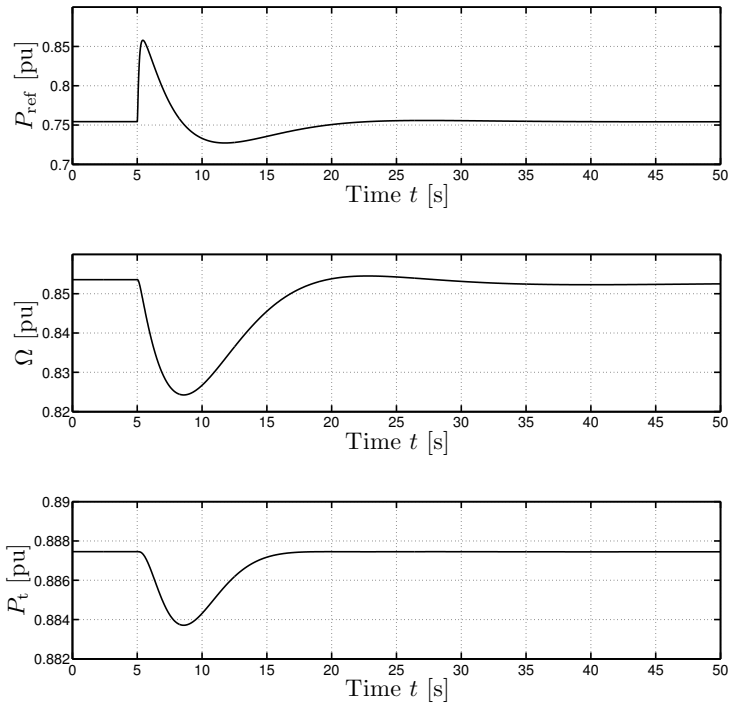

Figure 3.6: Example of the synthetic inertia for operation in the MPP.

control is the speed of this control strategy as it is obtained by the converter controller. Furthermore, in case of a frequency dip, kinetic energy can be released immediately, since the turbine is operating at a higher speed. As the rotor speed is decreasing, the power input is increasing, which is beneficial to provide inertial response and frequency control. However, it is difficult to obtain reliable speed control if the $C_{\mathrm{p}}(\lambda)$-curve is not known.

Pitch control makes use of the pitch mechanism in wind turbines. If the pitch angle of the turbine blades is increased, the captured wind power is decreased. Using a non-zero pitch angle in normal operation results in deloaded operation. To track the maximum of the deloaded curve, an optimal speed controller can be used. The simplicity of this control strategy is its main advantage: the optimal speed controller can still be used, only the blades have to be pitched. However, this strategy is slow as it relies on the mechanical pitch mechanism. Therefore, this control strategy is less suitable for inertial response.

By operating the wind turbines below their MPP, their inertial response behavior is completely equivalent to the one of conventional generators. No

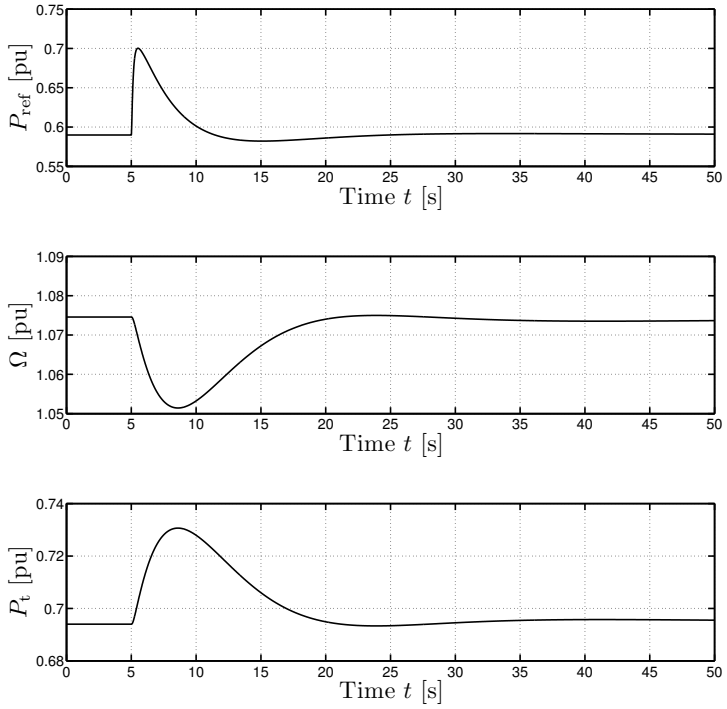

Figure 3.7: Example of the synthetic inertia for operation below the MPP.

recovery period is needed after the inertial response as a power reserve is available to increase the power output of the wind turbine. This is shown in Fig. 3.7 for speed control by means of over-speeding (cfr. the higher rotational speed Ω in Fig 3.7 compared to Fig. 3.6). Similar to the synthetic inertia with operation in the MPP, the power output of the wind turbine is increased immediately after the disturbance by injecting kinetic energy in the grid. This causes the wind turbine to slow down, as can be seen in the rotational speed Ω. However, contrary to the operation in the MPP, due to the decreasing rotational speed Ω, the wind turbine power P_{t} starts to increase as the wind turbine operates closer to the MPP. As the power input P_{t} increases during the inertial response, almost no recovery period is needed to regain normal operation.

As operation in the MPP is the most challenging concerning the provision of emulated inertial response and no continuous energy yield losses are needed to apply this strategy to wind turbines, only maximum power point tracking will be considered in the remainder of this chapter.

3.4.2.3 Influence of the operating point

When providing emulated inertial response, it is important to consider the influence of the operating point of the wind turbine. The operating range of a wind turbine is confined within some limits. There are lower and higher rotor speed limits $\Omega_{\min}$ and $\Omega_{\max}$ to prevent stalling of the turbine and avoid excessive wear. Furthermore, current, voltage and power ratings of the generator and converter have to be respected [79, 80, 82]. At high wind speeds, for example, the power input from the wind is curtailed by pitching the wind turbine blades.

In the following, only non-deloaded wind turbines are considered. Three distinct cases can be considered [79]:

1. low wind speed
2. medium wind speed
3. high wind speed (above the nominal wind speed)

In low wind speed conditions, the wind turbine is operating near the lower speed limit $\Omega_{\min}$. Only a limited amount of kinetic energy E_{kin} can be extracted from the rotor, which results in a reduced inertial response. When the wind turbines are equipped with the synthetic inertia strategy, their power output is altered by the wind turbine control to respect the lower speed limit $\Omega_{\min}$.

For medium wind speeds, the turbine is operating well above the lower speed limit $\Omega_{\min}$, but the power input from the wind is not curtailed by the pitch control, so the wind turbine operates below rated power. In this region, a normal inertial response is obtained from the wind turbines, as enough kinetic energy can be extracted from the rotor. The period of overproduction is then followed by a recovery period of underproduction to resume normal operation.

For wind speeds above the nominal wind speed, the pitch control is activated to limit the captured wind energy. Again, a normal inertial response can be expected, but only if the generator and converter ratings allow a short overproduction. Since the turbine was already operating at the maximum power, the emulated inertial response action would result in an even higher power output. The ratings of the generator and turbine will then determine which inertial response is obtained. Usually, over-currents of about 1.1 pu are allowed, which suffices for the optimal inertial response [87]. After the frequency event, normally no recovery period is needed, since the captured wind power can be increased by decreasing the pitch angle to accelerate the rotor. However, the design limits of the turbine should be respected when increasing the captured wind power. If the captured wind power may not

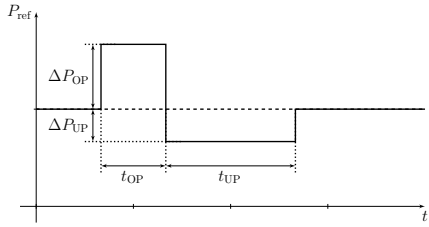

Figure 3.8: Example of a predefined power reference curve.

be increased enough, again, a (smaller) recovery period is needed to resume normal operation.

3.4.2.4 Choice of the control parameters

In the reference power P_{ref} there are two parameters that have to be chosen correctly: K_{in} and K_{droop}:

$$P_{\mathrm{ref}} = P_{\mathrm{mppt}} - K_{\mathrm{in}} \frac{df'}{dt} + K_{\mathrm{droop}} \Delta f' \tag{3.22}$$

The optimal combination depends strongly on the composition of the power system. Therefore, the optimal parameter selection for the synthetic inertia strategy is investigated thoroughly in § 3.6.

3.5 Temporary power surge

The temporary power surge (PS) strategy can be divided into different categories. The general operating principle of this strategy, however, is the same for the different categories. Therefore, the general behavior of this control strategy is explained first. Then, the different implementations of the strategy in the overproduction and underproduction periods of the wind turbine are explained.

3.5.1 General control strategy

In the synthetic inertia strategy, the increase in power output is proportional to the rate of change of the grid frequency df/dt and to the deviation of the grid frequency from the nominal value Δf. There, the shape of the additional power output is determined by the shape of the grid frequency, which is not the case for the temporary power surge strategy. Here, the shape of the increase in power output is determined by a predefined power reference curve, as shown in Fig. 3.8.

When a frequency dip is detected, e.g. the frequency falls below a certain threshold, the power output of the wind turbine is increased with an overproduction step ΔP_{OP} for a certain overproduction time t_{OP}. During this overproduction period, the wind turbine injects more power in the grid than there is available in the wind. Consequently, the wind turbine slows down while injecting kinetic energy E_{kin} from the rotor in the grid. To allow for a recovery of the wind turbine after the inertial response has finished, the overproduction period is followed by an underproduction period t_{UP} where the power output is decreased with ΔP_{UP} below the initial value. During the underproduction period, the turbine re-accelerates to the initial operational point before the disturbance. The duration of the underproduction period depends on both the overproduction period and the choice of the recovery strategy during the recovery period. Similar to the synthetic inertia strategy, no pitch control actions are needed during the inertial response.

As discussed in § 3.4.2.1 for the synthetic inertia, under-frequency events are the most challenging events for the emulated inertial response with wind turbines. The same holds for the temporary power surge, where the power output can be easily lowered according to a predefined reference curve. Therefore, also for the temporary power surge, only frequency dips will be considered in the remainder of this work.

In literature, different options for the power reference curve during the overproduction and underproduction period are available, which are discussed in the following paragraphs.

3.5.2 Overproduction period

For the overproduction period, there are two options for calculating the resulting output power reference P_{ref} for the wind turbine [69]. The first option is to add the desired power increase ΔP_{OP} to the reference value obtained by the maximum power point tracker P_{mppt}. The MPPT is kept active during the inertial response, which results in a decreasing reference value P_{mppt} due to the decrease in rotational speed Ω. This is shown in Fig. 3.9a. The other option is to calculate the power reference P_{ref} as the sum of the pre-disturbance reference value $P_{\mathrm{ref},0}$ and the desired power increase ΔP_{OP}, which is illustrated in Fig. 3.9b. In this way, the decrease in the power reference of the MPPT P_{mppt} (dashed) is excluded from the controller and the power reference P_{ref} is constant during the overproduction period. It can be noted that in case of the constant reference value (Fig. 3.9b), the total released energy during the overproduction period is larger. Consequently, the rotor speed is further decreased and the recovery time will be longer compared to the strategy with the activated maximum power point tracker. In literature, usually the power surge with constant

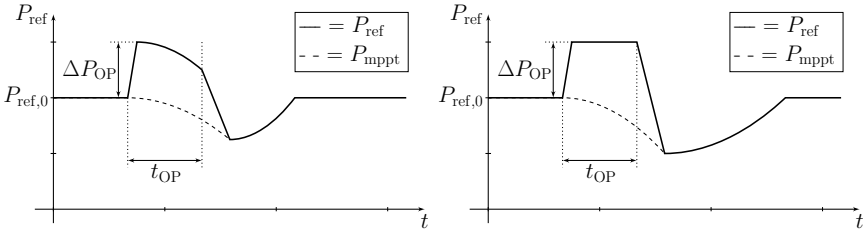

(a) P_{ref} depends on P_{mppt}. **(b)** Constant P_{ref}.

Figure 3.9: Control strategies during the overproduction period.

reference value is used [69, 91–95].

The overproduction period is triggered by a dip in the grid frequency. Usually, the temporary power surge is activated when the frequency falls below a certain threshold (frequency dead-band). This threshold should be low enough to prevent an activation of the temporary frequency support for small frequency variations during the normal operation of the power system. However, the threshold should not be too low either to ensure a proper functioning of the frequency support.

3.5.3 Underproduction period

There are three different strategies to obtain the power reference P_{ref} value during the underproduction period. These methods are summarized in Fig. 3.10. The first underproduction strategy is the optimal speed strategy (Fig. 3.10a) [69]. When the overproduction period t_{OP} has ended, the reference value is again determined by the MMPT. As can be seen in Fig. 3.5, the maximum power point tracker results in a reference value P_{ref} which is much lower than the available wind power P_{t} when the turbine is operating at a reduced rotational speed $\Omega < \Omega_{\text{opt}}$. Consequently, the turbine will re-accelerate to the initial speed and regain normal operation. The initial underproduction step ΔP_{UP} and underproduction time t_{UP} depend on the operating point of the wind turbine after the overproduction period. If more energy is extracted from the wind turbine during the overproduction period, the initial underproduction step ΔP_{UP} will be larger and the underproduction time t_{UP} will be longer. Both parameters are determined by the maximum power point tracker and can, therefore, not be altered manually.

The second option is the constant underproduction strategy (Fig. 3.10b) [95]. After the overproduction period, the power output is decreased with a value ΔP_{UP} under the pre-disturbance value $P_{\text{ref,0}}$. The duration of the underproduction period t_{UP} is determined by the equal area condition:

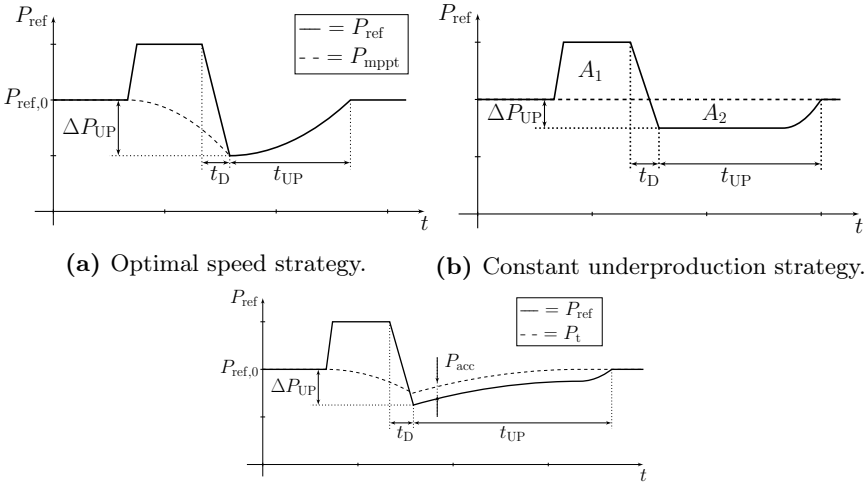

(a) Optimal speed strategy.

(b) Constant underproduction strategy.

(c) Constant accelerating power (P_{acc}) strategy.

Figure 3.10: Power reference curves during the underproduction period.

$A_1 \approx A_2$. The area A_1 in Fig. 3.10b is approximately equal to the excess energy injection of the wind turbine during the overproduction period. Area A_2 is roughly the energy deficit during the underproduction period. Small differences exist due to the suboptimal operation during the temporary frequency support. These energy yield losses are discussed in Chapter 4. Consequently, the excess energy injection will be higher than A_1, whereas the energy deficit will be lower than A_2, but the differences are quite small. Therefore, the equal area condition could be used to dimension the parameters ΔP_{UP} and t_{UP}. A low underproduction step ΔP_{UP} results in a longer underproduction period t_{UP} and vice versa. When the reference value P_{ref} equals the maximum power point tracking reference value P_{mppt}, the output is again determined by the MPPT.

In Fig. 3.10c, the third option, i.e., the constant accelerating power strategy, is illustrated [91, 94]. After the overproduction period t_{OP}, the reference value P_{ref} is reduced with ΔP_{UP} below the initial reference value $P_{\text{ref,0}}$. In this way, the reference value P_{ref} is lower than the available wind power P_{t} and the difference is the accelerating power P_{acc}:

$$P_{\text{acc}} = P_{\text{t}} - P_{\text{ref}} \tag{3.23}$$

Usually, the accelerating power P_{acc} is kept constant during the acceleration of the wind turbine. However, a varying accelerating power P_{acc} can also be used [91]. As the output power is below the available wind power, the wind

turbine recovers to the maximum power point. After the recovery, the power set point P_{ref} is again determined by the maximum power point tracker. The duration of the underproduction period can be altered by changing P_{acc}. To use this strategy, knowledge of the wind speed (measurement or estimation) is needed to determine P_{t}, which is a disadvantage of this strategy.

For all the recovery strategies, the power output is not immediately decreased after the overproduction period, but the reference value slowly decreases during a time t_{D} to allow a smoother transition from overproduction period to underproduction period. If this transition period is not used, there is a higher risk on a second, undesired frequency dip.

3.5.4 Choice of the control parameters and recovery period

Similar to the synthetic inertia strategy, the control parameters ΔP_{OP}, ΔP_{UP}, t_{UP} and t_{OP} have to be tuned properly to obtain the desired response in function of the system composition. Furthermore, the choice of the recovery period also has an important impact on the inertial response behavior. The optimal parameter selection for the temporary power surge strategy is discussed in § 3.7.

3.6 Optimal parameter selection for the synthetic inertia strategy

When using the synthetic inertia strategy, it is important to tune the parameters K_{in} and K_{droop} properly, otherwise it may result in a poor emulated inertial response from the wind turbine. If K_{in} is chosen too high, this may lead to an oscillatory response behavior of the synthetic inertia strategy. A slow reaction of the conventional generators can arise when the droop constant K_{droop} is too high. Conversely, low values for K_{in} and K_{droop} give a low inertial response, which may result in a very poor frequency response after a disturbance. Poor parameter tuning may result in a frequency response that is worse compared to the case without synthetic inertia or even without wind turbines at all. On the other hand, there exists an optimal combination of K_{in} and K_{droop} which results in the highest frequency nadir after the disturbance. Another combination of both parameters results in the lowest rate of change of frequency (ROCOF). As is shown further in the simulations, the highest frequency nadir is usually achieved for low values of K_{in}, whereas the lowest ROCOF is obtained for high values of K_{in} and K_{droop}. Therefore, often a trade-off has to be made to obtain the best emulated inertial response. Furthermore, the operational limits of the wind

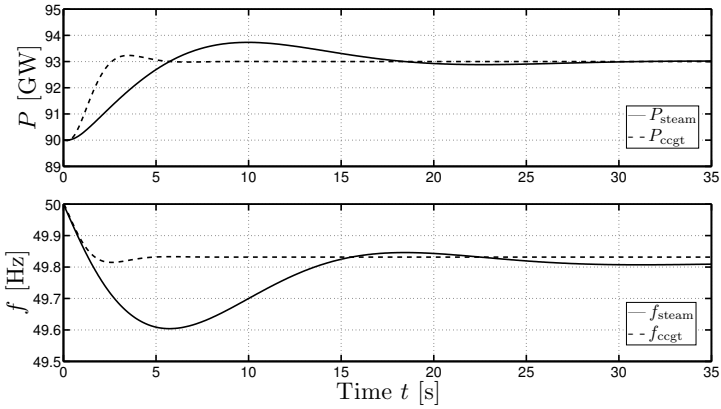

Figure 3.11: Influence of the power plant type on the system frequency response.

turbine, such as the current limit and the rotational speed control range, are considered by limiting $P_{\text{in}} + P_{\text{droop}}$ and Ω in the wind turbine control.

The optimal parameter selection strongly depends on the composition of the power system. Both the types of power plants as the penetration of wind turbines in the power system have an important influence on the frequency response.

Consequently, the parameters should be tuned to obtain a similar or even better frequency response when conventional generators are replaced by wind turbines. In this section, the optimal parameter selection for the synthetic inertia strategy will be determined for different power systems.

3.6.1 Influence of power plant type

In Fig. 3.11, the power and frequency responses of a combined cycle gas turbine (CCGT) and a conventional steam-based turbine on a loss of generation are shown. A power system with only steam-based turbines (70 %) and nuclear power plants (30 %) is used to obtain the solid curves, whereas a power system with only gas turbines (70 %) and nuclear power plants (30 %) results in the dashed curves.

After the loss of generation of 3 GW at $t = 0$ s, the power output of the gas turbine quickly increases due to the primary controller. Only a small overshoot can be observed. This results in a limited variation of the system frequency and a low ROCOF. For the steam-based turbines, the increase in power output is much slower and a larger overshoot arises. This results in a much lower frequency nadir combined with a slightly higher ROCOF.

Considering the above, it is obvious that the power system composition has a huge impact on the frequency response. Systems with many gas turbines will usually have a higher frequency nadir $f_{\min}$ and lower ROCOF compared to systems with mostly steam-based generators. This frequency response can hardly be changed as it mainly depends on the time constants of the power plants, which depend on the type of power plant. The steam-based power plants have higher thermal time constants than the units with a gas turbine. However, when wind turbines start to replace conventional generators, the frequency response can be altered by tuning K_{in} and K_{droop} appropriately. Considering the differences in the frequency response of the different power plant types, the optimal parameter selection will depend on the composition of the power system.

3.6.2 Influence of wind power penetration

Besides the composition of the different conventional generators in the power system, also the wind power penetration influences the optimal parameter selection. As discussed in § 3.1.4, the amount of system inertia J has an impact on the frequency response. When the wind power penetration increases, the system inertia decreases, which results in a higher ROCOF and a lower frequency nadir. The synthetic inertia strategy can enhance the frequency response, but for high wind power penetrations, it is crucial to tune the parameters properly as instability of the system may arise, as is discussed in § 3.6.4. The higher the wind power penetration, the smaller the range of stable K_{in} and K_{droop} values will be.

3.6.3 Details of the parameter tuning

All the wind turbines that are connected to the power system should contribute to the inertial response. This is similar to the current power system, where the inertial response of the conventional generators is only determined by the inertia of these generators and not by the operating conditions of the generator. If a generator is synchronously connected to the system, the rotational speed changes proportional to the frequency. Ideally, the wind turbines should participate in the inertial response according to their physical inertia, hence, all wind turbines with the same rotor inertia should have the same K_{in} and K_{droop}.

As it might be hard to obtain the inertia for all the wind turbines in the system, it is suggested to scale the inertial response constants proportional to the rated power if the physical inertia is not known. Consequently, wind turbines with a higher rated power have higher inertial response constants K_{in} and K_{droop}. In this case, the same per-unit inertial response constants

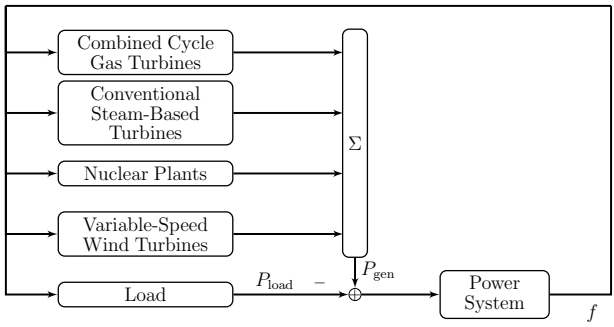

Figure 3.12: Electrical power system model.

are obtained for every wind turbine (in a per-unit system where the rated power of every wind turbine is used as a reference).

In this section, only wind turbines of the same rated power and rotor inertia are used, so every wind turbine has the same inertial constant. For very low wind speeds, when the wind turbine could hit the lower rotational speed limit, the additional power output is limited by the wind turbine control system. Here, a single, constant wind speed v of 10 m/s is assumed to show the importance of a correct parameter selection.

3.6.4 Simulations

In this section, different case studies are discussed to determine the optimal parameter selection for the synthetic inertia strategy.

3.6.4.1 Electrical power system model and wind turbine model

An overview of the electrical power system model is given in Fig. 3.12. The power system is modeled as a single busbar, hence, only frequency control is taken into account and voltage control is not considered. The simulated frequency f is used as the input of the generator and load models [96]. The grid frequency f is calculated by the integration of the imbalance between P_{load} and P_{gen}. Models of different types of power plants are included in the system according to [71, 97–102] (see Appendix A). This includes dynamic models of nuclear, conventional steam-based and CCGT power plants. In steady state, the frequency f equals the nominal frequency f_{nom} and the power outputs of the load and generators are constant. The loads are modeled as constant power loads. The self-regulation effect of the loads is included: the load decreases with 1.5 %/Hz in case of a frequency drop [71]. Then, a loss of production is simulated which results in a frequency deviation from its nominal value. A frequency response from the different

generators is obtained, dependent on the type of generator. The gas turbines and conventional steam-based turbines (such as coal-fired plants) are equipped with a primary controller, whereas the nuclear power plants do not participate in the primary control. For the variable-speed wind turbines, a synthetic inertia response with energy recovery period is obtained, but no primary control is provided by the wind turbines. The additional set-point associated with the inertial response, i.e. $P_{\text{in}} + P_{\text{droop}}$, is limited to 0.1 p.u. in order to respect the current limits of the IGBTs in the converter. In this way, the total current is still below 1.1 p.u. when the wind turbine is operating at rated power when a frequency disturbance occurs. Note that this upper limit on $P_{\text{in}} + P_{\text{droop}}$ was never exceeded during the simulations. No fixed-speed wind turbines were considered in the system as it is expected that in the future, mainly variable-speed wind turbines will be built due to their higher energy yield and better controllability.

Variable-speed wind turbines of the full-scale converter (FSC) type are considered. A permanent magnet synchronous generator is used with a passive rectifier and boost chopper connected to its terminals to inject the rectified current into a DC-link. The electric power is injected into the grid by means of a PWM-switched three-phase inverter with IGBTs as switches. The active power control is performed by controlling the switching actions of the boost chopper. The DC-bus voltage is kept constant by controlling the power balance with the grid-connected inverter. Since time periods of 100 s have to be simulated to investigate the synthetic inertial response, this detailed model, which models all the switching actions, results in overly-long simulation times. Consequently, an averaged model of the wind turbine system is used, where the converter is treated as a current source as is suggested in [32]. In this way, the simulation time can be shortened while still retaining sufficient accuracy.

3.6.4.2 Results

The most important simulation parameters are listed in Table 3.3. A power system of 150 GW is considered with a loss of 3 GW of production. This is a good representation of the reference incident in the European power system [10]. Wind power penetrations of 15 % and 50 % are considered, where conventional steam-based generators and CCGTs are replaced by wind turbines to obtain these penetrations. The primary frequency response is still provided by the conventional generators, the wind turbines only provide inertial response. The frequency nadir f_{min} and the initial rate of change of frequency df/dt_{init} averaged over the first 2 s are calculated for a range of K_{in} and K_{droop}. For each case, 9234 gain combinations (57 values for K_{droop} and 162 values for K_{in}) are tested. The droop constant K_{droop}

Param.	Value	Unit	Param.	Value	Unit
$P_{\mathrm{t,nom}}$	3.0	MW	P_{load}	150	GW
v	10.0	m/s	P_{reserve}	6	GW
f_{nom}	50	Hz	P_{disturb}	3.0	GW
T_{h}	25	s	T_{l}	0.64	s
Ω_{min}	0.85	rad/s	Ω_{max}	2	rad/s
Case 1			**Case 2**		
P_{nuc}	25	%	P_{nuc}	25	%
P_{steam}	0	%	P_{steam}	60	%
P_{ccgt}	60	%	P_{ccgt}	0	%
P_{wind}	15	%	P_{wind}	15	%
Case 3			**Case 4**		
P_{nuc}	25	%	P_{nuc}	25	%
P_{steam}	0	%	P_{steam}	25	%
P_{ccgt}	25	%	P_{ccgt}	0	%
P_{wind}	50	%	P_{wind}	50	%
No wind turbines					
P_{nuc}	25	%	P_{ccgt}	$0-75$	%
P_{wind}	0	%	P_{steam}	$75-0$	%

Table 3.3: Simulation parameters.

is varied between 0 and 2.7 MW/Hz, whereas K_{in} varies between 0 and 7.8 MWs/Hz. The frequency nadir and ROCOF values are compared with the values obtained for the power system without wind turbines. It is indeed more interesting to compare this frequency response to the power system without wind turbines than to the power system with wind turbines without synthetic inertia as the frequency response is always worse for the latter due to the lower system inertia. This can be seen in the simulations for all different cases. Consequently, the system without any wind turbines is used as reference situation. The desired result is a high frequency nadir and a low ROCOF. The objective is to obtain a frequency response with the synthetic inertia strategy which is as good as or even better than the frequency response for the system without wind turbines.

3.6.4.3 Case 1: Low wind power penetration, 60 % CCGT

The first case has a wind power penetration of 15 % and consists of 60 % CCGTs and 0 % steam-based power plants. This means that all primary control is provided by fast reacting CCGTs. The frequency nadir and RO-

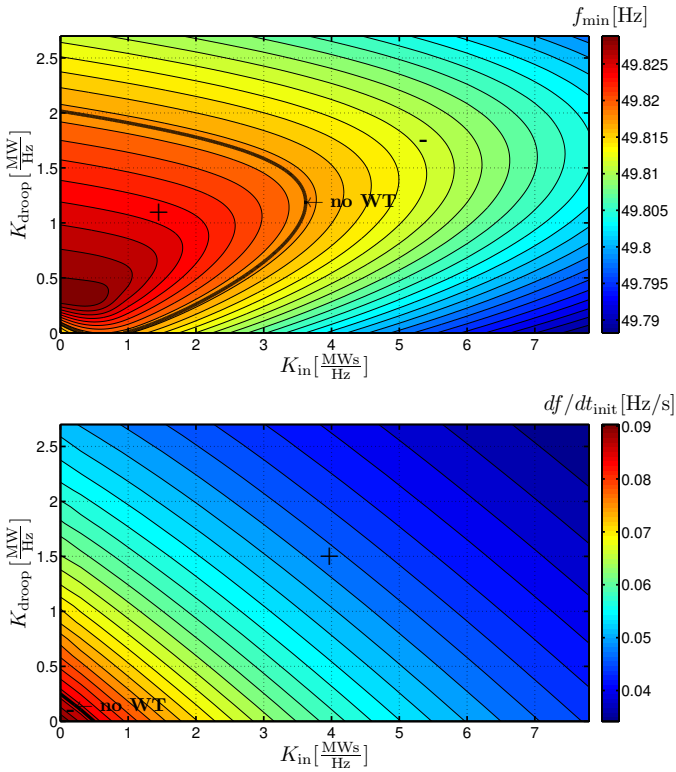

Figure 3.13: Case 1: Frequency nadir and ROCOF for a wind power penetration of 15 % and 60 % CCGT.

COF are shown in Fig. 3.13. The thick black lines represent the values of $f_{\min}$ and df/dt_{init} for the equivalent power system without wind turbines, whereas the contour plots represent the values of $f_{\min}$ and df/dt_{init} for the system with wind turbines equipped with the synthetic inertia strategy for different values of K_{in} and K_{droop}.

Considering only the frequency nadir, the optimal parameters (i.e., resulting in the highest frequency nadir) are $K_{\text{in}} = 0$ MWs/Hz and $K_{\text{droop}} = 0.45$ MW/Hz. Furthermore, all the parameter combinations which have a frequency nadir above the value for $f_{\min}$ without wind turbines result in a better frequency response than the case without wind turbines (area inside the thick black curve, indicated by the plus sign in Fig. 3.13).

As expected, the ROCOF decreases for increasing values of K_{in} and K_{droop}, which is the desired result. A lower ROCOF gives the generators participating in the primary control more time to adapt their power output. High values for K_{in} and K_{droop} would, however, result in a low frequency

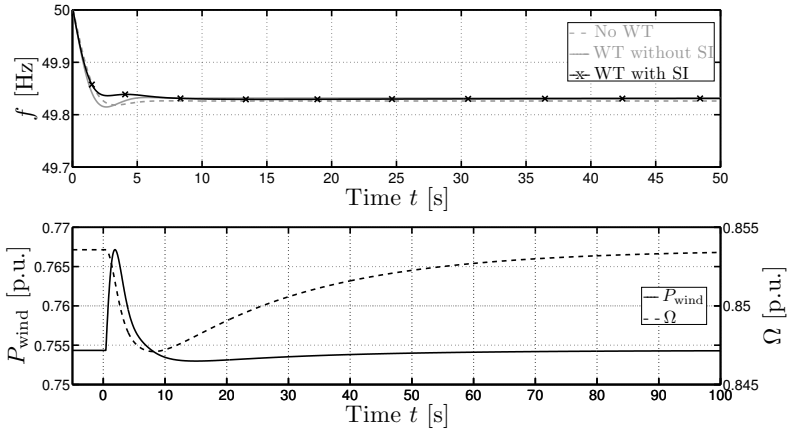

Figure 3.14: Case 1: Frequency response for different scenarios and wind turbine behavior for SI. Optimal parameters for WT with synthetic inertia: $K_{\text{in}} = 0$ MWs/Hz, $K_{\text{droop}} = 0.45$ MW/Hz.

nadir, which is unacceptable. All parameter combinations which have a ROCOF below the value for df/dt_{init} without wind turbines are indicated by the plus sign in Fig. 3.13. Consequently, it is clear from Fig. 3.13 that only parameters near the origin ($K_{\text{in}} \approx 0$, $K_{\text{droop}} \approx 0$) worsen the ROCOF.

Consequently, the parameters K_{in} and K_{droop} that result in the highest frequency nadir also result in a slightly better ROCOF and are therefore chosen as the optimal parameters for this system composition. As is shown in the following cases, the parameter combination that results in the highest frequency nadir, always results in an enhanced ROCOF, also for other system compositions. Therefore, when there is referred to the 'optimal' parameters in this section, this corresponds to the parameters that result in the highest frequency nadir. In § 3.6.4.7, the parameter ranges which result in both a higher frequency nadir and lower ROCOF are presented.

In Fig. 3.14, the frequency response is shown for three different scenarios. The frequency response is slightly worsened when the wind power penetration increases, but no synthetic inertia is used in the wind turbines. Wind turbines with synthetic inertia slightly improve the frequency response, though the differences are small. The frequency nadir f_{min} is slightly higher and the ROCOF is almost the same. This is due to the high amount of gas turbines in the system, which quickly change their power output in case of a disturbance, leaving only little room for improvement.

When looking at the turbine-side behavior in Fig. 3.14, it can be seen that the rotational speed Ω only deviates little from the pre-disturbance value and the additional power output is quite modest.

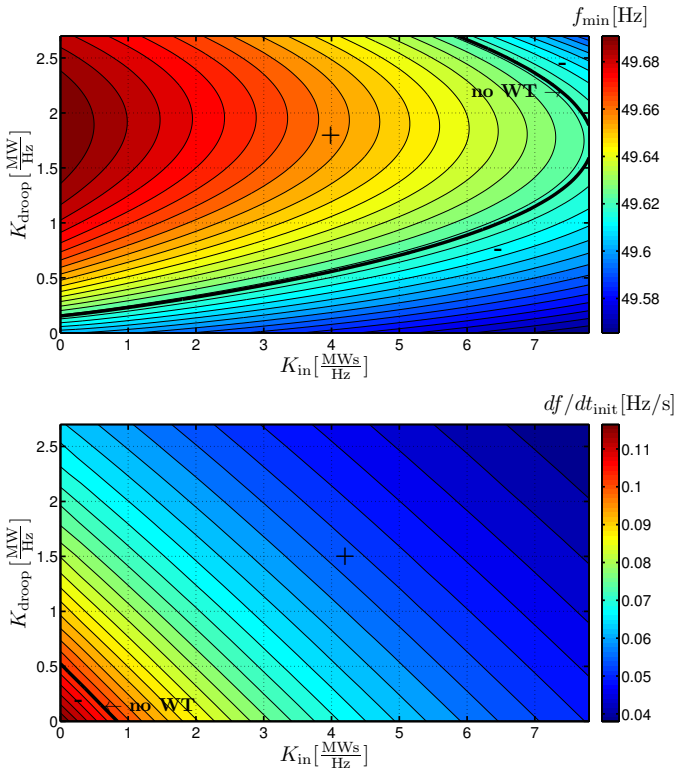

Figure 3.15: Case 2: Frequency nadir and ROCOF for a wind power penetration of 15 % and 60 % steam.

3.6.4.4 Case 2: Low wind power penetration, 60 % steam

In case 2, again a wind power penetration of 15 % is considered, but 100 % of the primary control action is now provided by steam-based generators. For the frequency nadir, the optimal droop constant has shifted towards a higher value ($K_{\text{droop}} = 1.8$ MW/Hz), whereas K_{in} remains the same (see Fig. 3.15). For systems with mainly slower generators, this higher K_{droop} for the fast-reacting wind turbines results in a faster response immediately after the disturbance, which enhances the frequency response. The zone of improvement for the ROCOF is almost the same as in case 1, but due to the slower reaction of the power plants in the system, the ROCOF has increased.

The extent of the parameter range which results in a better frequency nadir, however, has increased compared to the first case. As the power system consists of power plants that can only increase their power output slowly, the frequency response can be increased by replacing these steam-

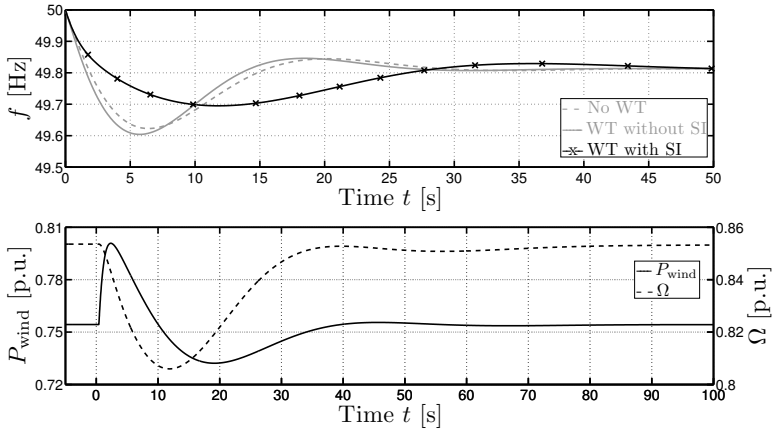

Figure 3.16: Case 2: Frequency response for different scenarios and wind turbine behavior for SI. Optimal parameters for WT with synthetic inertia: $K_{\text{in}} = 0$ MWs/Hz, $K_{\text{droop}} = 1.8$ MW/Hz.

based units with wind turbines with the synthetic inertia strategy, which react faster on frequency deviations. Even a non-optimal parameter selection results in an enhanced frequency response.

Considering Fig. 3.16, the synthetic inertia strategy results in a higher frequency nadir and a lower ROCOF compared with the situation without wind turbines in the system. Furthermore, steady state is reached as fast as in the case without wind turbines. Compared to case 1, a much larger improvement in the frequency response can be obtained by applying the synthetic inertia strategy. The additional power output is higher compared to case 1 and consequently, more kinetic energy is extracted from the rotor, resulting in a higher rotational speed deviation. The wind turbines remain within their operational limits (rotational speed, power, etc.) at all times.

3.6.4.5 Case 3: High wind power penetration, 25 % CCGT

For case 3, a wind power penetration of 50 % is considered and all the primary control action is provided by the CCGTs. Compared to the low wind power penetration case (case 1), the optimal droop constant K_{droop} has decreased as is shown in Fig. 3.17. Also the parameter range which results in a higher frequency nadir than without wind turbines has shrunk. Especially the range of K_{droop} is smaller. This is due to the lower penetration of conventional generators. For high values of K_{droop}, the inertial response of the wind turbines dominates the frequency response by initially injecting much additional power. The high initial power injection limits the frequency deviation and the primary response of the conventional genera-

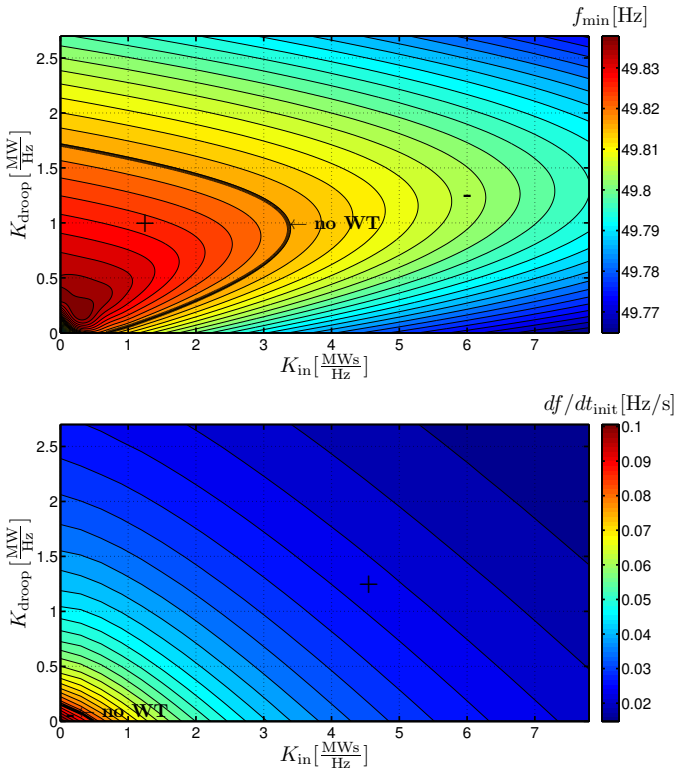

Figure 3.17: Case 3: Frequency nadir and ROCOF for a wind power penetration of 50 % and 25 % CCGT.

tors. When the inertial response from the wind turbines has finished, the power output of these conventional generators has not yet increased enough to restore the frequency, resulting in a deferred and lower frequency nadir, as can be seen in Fig. 3.19. Shortly after the disturbance, the output of the wind turbines increases due to the high droop constant. Then, the maximum power point tracker tries to bring the wind turbine to the maximum power point again, resulting in a lower output when the recovery period starts (around 15 s). The CCGTs start to increase their power output after the disturbance by means of their primary controller. As the wind turbines inject too much additional power in the first 15 s, the frequency nadir and ROCOF are initially limited, so the primary droop controller of the CCGTs gives only a limited additional power output. After 15 s, the wind turbines start to recover again and the output of the CCGTs has not yet increased enough to limit the frequency deviation, which results in the lower frequency nadir. Therefore, it is important not to exaggerate the inertial response, as

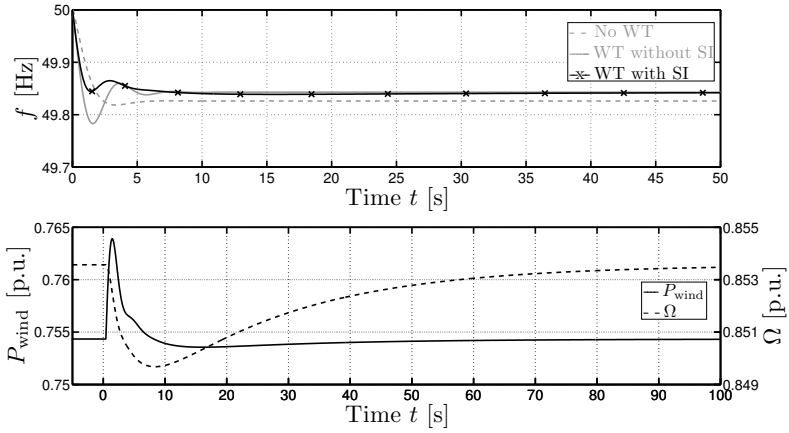

Figure 3.18: Case 3: Frequency response for different scenarios and wind turbine behavior for SI. Optimal parameters for WT with synthetic inertia: $K_{\text{in}} = 0$ MWs/Hz, $K_{\text{droop}} = 0.3$ MW/Hz.

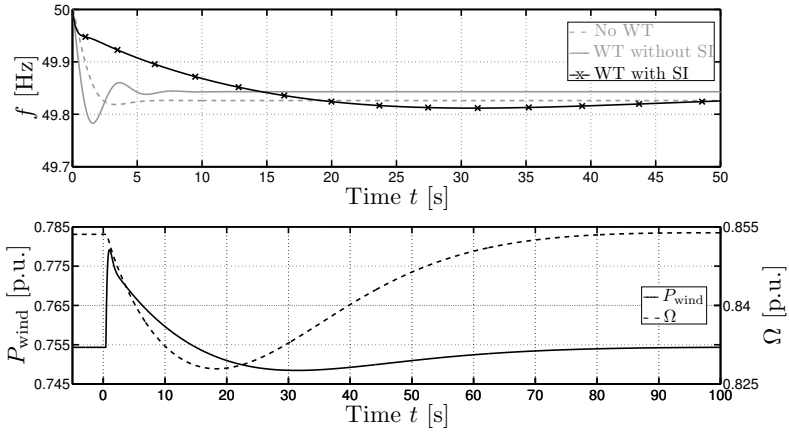

Figure 3.19: Case 3: Frequency response for different scenarios and wind turbine behavior for SI. Suboptimal parameters for WT with synthetic inertia: $K_{\text{in}} = 0$ MWs/Hz, $K_{\text{droop}} = 2.1$ MW/Hz.

it might initially limit the frequency deviation too much for the CCGTs to start responding fast enough. The primary controllers do not increase the power output enough, as they only "see" a small disturbance. Consequently, when the wind turbines start to recover again, this causes the lower dip. For high wind power penetrations, this effect is much more pronounced, which explains the smaller droop constant range. Using only inertial control K_{in} is also not beneficial for the frequency response for high wind power penetrations, as it might lead to an oscillatory behavior. Too much additional

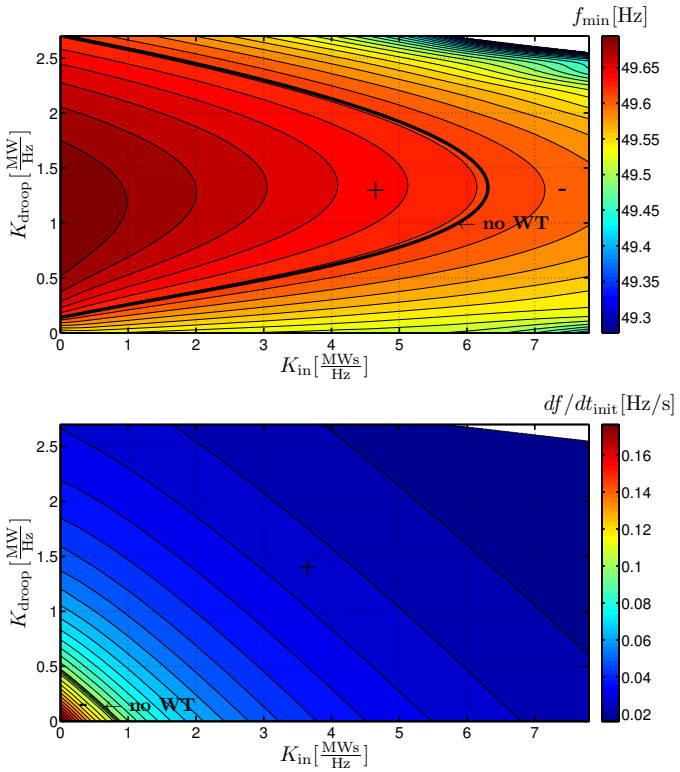

Figure 3.20: Case 4: Frequency nadir and ROCOF for a wind power penetration of 50 % and 25 % steam.

power is injected in the first few seconds and the output of the conventional generators does not increase enough to limit the frequency deviation during the recovery period. Therefore, it is important to tune the parameters K_{in} and K_{droop} together to avoid unexpected behavior of the synthetic inertia strategy.

The frequency responses for the optimal parameter selection in Fig. 3.18 are similar to the ones that are obtained in Fig. 3.14. However, the influence of the synthetic inertia strategy on the frequency response is more distinct due to the lower penetration of conventional generators. Also for the higher wind power penetration, the wind turbines stay within their operational limits.

3.6.4.6 Case 4: High wind power penetration 25 % steam

The last case also has a wind power penetration of 50 %, but has steam-based generators instead of CCGTs. The optimal value for K_{droop} has again

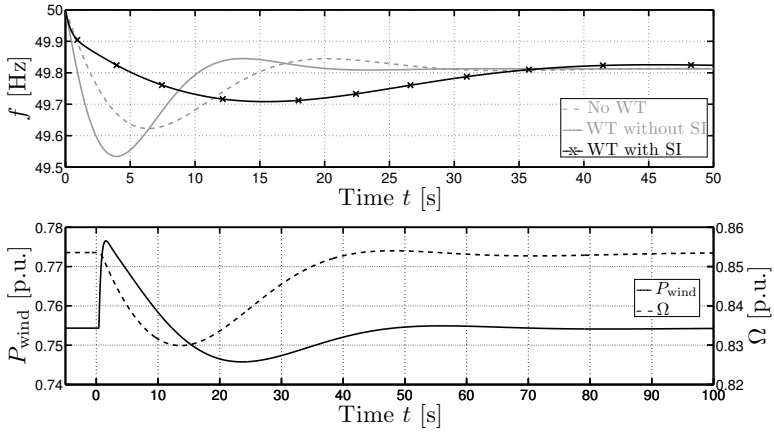

Figure 3.21: Case 4: Frequency response for different scenarios and wind turbine behavior for SI. Optimal parameters for WT with synthetic inertia: $K_{\text{in}} = 0$ MWs/Hz, $K_{\text{droop}} = 1.05$ MW/Hz.

decreased and the optimal parameter range is smaller compared to case 2 (lower wind power penetration). The same explanation as for case 3 is applicable.

The difference between the optimal value for K_{droop} in case 2 and 4 is larger than for case 1 and 3 (i.e., 1.8 MW/Hz vs. 1.05 MW/Hz and 0.45 MW/Hz vs. 0.3 MW/Hz respectively), which makes the parameter sensitivity higher for systems with mainly steam-based generators. As the steam-based generators have a longer response time than the CCGTs, it is important not to exaggerate the inertial response of the wind turbines for increasing wind power penetrations. If the additional power output of the wind turbines is too high, the frequency deviation is initially limited which results in a reduced primary response from the conventional units. However, the wind turbines cannot maintain this high power output, so eventually, the conventional units have to take over. As the response time for CCGTs is closer to the response time of the wind turbines, this parameter sensitivity is less pronounced as these units increase their power output faster. In summary, for systems with mainly fast generators, K_{droop} will be lower, but less sensitive for an increasing wind power penetration, whereas for systems with slower generators, the optimal K_{droop} is higher, but more dependent on the wind power penetration. However, for all system compositions it is important not to exaggerate the inertial response of the wind turbines in order to trigger the conventional generators to increase their power output.

According to Fig. 3.21, it is important to use the synthetic inertia strategy to enhance the frequency response. When no synthetic inertia is applied

to the wind turbines, the frequency drops fast after the loss of generation. The frequency nadir is significantly lower than for the case without wind turbines. A properly tuned synthetic inertia strategy is able to decrease the ROCOF and increase the frequency nadir. Furthermore, when the frequency response of Fig. 3.21 is compared to the one of Fig. 3.18, a similar response is obtained for a wind power penetration of both 15 % and 50 % when the synthetic inertia strategy is applied.

3.6.4.7 Optimal parameter range

Considering the four case studies, some general conclusions can be drawn. For systems with mainly fast reacting generators (CCGTs), only limited inertial response from the wind turbines is needed, which results in low values for K_{in} and K_{droop}. For systems with mainly slower generators, a higher value for K_{droop} is preferable. The optimal parameter selection shows that K_{in} should be zero or close to zero. This is an important outcome, as it means that no measurement (or calculation) of df/dt is needed. Differentiation of the grid frequency f usually results in a noisy signal, which could result in undesired oscillations of the output power of the wind turbine. As the converter of the wind turbine is able to control its power output very fast, the droop controller K_{droop} is fast enough to enhance the frequency response, so no inertial term K_{in} is needed. Consequently, a droop controller is a viable alternative for the synthetic inertia strategy, as is shown by the simulations. In literature, only the behavior of emulated inertial control is investigated without taking into account the influence of the system composition. This investigation shows the importance of considering the system composition.

In Fig. 3.22, the parameter ranges which result in a better frequency response than for the case without wind turbines are shown as the intersection of the limits for f_{min} and df/dt_{init}. The innermost curve represents the situation with only CCGTs participating in the primary control, whereas the outermost curve is a power system with only steam-based generators providing primary control. The curves in between are obtained for different intermediate compositions. If a parameter combination in the shaded area is used, this results in an enhanced frequency response. Consequently, a combination of inertial control (K_{in}) and droop control (K_{droop}) can still enhance the frequency response, but for the optimal response no inertial term is needed ($K_{\text{in}} = 0$). As expected, the area for the high wind power penetration is smaller than for the low wind power penetration. By combining the general conclusions from the case studies with Fig. 3.22a and Fig. 3.22b, the optimal parameter configuration for each power system can be determined. Firstly, the parameters should be chosen inside the shaded

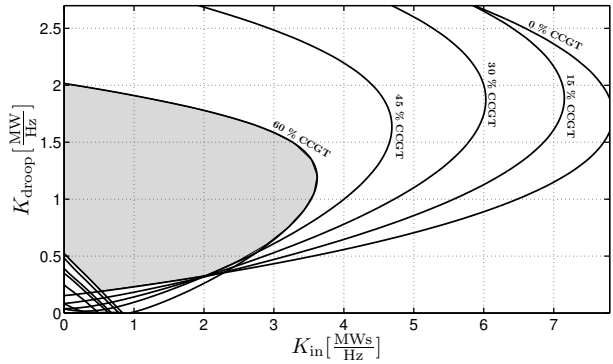

(a) 15 % wind power penetration

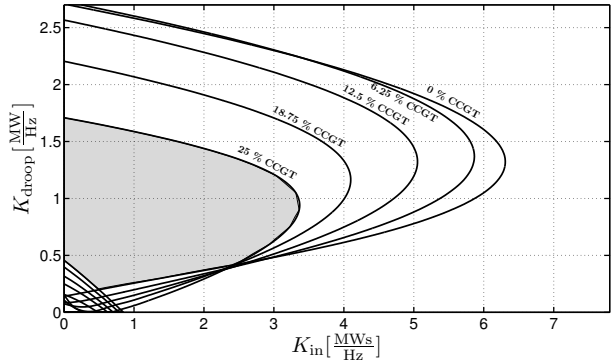

(b) 50 % wind power penetration

Figure 3.22: Parameter range.

area of Fig. 3.22 to make sure that the emulated inertial response enhances the frequency response. This is a first, coarse tuning of the parameters to make sure the frequency response is enhanced. Secondly, the optimal fine-tuned parameters could be selected by using information about the exact composition of the power system.

3.6.4.8 Optimal synthetic inertia response for a varying system composition

In the previous paragraphs, four different case studies were performed to show the importance of a correct parameter selection. In this paragraph, the system composition is varied according to the simulation parameters listed in Table 3.4. Again, two distinct scenarios are considered: a system with

Param.	Value	Unit	Param.	Value	Unit
Low wind penetration			**High wind penetration**		
P_{nuc}	25	%	P_{nuc}	25	%
P_{steam}	$0-60$	%	P_{steam}	$0-25$	%
P_{ccgt}	$60-0$	%	P_{ccgt}	$25-0$	%
P_{wind}	15	%	P_{wind}	50	%
No wind turbines					
P_{nuc}	25	%	P_{ccgt}	$0-75$	%
P_{wind}	0	%	P_{steam}	$75-0$	%

Table 3.4: Simulation parameters for a varying system composition.

a low wind power penetration (15 %) and a high wind power penetration (50 %). The wind turbines are equipped with the synthetic inertia strategy with the optimal parameters K_{in} and K_{droop} for each system composition.

In Fig. 3.23, the frequency nadir f_{min} and ROCOF df/dt_{init} are shown for a wind power penetration of 15 %. The dashed gray line represents the system without wind turbines, the solid gray line is the system with wind turbines but without synthetic inertia and the solid black line is for the system with wind turbines equipped with the synthetic inertia strategy. The system without wind turbines can be regarded as the reference situation. As expected, the frequency nadir is the lowest for the power system which is dominated by the steam-based generation and increases with increasing CCGT-levels. Also the ROCOF improves with an increasing share of CCGTs in the power system.

Replacing 15 % of the generators by wind turbines without synthetic inertia results in a minor change of the frequency nadir. Only for the power systems with a high amount of steam-based generation, the frequency nadir is slightly worsened due to the slower increase of the power output of these power plants in case of a frequency dip. The ROCOF, on the other hand, has increased compared to the reference case. This could be expected, since the wind turbines replace conventional generation and cause a decrease of the system inertia J. The difference is the smallest for systems with a high share of CCGTs, as these power plants can increase their power output faster and thus reduce the ROCOF.

When the wind turbines are equipped with the synthetic inertia strategy and the control parameters are properly tuned, both frequency nadir and ROCOF can be greatly improved. Especially the frequency response of systems with a high share of steam-based generation can be enhanced. The wind turbines with synthetic inertia react much faster than the steam-based

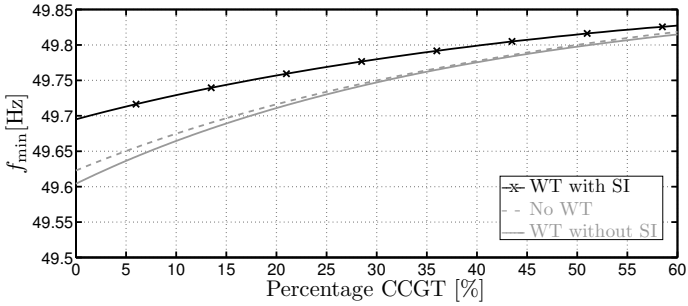

(a) Frequency nadir.

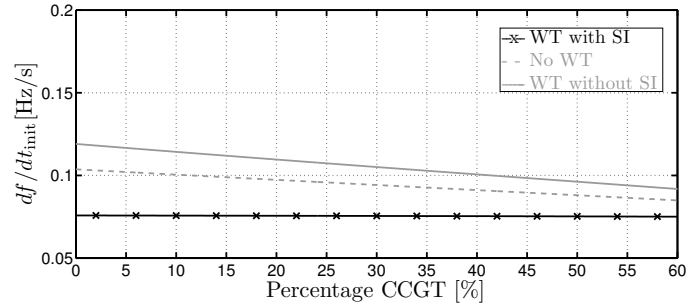

(b) ROCOF.

Figure 3.23: Frequency nadir and ROCOF in function of the system composition for a low wind power penetration.

generators resulting in an enhanced frequency response. As the CCGTs already react fast on frequency dips, only little improvement can be obtained by replacing part of these generators with wind turbines.

The frequency nadir and ROCOF for a wind power penetration of 50 % are depicted in Fig. 3.24. When 50 % of the generation capacity is replaced by wind turbines without synthetic inertia strategy, the inertial response is clearly deteriorated as the frequency nadir decreases and the ROCOF increases for all the system compositions. This is a major difference with the first case, where there was only a minor impact on both the frequency nadir and the ROCOF. Similar to the first case, the impact on the frequency nadir and ROCOF is the highest for the systems with mainly steam-based generation.

When the wind turbines are equipped with the synthetic inertia strategy, however, both frequency nadir and ROCOF can be enhanced. The

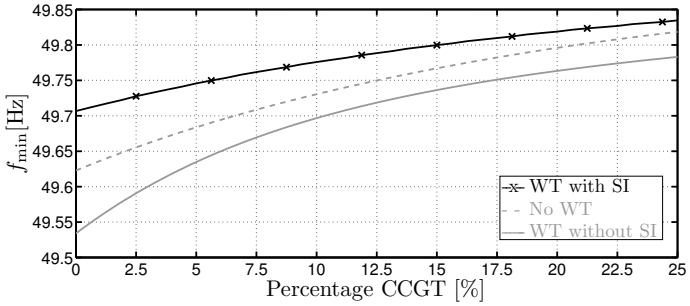

(a) Frequency nadir.

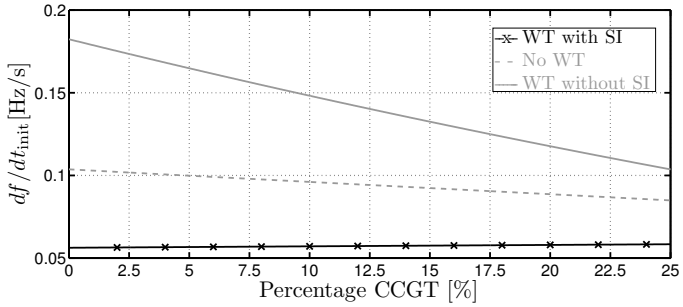

(b) ROCOF.

Figure 3.24: Frequency nadir and ROCOF in function of the system composition for a high wind power penetration.

frequency nadir and ROCOF that can be obtained with the optimal parameter selection are almost equal for both cases (15 % and 50 % wind power). This means that the inertial response can be as good for high wind power penetrations as for low wind power penetrations.

Fig. 3.24 shows the need for wind turbines equipped with the synthetic inertia strategy. The inertial response clearly deteriorates for an increasing wind power penetration without the use of the synthetic inertia strategy. Using wind turbines with SI, however, can enhance the frequency response for different system compositions.

3.6.5 Conclusion

In this section, it was shown that the droop control strategy is a viable alternative for the synthetic inertia strategy. The optimal parameter tuning of the synthetic inertia strategy for wind turbines was investigated. First, it

was shown that there exists quite a broad range of parameters that enhance the frequency response, but that the optimal value for K_{in} is zero. This means that no differentiation of the frequency is needed, which simplifies the control system and makes it more robust to measurement noise. In this way, the synthetic inertia strategy reduces to a fast droop control strategy. Furthermore, the optimal parameter combination, which results in $K_{\text{in}} = 0$, shows that mimicking the behavior of a synchronous machine (with $K_{\text{in}} \neq 0$) does not result in the optimal inertial response.

Second, it was shown that the optimal selection of the synthetic inertia strategy strongly depends on the composition of the power system. For power systems consisting of mainly fast reacting generators, a low value for K_{droop} (and K_{in}) is needed, whereas for slower power systems, a higher value for K_{droop} is desired. Furthermore, simulations show that only a limited parameter range results in a better frequency response compared to the case without wind turbines. All the parameter combinations outside this range result in a deterioration of the frequency response. Care should be taken when selecting the parameters for the synthetic inertia strategy and droop control strategy, otherwise, the use of emulated inertial response strategies may deteriorate the frequency response instead of improving it.

Third, an optimal parameter range for different wind power penetrations was derived, which shows that the parameter tuning is more crucial for higher wind power penetrations. Furthermore, for 'fast' power systems, the range is much smaller than for 'slow' power systems. Due to the inherently worse frequency response in 'slow' power systems, there is more room to improve the frequency response by adding synthetic inertia to the system. By applying some basic rules based to the sensitivity analysis for K_{in} and K_{droop}, it is possible to achieve an optimal parameter selection for every power system composition.

Finally, the frequency response was investigated for a broad range of system compositions. It was shown that the inertial response can be enhanced the most for systems with a large share of steam-based generation. For these systems, the replacement of the conventional generation results in a power system that reacts faster on frequency changes, as the converter-connected wind turbines can increase their power output faster than the steam-based generators. This results in a reduced ROCOF and an increased frequency nadir. For systems with many CCGTs, this effect is less pronounced as these generators can change their power output quite fast. The simulations show that the optimal parameter selection results in an inertial response that is equally good for low and high wind power penetrations.

3.7 Optimal parameter selection for the temporary power surge

Similar to the synthetic inertia strategy, it is important to tune the parameters of the temporary power surge properly. If the overproduction step ΔP_{OP} is chosen too high and/or too long, fast depletion of the kinetic energy can occur. This can result in an unstable operation of the wind turbine. If ΔP_{OP} is too low, poor emulated inertial response behavior is obtained from the wind turbine. Furthermore, the transition to the underproduction period t_{D}, the depth ΔP_{UP} and duration t_{UP} of this period are important parameters as well. If the power reference is decreased too fast after the overproduction period, a second (undesired) frequency dip could occur in the electric power system. The same holds for the depth of the recovery period ΔP_{UP}. The choice of the recovery strategy has an important impact on the stability of the temporary power surge. Consequently, poor parameter tuning may result in a frequency response that is worse compared to the case without emulated inertial response or without wind turbines at all or even unstable operation of the wind turbine, as will be shown further in this section.

The optimal parameter selection, which results in a higher frequency nadir f_{min} and lower ROCOF df/dt than for the system without wind turbines with emulated inertial response, depends strongly on the composition of the power system. Both the present types of power plants as the penetration of wind turbines in the power system have an important impact on the frequency response, as was shown in § 3.6 [87]. Systems with mainly gas turbines usually have a higher frequency nadir f_{min} and lower ROCOF df/dt as these generators can react faster. The amount of wind turbines in the system influences the systems inertia and, consequently, the frequency response.

In this section, the influence of the parameter selection on the inertial response capability and stability of the temporary power surge is investigated for different system compositions. Different recovery strategies are considered.

3.7.1 Simulation results

3.7.1.1 Electrical power system model and wind turbine model

The same electrical power system as in § 3.6.4.1 is considered. The most important simulation parameters are listed in Table 3.5. Again, for every system composition, the frequency nadir f_{min} and rate of change of frequency df/dt_{init} in the first 2 s are calculated. The parameters ΔP_{OP}

Param.	Value	Unit	Param.	Value	Unit
$P_{\mathrm{t,nom}}$	3.0	MW	P_{load}	150	GW
f_{nom}	50	Hz	P_{disturb}	3.0	GW
ΔP_{UP}	$0.5 \cdot \Delta P_{\mathrm{OP}}$	p.u.	t_{D}	5	s
P_{acc}	$0.25 \cdot \Delta P_{\mathrm{OP}}$	p.u.	dP/dt_{max}	300.0	kW/s
With wind turbines					
P_{nuc}	25	%	P_{ccgt}	$0-60$	%
P_{wind}	15	%	P_{steam}	$60-0$	%
No wind turbines					
P_{nuc}	25	%	P_{ccgt}	$0-75$	%
P_{wind}	0	%	P_{wind}	$75-0$	%

Table 3.5: Simulation parameters for the temporary power surge strategies.

and t_{OP} are varied as they have an important impact on the frequency response (f_{min} and df/dt_{init}) immediately after the disturbance. The recovery parameters are determined according to Table 3.5. Only a wind power penetration of 15 % is considered as the influence of the wind power penetration is quite similar as for the synthetic inertia strategy. Here, the influence of the recovery strategy is of greater importance.

The frequency nadir and ROCOF values are compared with the values obtained for the power system without wind turbines. The desired result is a high frequency nadir and a low ROCOF as it is the objective to achieve a frequency response with the temporary power surge which is as good or even better than the case without wind turbines in the system.

In Figs. 3.25, 3.26 and 3.27 the frequency nadir f_{min} and ROCOF df/dt_{init} for two extreme cases (60 % steam-based turbines vs. 60 % CCGTs, both with 25 % nuclear and 15 % wind power) are shown to illustrate the importance of correct parameter tuning. Three different recovery strategies are compared in these figures: optimal speed recovery, constant underproduction recovery and constant accelerating power recovery. The thick black lines represent the values for f_{min} and df/dt_{init} for the equivalent power system without wind turbines, whereas the contour plots represent the values for f_{min} and df/dt_{init} for the system with wind turbines equipped with the temporary power surge for different values of ΔP_{OP} and t_{OP}. Areas denoted with a plus sign result in a better inertial response than the system without wind turbines, a minus sign means that the inertial response is worse. The white areas show parameter combinations that result in an unstable operation of the wind turbines (i.e., the wind turbines slow down and stop operating). It is clear that both the recovery strategy and the system

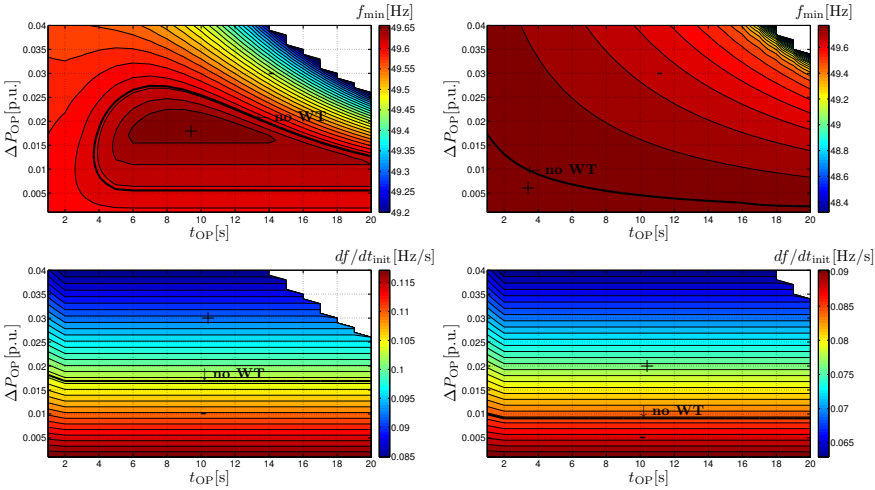

(a) 60% steam-based **(b)** 60% CCGTs

Figure 3.25: Frequency nadir and ROCOF in function of ΔP_{OP} and t_{OP} for the optimal speed recovery strategy.

composition have a huge impact on the frequency response, so the parameter tuning and choice of recovery strategy are important. Both aspects are discussed in detail in the following paragraphs.

3.7.1.2 Parameter selection in function of system composition

First, the influence of the system composition on the optimal parameter selection is discussed. Considering the frequency nadir $f_{\min}$, it can be noted that the higher the penetration of steam-based generators is, the higher the overproduction step ΔP_{OP} should be to obtain the best inertial response (see Figs. 3.25, 3.26 and 3.27). When Fig. 3.25a and 3.25b are compared, it can be seen that the optimal parameter combination resulting in the highest frequency nadir has a low ΔP_{OP} for 60 % CCGTs (near zero). For 60 % steam-based generation, a higher ΔP_{OP} is optimal. This also applies to the two other recovery strategies. The reason is that in systems with a high penetration of steam-based generators, the reaction on disturbances is quite slow due to the larger thermal time constants of these type of generators [87]. Replacing these generators with fast-reacting wind turbines enhances this response. In gas-based systems, the need for wind turbine support is less crucial as these generators already react fast on disturbances. Secondly, the dependence on the overproduction time t_{OP} is quite limited: an overproduction time of about 7 seconds usually results in a good frequency response,

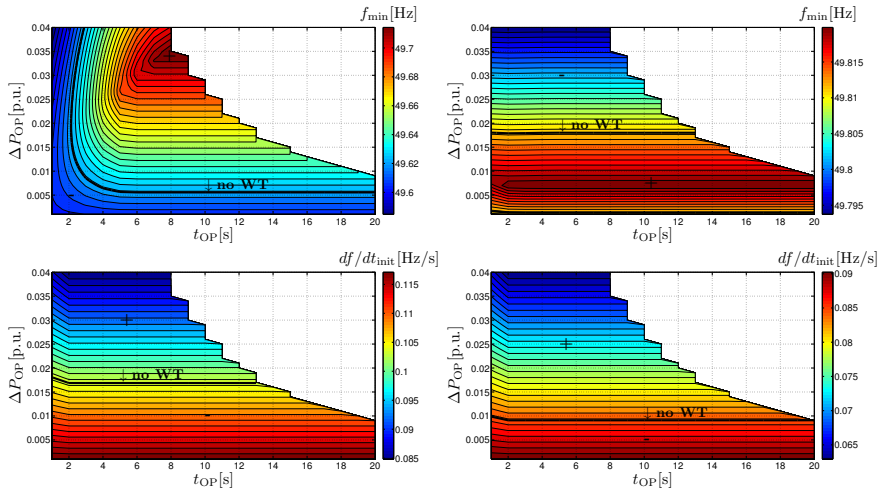

(a) 60% steam-based **(b)** 60% CCGTs

Figure 3.26: Frequency nadir and ROCOF in function of ΔP_{OP} and t_{OP} for the constant underproduction recovery strategy.

but the sensitivity is low. However, the combination of both a high overproduction step ΔP_{OP} and overproduction time t_{OP} could result in instability (shown by the white areas in Fig. 3.25) as too much kinetic energy is extracted from the wind turbine rotor. The wind turbine slows down and eventually stops rotating, as is discussed in § 3.7.1.3.

In Figs. 3.25, 3.26 and 3.27, also the ROCOF is shown for the different system compositions and recovery strategies. As expected, the ROCOF decreases with increasing ΔP_{OP}. The more power is injected into the grid immediately after the disturbance, the slower the frequency f will decrease resulting in a lower ROCOF. As expected, the overproduction time t_{OP} has almost no influence on the ROCOF as df/dt_{init} is mainly determined by the additional amount of power ΔP_{OP} that is injected in the first instants after the disturbance. Only for very short overproduction periods ($t_{OP} = 1-2$ s), the ROCOF depends on t_{OP} as the overproduction lasts not long enough to limit the ROCOF. The ROCOF is higher for systems with mainly steam-based generators as these generators only slowly adjust their power output in case of a disturbance.

In order to obtain the desired inertial response, the frequency nadir $f_{\min}$ should be as high as possible, whereas the ROCOF should be as low as possible. As can be seen in Figs. 3.25a, 3.26a and 3.27a for 60 % steam-based generation, the parameter combination which results in the highest frequency nadir also results in a ROCOF that is lower than the

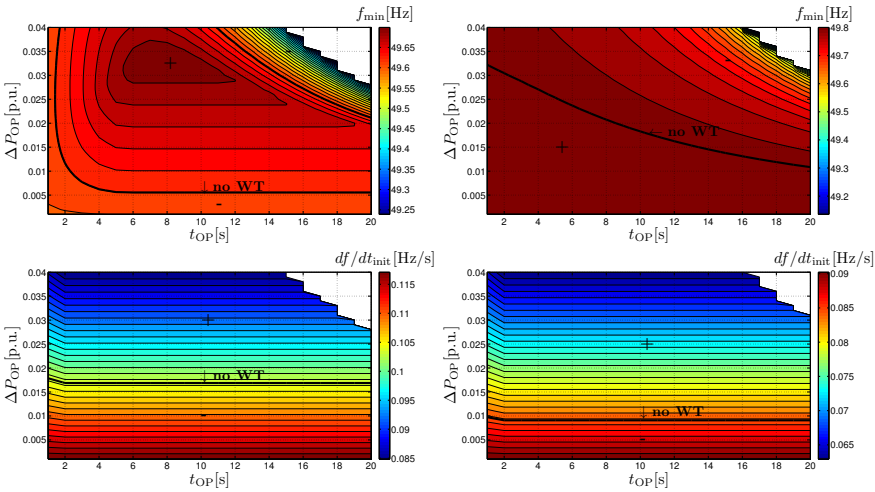

(a) 60% steam-based **(b)** 60% CCGTs

Figure 3.27: Frequency nadir and ROCOF in function of ΔP_{OP} and t_{OP} for the constant accelerating power P_{acc} recovery strategy.

case without wind turbines. Consequently, no trade-off has to be made to obtain the optimal inertial response as both frequency nadir and ROCOF are enhanced compared to the case without wind turbines in the system. However, for 60 % CCGTs in the power system (Figs. 3.25b, 3.26b and 3.27b), the optimal parameter combination for the frequency nadir results in a slightly higher ROCOF than the case without wind turbines in the system. Consequently, a trade-off has to be made. Here, the parameter combination which maximizes the frequency nadir $f_{\min}$ is chosen as the optimal solution, as the differences for the ROCOF are only very small (see Section 3.7.1.4).

From this paragraph, the following can be concluded:

- The system composition has an important impact on the optimal parameter selection: a higher overproduction step ΔP_{OP} is needed for systems with mainly steam-based generators.

- The ROCOF is mainly determined by the overproduction step ΔP_{OP} and not by the overproduction time t_{OP}.

- Sometimes, a trade-off has to be made between a slightly higher ROCOF and a higher frequency nadir.

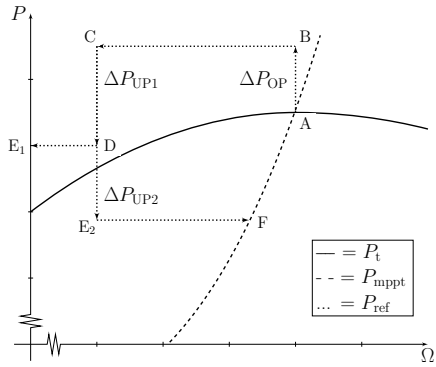

Figure 3.28: Instability for the constant underproduction period.

3.7.1.3 Influence of recovery strategy on parameter selection

Besides the system composition, the choice of the recovery strategy also has an important impact on the optimal parameter selection and frequency response. It can be noted that the optimal speed recovery and constant accelerating power recovery strategy show similar behavior concerning the stable range: only the combination of a high ΔP_{OP} and a large t_{OP} result in unstable operation. This is clearly shown by the size of the white area in Figs. 3.25a, 3.25b, 3.27a and 3.27b. The reason for the instability is the fact that too much kinetic energy is extracted from the rotor, so the wind turbine is exhausted and stops rotating. However, the optimal parameter combination is far away from this unstable region, so this is not a problem.

For the constant underproduction recovery strategy in Figs. 3.26a and 3.26b, unstable operation is reached faster as instability can occur when the underproduction step ΔP_{UP} is chosen too small. This is shown in Fig. 3.28 for the underproduction step ΔP_{UP1}. Initially, the wind turbine is operating in the MPP (A). Then, the power output is increased with ΔP_{OP} (B). As the power output is higher than the power input P_t, kinetic energy is extracted from the wind turbine inertia which causes the wind turbine to slow down (C). When the overproduction period t_{OP} is over, the power output is decreased with ΔP_{UP1} (D). Here, the reference value P_{ref} for the power output is still higher than the power input P_t during the recovery period, which means that the wind turbine will not recover but slows down further (E_1). For a larger underproduction step ΔP_{UP2}, the power output P_{ref} decreases below the power input P_t (E_2). This results in a recovery of the wind turbine (first to F and then to A). Consequently, also the underproduction step should be tuned according to the operating conditions of the wind turbine for this recovery strategy. Furthermore, the optimal

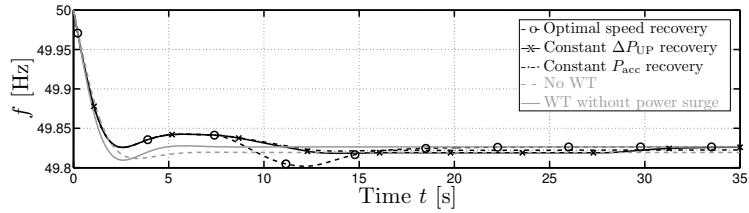

Figure 3.29: Frequency for $\Delta P_{\mathrm{OP}} = 0.01$ p.u., $t_{\mathrm{OP}} = 7$ s and 60 % CCGT.

parameter combination is very close to the unstable region, so instability could indeed be a problem.

Furthermore, it is clear that the recovery strategy has an impact on the exact optimal parameter combination as well, so the parameters t_{OP} and ΔP_{OP} should be tuned together with the recovery strategy.

Concerning the ROCOF df/dt_{init}, the influence of the recovery strategy is limited. As the ROCOF is only determined by the first few seconds of the inertial response, the different recovery strategies all have the same ROCOF for a certain combination of the control parameters t_{OP} and ΔP_{OP} as can be seen when the ROCOF is compared for the different strategies in Figs. 3.25, 3.26 and 3.27.

In Fig. 3.29, the frequency response is shown for the different recovery strategies. It is important to notice that all the strategies result in two frequency dips: a high one due the disturbance and counteracted by the overproduction period and a low one, caused by the underproduction period. The optimal speed recovery strategy performs the worst as the power reference P_{ref} drops significantly during the recovery period. This can be seen in Fig. 3.28, where the optimal speed curve is shown by the dashed line. For a given rotational speed Ω, the power reference P_{ref} is indeed lower than for the constant underproduction strategy.

Three major conclusions can be derived:

- The choice of the recovery strategy has an important impact on the inertial response. The optimal speed and constant accelerating power recovery strategy have only a limited chance of unstable operation, whereas the constant underproduction power recovery is prone to instability.
- The parameters t_{OP} and ΔP_{OP} should be tuned together with the recovery strategy.
- All the temporary power strategies result in a second frequency dip, regardless of the recovery strategy. However, the optimal speed recovery strategy performs the worst.

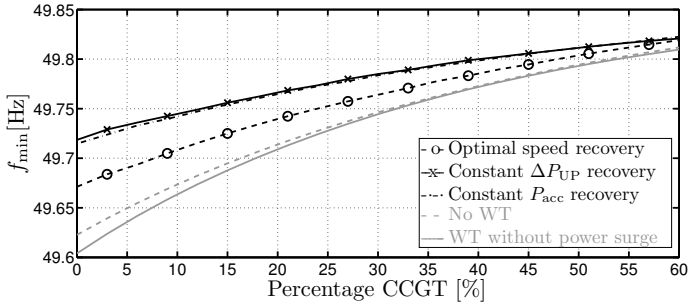

(a) Frequency nadir.

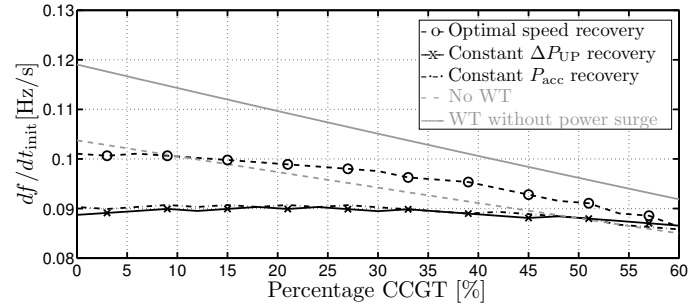

(b) ROCOF.

Figure 3.30: Frequency nadir and ROCOF in function of the system composition.

3.7.1.4 Optimal temporary power surge response for a varying system composition

In Fig. 3.30, the frequency nadir and ROCOF for optimal parameter selection for the different recovery strategies (i.e., highest frequency nadir $f_{\min}$) are shown. As expected, the frequency nadir is higher and the ROCOF is lower for systems with mainly CCGTs, as they respond faster on frequency changes. When wind turbines without emulated inertial response are added to the system, the frequency nadir decreases slightly and the ROCOF increases compared to the case without wind turbines in the system (gray curves). The black curves show that the temporary power surge is able to enhance the frequency response compared to the case without wind turbines for all the system compositions. The frequency response can be enhanced most for systems with mainly steam-based generators, as wind turbines can react faster than the units they replace.

When the different recovery strategies are considered, the constant underproduction strategy and the constant accelerating power strategy give the best results. The frequency nadir $f_{\min}$ and ROCOF df/dt_{init} are enhanced the most. The optimal speed recovery strategy performs worse than the other strategies, as the frequency nadir is much lower. Also the ROCOF is higher for the optimal speed recovery, as the optimal parameter selection results in a lower ΔP_{OP} (see Fig. 3.25a and 3.25b).

3.7.2 Conclusions

This section illustrates that the system composition has a huge impact on the optimal parameter selection of the temporary power surge strategy. Higher values for the overproduction step ΔP_{OP} are needed for power systems with mainly steam-based generators (i.e., 'slow' systems). The optimal parameter selection for one system could be very suboptimal for another system. Also, the recovery strategy has a tremendous impact on the optimal inertial response as well as on the parameter selection. The optimal speed recovery strategy results in a severe second frequency dip and consequently, the worst frequency response of the three considered strategies. The constant underproduction strategy results in a good inertial response, but might lead to unstable operation. The constant accelerating power strategy seems the most promising strategy as there is only little possibility of instability. However, knowledge of the wind speed is necessary to use this strategy as the wind speed is needed to keep the accelerating power P_{acc} constant. Consequently, the constant accelerating power strategy is the best recovery strategy, followed by the constant underproduction strategy. For the latter one, the parameters t_{OP} and ΔP_{OP} should be properly tuned to avoid instability.

3.8 Comparison between synthetic inertia and temporary power surge

In the previous sections, the optimal parameter selection of the synthetic inertia strategy and the temporary power surge were considered separately. Here, a comparison between the inertial response behavior of both strategies is made.

3.8.1 Frequency nadir and rate of change of frequency

When the frequency nadir $f_{\min}$ and the rate of change of frequency df/dt_{init} are compared for the optimal parameters of both strategies, the results are

quite similar as can be seen in Fig. 3.23 and Fig. 3.30.

Considering the frequency nadir, the temporary power surge with constant accelerating power and constant underproduction recovery strategy results in the highest frequency nadir, especially for low CCGT-percentages. The synthetic inertia strategy has a slightly lower frequency nadir, whereas the temporary power surge strategy with optimal speed recovery strategy has the lowest frequency nadir. The differences, however, are small. For high CCGT-percentages, all the emulated inertia strategies have the same frequency nadir. It is important to note that both strategies result in an enhanced frequency nadir compared to the cases without wind turbines or with wind turbines without emulated inertial response in the system.

When the rate of change of frequency is considered, some differences can be noted. The synthetic inertia strategy clearly results in the lowest rate of change of frequency, as is desired. A quasi-constant ROCOF can be obtained independent of the system composition. For the temporary power surge, however, the ROCOF depends strongly on the recovery strategy as the parameter selection that results in an enhanced frequency nadir might have an negative impact on the rate of change of frequency. Besides the temporary power surge with optimal speed recovery strategy, however, the ROCOF can be enhanced by using the emulated inertial response. Even for the optimal speed recovery strategy, the ROCOF is almost the same as for the power system were no wind turbines were considered. The ROCOF is clearly better than when the wind turbines were not equipped with the temporary power surge strategy.

In conclusion, when the frequency nadir $f_{\min}$ and ROCOF df/dt_{init} are considered, it is clearly beneficial to equip the wind turbines with an emulated inertial response strategy. Both strategies give similar results concerning the inertial response behavior. However, the parameter selection is more difficult for the temporary power surge than for the synthetic inertia.

3.8.2 Risk of instability

When the parameters of the different emulated inertial response strategies are tuned, care should be taken to avoid unstable operation of the wind turbine (i.e., extracting too much kinetic energy from the wind turbine which causes the wind turbine to slow down and eventually stop rotating).

For the synthetic inertia strategy, the risk of instability is very small. Only for high wind power penetrations and a system consisting of mainly 'slow' generation, e.g., steam-based generators, there is a small change of instability when both K_{in} and K_{droop} are chosen very high (see the small white area in Fig. 3.20). Furthermore, the optimal parameters are located far away from the instability range (i.e., $K_{\text{in}} \approx 0$), which further reduces

the risk of unstable behavior.

The main reason for the stability of the synthetic inertia strategy is the fact that the inertia and droop control loop are added to the maximum power point tracker. As the maximum power point tracker keeps activated during the inertial response, this provides a stabilizing effect on the control of the wind turbine.

For the temporary power surge strategy, however, the risk of instability is much larger (see Figs. 3.25, 3.26 and 3.27). There arises a risk of instability for high values of both ΔP_{OP} and t_{OP}. The power surge with optimal speed recovery or constant accelerating power recovery have the lowest chance of instability. Furthermore, the optimal parameter combination is far away for the unstable area, which reduces the risk of unstable behavior. The constant underproduction recovery strategy is prone to instability as the optimal parameter combination is close to the large unstable area.

Contrary to the synthetic inertia strategy, the maximum power point tracker is deactivated during the inertial response, so the stabilizing impact is not present here. Consequently, for the temporary power surge, it is very important to properly tune the control parameters and recovery strategy to avoid unstable operation.

3.8.3 Distributed recovery of wind turbines

As the temporary power surge results in a second frequency dip due to the recovery period, it is possible to allow a distributed recovery of the wind turbines in the power system to mitigate this secondary frequency dip [78]. Instead of allowing a simultaneous start of the underproduction period of all the wind turbines, a distributed recovery could be implemented. Due to the structure of the optimal speed recovery strategy and the constant accelerating power recovery strategy, it is not possible to alter the duration, start and depth of the underproduction period. Therefore, it is not possible to use the distributed recovery period without changing the type of recovery period. Therefore, the distributed recovery strategy is only applicable for the constant underproduction strategy. For the synthetic inertia strategy, there is no secondary frequency dip, so no distributed recovery is needed.

Moreover, the distributed recovery of wind turbines in the power system requires a certain coordination between the different turbines. This might require communication between the different wind farms. As primary frequency control and inertial response is an automatic (and necessarily rapid) response of the generators in the power system, it should rely as less as possible on inter-unit communication. Therefore, in this work, only an optimal parameter selection for all the wind turbines was assumed without the use of a distributed recovery strategy.

3.8.4 Advantages and disadvantages

Finally, now the optimal parameter selection for both strategies is discussed, the advantages and disadvantages of both strategies are summarized. Both strategies have the potential to enhance the frequency response by using the kinetic energy in the rotor, which is an advantage. Additional energy yield losses due to the suboptimal operation and additional torque variations arise due to the use of both emulated response strategies. These disadvantages are discussed in detail in Chapter 4. Here, some advantages and disadvantages that are specific for both strategies are listed.

3.8.4.1 Synthetic inertia strategy

Advantages

- **Simple control strategy:** the power reference P_{ref} is obtained as a combination of MPPT value P_{mppt} and a synthetic inertial response value. The synthetic inertial response reference can comprise a pure inertial response part P_{in}, which imitates the response behavior of a synchronous generator, and a droop part, which counteracts the initial behavior of the MPPT. As the synthetic inertial response value and the MPPT reference value are calculated independently, the synthetic inertial response strategy can be added easily to existing and new wind turbines.

- **No differentiation of the grid frequency needed:** as shown in this work, the inertial response term P_{in} can be omitted to obtain the optimal inertial response. Consequently, no differentiation of the grid frequency is needed which might result in oscillations in the wind turbine drive-train.

- **Stable control strategy:** as the MPPT is kept active during the inertial response, it is very difficult to obtain unstable operation with this strategy. Furthermore, the range of parameters that still enhance the frequency response is quite large, which reduces the risk of bad parameter selection.

- **Conventional frequency behavior:** as the additional power output is a combination of inertial control and droop control, the frequency behavior remains almost the same as in the conventional power system.

Disadvantages

- **Accurate measurement of the grid frequency needed:** as the set-points of the wind turbine are determined by the grid frequency, an accurate measurement is needed to apply this strategy.

3.8.4.2 Temporary power surge strategy

Advantages

- **Simple control strategy:** the power reference P_{ref} is obtained as a predefined function, which can be easily programmed into the control system of the wind turbines.
- **No accurate frequency measurement needed:** contrary to the synthetic inertia strategy, the additional power output is not dependent on the grid frequency. To activate the temporary power surge strategy, only a trigger based on the grid frequency (a certain threshold that is exceeded) is needed. Therefore, a less accurate frequency measurement can be used.
- **Commercially available:** some temporary power surge strategies are already available, e.g., *GE's WindInertia* and *Enercon Inertia Emulation* [103, 104].

Disadvantages

- **Difficult parameter selection:** as explained in § 3.7, the optimal parameter selection depends strongly on the choice of the recovery strategy. Furthermore, care has to be taken to avoid the unstable parameter range, which is much more pronounced than in the synthetic inertia strategy due to the deactivation of the MPPT during the inertial response.
- **Unknown frequency behavior:** as the additional power output is determined by a predefined function, it is very hard to predict the frequency behavior of the entire power system. The frequency response will be highly dependent on the amount of online wind turbines at the instant of the frequency event. In the case of little wind turbines in operation, the response will resemble the frequency response of the present system. When many wind turbines participate in the inertial response by means of a temporary power surge, the response will be be completely different (e.g., a pronounced secondary frequency dip might occur).

3.9 Conclusion

In this chapter, emulated inertial response with variable-speed wind turbines was discussed.

First, the need for inertia in the power system was clarified. Therefore, the inertial response in a power system with conventional generators was studied. Then, the inertial response behavior of wind turbines was investigated. It was shown that variable-speed wind turbines such as FSCs and DFIGs show no natural inertial response behavior due to the decoupling of the grid frequency f and the rotational speed Ω of the wind turbines.

Second, the possibility to use wind turbines for inertial response enhancement were summarized. As wind turbines have a similar amount of kinetic energy in their rotor inertia, they are perfectly suited to inject this kinetic energy into the power system when needed. In order to obtain this, an additional control loop has to be added in the wind turbine converter to inject the appropriate amount of power at the right time.

Third, two wide-spread options in literature to emulate inertial response with wind turbines are presented: the synthetic inertia strategy and the temporary power surge. When these strategies are studied in literature, they usually try to maximize the amount of kinetic energy that is injected into the system. However, the optimal amount of kinetic energy injection depends strongly on the system composition, as is explained in this chapter.

Therefore, in this work, a new method to determine the optimal parameter selection is derived for both strategies for different system compositions. It is shown that a correct parameter selection is important to obtain the desired inertial response. Furthermore, it is not necessary to inject much additional power, it just has to be injected at the right time in the right amount. The synthetic inertia strategy seems the most promising as it is the most stable emulation strategy. Obtaining the correct parameters for the temporary power surge is much more difficult as the recovery strategy has an important impact.

Another important outcome of this work, is that it makes no sense to mimic the inertial response behavior of a conventional synchronous generator. The optimal parameter selection shows that the inertial term (which mimics this behavior) can be omitted for the synthetic inertia strategy so it reduces to a droop control strategy. Also with the temporary power surge, it is possible to obtain a similar inertial response.

4

Side-effects of inertial response with wind turbines

In the previous chapter, the optimal parameter selection for both emulated inertial response strategies, i.e., synthetic inertia, and temporary power surge, was discussed in order to obtain an enhanced frequency response in the electric power system. However, providing emulated inertial response with wind turbines also has some side-effects. First, the additional energy yield losses due to the emulated inertial response are discussed. Contrary to the results found in literature, realistic cases without exaggerating the inertial response are discussed in this chapter. It is shown that the yield losses are quite limited, which is an advantage. Second, the additional load on the wind turbine drive-train due to the inertial response is discussed. A new control algorithm to avoid these rapid torque variations is developed in this PhD and presented in this chapter.

4.1 Energy yield losses due to emulated inertial response

In this section, the energy yield losses due to emulated inertial response are calculated for different situations. First, the reason for the energy yield

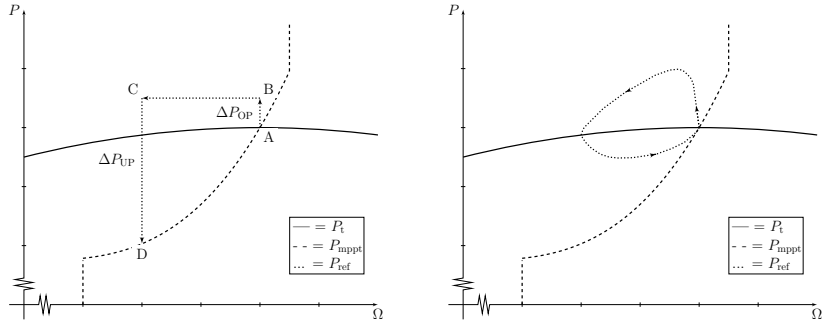

(a) Temporary power surge. **(b)** Synthetic inertia strategy.

Figure 4.1: Origin of the energy yield losses due to emulated inertial response.

losses is explained. Then, the losses are calculated for different scenarios for both inertial response strategies. As discussed in Chapter 3, only operation in the MPP before the disturbance is considered. If the wind turbines are operating in deloaded mode before the disturbance, this would result in continuous energy yield losses. The amount of losses then strongly depends on the percentage of deloading. However, the same calculation method can be used to calculate the energy yield losses in deloaded operation mode.

4.1.1 Origin of the energy yield losses

When wind turbines are operated in the maximum power point (MPP), kinetic energy has to be extracted from the rotor to provide an emulated inertial response. This results in operation below the MPP and therefore energy yield losses.

The origin of the energy losses is explained for the temporary power surge strategy with optimal speed recovery in Fig. 4.1a. A similar explanation can be given for the synthetic inertia strategy or for the temporary power surge strategy with another recovery strategy. Before the frequency disturbance, the wind turbine is operating in the MPP (A). When the control loop is triggered by a frequency dip, the power output P_{ref} is increased with ΔP_{OP}, so operating point B is reached. During the overproduction period t_{OP}, the turbine is decelerating until operating point C is reached. Then, the overproduction period is ended and the power output P_{ref} is decreased to allow an acceleration of the wind turbine. The reference value P_{ref} is again determined by the MPPT ($P_{\mathrm{ref}} = P_{\mathrm{mppt}}$) (D). The MPPT will drive the wind turbine to the original operating point (A) to end the emulated inertial response.

It is clear that during the inertial response the operating point is devi-

ating from the maximum power point, which results in an energy yield loss. This can be seen in Fig. 4.1a, where the mechanical input power P_{t} is slowly decreasing when the turbine changes from point B to C, which means that less energy is captured from the wind.

For the synthetic inertia strategy and the other recovery strategies, the reasoning is the same, but the path ABCD of the operating points during the frequency response will be different. An example of the operating point path during the synthetic inertia strategy is shown in Fig. 4.1b.

In [91], the energy yield losses are calculated for wind turbines equipped with the temporary power surge strategy. However, it is assumed that all the kinetic energy is extracted from the rotor during the frequency disturbance. This results in an extremely long recovery period and consequently very high energy yield losses. This is an unrealistic case, as it may result in a severe secondary frequency dip [67, 82]. Furthermore, as shown in § 3.6 and § 3.7, it is not beneficial to exaggerate the additional power output during the frequency dip. Therefore, here, the energy losses are calculated for more realistic cases for the synthetic inertia strategy and the temporary power surge strategy.

The energy yield losses per wind turbine per frequency event are given by:

$$E_{\mathrm{loss}} = \int_{t_0}^{t_1} \left(P_{\mathrm{t,without}}(t) - P_{\mathrm{t,with}}(t)\right) dt \tag{4.1}$$

with t_0 and t_1 the start and end time of the inertial response and $P_{\mathrm{t,with}}$ and $P_{\mathrm{t,without}}$ the mechanical power respectively with and without emulated inertial response. The start time t_0 is determined by the moment that the inertial response starts, i.e., the moment that the frequency dip is detected and the power output is increased. The end time t_1 is the moment that the power output of the wind turbine reaches again steady state operation in the MPP after the inertial response has finished.

4.1.2 Energy yield losses for the synthetic inertia strategy

In the following paragraphs, the energy yield losses per wind turbine per frequency event for the synthetic inertia strategy are calculated. First, the yield losses are calculated for the optimal parameters derived in § 3.6.4.8. Second, the yield losses are calculated for non-optimal parameters to study the effect of a non-optimal parameter selection on the energy yield losses.

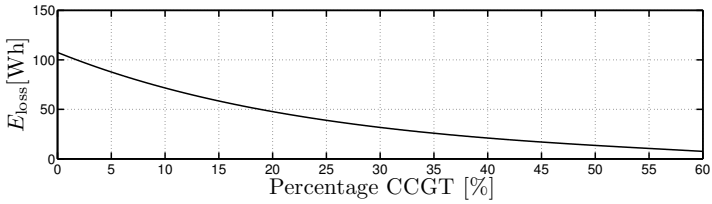

Figure 4.2: Energy yield losses per wind turbine per frequency event for the optimal parameter selection of the synthetic inertia strategy for a low wind power penetration (15 % wind power).

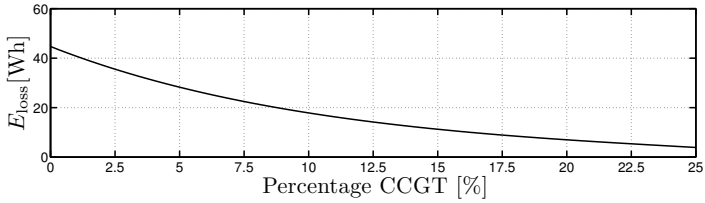

Figure 4.3: Energy yield losses per wind turbine per frequency event for the optimal parameter selection of the synthetic inertia strategy for a high wind power penetration (50 % wind power).

4.1.2.1 Optimal parameter selection

For the simulations with the optimal parameter selection, the same situation as in § 3.6.4.8 is considered. The simulation parameters are listed in Table 3.4. Two distinct scenarios are considered: a system with a low wind power penetration (15 %) and a high wind power penetration (50 %).

The results for the low wind power penetration are shown in Fig. 4.2. Here, the energy yield losses per frequency event for a single wind turbine are calculated. It is immediately clear that the losses are very limited for the optimal parameter selection. The losses are the highest for the system with mainly steam-based generators as the optimal droop constant K_{droop} is the highest for these power systems. Consequently, the additional power output is the highest for these systems and the suboptimal operation lasts longer than for systems with mainly CCGTs which explains the higher energy yield losses.

Similar results can be found for the high wind power penetration in Fig. 4.3. Again, the losses decrease with increasing percentages of CCGTs. Compared to the low wind power penetration case of Fig. 4.2, the energy yield losses are lower when the penetration of wind turbines increases. This

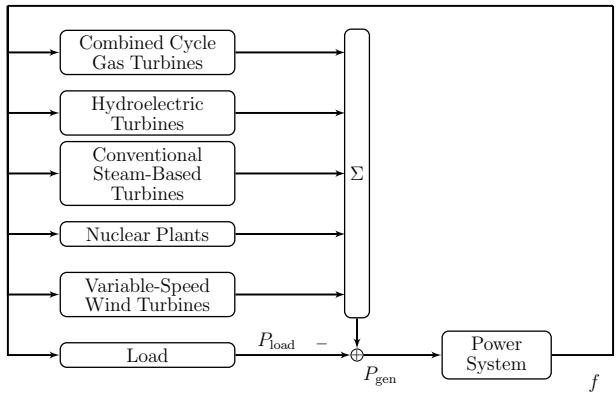

Figure 4.4: Electrical power system model.

is due to the lower optimal value for K_{droop} for a higher wind power penetration which results in lower energy yield losses.

Overall, it can be concluded that the use of the synthetic inertia strategy with optimal parameter selection only results in very limited energy yield losses. Consequently, the synthetic inertia strategy is perfectly suited to be used in wind turbines without affecting the energy yield.

4.1.2.2 Non-optimal parameter selection

For the simulations of the non-optimal parameter selection of the synthetic inertia strategy and the temporary power surge strategy, the power system of Fig. 4.4 is used. Besides the nuclear, steam-based and CCGT plants, also hydroelectric power plants are considered. The most important simulation parameters are listed in Table 4.1. Again, a power system of 150 GW is considered with a loss of 3 GW of production.

In this section, the energy yield losses per wind turbine per frequency event are calculated for the synthetic inertia strategy for varying parameters K_{in} and K_{droop}. A wind power penetration of 15 % is considered. In order to obtain the best inertial response, both parameters should be changed independently as was shown in § 3.6. Here, only the energy yield losses are of interest, so both parameters are altered together by multiplication with a scaling factor α:

$$K_{\text{in}} = \alpha \cdot K_{\text{in,n}} \qquad K_{\text{droop}} = \alpha \cdot K_{\text{droop,n}} \tag{4.2}$$

where $K_{\text{in,n}}$ and $K_{\text{droop,n}}$ are listed in Table 4.1.

From Fig. 4.5 and 4.6, the effects of the parameter variation are immediately clear. An increasing α results in a higher increase of electrical

Param.	Value	Unit	Param.	Value	Unit
$P_{\mathrm{t,nom}}$	3.0	MW	P_{ccgt}	23	%
r	56	m	P_{hydro}	7	%
ρ	1.225	kg/m^3	P_{steam}	30	%
v	10.0	m/s	P_{nuc}	25	%
$K_{\mathrm{in,n}}$	$5.19 \cdot 10^5$	Ws/Hz	P_{wind}	15	%
$K_{\mathrm{droop,n}}$	$1.62 \cdot 10^5$	W/Hz	P_{disturb}	3.0	GW
$\Delta P_{\mathrm{OP,n}}$	0.001	pu	P_{load}	150.0	GW
$t_{\mathrm{OP,n}}$	1.0	s	dP/dt_{max}	300.0	kW/s
ΔP_{UP}	$0.5 \cdot \Delta P_{\mathrm{OP}}$	p.u.	t_{D}	5	s
P_{acc}	$0.25 \cdot \Delta P_{\mathrm{OP}}$	p.u.			

Table 4.1: Simulation parameters for § 4.1.2.2 and § 4.1.3.2.

power during the inertial response. Consequently, the rate of change of frequency (ROCOF) df/dt_{init} decreases for increasing α as is expected when more inertia is emulated. The frequency nadir f_{min}, however, behaves differently. First, the minimum frequency is improved for increasing α. When α is higher than 5, the minimum frequency starts to decrease again. The reason for this behavior is an excessive power increase during the inertial response. The excessive inertial response of the wind turbines causes a slower response of the primary control of the conventional plants, which reduces the minimum frequency, as was explained in the previous chapter.

The energy yield losses increase with increasing α and are very low for all values of α. When α is 5, which gives the highest frequency nadir of the simulated cases, an energy yield loss of only 26.4 Wh per wind turbine is observed. Even for the worst parameter combination that is simulated ($\alpha = 15$), the energy yield losses are only 430 Wh, which is still very low. Consequently, it can be concluded that the energy yield losses are very low for the synthetic inertia strategy, even if the response is exaggerated (high α) and non-optimal parameters are selected. Furthermore, from a system point of view, it makes no sense to provide an excessive inertial response, since it only worsens the frequency nadir f_{min}.

4.1.3 Energy yield losses for the temporary power surge strategy

Similar to the synthetic inertia strategy, the energy yield losses per wind turbine per frequency event are calculated for the temporary power surge

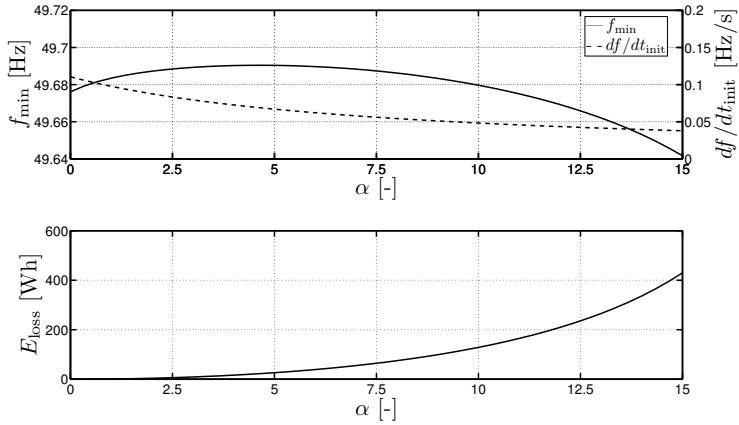

Figure 4.5: Frequency nadir, ROCOF and energy yield losses per wind turbine per frequency event for different non-optimal parameter selections of the synthetic inertia strategy.

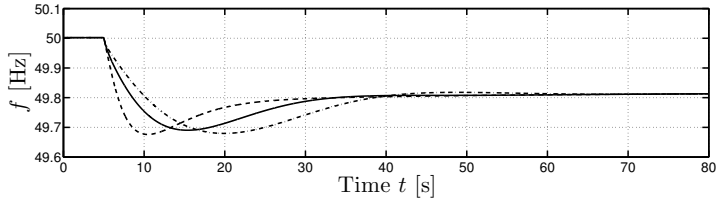

Figure 4.6: Frequency variation for $\alpha = 0$ (- -), $\alpha = 5$ (—) and $\alpha = 10$ ($\cdot$—) for the synthetic inertia strategy.

for both optimal parameter selection (derived in § 3.7) and non-optimal parameters.

4.1.3.1 Optimal parameter selection

In Fig. 4.7, the simulation results for the optimal parameter selection for the temporary power surge strategy are summarized. The three different recovery strategies are considered. Similar to the synthetic inertia strategy, the losses depend strongly on the system composition. The higher the amount of CCGTs, the lower the energy yield losses are. For systems with mainly gas turbines, the need for additional inertial response from the wind turbines is lower, so the wind turbines only have to work in a suboptimal operating point for a very limited amount of time. Consequently, the yield losses are limited.

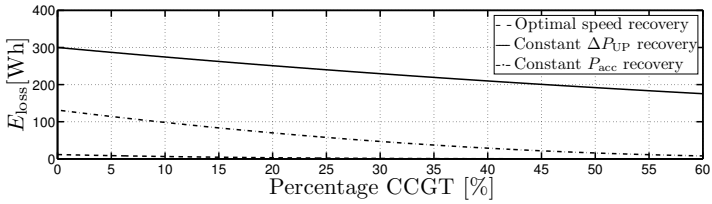

Figure 4.7: Energy yield losses per wind turbine per frequency event for the optimal parameter selection of the temporary power surge strategy for a low wind power penetration.

However, there is a strong difference between the three recovery strategies. The optimal speed recovery strategy results in the lowest energy yield losses. This is due to the rapid re-acceleration to the optimal operating point after the overproduction period. The constant accelerating power strategy has the second lowest energy yield losses of the three strategies as the recovery period is here longer than for the constant underproduction strategy. However, for the two last strategies, the length of the underproduction period can be affected by changing P_{acc} and ΔP_{UP}. Shortening the underproduction period results in lower energy yield losses, but increases the risk of a severe second frequency dip (see § 3.7).

Similar to the synthetic inertia strategy, the temporary power surge with optimal parameter selection results in only limited energy yield losses. Therefore, it can also be used to enhance the frequency response without affecting the energy yield of the wind turbine.

4.1.3.2 Non-optimal parameter selection

For the simulations of the non-optimal parameter selection for the temporary power surge strategy, the same simulation model and simulation procedure as in § 4.1.2.2 is used. The parameters ΔP_{OP} and t_{OP} are scaled with α:

$$\Delta P_{\mathrm{OP}} = \alpha \cdot \Delta P_{\mathrm{OP,n}} \qquad t_{\mathrm{OP}} = \alpha \cdot t_{\mathrm{OP,n}} \tag{4.3}$$

where $\Delta P_{\mathrm{OP,n}}$ and $t_{\mathrm{OP,n}}$ are listed in Table 4.1. For the constant underproduction recovery strategy and the constant accelerating power strategy, also ΔP_{UP} and P_{acc} are scaled with α according to Table 4.1.

The energy yield losses and frequency behavior for the temporary power surge with optimal speed recovery strategy are shown in Figs. 4.8 and 4.9. The ROCOF decreases only slightly for increasing α. Initially, for low α, the frequency nadir is improved. For high values of α, the additional power

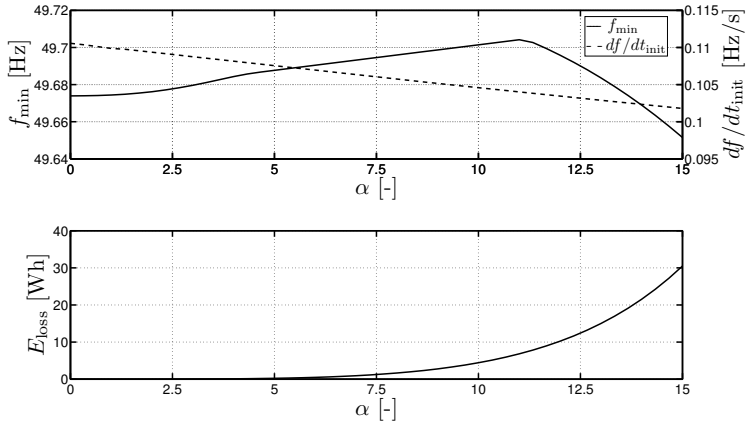

Figure 4.8: Frequency nadir, ROCOF and energy yield losses per wind turbine per frequency event for different non-optimal parameter selections of the temporary power surge with optimal speed recovery.

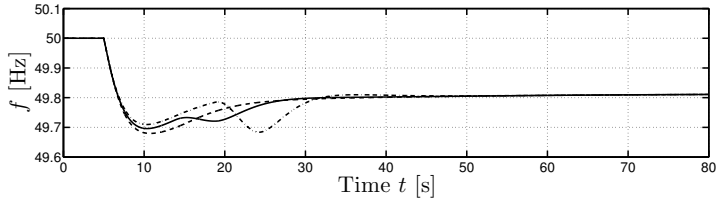

Figure 4.9: Frequency variation for $\alpha = 3$ (- -), $\alpha = 8$ (—) and $\alpha = 13$ ($\cdot$—) for the temporary power surge with optimal recovery strategy.

output is too high, which results in a second, lower frequency dip, as can be seen in Fig. 4.9. This second dip is caused by the recovery of the wind turbines, as explained earlier.

The energy yield losses are lower compared to the synthetic inertia case due to the very fast optimal speed recovery of the wind turbines after the inertial response. This very fast recovery causes the second frequency dip and complicates the parameter tuning. Again, excessive inertial response has to be avoided as the energy yield losses increase for increasing α without improving the frequency response.

In Figs. 4.10 and 4.11, the energy yield losses and frequency behavior for the temporary power surge with constant underproduction recovery are summarized. Again, the ROCOF decreases slightly with increasing α. The frequency nadir $f_{\min}$ increases with increasing α. Contrary to the previ-

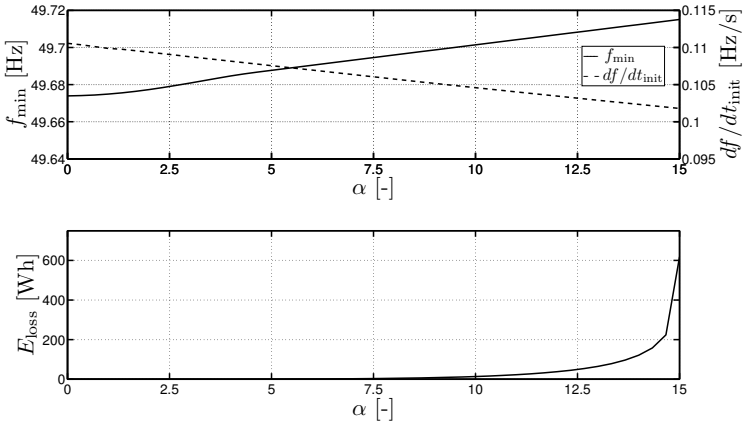

Figure 4.10: Frequency nadir, ROCOF and energy yield losses per wind turbine per frequency event for different non-optimal parameter selections of the temporary power surge with constant underproduction recovery.

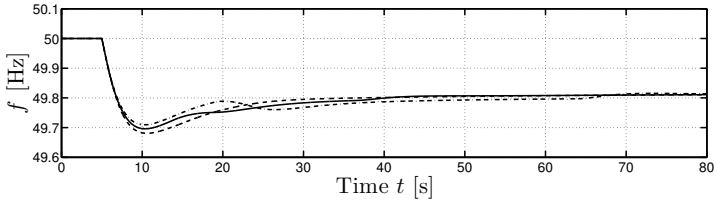

Figure 4.11: Frequency variation for $\alpha = 0$ (- -), $\alpha = 5$ (—) and $\alpha = 10$ ($\cdot-$) for the temporary power surge with constant underproduction recovery.

ous recovery strategy, the frequency nadir keeps increasing for increasing α. However, if α is further increased, the inertial response strategy with constant underproduction becomes unstable. As explained in § 3.7, the optimal parameter combination is indeed close to the unstable region, which increases the risk of instability.

The energy yield losses are clearly higher for the constant underproduction strategy and are similar to the ones that are obtained for the synthetic inertia strategy. Due to the slower recovery of the wind turbine for this strategy, the wind turbine operates in a suboptimal operating point for a longer amount of time, which explains the higher yield losses.

Finally, the results for the constant accelerating power strategy are

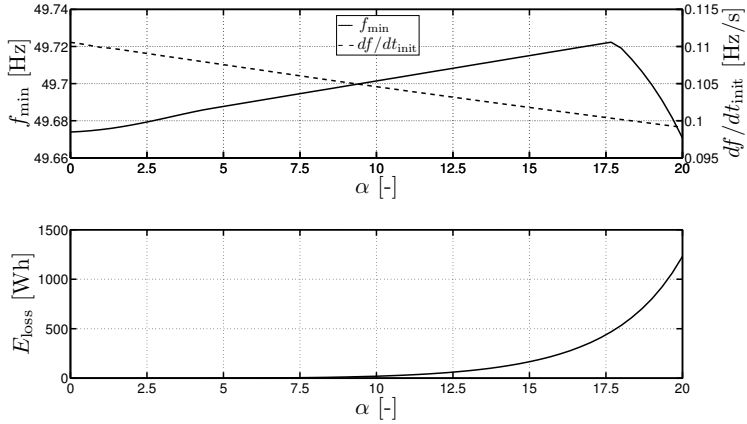

Figure 4.12: Frequency nadir, ROCOF and energy yield losses per wind turbine per frequency event for different non-optimal parameter selections of the temporary power surge with constant accelerating power recovery.

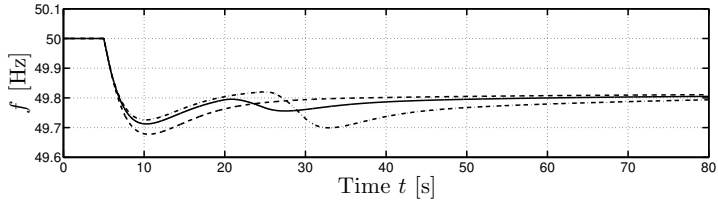

Figure 4.13: Frequency variation for $\alpha = 2$ (- -), $\alpha = 14$ (—) and $\alpha = 19$ ($\cdot-$) for the temporary power surge with constant accelerating power recovery.

shown in Figs. 4.12 and 4.13. The behavior of this strategy is in between the two previous strategies. The recovery step ΔP_{UP} is usually steeper than for the constant underproduction strategy but less pronounced than for the optimal speed recovery. Consequently, the recovery time t_{UP} is longer than for the optimal speed strategy but shorter than for the constant underproduction strategy. Consequently, the energy yield losses are also in between. Again, the yield losses increase with increasing α, but are still low. Similar to the optimal speed recovery strategy, the frequency nadir $f_{\min}$ improves with increasing α, but rapidly decreases for very high values of α. Excessive inertial response should be avoided.

Overall, for the three strategies, the energy yield losses are very low

for all the parameter combinations. Dependent on the recovery strategy, they are lower than or equal to the values obtained for the synthetic inertia strategy.

4.1.4 Conclusion

In this section, the energy yield losses per wind turbine per frequency event were calculated for the synthetic inertia strategy and the temporary power surge strategy with different recovery strategies. Furthermore, the losses were calculated for optimal and non-optimal parameter selection. For both strategies and all the considered parameter combinations, the energy yield losses are very small, which is the desired result.

The reason for these low losses is the shape of the $C_\mathrm{p}(\lambda)$-curve. During the inertial response, the change of rotational speed Ω is limited, because excessive inertial response is usually avoided. As the $C_\mathrm{p}(\lambda)$-curve is quite flat around the MPP, the power coefficient only slightly deviates from its optimal value, which explains the low losses. This means that emulated inertial response can be provided with wind turbines with very little energy yield losses and a negligible loss of revenue. Consequently, emulated inertial response with wind turbines is a good way to support the grid in case of frequency disturbances.

4.2 Torque variations due to emulated inertial response

In this section, the impact of the emulated inertial response on the drive-train dynamics is investigated. To emulate the inertial response, rapid power variations are needed. This results in a fast variation of the load torque of the wind turbine, which is undesired. Therefore, a control strategy which mitigates these fast variations is presented.

4.2.1 Torque variations

In order to be able to provide emulated inertial response with wind turbines, additional electrical power has to be injected into the grid immediately after the disturbance. As the wind turbine is usually operating in the MPP, this additional energy has to be extracted from an energy buffer in the wind turbine, which is the total turbine inertia J_wt. The power controller of the generator-side converter controls the power that is extracted from the wind turbine rotor by changing the generator current I_g and consequently changing the generator torque T_g. The fast changes in the reference power

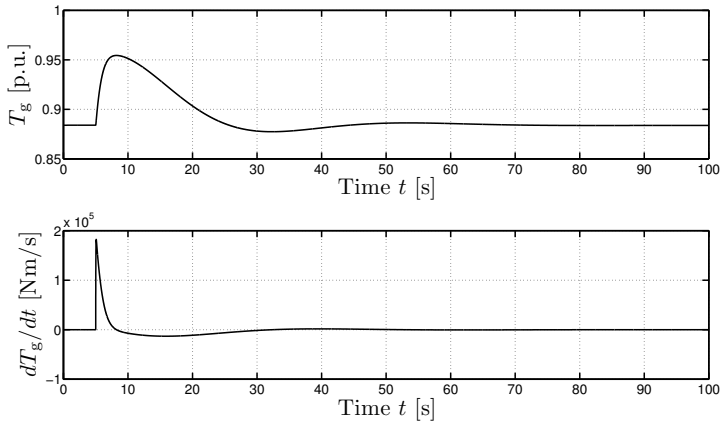

Figure 4.14: Example of the torque variation for the synthetic inertia strategy.

output P_{ref} result in a rapidly varying generator torque, as is shown in the following paragraphs. These rapid torque variations might result in additional loading of the wind turbine drive-train and can excite mechanical oscillations in the drive-train or even the tower [105–108]. The additional loading and excitation of mechanical oscillations might result in a reduced lifetime of the wind turbine, which is undesired [106–108]. Therefore, these torque variations should be avoided as much as possible.

For the simulations in this section, the same simplified model for the wind turbine rotor and generator is used. The converter model is expanded to an averaged model of the generator-side converter, DC-bus and grid-side converter. A single mass model for the wind turbine drive train is used. This suffices to estimate the additional torque variations caused by the emulated inertial response. However, in order to study the impact of these variations on the drive train dynamics, mechanical oscillations, etc., a more detailed multiple mass model should be used, but this is out of the scope of this work.

4.2.1.1 Synthetic inertia

In Fig. 4.14, an example of the variation of the generator torque T_g and the variation rate dT_g/dt for the synthetic inertia strategy is shown. The optimal parameters for a system with 60 % steam and low wind power penetration (see § 3.6.4.4) are considered here, as this situation results in the highest emulated inertial response of the different cases that were studied in this work. The torque clearly increases due to the inertial response, but

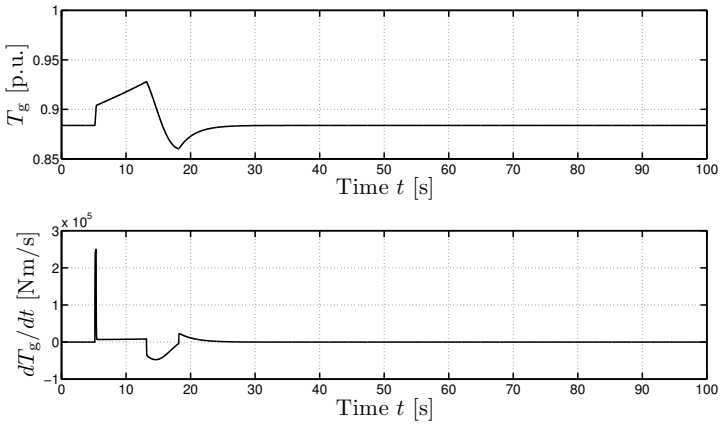

Figure 4.15: Example of the torque variation for the temporary power surge with optimal speed recovery strategy.

remains below 1 p.u.. As explained earlier, the power and torque are always below 1.1 p.u. for all the simulated cases.

However, when the rate of the torque variation dT_g/dt is considered, a sharp and steep peak can be noted immediately after the initiation of the inertial response. This means that the generator torque T_g varies rapidly due to the emulated inertial response. The power controller of the generator-side converter is able to track the rapidly varying reference power P_{ref} and change the generator current I_g accordingly which causes the fast torque variation. It is clear that the provision of synthetic inertia results in an additional loading of the drive-train.

4.2.1.2 Temporary power surge

In Figs. 4.15, 4.16 and 4.17, the generator torque variations for the temporary power surge with different recovery strategies are shown. Again, a power system consisting of 60 % steam-based generation and a low wind power penetration is considered. The optimal parameters for the different temporary power surge strategies derived in § 3.7.1.2 are used.

The results are in line with the ones obtained in § 3.7.1.2. The lowest inertial response is obtained for the temporary power surge with optimal speed recovery, followed by the temporary power surge with constant accelerating power and constant underproduction. Similar to the synthetic inertia strategy, the power output remains well below 1 p.u.. The longer recovery periods for the constant underproduction and constant accelerating power strategy are clearly visible in the variation of the generator torque

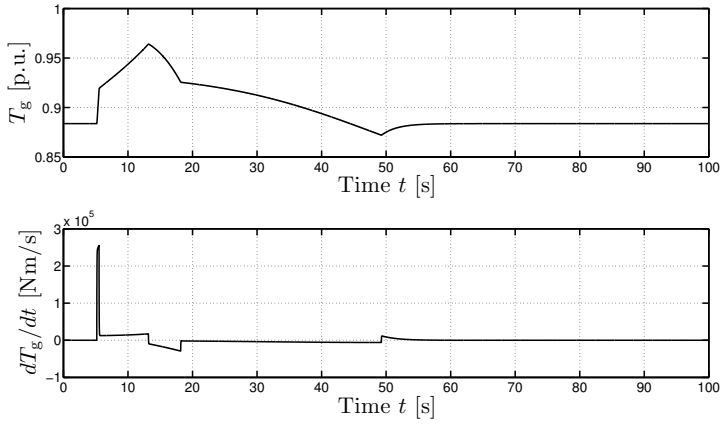

Figure 4.16: Example of the torque variation for the temporary power surge with constant underproduction recovery.

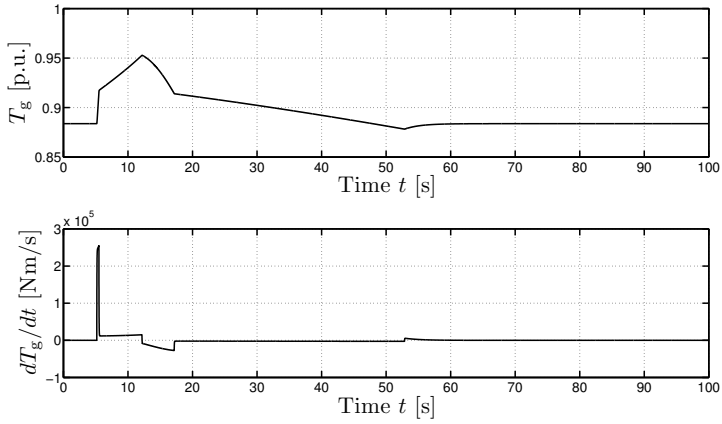

Figure 4.17: Example of the torque variation for the temporary power surge with constant accelerating power recovery.

T_g.

However, when the torque variation rate dT_g/dt is considered, the differences between the temporary power surges with different recovery strategies are less pronounced. All the temporary power surges have a very sharp peak in the torque variation rate dT_g/dt immediately after the activation of the emulated inertial response. The height of this peak is independent of the amount of additional power output ΔP_{OP}, but is solely determined by the fast increase rate of the power output immediately after the frequency dip. Furthermore, the torque variation rate dT_g/dt is higher for the temporary power surge strategy than for the synthetic inertia strategy. This is due to the steeper power increase for the temporary power surge compared to the synthetic inertia strategy.

A second difference between both emulated inertial response strategies is the smoother variation of the generator torque T_g for the synthetic inertia strategy. This is inherent to the synthetic inertia strategy as the additional power output varies proportional to the grid frequency f and the MPPT is kept active during inertial response. For the temporary power surge, the MPPT is deactivated and the power output is determined by a predefined curve, which results in a less smooth variation of the generator torque T_g.

4.2.1.3 Conclusion

As shown in the previous paragraphs, both emulated inertial response strategies result in a rapidly varying generator torque T_g. Especially the high peaks in the torque variation rate dT_g/dt immediately after the inertial response should be noted. These rapid variations in the generator torque result in an additional loading of the wind turbine drive-train. Therefore, in the next sections, a control method is proposed to mitigate these undesired torque variations.

4.2.2 DC-bus voltage modulation

In this section, a control strategy to mitigate the rapid torque variations, i.e., the DC-bus voltage modulation strategy, is presented. First, the energy buffers in a wind turbine system are identified. Second, the operating principle of the control strategy is explained.

4.2.2.1 Energy buffers

As discussed in § 4.2.1, the use of emulated response strategies such as the synthetic inertia strategy or temporary power surge strategies results in rapid torque variations that are caused by the sudden increase of the power output after a frequency dip.

In order to be able to increase the power output from a wind turbine that is operating in the maximum power point, energy should be extracted from an energy buffer. In the emulated inertial response strategies that are presented here, the inertia J_{wt} of the wind turbine is used as the energy buffer from which kinetic energy can be extracted by changing the rotational speed Ω from Ω_0 to Ω_1 (with $\Omega_1 < \Omega_0$):

$$\Delta E_{\mathrm{kin}} = \frac{1}{2} J_{\mathrm{wt}} \left(\Omega_0^2 - \Omega_1^2 \right) \tag{4.4}$$

After the disturbance, the rotational speed Ω returns to Ω_0 by allowing a recovery period of the wind turbine. Then, kinetic energy is stored in the inertia J_{wt}.

However, due to the configuration of modern wind turbines, there is also a second energy buffer in the system: the DC-bus. The DC-bus consists of capacitors C_{dc} that ensure a smooth operation of the back-to-back converter. Similar to the inertia J_{wt}, energy can be extracted from the DC-bus. In a capacitor C operating at a voltage V, the energy stored in the capacitor is given by:

$$E_c = \frac{1}{2} C V^2 \tag{4.5}$$

Consequently, by changing the voltage of the DC-bus V_{dc} from $V_{\mathrm{dc},0}$ to $V_{\mathrm{dc},1}$ (with $V_{\mathrm{dc},1} < V_{\mathrm{dc},0}$), energy can be extracted from the DC-bus capacitor:

$$\Delta E_{\mathrm{c}} = \frac{1}{2} C_{\mathrm{dc}} \left(V_{\mathrm{dc},0}^2 - V_{\mathrm{dc},1}^2 \right) \tag{4.6}$$

More energy can be stored in the DC-bus by increasing the DC-bus voltage.

Considering the storage capacity of the DC-bus, a difference should be made between the full-scale converter type and DFIG. In the full-scale converter wind turbines, the generator-side converter and grid-side converter are linked by means of a DC-bus. All the power that is produced by the wind turbine has to pass through both power-electronic converters and the DC-bus. For the doubly-fed induction generator wind turbines, there also is a DC-bus that links both power-electronic converters, but only part of the produced power passes through the rotor circuit of the DFIG and consequently through the power-electronic converters and DC-bus. Consequently, the rated power of the converters of the DFIG is lower and the DC-bus capacitors are smaller compared to the full-scale converter wind turbines. Consequently, the control strategy that is presented here is more suited for FSCs than for DFIGs. Therefore, we will only discuss FSCs from here on as they have the largest potential for mitigating the torque variations.

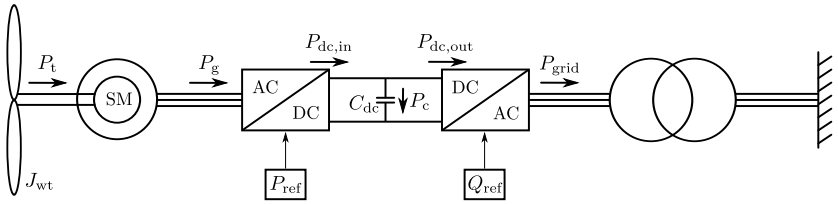

Figure 4.18: Power flow in a full-scale converter wind turbine.

4.2.2.2 Overview of the control strategy

In Fig. 4.18, an overview of the power flows in a FSC wind turbine is presented. The operation principle of the complete system, which was shortly described in § 2.2.2, is elaborated in more detail in order to explain the DC-bus voltage modulation strategy.

In a conventional wind turbine without inertial response, the power output of the wind turbine is maximized by means of the MPPT. The maximum power point tracker provides the reference value P_{ref} to the generator-side converter. This converter controls the generator current I_{g} to achieve a generator power P_{g} that equals P_{ref}:

$$P_{\mathrm{g}} = P_{\mathrm{ref}} \tag{4.7}$$

This is usually the case, as the PI current controller has a high bandwidth. If there was no inertia J_{wt} and a perfect MPPT was assumed, the wind turbine power P_{t} would equal the generator power P_{g}, taking into account the efficiency of the generator η_{g}:

$$P_{\mathrm{g}} = \eta_{\mathrm{g}} \cdot P_{\mathrm{t}} \tag{4.8}$$

The generator efficiency η_{g} depends on the generator torque T_{g} and rotational speed Ω [109]. In this idealized case, the MPPT is able to track the maximum power point perfectly which would result in a constant TSR:

$$\lambda = \lambda_{\mathrm{opt}} \tag{4.9}$$

This implies that the rotational speed Ω follows the variations of the wind speed v perfectly. However, in reality, the inertia J_{wt} is non-zero and the MPPT is not perfect which means that the wind turbine will always be operating around the MPP and the rotational speed Ω will be in the vicinity of Ω_{opt}. The lower the inertia J_{wt} and the better the MPPT performs, the closer the MPP will be tracked.

The generator power P_{g} is then injected into the DC-bus by the generator-side converter. When the losses of the converter are included, the power

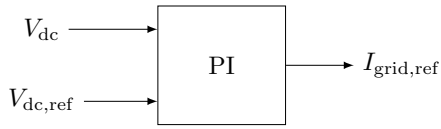

Figure 4.19: DC-bus voltage controller.

$P_{dc,in}$ is injected in the DC-bus:

$$P_{dc,in} = \eta_{rec} \cdot P_g \tag{4.10}$$

with η_{rec} the efficiency of the rectifier, which is again dependent on the operating point of the wind turbine (i.e., T_g and Ω) [109].

In order to balance the power $P_{dc,in}$ that is injected in the DC-bus and the power $P_{dc,out}$ that is extracted from the DC-bus, the grid-side converter is equipped with a DC-bus voltage controller. A schematic overview of the bus voltage controller is given in Fig. 4.19. The bus voltage V_{dc} is controlled to a set value $V_{dc,ref}$ by changing the current I_{grid} that is injected in the grid. The DC-bus voltage PI controller compares the measured DC-bus voltage V_{dc} to the set-point value $V_{dc,ref}$. If V_{dc} is below its set-point, more power is injected into the grid than there is injected into the bus. Consequently, the grid current I_{grid} has to be lowered. If the voltage is above the set-point, I_{grid} has to be increased. In this way, the DC-bus voltage is controlled by balancing AC and DC power. In the conventional control strategy, a constant DC-bus voltage set-point $V_{dc,ref}$ is used. The DC-bus voltage V_{dc} should not be too low in order to make sure that the injected current has an acceptable total harmonic distortion (THD).

The grid-side converter injects the power P_{grid} in the grid:

$$P_{grid} = \eta_{inv} \cdot P_{dc,out} \tag{4.11}$$

where η_{inv} is the efficiency of the grid-side inverter [109]. By controlling the phase angle of the injected grid current I_{grid}, the reactive power Q_{grid} can be controlled to the desired set-point Q_{ref}. In the conventional operation of a wind turbine, Q_{ref} is usually zero.

When the wind turbine is equipped with a standard emulated inertial response strategy such as the synthetic inertia or the temporary power surge, the active power reference value P_{ref} is not always determined by the MPPT. When a frequency disturbance occurs, P_{in} and P_{droop} are added to P_{mppt} to obtain the complete reference power P_{ref} for the synthetic inertia strategy. For the temporary power surge, the predefined power surge curve takes over during the inertial response. This means that kinetic energy will first

be extracted from the inertia J_{wt} and injected in the DC-bus. The bus voltage controller will keep the DC-bus voltage constant and consequently the additional power output will be injected in the grid. During the recovery period, less energy will be injected into the DC-bus by the rectifier and consequently the wind turbine will regain normal operation. Again, the DC-bus voltage controller will keep the DC-bus voltage constant by lowering the injected power in the grid. Consequently, the DC-bus voltage remains constant and the inertial response power is transferred to the grid. The wind turbine operates exactly the same as if no emulated inertial response was used, except the power output is adapted.

Here, the DC-bus voltage modulation strategy is presented in order to effectively use the second energy buffer that is present in the wind turbine system. Instead of injecting only kinetic energy from the inertia J_{wt} in the grid during the inertial response, also electrical energy stored in the DC-bus capacitor C_{dc} can be injected in the grid. If the moments of the energy injections are properly coordinated, this strategy can be used to limit the torque variations by limiting E_{kin}. Additional power can be extracted from the capacitors and injected in the grid by varying the DC-bus voltage. The relationship between the additional power and the voltage variation is derived next.

Considering Fig. 4.18, the power balance of the DC-bus is given by:

$$P_{\mathrm{dc,out}} = P_{\mathrm{dc,in}} - P_{\mathrm{c}} \tag{4.12}$$

which results in:

$$C_{\mathrm{dc}} \cdot V_{\mathrm{dc}} \frac{dV_{\mathrm{dc}}}{dt} = P_{\mathrm{dc,in}} - P_{\mathrm{dc,out}} \tag{4.13}$$

In normal operation, $P_{\mathrm{dc,in}}$ and $P_{\mathrm{dc,out}}$ are balanced so V_{dc} remains constant. If we want to extract additional inertial response power $P_{\mathrm{incdc}}(t)$ from the DC-bus, (4.13) reduces to:

$$C_{\mathrm{dc}} \cdot V_{\mathrm{dc}} \frac{dV_{\mathrm{dc}}}{dt} = -P_{\mathrm{incdc}}(t) \tag{4.14}$$

By rearranging (4.14) we can obtain V_{dc} as a function of the desired additional inertial response power $P_{\mathrm{incdc}}(t)$:

$$C_{\mathrm{dc}} \cdot \frac{1}{2} \frac{d}{dt} \left(V_{\mathrm{dc}}^2\right) = -P_{\mathrm{incdc}}(t) \tag{4.15}$$

$$\frac{d}{dt} \left(V_{\mathrm{dc}}^2\right) = -\frac{2P_{\mathrm{incdc}}(t)}{C_{\mathrm{dc}}} \tag{4.16}$$

$$V_{\mathrm{dc}}^2 = \int_{t_1}^{t_2} -\frac{2P_{\mathrm{incdc}}(t)}{C_{\mathrm{dc}}}\, dt + \mathrm{cst} \tag{4.17}$$

The constant term can be determined by assuming that the DC-bus voltage V_{dc} was the nominal set-value $V_{\mathrm{dc,nom}}$ before the disturbance. Consequently, (4.17) reduces to:

$$V_{\mathrm{dc}}^2 = \int_{t_1}^{t_2} -\frac{2P_{\mathrm{incdc}}(t)}{C_{\mathrm{dc}}}\,dt + V_{\mathrm{dc,nom}}^2 \tag{4.18}$$

$$V_{\mathrm{dc}} = \sqrt{\frac{-2\int_{t_1}^{t_2} P_{\mathrm{incdc}}(t)\,dt + C_{\mathrm{dc}}V_{\mathrm{dc,nom}}^2}{C_{\mathrm{dc}}}} \tag{4.19}$$

where t_1 and t_2 represent the start and the end time of the inertial response (t_1 is considered as zero when the inertial response starts). Consequently, by using (4.19), the set-point for the DC-bus voltage V_{dc} can be calculated which results in an additional power output $P_{\mathrm{incdc}}(t)$ at time t.

In the next sections, this method is applied to both inertial response strategies in order to limit the torque variations. By using an appropriate time sequence for $P_{\mathrm{incdc}}(t)$, the torque variations can be limited.

4.2.3 Application of the DC-bus voltage modulation

In the previous section, the overall control principle of the DC-bus voltage modulation strategy was presented. Here, the strategy will be applied to the two emulated inertial response strategies. As the actual implementation differs strongly for the two strategies, they are discussed separately. Simulations are performed to show the advances of the DC-bus voltage modulation strategy.

4.2.3.1 Application to the synthetic inertia strategy

From § 4.2.1.1, it is clear that the strongest torque variation occurs immediately after the frequency disturbance. Ideally, this initial and fast increase in the power output is covered by additional power extracted from the DC-bus. The desired power flow is as follows:

- Immediately after the disturbance, the DC-bus voltage modulation strategy is activated. An additional power P_{incdc} is extracted from the DC-bus by lowering the DC-bus voltage V_{dc}.
- Then the reference power P_{ref} is slowly increased to extract kinetic energy from the inertia J_{wt}. At the same time, the additional power output P_{incdc} is slowly decreased until all the additional power is extracted from the inertia J_{wt}.
- During the recovery period, the wind turbine is brought back to the optimal operating point by restoring the rotational speed Ω to the optimal speed Ω_{opt} and restoring V_{dc} to $V_{\mathrm{dc,ref}}$.

Unfortunately, it is hard to obtain this desired inertial response sequence for the synthetic inertia as the power output during the inertial response depends strongly on the rotational speed Ω. As can be seen in Fig. 4.20, the power output during the inertial response depends on the power output P_{mppt} of the maximum power point tracker. During the inertial response, the rotational speed Ω decreases due to the injection of kinetic energy in the grid. As P_{mppt} is a cubic function of the rotational speed Ω, this power reference decreases with decreasing rotational speed. As explained in § 3.4, the droop term P_{droop} is mainly added to the synthetic inertial response to counteract the behavior of this maximum power point tracker. Consequently, if P_{mppt} would be removed from the inertial response reference power P_{ref} and replaced by a constant pre-disturbance power value, this would result in an overreaction of the synthetic inertia strategy. This could result in a fast depletion of the kinetic energy and unstable operation of the wind turbine. Therefore, the MPPT is kept active during the inertial response.

This behavior of the MPPT complicates the use of the suggested DC-bus modulation sequence. If the additional power is initially only extracted from the DC-bus, the rotational speed Ω remains constant (when a constant wind speed v is assumed during the inertial response). If the conventional calculation method for P_{in} and P_{droop} is used, this would result in an excessive power output during the first seconds of the inertial response as the MPPT results in a constant power output. The rotational speed Ω remains unchanged as long as only energy from the DC-bus is extracted. Consequently, the inertial response would differ strongly from the optimal inertial response derived in § 3.4. Furthermore, it would be very difficult to obtain a smooth transition to the injection of kinetic energy from the inertia J_{wt} as then suddenly the MPPT starts to affect the inertial response.

From the above, it is clear that it is difficult to obtain a similar inertial response as in § 3.4 by applying the desired inertial response sequence. This makes it hard to compare the effect of the DC-bus voltage modulation strategy on the torque variations. Therefore, an alternative approach is used here for the synthetic inertia strategy. This approach results in a similar additional power output while reducing the torque variations.

In Fig. 4.20, the control scheme for the synthetic inertia strategy with DC-bus voltage modulation is shown. The total inertial response power $P_{\mathrm{ref,tot}}$ is calculated in the same way as for the conventional synthetic inertia strategy. However, for the same operating conditions (i.e., wind speed v, etc.), the power output will deviate slightly as the rotational speed variation will be different due to the use of the DC-bus as a second energy buffer. The total power reference $P_{\mathrm{ref,tot}}$ is then scaled with K_{J} in order to obtain the

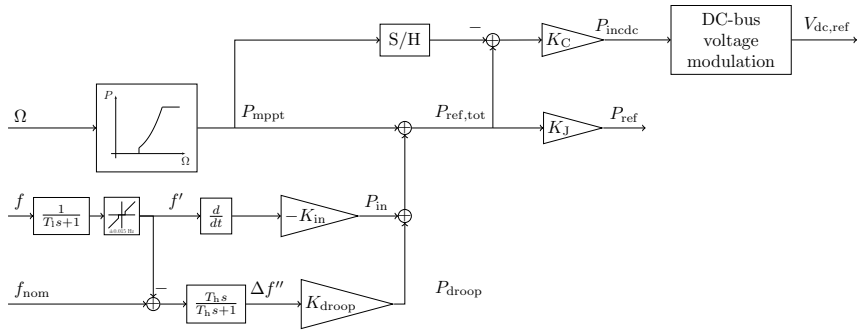

Figure 4.20: Control loop of the synthetic inertia strategy with DC-bus voltage modulation.

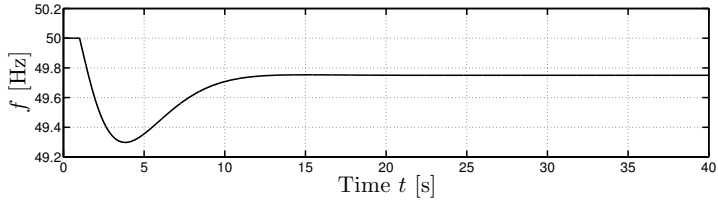

Figure 4.21: Frequency variation for the synthetic inertia strategy.

reference value P_{ref} for the generator-side converter. The additional power P_{incdc} is calculated by scaling the difference of $P_{\text{ref,tot}}$ and a sample and hold value (S/H) of P_{mppt} with K_{C}. At the moment the synthetic inertia strategy is activated, the MPPT power P_{mppt} is sampled and held constant until the inertial response has ended. In this way, P_{incdc} is only non-zero during the inertial response. In order to obtain a similar inertial response as without the DC-bus voltage modulation strategy, K_{J} and K_{C} are between 0 and 1 and their sum is 1. Here a value of 0.5 for K_{J} and K_{C} is used. Then the set-point for the DC-bus voltage $V_{\text{dc,ref}}$ is calculated by applying (4.19). Using this value as the set-point for the DC-bus voltage V_{dc} will result in an additional power injection from the DC-bus into the grid. When the inertial response has finished, the set-point for the DC-bus voltage $V_{\text{dc,ref}}$ is again determined by the nominal value and the power output P_{ref} is again determined by the maximum power point tracker. During the inertial response, the wind turbine remains within the operational limits (i.e., [Ω_{min} ... Ω_{max}], [$V_{\text{dc,min}}$ ... $V_{\text{dc,max}}$]). Next, some simulations are performed to show the functioning of the DC-bus voltage modulation strategy.

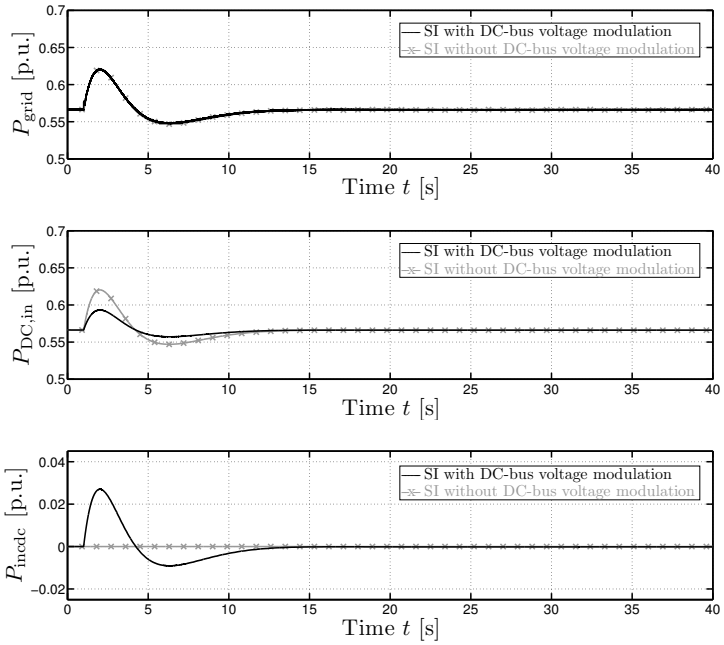

Figure 4.22: Power variations for the synthetic inertia strategy.

In Fig. 4.21, the frequency dip that occurs in the power system is shown. This frequency variation is used as an input for the synthetic inertia strategy. The additional power output due to the synthetic inertia strategy is presented in Fig. 4.22. It is immediately clear that there is a negligible difference between the power output P_{grid} for the conventional synthetic inertia strategy and the synthetic inertia strategy with DC-bus voltage modulation. Consequently, the resulting torque variations can be effectively compared. As expected, the power $P_{\text{DC,in}}$ that is injected in the DC-bus is smaller for the synthetic inertia with DC-bus voltage modulation as it is scaled with K_{J} and part of the additional power is extracted from the DC-bus. Indeed, P_{incdc} is non-zero for the DC-bus voltage modulation strategy and zero for the conventional synthetic inertia strategy. When the inertial response has ended, the power output P_{grid} returns back to the pre-disturbance value.

When the behavior of the energy buffers is compared in Fig. 4.23, it can be seen that for the conventional synthetic inertia strategy only energy is extracted from the inertia J_{wt}. This results in a strongly varying rotational speed Ω. The DC-bus voltage V_{dc} remains constant for the conventional strategy, as the DC-bus voltage is kept constant by the DC-bus voltage controller which balances AC and DC-power. For the SI with DC-bus volt-

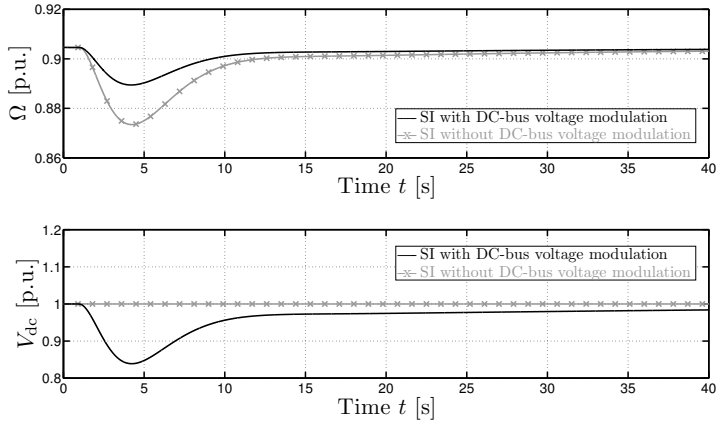

Figure 4.23: Variations of the rotational speed Ω and the DC-bus voltage V_{dc} for the synthetic inertia strategy.

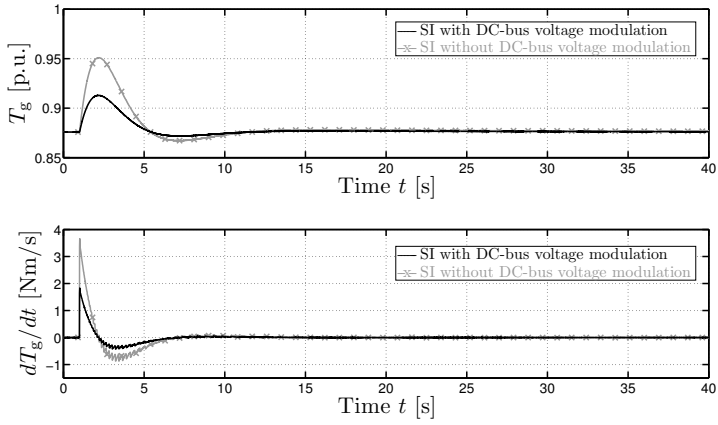

Figure 4.24: Torque variations for the synthetic inertia strategy.

age modulation, energy is extracted from both the inertia J_{wt} and DC-bus capacitors C_{dc}. This can be seen in the varying rotational speed Ω and DC-bus voltage V_{dc}. The variation in the rotational speed Ω is indeed smaller compared to the conventional case as part of the energy is extracted from the DC-bus. After the inertial response has finished, the rotational speed Ω and DC-bus voltage V_{dc} return to their pre-disturbance values.

Finally, in Fig. 4.24, the torque variations during the inertial response are presented. First, it can be noted that the increase in generator torque T_{g}

is much smaller for the synthetic inertia strategy with DC-bus voltage modulation than without the DC-bus voltage modulation. More importantly, also the torque variation rate dT_g/dt has decreased significantly when the DC-bus voltage modulation is applied, which is the desired result.

In conclusion, the DC-bus voltage modulation strategy seems a promising strategy to reduce the torque variations dT_g/dt for the synthetic inertia. The power output remains equivalent to the conventional SI strategy, while the torque variations are strongly reduced.

4.2.3.2 Application to the temporary power surge strategy

Here, the DC-bus modulation is applied to the temporary power surge strategy. Considering the different recovery strategies, a similar problem as for the synthetic inertia strategy arises: the power output depends on the maximum power point tracker, which makes it difficult to compare the torque variations with and without the DC-bus voltage modulation strategy. For the synthetic inertia strategy, the power output depends on the MPPT for the complete inertial response period, whereas for the considered temporary power surge strategies only the recovery period is affected:

- For the optimal speed recovery strategy, the power output during the recovery period is determined by the MPPT and consequently depends on the rotational speed Ω. The additional power output during the overproduction period remains unaffected.

- For the constant accelerating power recovery, the power output during the recovery period is determined by the wind turbine power P_t, which depends on the rotational speed Ω. Again, the power output during the overproduction period is unaffected.

- For the constant underproduction strategy, the power output does not depend on the rotational speed Ω for the overproduction period. For the underproduction period, the power output only depends on the rotational speed Ω for the transition to normal operation at the end of the underproduction period.

As the power output during the overproduction period does not depend on the MPPT for all the temporary power surge strategies and the fastest torque variations occur during the overproduction period, the results will be similar for the different recovery strategies. Therefore, here, only the temporary power surge with the constant underproduction recovery strategy is considered.

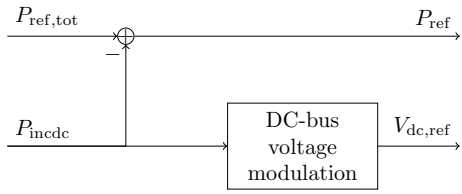

Figure 4.25: Control loop of the temporary power surge strategy with DC-bus voltage modulation.

Contrary to the synthetic inertia strategy, for the temporary power surge the desired power flow can be applied as the power output during the overproduction period does not depend on the rotational speed Ω:

1. Initially, inject only power from the DC-bus to limit fast torque variations.

2. Slowly increase the power extracted from the inertia while decreasing the power output from the DC-bus.

3. Recovery from both the rotational speed Ω and DC-bus voltage V_{dc}.

In Fig. 4.25, the control scheme for the temporary power surge with DC-bus voltage modulation is presented. The total inertial response power $P_{\mathrm{ref,tot}}$ that is desired for the inertial response, is given by one of the predefined reference curves presented in § 3.5. A second curve is constructed for the power P_{incdc} that has to be extracted from the DC-bus. By using an appropriate shape for this power set-point, the torque variations can be limited. This reference power is used as an input for the DC-bus voltage modulation strategy, which results in a set-point $V_{\mathrm{dc,ref}}$ for the DC-bus voltage V_{dc}. The DC-bus power set-point P_{incdc} is then subtracted from $P_{\mathrm{ref,tot}}$ to obtain the power reference P_{ref} for the generator-side converter. By applying this control to the wind turbine, the same inertial response as for the conventional temporary power surge is obtained, while reducing the generator torque variations. This is shown in the following simulations.

Again, the same frequency event is used to trigger the additional power output of the wind turbine (see Fig. 4.26). When the power output P_{grid} of the conventional temporary power surge strategy and the power surge with DC-bus voltage modulation are compared, the similarities are immediately clear. The additional power output during the overproduction period is the same for both strategies. Also the behavior during the underproduction period is quite similar. The underproduction period is slightly shorter for the temporary power surge with DC-bus voltage modulation as the wind

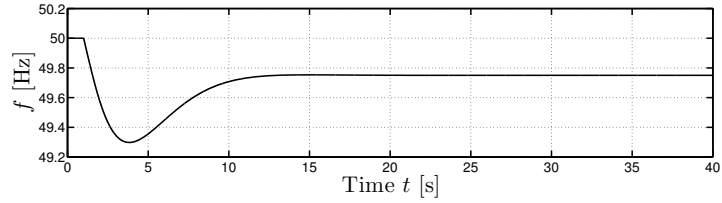

Figure 4.26: Frequency variation for the temporary power surge with constant underproduction strategy.

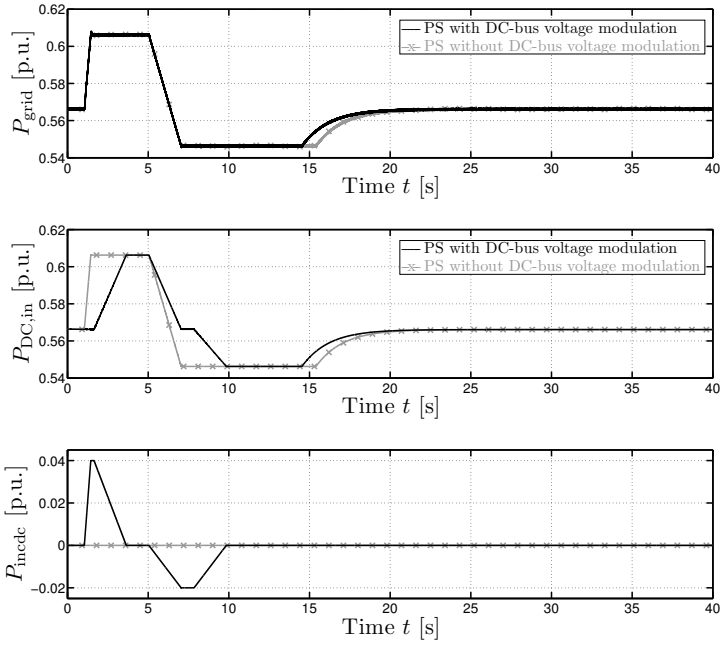

Figure 4.27: Power variations for the temporary power surge with constant underproduction strategy.

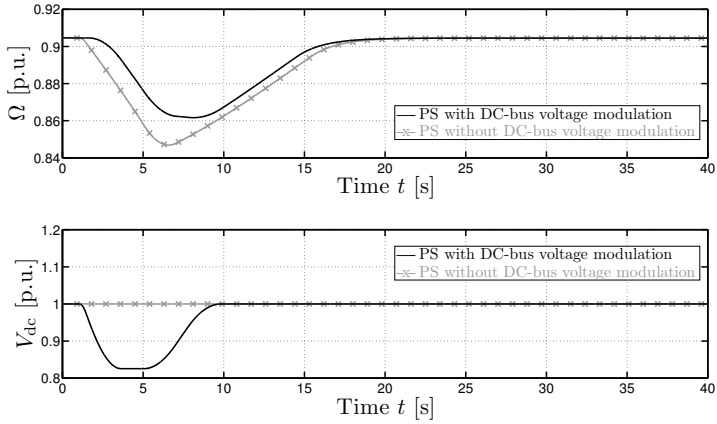

Figure 4.28: Variations of the rotational speed Ω and the DC-bus voltage V_{dc} for the temporary power surge with constant underproduction strategy.

turbine operates for a shorter period below the MPP which results in less energy yield losses. The reference value for the additional power P_{incdc} extracted from the DC-bus follows the desired sequence. First, the steep power increase is completely covered by additional power from the DC-bus. Then the additional power output from the DC-bus is slowly increased. As the power reference P_{ref} for the generator-side converter is calculated as the difference between $P_{\mathrm{ref,tot}}$ and P_{incdc}, this results in a slowly increasing power $P_{\mathrm{DC,in}}$ that is injected in the DC-bus. When the overproduction period has finished, the recovery of both the rotational speed Ω and DC-bus voltage V_{dc} starts.

The behavior of the energy buffers J_{t} and C_{dc} is similar for the temporary power surge and the synthetic inertia strategy. For the temporary power surge with DC-bus voltage modulation, energy is extracted from both the inertia J_{t} and the DC-bus capacitors C_{dc}, whereas only energy from the inertia is extracted for the conventional temporary power surge.

Finally, the variation of the generator torque T_{g} is summarized in Fig. 4.29. It is clear that the variation of the torque is much smoother when the DC-bus voltage modulation strategy is applied. Furthermore, the peak torque is slightly lower for the temporary power surge with DC-bus voltage modulation. When the torque variation rate dT_{g}/dt is considered, the benefits of the DC-bus voltage modulation are clearly visible. The high torque variation rate immediately after the disturbance is reduced tremendously by applying this strategy. Consequently, the application of the DC-bus voltage

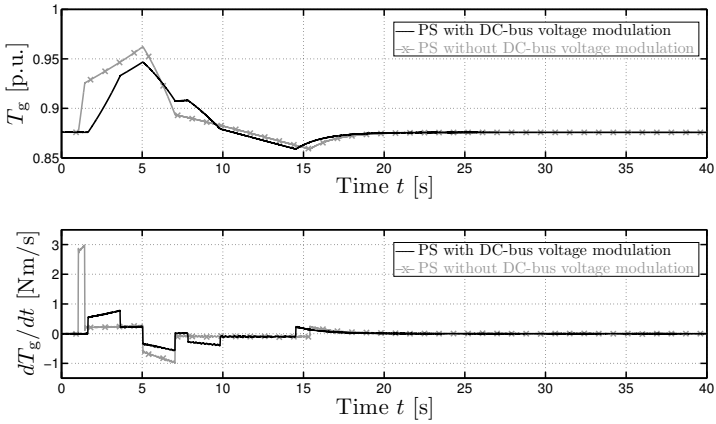

Figure 4.29: Torque variations for the temporary power surge with constant underproduction strategy.

modulation to the temporary power surge strategy results in lower torque variations without affecting its inertial response capability.

4.2.3.3 Size of the DC-bus capacitor

In order to effectively apply the DC-bus voltage modulation strategy, sufficient energy should be stored in the DC-bus capacitor. For the simulations in this section, the highest inertial response for all the considered system compositions were considered. For both emulated inertial response strategies, a substantial part of the energy was extracted from the DC-bus. For a wind turbine with a rated power of 3 MW and a DC-bus voltage that varies between 1150 V and 1000 V, a DC-bus capacitor of about 1 F is needed. Consequently, additional capacitance should be added to the existing DC-bus to apply the DC bus voltage modulation strategy. However, by further optimizing the extraction of energy from the DC-bus, a lower capacitor value could be achieved.

4.2.4 Conclusion

In this section, the torque variations due to the emulated inertial response were discussed. First, it was shown that the use of emulated inertial response strategies such as the synthetic inertia strategy and the temporary power surge strategy results in very fast variations of the generator torque. This induces additional loading of the wind turbine drive-train, which is undesired. Then, the DC-bus voltage modulation strategy was presented

in order to limit these torque variations. It was shown that the DC-bus voltage modulation strategy is able to reduce the torque variations for both emulated inertial response strategies.

4.3 Conclusion

In this chapter, the negative side-effects of the emulated inertial response with wind turbines were discussed.

First, the energy yield losses due to the emulated inertial response were calculated for optimal and non-optimal parameter selections. Both inertial response strategies were considered. The energy yield losses are very low for all the considered cases, which is the desired result. The reason for the low energy yield losses is the shape of the $C_{\mathrm{p}}(\lambda)$-curve, which is quite flat around the top and the limited variations of the rotational speed Ω that are needed to obtain the desired inertial response.

Second, the additional torque variations due to the emulated inertial response were considered. It was shown that the emulated inertial response strategies result in a steep increase in the generator torque immediately after the disturbance. These fast variations may result in additional loading of the wind turbine drive-train, which is undesired. Therefore, the DC-bus voltage modulation strategy was developed in this PhD. This strategy reduces the heavy torque variations by using the storage capacity of the DC-link. Simulations show that this strategy can be successfully applied on both inertial response strategies.

In conclusion, two important side-effects of the emulated inertial response with wind turbines were investigated. It was shown that the negative effects are either quite limited (energy yield losses) or can be effectively mitigated by introducing proper control strategies in the wind turbine controls (torque variations). Consequently, the negative effects of the inertial response do not outweigh its positive effects, i.e., a better integration of wind turbines in the power system. By adding the DC-bus voltage modulation strategy to the emulated inertial response strategies, a better grid integration of wind turbines could be achieved, while limiting the impact on the wind turbine drive-train dynamics.

5

Primary frequency control with wind turbines

In this chapter, first, an overview of primary frequency control with wind turbines is given. The deloaded operation of wind turbines to provide positive reserves is explained and different deloading strategies are presented. A new algorithm to determine the power reference values for constant power control and balance control is derived in this work. Then, a comparison is made between different control strategies to provide positive primary reserves with wind turbines. Finally, the adaptive droop control method is developed, which is a new method that allows a fair power sharing of the primary control action between different wind turbines in case of over-frequency events.

5.1 Primary frequency control

In this section, primary control with wind turbines is discussed. First, a short introduction is given and the control strategy is presented. Then, deloaded operation of wind turbines is discussed, together with the different deloading power references.

5.1.1 Introduction

At any given point in time, the amount of electricity that is produced equals the amount that is being consumed. This balance guarantees a stable operation of the electricity grid at the rated frequency f_{nom}. When there is a sudden disturbance in the grid (such as a drop in the electricity production or consumption), frequency deviations occur. To restore the frequency to its nominal value, the input of the generators has to be rapidly increased or decreased by means of the frequency control. This frequency regulation is achieved in three stages, of which the primary control is the first, automated one. In order to provide primary control, active power reserves have to be maintained at any point in time, which are often provided by conventional generators operating below their maximum power output.

As long as the wind power penetration is rather low, the necessary amount of primary control reserves can be provided by conventional power plants. However, when the penetration of wind turbines increases and they start to replace conventional power plants when they are taken out of service, this has a negative impact on the amount of available power reserves. This could endanger the proper functioning of the electric power system. A possible solution is to provide power reserves with wind turbines so they can participate in the balancing of the power system. Furthermore, by participating in the reserves market optimally, wind turbines can obtain a remuneration for these services and make profit, as is shown in [110, 111].

5.1.2 Control strategy

Primary control with wind turbines is achieved by adding an additional control loop to the wind turbine controller. Similar to the primary controller in a conventional power plant, a droop controller is used in the wind turbines. The control scheme is shown in Fig. 5.1. Consequently, the total reference power P_{ref} is given by:

$$P_{\text{ref}} = P_{\text{ref},0} + \Delta P_{\text{prim}} \tag{5.1}$$

where ΔP_{prim} is obtained as [42]:

$$\Delta P_{\text{prim}} = K_{\text{prim}} \left(f_{\text{nom}} - f \right) \tag{5.2}$$

The pre-disturbance power output $P_{\text{ref},0}$ depends on the operating strategy of the wind turbine, i.e., operation in the MPP or deloaded operation. The choice of this operating strategy depends on the desired primary control capability of the wind turbine, which is determined by the P/f-droop characteristic. In Fig. 5.2, two different P/f-droop characteristics are shown. The factor K_{prim} is determined as the slope of this characteristic.

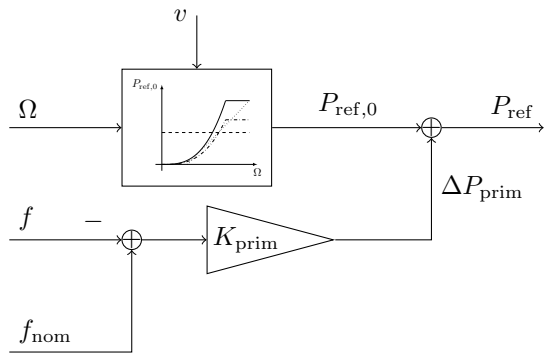

Figure 5.1: Control loop for primary frequency control.

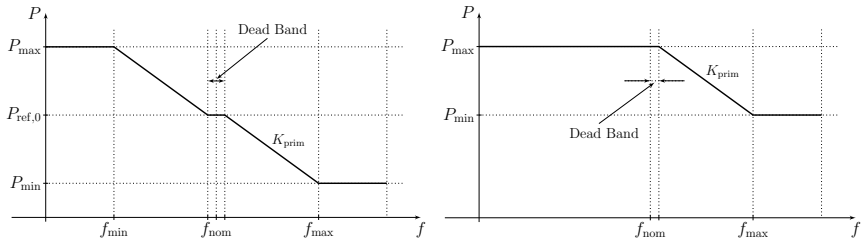

(a) Symmetric P/f-droop characteristic.

(b) Asymmetric P/f-droop characteristic.

Figure 5.2: P/f-droop characteristics.

If the asymmetric characteristic of Fig. 5.2b is used, only primary control in case of over-frequency events can be provided. The symmetric characteristic (Fig. 5.2a) enables the provision of complete primary frequency control, both in over- and under-frequency events. When the frequency exceeds the nominal frequency f_{nom}, the power output of the wind turbine is decreased (both characteristics). When the frequency is lower than the nominal frequency f_{nom}, the power output is increased (only for the symmetric characteristic). A dead band can be applied to prevent a frequency response from the wind turbine when the frequency deviation is small.

Decreasing the power output of the wind turbine is always possible by using either speed control or pitch control, so the asymmetric characteristic can be used on any wind turbine. Therefore, $P_{\mathrm{ref,0}}$ is determined by the maximum power point tracker P_{mppt} for the asymmetric droop curve. In order to obtain the complete primary control with the symmetric characteristic, the wind turbine has to be operated in deloaded mode. The deloaded

operation was shortly introduced in § 2.3.1.2. Here, a more extensive discussion will be presented. Another option is to include a storage facility (whether or not in the wind farm itself) to provide additional power in case of a frequency dip, but this is beyond the scope of this study.

Consequently, two distinct types of power reserves are needed to assist in primary frequency control:

1. **Negative reserves:** When there is a decrease in electricity consumption, the generation has to be decreased. The power output of wind turbines can be lowered quite easily by reducing the power coefficient C_p. Negative reserves can be provided anytime, which results in a temporary lower production.

2. **Positive reserves:** When there is an increase in electricity consumption, the generation has to be increased. If the turbine is operating in the MPP, the power production cannot be regulated upwards. Providing a positive power reserve with wind turbines implies that the wind turbine has to be operated suboptimally, which means a lower power production during normal operation.

The power reserve P_reserve of a wind turbine can be calculated as [90,112]:

$$P_\mathrm{reserve} = \eta_\mathrm{wt} \cdot (P_\mathrm{max} - P_\mathrm{t}) \tag{5.3}$$

with:

$$P_\mathrm{max} = \frac{1}{2}\rho\pi r^2 v^3 \cdot C_\mathrm{p,max} \tag{5.4}$$

and η_wt the efficiency of the wind turbine system given by:

$$\eta_\mathrm{wt} = \eta_\mathrm{g} \cdot \eta_\mathrm{rec} \cdot \eta_\mathrm{inv} \tag{5.5}$$

As the provision of positive reserves with wind turbine is clearly a challenging issue, this will be considered in the next paragraphs.

5.1.3 Deloaded operation of wind turbines

Complete primary frequency control with wind turbines is only possible if a power reserve is maintained at any point in time. To obtain a power reserve, the wind turbine has to be operated below the maximum power point, i.e. the deloaded operation mode. Deloaded operation is divided into two different methods: pitch control and speed control [80, 113]. Both methods are shown in Fig. 5.3.

5.1.3.1 Pitch control

This control strategy makes use of the pitch mechanism in wind turbines. Nowadays, wind turbines are usually operated to extract the maximum wind power. This implies operation at the minimum pitch angle, as can be seen in Fig. 5.3a. Only for wind speeds above the nominal wind speed, the power output of the wind turbine is limited to the rated power by means of pitch control. Indeed, increasing the pitch angle results in a lower power coefficient C_p and consequently a lower power yield for the wind turbine.

However, pitch control can also be used to obtain a power reserve for the provision of primary control with wind turbines. During normal operation, an increased pitch angle is used to obtain deloaded operation. In this way, the power output of the wind turbine is limited to a value lower than the maximum power output for the given wind speed. The resulting power reserve can be delivered by decreasing the pitch angle so that the turbine can extract more power from the wind in case of a frequency dip. Since the deloading is obtained by pitching the turbine blades, the turbine can be operated in the maximum power point of the deloaded curve. The optimal speed controller of the wind turbine can be used to track this maximum.

The main advantage of pitch control is its simplicity: the optimal speed controller can still be used, only the blades have to be pitched. Furthermore, the wind turbine can operate in deloaded mode without the need for an accurate measurement of the wind speed. When this strategy is used, measures should be taken to avoid excessive pitch control actions in case of small frequency deviations. A dead band or a filter on the frequency measurement or the rotational speed measurement could be added to avoid this. However, pitch control will still result in additional pitch control actions in order to deload the wind turbine, which will cause more wear of the pitch mechanism. Furthermore, the response of pitch control is slower than for speed control due to delays in the actuation of the pitch mechanism [113]. This limits the use of pitch control in inertial response strategies. This is less a problem for the provision of primary reserves, since this occurs on a longer timescale than the inertial response.

5.1.3.2 Speed control

Another way to deload a wind turbine, is by means of rotational speed control. From Fig. 5.3b, it is clear that there exists an optimal rotational speed Ω_opt for every wind speed. This optimal rotational speed Ω_opt results in the maximum power output for the given wind speed v. However, if the turbine operates at a lower or higher rotational speed, the power coefficient C_p decreases and the power output is lower. This behavior is used in the

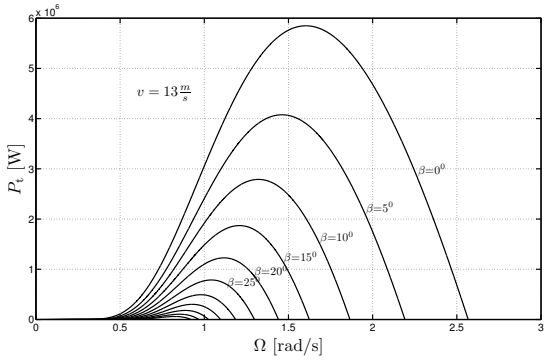

(a) Pitch control.

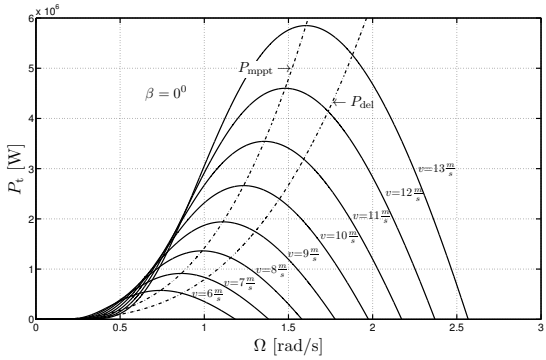

(b) Speed control.

Figure 5.3: Deloaded operation of wind turbines.

speed control strategy.

The rotational speed Ω of the wind turbine is controlled by means of the power electronic converter. For a given pitch angle β, the maximum power point reference curve P_{mppt} is a cubic function of the rotational speed Ω [37, 114]:

$$P_{\text{mppt}} = \frac{1}{2}\rho\pi r^5 \frac{C_{\text{p,max}}}{\lambda_{\text{opt}}^3} \cdot \Omega^3 \tag{5.6}$$

$$= K_{\text{mppt}}\Omega^3 \tag{5.7}$$

When the power output of the converter is controlled according to this reference value, the maximum power is extracted from the wind. If, however, a suboptimal reference curve is used in the power electronic converter, the rotational speed Ω will be altered and less power will be extracted from the wind. According to Fig. 5.3b, it is possible to shift the maximum power

point curve P_{mppt} to the left, which results in a lower rotational speed Ω or to the right, towards a higher rotational speed Ω. Shifting the reference curve to the left may result in stability problems [80, 113], so deloading via underspeeding will be ignored. The reason for these stability problems is illustrated in Fig. 5.4. To obtain a stable operation of the wind turbine in steady state, the tip-speed ratio λ should be higher than the one corresponding to the maximum of the torque coefficient C_{t}. For all the tip-speed ratios to the right of the top of the C_{t}-curve, an increasing rotational speed Ω results in a decreasing wind turbine torque T_{t} and vice versa. For a given load torque T_{g}, a small disturbance from the equilibrium point will always result in a stabilizing effect of the wind turbine torque. If the rotational speed slightly increases, the wind turbine torque will decrease, which results in a torque deficit (the driving torque is smaller than the load torque). This causes the wind turbine to slow down again. The opposite holds for a small decrease in the rotational speed Ω as the wind turbine torque will increase, causing the wind turbine to accelerate to the equilibrium point again. For all values of λ to the left of the top, this stabilizing effect is not present as a decreasing rotational speed Ω results in a decreasing wind turbine torque T_{t}, which is unstable behavior. Transiently, it is allowed to operate at a lower tip-speed ratio λ for a short time. However, if the tip-speed ratio λ is too low for a longer time, the wind turbine will stall, which has to be avoided. In Fig. 5.4, the stable part of the C_{p} is highlighted in bold. It is immediately clear that the risk of stability problems is much higher for underspeeding than for overspeeding. Therefore, only speed control by means of over-speeding will be considered. An example of a shifted, deloaded, reference curve P_{del} is given in Fig. 5.3b. When this curve is used to obtain the power reference P_{ref} for the power electronic converter, the wind turbine operates in deloaded mode and a power reserve is available at any point in time.

It is important to note that every wind turbine has a maximum rotational speed Ω_{max}. This maximum rotational speed may limit the applicability of deloading via speed control when the desired rotational speed to obtain a power reserve is higher than the maximum rotational speed Ω_{max}. Therefore, three different wind speed regimes can be identified:

- **low wind speed:** deloading can be achieved by speed control alone
- **medium wind speed:** deloading is achieved by a coordinated use of speed and pitch control
- **high wind speed (above the nominal wind speed):** deloading can only be achieved by pitch control, since the desired rotational speed is always higher than the maximum rotational speed

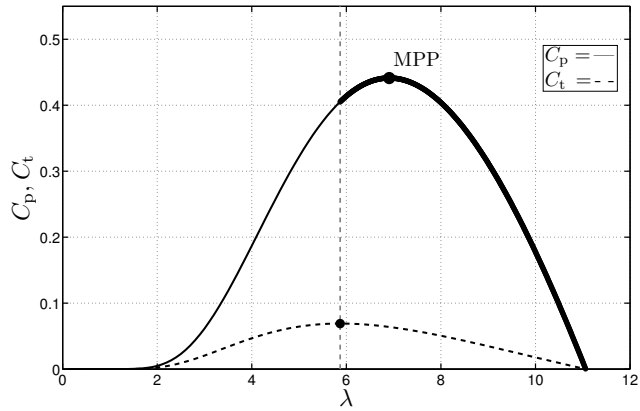

Figure 5.4: C_p and C_t -curves.

The main advantage of speed control is that the power output of the wind turbine can be increased or decreased very fast due to the converter control. Furthermore, since no pitching actions are needed (except for high wind speeds), it will cause no additional wear of the pitching mechanism. On the other hand, since the wind turbine is operated at a higher rotational speed Ω, this results in higher mechanical stresses due to centrifugal forces. Furthermore, an accurate measurement of the wind speed and a good knowledge of the $C_p(\lambda)$-curve is needed to obtain a reliable deloaded operation, which is a disadvantage of this strategy.

5.1.3.3 Combined speed and pitch control

From the previous sections, it is clear that both methods have advantages and disadvantages. In order to achieve a better performance, a combination of both speed and pitch control can be used to obtain the desired power reserve at any point in time. In [113], it is shown that a smart combination of both strategies can result in a better performance than the individual controllers.

5.1.4 Deloading power references

In the previous section, two different methods were presented to decrease the power output of a wind turbine and obtain a deloaded operation: pitch control and speed control. In this section, different power references for deloaded operation will be presented. These deloaded power references are then used to control the power output of the wind turbine by using either

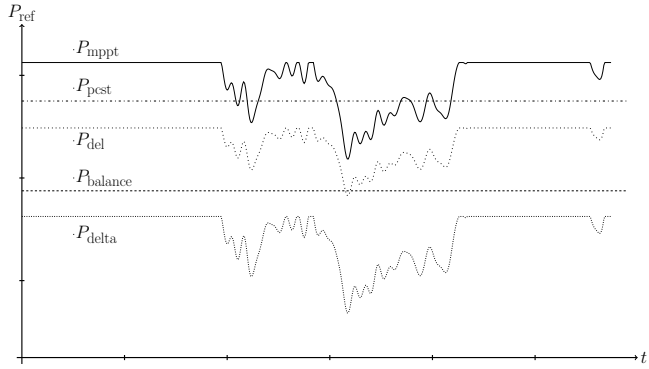

Figure 5.5: Balance, delta, percentage and constant power control in a variable-speed wind turbine.

of the presented methods. An overview of the different reference curves is given in Fig. 5.5. Since all of these reference curves ensure the availability of a certain power reserve, it is possible to increase the power production in case of a frequency dip and provide primary control.

5.1.4.1 Available wind power

The upper curve P_{mppt} of Fig. 5.5 shows the maximum power that can be produced by the wind turbine by using a maximum power point tracker. If the power exceeds the rated power of the wind turbine, the power output is curtailed by pitching the turbine blades. This curve is not a deloaded reference curve, but is shown for comparison of the different deloaded reference curves.

5.1.4.2 Constant power control

When constant power control is applied, a constant power reference P_{pcst} is used for a predefined time interval (see the dash-dotted curve in Fig. 5.5) [88,115]. The power reference is kept constant for a predefined period, after which a new power reference can be chosen for the next time interval. A prediction of the wind speed v is needed to determine the power reference P_{pcst}. This reference value can only be tracked properly by means of speed control. It is immediately clear that this control strategy results in a non-constant power reserve. The selection of the constant power reference value is crucial, as it determines the operational behavior of the wind turbine. If the reference power is chosen too low, the power output of the wind turbine is decreased too much. A reference value that is too high results in unstable behavior of the wind turbine as not enough power is available from the

wind and consequently the wind turbine starts to slow down unacceptably. Therefore, in § 5.2.3.1, an algorithm to obtain the optimal reference value for the constant power control strategy is derived. Furthermore, in § 5.2.4, it is shown that this strategy has the ability to provide power reserves with wind turbines, especially when they are aggregated in wind farms [115].

5.1.4.3 Balance control

Balance control is a special case of constant power control. When balance control is applied, the reference curve P_{balance} is chosen below the available power to obtain a power reserve at any point in time [42, 115–117]. Similar to the constant power control, the power reference is kept constant for a predefined period, after which a new power reference can be chosen for the next time interval. Again, this control strategy results in a non-constant power reserve.

5.1.4.4 Delta control

For delta control, the power output P_{delta} of the wind turbine is reduced by a predefined set-point compared to the maximal available power P_{mppt} (e.g. 100 kW). In this way, a constant power reserve is available at any point in time which can be used in the primary frequency control [42, 116, 117]. Delta control can be achieved by using speed control, pitch control or a combination of both strategies.

5.1.4.5 Percentage control

A commonly used deloading strategy is percentage control [43,80,89,90,113]. Percentage control is achieved by using a power reference curve which is reduced with a fixed percentage compared to the maximum power point curve. The P_{del}-curve in Fig. 5.3b is an example of percentage control by means of speed control. From Fig. 5.5, it is clear that the power reserve is not constant, but depends on the available power. For high wind speeds, the power reserve is higher than for low wind speeds. This is beneficial since higher power reserves are needed in case of high wind power production. If the $C_{\text{p}}(\lambda)$-curve of the wind turbine is known, it is possible to determine the reference curve for percentage control. Otherwise, it may be difficult to obtain the desired deloading percentage.

5.1.5 Improvements of the primary controller

In [89], a slightly modified primary control strategy is presented. Percentage control is used as power reference and the turbines are deloaded by means

of speed control (P_{del} in Fig. 5.3b). When a frequency dip occurs, the output power of the wind turbine is increased by decreasing the rotational speed Ω. However, since the turbine is slowed down, an amount of kinetic energy from the rotor is injected during the disturbance. If this kinetic energy is taken into account, percentage control that is achieved by means of speed control, results in a higher power reserve for certain operating points. Therefore, another power reference is suggested which takes the additional kinetic energy into account. This results in a reference curve that is slightly higher than P_{del} in Fig. 5.3b for certain rotational speeds Ω. Using this modified power reference results in a lower energy loss due to deloading. However, the difference is small.

In [90], another modification of the primary controller is investigated. Again, percentage control is used to obtain a power reserve. A wind farm is considered where all the turbines are equipped with a primary droop controller. The droop constant of the different turbines is not fixed, but depends on the power reserve of the considered wind turbine. As percentage control is used, the turbines that are operating at a (locally) higher wind speed v, have a higher power reserve that can be used to assist in the primary control. However, this is a complex strategy with only a very limited enhancement of the primary control results.

5.1.6 Conclusion

From this section, it can be concluded that wind turbines can assist in the primary frequency control if an additional control loop is added to the wind turbine controller. Decreasing the power output in case of an over-frequency event is always possible, whereas increasing the power output has to be achieved by deloading the wind turbines or by including storage. The behavior of the droop controller is equivalent to the traditional droop controller in conventional power plants. It should be noted, however, that the amount of reserves depends strongly on the wind speed. For high wind speeds, the power reserves may be high, but for low wind speeds it may be impossible to provide any reserves. This is not really a problem, since wind turbines should only assist in the primary control for a high wind power penetration. For low wind speeds, the share of wind turbines in the total production is lower and conventional power plants are needed to cover the load. These power plants can maintain enough reserves to provide the frequency control. For high wind speeds, on the other hand, it may be beneficial to assist in the primary control. Sometimes, limits are imposed on the maximum amount of wind power that may be injected into the system to prevent stability problems. If wind turbines participate actively in the frequency control, this may relax those limitations [42]. The energy that is

lost due to the deloaded operation of the wind turbine should be considered as the main drawback of primary control with wind turbines. Storage could be a solution to minimize the lost energy, but might be expensive. Therefore, in the next section, the provision of active power reserves with different control strategies is discussed. Using these strategies allows wind turbines to participate in the primary frequency control during a frequency dip. In the last section of this chapter, a new control algorithm that allows equal power sharing during over-frequency events is presented.

5.2 Comparison of the deloading strategies

In this section, the different control strategies to provide active power reserves with wind turbines are compared. First, the different control strategies to obtain deloaded operation with wind turbines are presented. Then, the selection of the control parameters for the different strategies is discussed. For the constant power control strategy, the choice of the reference power is crucial, so an optimization algorithm to determine the power reference is developed [115]. Finally, the ability to maintain active power reserves with a single wind turbine and a wind farm is shown by means of simulations. The different control strategies are compared to find the strategy that is best suited to maintain active power reserves.

5.2.1 Power control strategies

In Fig. 5.6, the different power control strategies that can be used to determine P_{ref} are shown as dashed lines [88, 90, 115, 118]. The solid lines represent the wind power at different wind speeds v for a fixed pitch angle β. As pitch control is not fast enough to follow the rapid wind speed variations, the pitch angle β is considered zero here. In this section, the following power control strategies are considered: maximum power point tracking P_{mppt}, constant power control P_{pcst}, percentage control P_{del}, linear slope control P_{lsc} and delta control P_{delta}. As already explained, the balance control strategy P_{balance} can be seen as a special case of the constant power control strategy and is therefore not discussed separately:

1. *Maximum Power Point Tracking (MPPT, P_{mppt})*: For each wind speed v, there exists a TSR and consequently a rotational speed Ω_{opt} for which the acquired wind power reaches a maximum. The curve that passes through these maxima, is a cubic function of Ω (see eq. (5.7)). When P_{mppt} is used as reference power P_{ref}, the maximum power is acquired.

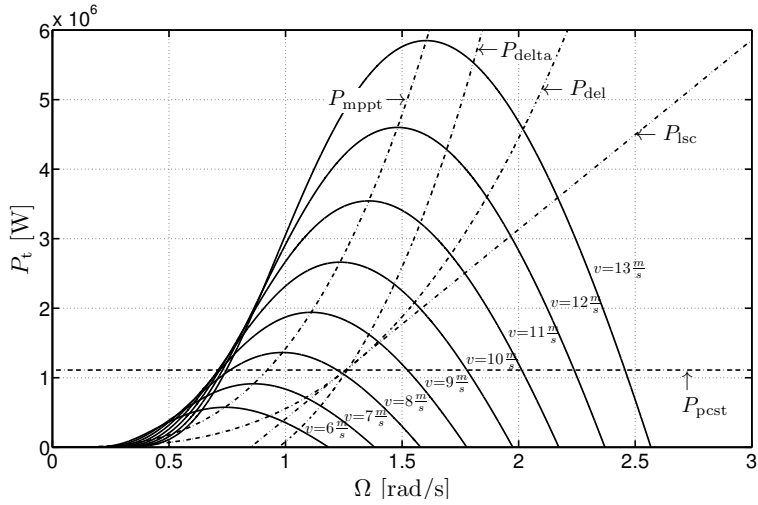

Figure 5.6: Illustration of different control strategies. Solid lines: wind power curves, dashed lines: control strategies.

2. *Constant power control (PCST, P_{pcst})*: In the constant power strategy, the generator is loaded with a constant power $P_{\mathrm{ref}} = P_{\mathrm{pcst}}$ for a certain period of time (e.g., 550 s in this section). The choice of this reference power is difficult, as it depends on the wind speed profile during the time interval of interest. If the reference value is too high, the turbine will slow down too much. Conversely, if the reference is too low, the turbine will accelerate unacceptably. Thus, the better the wind speed profile can be predicted, the better this strategy works. In the following paragraphs, a method to obtain the optimal value for P_{pcst} is proposed.

3. *Percentage control (DEL, P_{del})*: By shifting the operating point to the right of the maximum power point, the wind turbine is deloaded by a certain percentage. This is achieved by shifting the rotor speed from Ω_{opt} to the deloaded speed Ω_{del}. The deloaded reference power P_{del} is given by [89, 90, 118]:

$$P_{\mathrm{del}} = K_{\mathrm{del}}\Omega^3 \tag{5.8}$$

By using P_{del} as reference power, a power margin, which is a fraction (e.g. 80 %) of the maximum available power, is maintained at all times. Shifting the reference power to the right has two advantages compared to shifting it to the left. Firstly, the wind turbine is continuously operating on the stable part of the C_{p}-curve. Secondly,

kinetic energy can be immediately injected into the grid when the power output of the wind turbine has to be increased. A disadvantage is that the power losses in the generator and converter might increase as the mechanical losses and iron losses are higher. However, the Joule losses decrease for increasing rotational speeds. The calculation of these losses is an important topic, but out of the scope for this work [109].

4. *Linear slope control (LSC, P_{lsc})*: In general, linear slope control has the following reference power P_{lsc} [88]:

$$P_{\mathrm{lsc}} = P_{\mathrm{lsc},0} + T_{\mathrm{cst}}\Omega \tag{5.9}$$

When $P_{\mathrm{lsc},0} = 0$, the linear slope control strategy reduces to the constant torque strategy. In order to obtain a power reserve at any point in time, a negative $P_{\mathrm{lsc},0}$ is chosen in Fig. 5.6.

5. *Delta control strategy (DELTA, P_{delta})*: For the delta control strategy, a constant power margin $\Delta P_{\mathrm{delta}}$ compared to the the maximum power point tracker is maintained:

$$P_{\mathrm{delta}} = P_{\mathrm{mppt}} - \Delta P_{\mathrm{delta}} \tag{5.10}$$

This results in a polynomial expression for P_{delta} in function of Ω:

$$P_{\mathrm{delta}} = P_{\mathrm{delta},3}\Omega^3 + P_{\mathrm{delta},2}\Omega^2 + P_{\mathrm{delta},1}\Omega + P_{\mathrm{delta},0} \tag{5.11}$$

which can be obtained by solving $P_{\mathrm{t}} = P_{\mathrm{delta}}$ for the rotational speed Ω for different wind speeds v and fitting a curve through these values.

5.2.2 Reference tracking

The system dynamics are described by Newton's equation of motion:

$$J_{\mathrm{wt}}\frac{\mathrm{d}\Omega}{\mathrm{dt}} = T_{\mathrm{t}} - T_{\mathrm{g}} \tag{5.12}$$

where J_{wt} is the total inertia of the system, T_{t} is the turbine torque and T_{g} is the generator torque. Here, it is assumed that the converter is able to control the power of the generator P_{g} perfectly, i.e., $P_{\mathrm{g}} = P_{\mathrm{ref}}$ due to the high bandwidth of the controllers. Consequently, (5.12) can also be written as follows:

$$J_{\mathrm{wt}}\Omega\frac{\mathrm{d}\Omega}{\mathrm{dt}} = P_{\mathrm{t}} - P_{\mathrm{ref}} \tag{5.13}$$

The intersection of a solid line (wind power at a given wind speed v) with a dashed line (chosen reference strategy) in Fig. 5.6 defines the equilibrium

operating point. Intersections to the right of the maximum power point are certainly stable operating points. Usually, the fluctuations in the wind speed are too fast to settle an equilibrium. According to (5.13), the acceleration and deceleration of the generator make sure the power reference P_{ref} will be tracked.

5.2.3 Selection of the control parameters

For the different control strategies, the control parameters P_{pcst}, K_{del}, etc. should be properly tuned. Especially for the constant power control strategy, it is important to choose the correct reference power, as is shown next. Therefore, an optimization algorithm is developed to find the optimal reference power for the constant power control strategy.

5.2.3.1 Selection of the optimal reference power for the constant power control strategy

Problem statement

The choice of the reference power for constant power control is difficult. When the reference power P_{ref} is chosen, the following conditions must be satisfied:

- The wind speed profile has to be predicted as accurately as possible for the time interval of interest.
- The wind turbine can provide power reserves.
- The rotational speed Ω has to be within the speed limits: $\Omega_{\text{min}} < \Omega < \Omega_{\text{max}}$. In this way, the operating range of the wind turbine is respected.
- The turbine power P_{t} satisfies: $P_{\text{t}} > 0$.

All these conditions result in a range of possible power references: $P_{\text{ref,min}} < P_{\text{ref}} < P_{\text{ref,max}}$. The choice of P_{ref} with respect to these boundaries is determined by the accuracy of the wind speed prediction. If the prediction is accurate, P_{ref} can be chosen close to these boundaries, otherwise, safety margins should be respected.

Finding the range of reference values P_{ref} that satisfy all these conditions can be achieved by the algorithm described in the remainder of this section.

Optimization algorithm

The aim of the optimization algorithm is to find the range of possible

reference values P_{ref} for which the listed conditions are satisfied. In section 5.2.4.1, simulations are used to determine which reference power is optimal to provide power reserves.

A schematic overview of the optimization algorithm is shown in Fig. 5.7. The iterative process starts with:

- $P_{\text{ref}} = 0$
- $\Omega_{\text{start}} = \frac{v\lambda_{\text{opt}}}{r}$

with λ_{opt} the TSR that maximizes $C_{\text{p}}(\lambda)$. This choice for Ω_{start} corresponds to a wind turbine delivering the maximum power before the constant power control is enabled. The (predicted) wind speed $v(t)$ during the time interval of interest is needed to calculate the reference value. Furthermore, the operating range of the wind turbine, $[\Omega_{\text{min}}, \Omega_{\text{max}}]$, is specified. Then, $\Omega(t)$ is calculated for the given time interval by solving (5.13). As the initial value of the reference power P_{ref} is zero, the turbine will accelerate and exceed the upper speed limit Ω_{max}. Consequently, the reference value P_{ref} is increased with ΔP and the calculations are repeated until $\Omega(t)$ is within the operating limits. The choice of ΔP is a trade-off between speed and accuracy. The higher the value of ΔP, the faster the reference value is found, but the less accurate the solution is. The minimum power reference $P_{\text{ref,min}}$ is found as the lowest value for P_{ref} for which $\Omega(t) > \Omega_{\text{min}}$ and $P_{\text{t}} > 0$. To find the maximum power reference $P_{\text{ref,max}}$, the reference value P_{ref} is further increased with ΔP until the minimum of $\Omega(t)$ falls below the lower speed limit Ω_{min}. The iterative process is stopped and the reference value is decreased with ΔP to give the maximum power reference $P_{\text{ref,max}}$ for which a stable operating point was achieved. Finally, the calculations are done one last time with $P_{\text{ref,max}}$ and it is verified whether $\Omega(t)$ is indeed in the operating range. If this is the case, the power reference value $P_{\text{ref,max}}$ is obtained. Otherwise, no power reference value can be found for the given wind speed sample $v(t)$ and operating range $[\Omega_{\text{min}}, \Omega_{\text{max}}]$. In this case, the time interval for which a constant P_{ref} is maintained has to be shortened until a solution can be found.

In § 5.2.4.1, two reference values in the reference range are used to investigate the reserve capabilities of wind turbines under constant power control and balance control. It is assumed that the wind speed can be accurately predicted for the considered time interval, such that no safety margin with respect to the upper and lower power limits $P_{\text{ref,min}}$ and $P_{\text{ref,max}}$ has to be maintained.

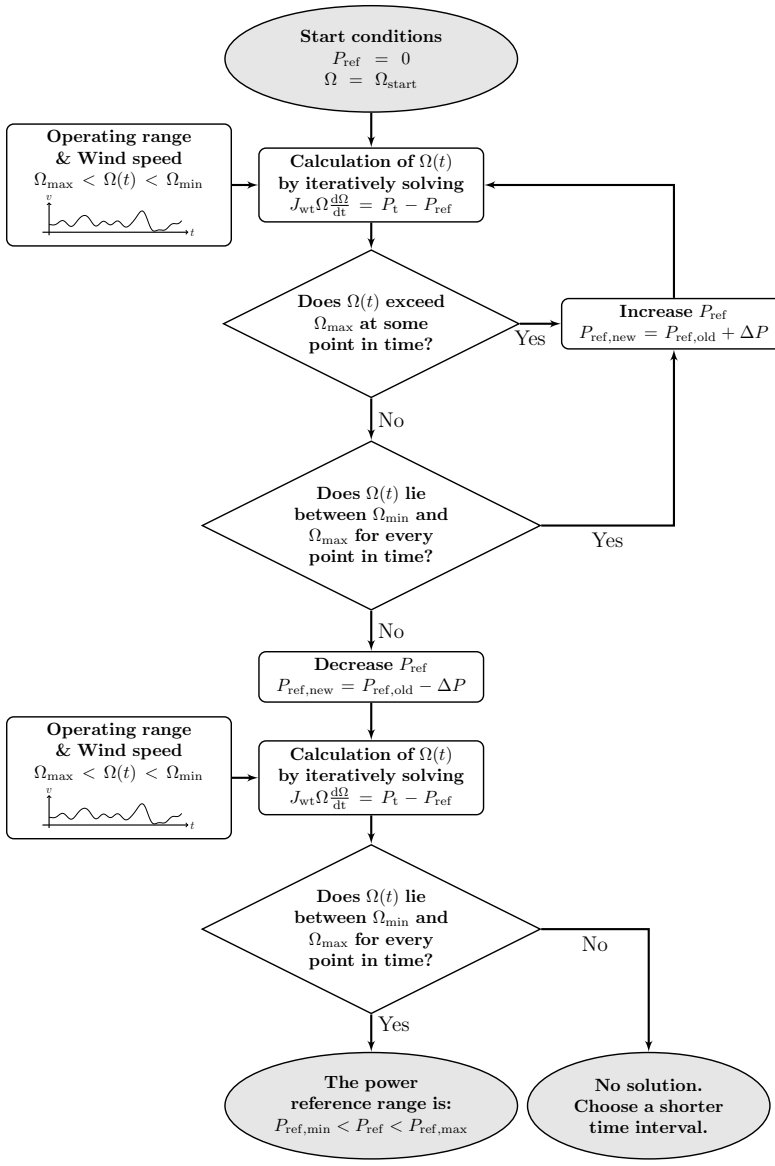

Figure 5.7: Schematic overview of the optimization algorithm.

5.2.3.2 Selection of the control parameters for the other strategies

The control parameters of the three other strategies, i.e., linear slope control, percentage control and delta control, are tuned to obtain the same average

Parameter	Value	Unit	Parameter	Value	Unit
P_{rated}	3.0	MW	Ω_{nom}	1.45	$\frac{\text{rad}}{\text{s}}$
r	56	m	ρ	1.225	$\frac{\text{kg}}{\text{m}^3}$
J	$1.24 \cdot 10^7$	kgm^2	ΔP	100.0	W
$C_{\text{p,max}}$	0.4412	–	λ_{opt}	6.908	–
Ω_{min}	0.85	$\frac{\text{rad}}{\text{s}}$	Ω_{max}	2.0	$\frac{\text{rad}}{\text{s}}$
K_{mppt}	1.4185	$\frac{\text{MWs}^3}{\text{rad}^3}$	K_{del}	0.5559	$\frac{\text{MWs}^3}{\text{rad}^3}$
$P_{\text{lsc,0}}$	−2.3163	MW	T_{cst}	2.725	$\frac{\text{MWs}}{\text{rad}}$
P_{pcst}	1.1108	MW	ΔP_{delta}	0.31	MW
$P_{\text{delta,0}}$	−0.8545	MW	$P_{\text{delta,1}}$	0.7206	$\frac{\text{MWs}}{\text{rad}}$
$P_{\text{delta,2}}$	−1.4208	$\frac{\text{MWs}^2}{\text{rad}^2}$	$P_{\text{delta,3}}$	1.6574	$\frac{\text{MWs}^3}{\text{rad}^3}$

Table 5.1: Simulation parameters for the comparison of the different power control strategies.

power production and consequently the same average power reserve as for the constant power control. Also the energy yield reduction is the same for all the strategies. In this way, it is possible to compare the behavior of the different strategies. For the percentage control, this results in a deloading of 22 % compared to the maximum power point tracking. For the linear slope control, $P_{\text{lsc,0}}$ has a negative value to ensure a stable operating point for a broad range of wind speeds. For the delta control strategy, a power margin ΔP_{delta} of 0.31 MW is selected, as this is the average power reserve for the constant power control for a single wind turbine in § 5.2.4.1. The values for these parameters are summarized in Table 5.1. Further optimization of the parameter selection could be investigated in the future.

5.2.4 Simulation results

In this section, the simulation results are summarized. Firstly, the constant power control and balance control on a single wind turbine are compared to determine the differences between these related strategies. Secondly, a single wind turbine equipped with the different control strategies is considered. Thirdly, the same control strategies are used in a wind farm. The parameters used in the simulations are listed in Table 5.1.

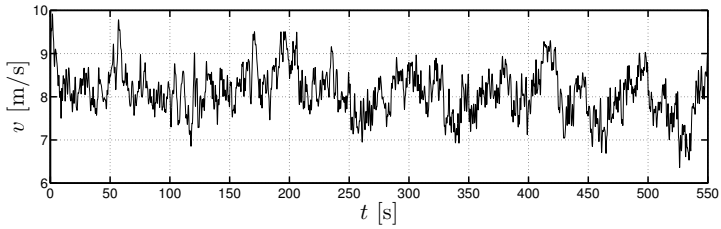

Figure 5.8: Simulated wind speed sample.

5.2.4.1 Constant power control and balance control on a single wind turbine

The wind speed sample used for the simulations is shown in Fig. 5.8. A wind model is used to simulate this wind sample. First, the simulations are conducted for the constant power control strategy, which corresponds with the maximum reference value $P_{\text{ref}} = P_{\text{ref,max}} = P_{\text{pcst}}$ obtained with the algorithm developed in section 5.2.3.1. The results of this simulation are shown in Fig. 5.9.

The maximum reference value $P_{\text{ref,max}}$ corresponding to the wind speed profile of Fig. 5.8 is 1.1108 MW. This corresponds quite well to the mean value of the wind power $P_{\text{t,avg}} = 1.1110$ MW, as may be noted in Fig. 5.9. This is in line with the expectations, since it indicates the balance between the energy delivered by the turbine and the energy extracted by the generator. As a result, the rotational speed Ω oscillates around the mean value of 1.24 rad/s. The minimum reference value $P_{\text{ref,min}}$ is 0.8906 MW. The simulation shows the capability of the wind turbine to provide power reserves when constant power control is applied. An average power reserve $P_{\text{reserve,avg}}$ of about 0.31 MW is available. The maximum power reserve is 1.06 MW, while the minimum is approximately 0 MW. These minima correspond to the maxima of the C_{p} curve, which means that the wind turbine already delivers the maximum power. Consequently, using P_{pcst} as the reference value allows to retain a power reserve during the majority of the time, however, there are some periods with very low power reserves.

It is interesting to compare the power output of the constant power strategy and the MPPT strategy.

$$P_{\text{pcst}} = 1.1108 \text{ MW} \leftrightarrow \begin{cases} P_{\text{mppt,avg}} = 1.423 \text{ MW} \\ P_{\text{mppt,min}} = 0.878 \text{ MW} \\ P_{\text{mppt,max}} = 2.08 \text{ MW} \end{cases}$$

With constant power control, the wind turbine generates on average about

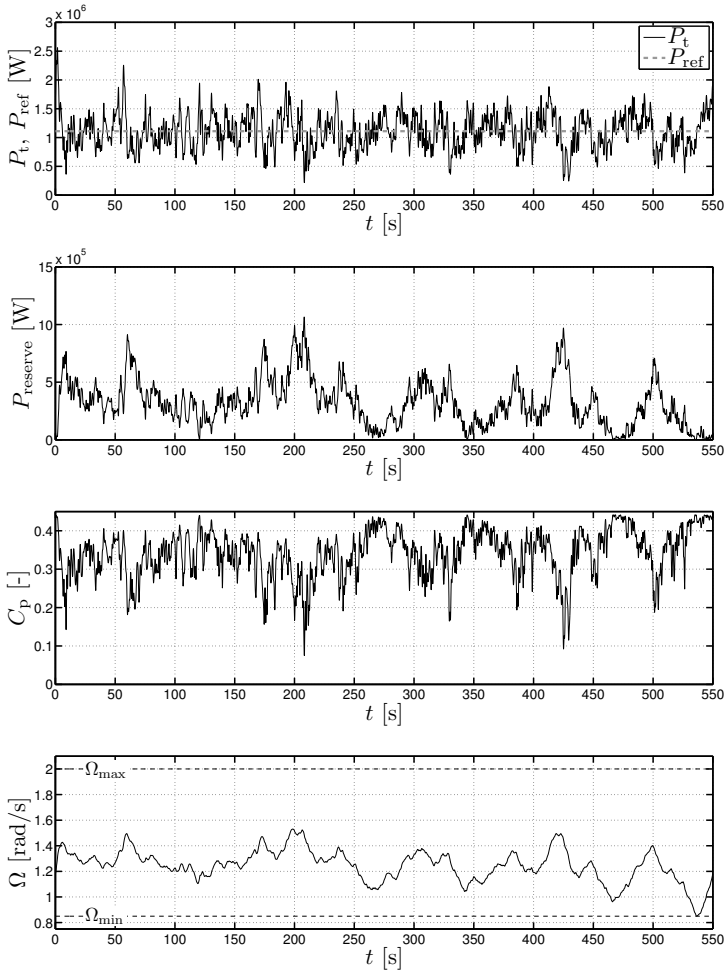

Figure 5.9: Simulation for the constant power control strategy ($P_{\text{ref}} = P_{\text{pcst}}$).

22 % less power for the given wind profile compared with MPPT, i.e, 1.1108 MW vs. 1.423 MW, which is a disadvantage. However, the use of constant power control makes it possible to maintain power reserves. Moreover, the power output is constant, where it fluctuates highly with the MPPT strategy, as indicated by $P_{\text{mppt,min}}$ and $P_{\text{mppt,max}}$. As expected, the rotational speed Ω varies more when applying the constant power control:

$$\Omega_{\text{pcst,min}} = 0.8501 \text{ rad/s} \leftrightarrow \Omega_{\text{mppt,min}} = 0.8522 \text{ rad/s}$$
$$\Omega_{\text{pcst,max}} = 1.5307 \text{ rad/s} \leftrightarrow \Omega_{\text{mppt,max}} = 1.1361 \text{ rad/s}$$

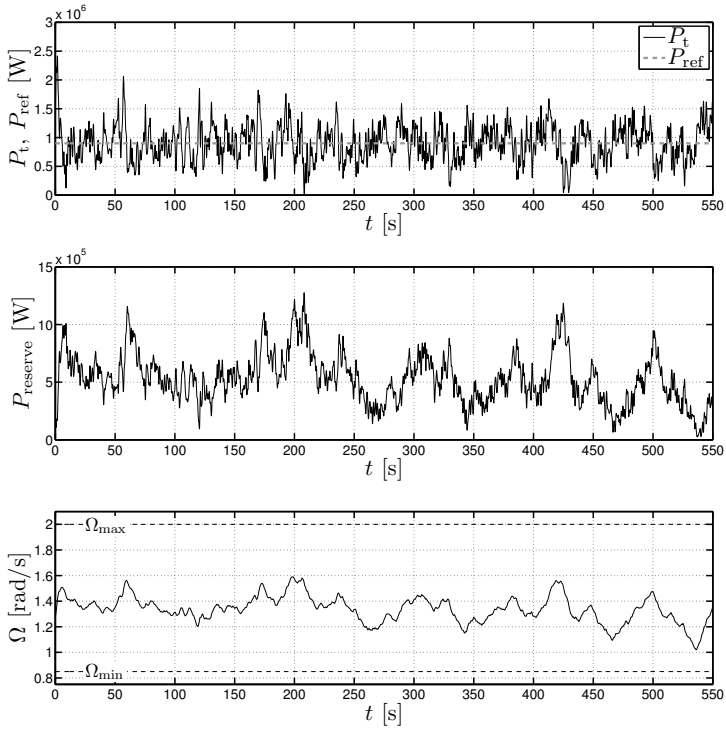

Figure 5.10: Simulation for the balance control strategy ($P_{\mathrm{ref}} = P_{\mathrm{balance}}$).

In the following, it is examined whether balance control could make it possible to maintain a power reserve at any point in time. Again, the wind profile presented in Fig. 5.8 is used in the simulations. Instead of $P_{\mathrm{ref,max}} = P_{\mathrm{pcst}}$ as the power reference, a lower reference value is used: $P_{\mathrm{ref}} = P_{\mathrm{balance}} = 0.9$ MW. The results are summarized in Fig. 5.10.

The behavior is quite similar as in the previous case. As expected, the reference power and the average wind power are balanced and the average rotational speed is slightly higher $\Omega_{\mathrm{avg}} = 1.33$ rad/s. Now, the average generated power is about 37 % lower than with the MPPT strategy.

Considering the ability to provide power reserves, there are some differences. First, the average power reserve is higher: 0.530 MW instead of 0.31 MW. Also the maximum power reserve is higher. However, the most interesting difference is found for the minimum power reserve. The minimum power reserve is 24.5 kW for balance control, whereas it was zero for constant power control. This indicates that it is possible to maintain a power reserve at any point in time by lowering the reference value. However,

Parameter	MPPT	PCST	LSC	DEL	DELTA	Unit
P_{avg}	1.4232	1.1108	1.1156	1.1169	1.1151	MW
P_{min}	0.8779	1.1108	0.6529	0.6951	0.3676	MW
P_{max}	2.0803	1.1108	1.5870	1.6195	2.2789	MW
Ω_{avg}	0.9985	1.2468	1.2594	1.2587	1.2610	$\frac{\text{rad}}{\text{s}}$
Ω_{min}	0.8522	0.8501	1.0896	1.0773	1.1590	$\frac{\text{rad}}{\text{s}}$
Ω_{max}	1.1361	1.5307	1.4324	1.4282	1.3521	$\frac{\text{rad}}{\text{s}}$
$P_{\text{reserve,avg}}$	0	0.3121	0.3156	0.3143	0.3172	MW
$P_{\text{reserve,min}}$	0	≈ 0	0.0510	0.0482	0.0117	MW
$P_{\text{reserve,max}}$	0	1.0655	0.6847	0.6723	0.6103	MW

Table 5.2: Simulation results for the comparison of the different power control strategies.

lowering the reference value with more than 0.2 MW results in a minimum power reserve of only 24.5 kW. Consequently, for the wind speed sample of Fig. 5.8, lowering the reference value strongly affects the average power reserve, but only has a minor effect on the minimum power reserve. When the simulations are repeated with other wind speed profiles, the same conclusions can be drawn. This suggests that lowering the reference value P_{ref} and using balance control instead of constant power control is not a sustainable way to ensure a minimum power reserve.

In summary, using constant power control makes it possible to maintain a power reserve during most of the time. The use of a lower reference value in balance control does not significantly alter the minimum power reference. Therefore, in the next paragraphs, only constant power control will be considered.

5.2.4.2 Comparison of the deloaded power control strategies on a single wind turbine

The same wind speed sample (Fig. 5.8) that is used for constant power control and balance control is used for the simulations in this section. Wind turbines equipped with the MPPT strategy are not able to maintain power reserves as they are already maximizing the energy yield. However, the maximum power point tracking results can be used to compare the results of the other strategies. Some interesting operational parameters during the given wind speed sample are shown in Table 5.2 for the different strategies.

The simulation results are shown in Figs. 5.9, 5.11, 5.12 and 5.13, where

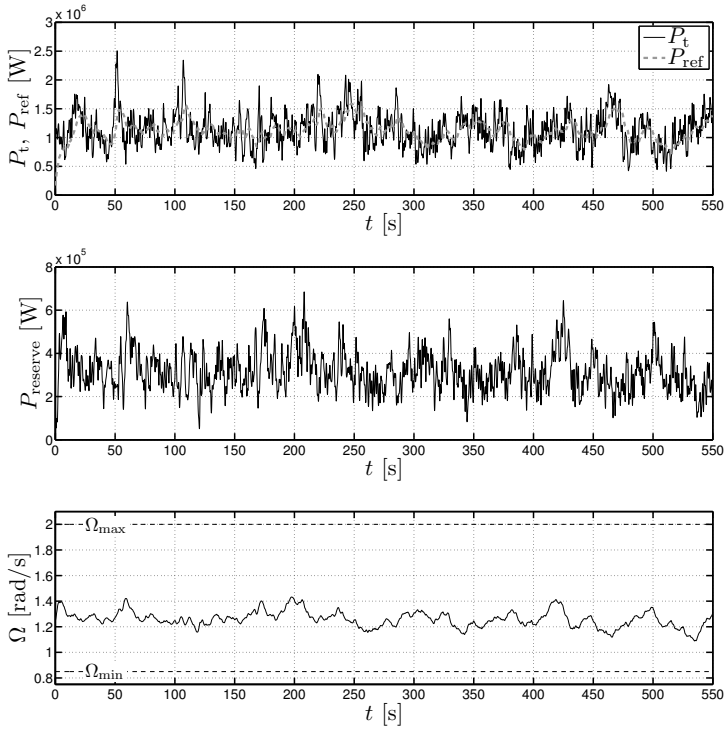

Figure 5.11: Simulation for the linear slope control strategy ($P_{\mathrm{ref}} = P_{\mathrm{lsc}}$).

the active power reference P_{ref}, the power reserves P_{reserve} and the rotational speed Ω are shown for the considered wind speed pattern and the different control strategies.

Firstly, it can be noted that the rotational speed Ω remains within the operational limits (Ω_{min} and Ω_{max}) for all the different control strategies. As the power reserves are obtained by increasing the rotational speed Ω (and thus decreasing the value of C_{p}), the average rotational speed Ω_{avg} is higher for the considered strategies than for the MPPT strategy:

$$\Omega_{\mathrm{pcst,avg}} \approx \Omega_{\mathrm{lsc,avg}} \approx \Omega_{\mathrm{del,avg}} \approx \Omega_{\mathrm{delta,avg}} \approx 1.25 \text{ rad/s}$$
$$\leftrightarrow \Omega_{\mathrm{mppt,avg}} = 0.9985 \text{ rad/s}$$

Furthermore, there is a clear difference in the fluctuations of the rotational speed Ω for the different control strategies. The smallest fluctuations can be found for the MPPT strategy (see $\Omega_{\mathrm{mppt,min}}$ and $\Omega_{\mathrm{mppt,max}}$ in Table 5.2), closely followed by delta control. The fluctuations are larger for the constant power control, linear slope control and percentage control as can be seen

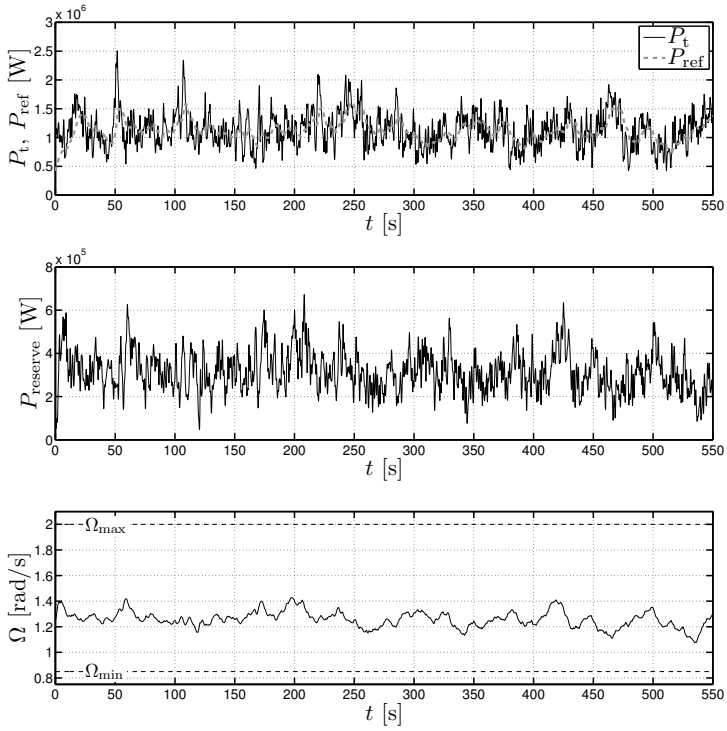

Figure 5.12: Simulation for the percentage control strategy ($P_{\mathrm{ref}} = P_{\mathrm{del}}$).

in Figs. 5.9, 5.11, 5.12, 5.13 and in Table 5.2. For linear slope control and percentage control, the minimum rotational speed Ω_{min} is approximately 1.08 rad/s, whereas the maximum rotational speed Ω_{max} is 1.43 rad/s for both strategies. The largest fluctuations in the rotational speed can be found for constant power control: $\Omega_{\mathrm{pcst,min}} = 0.8501$ rad/s and $\Omega_{\mathrm{pcst,max}} = 1.5307$ rad/s. Summarized:

- Constant power control gives the highest fluctuations in the rotational speed Ω.
- Delta control gives the lowest fluctuations in the rotational speed Ω, linear slope control and percentage control are in between.

A higher rotational speed Ω results in more wear of the drive-train components, so this is a disadvantage of the constant power control.

The opposite holds for the active power output of the wind turbines: the power output is constant for the constant power control strategy, whereas it fluctuates the most for the MPPT strategy and delta control. As delta

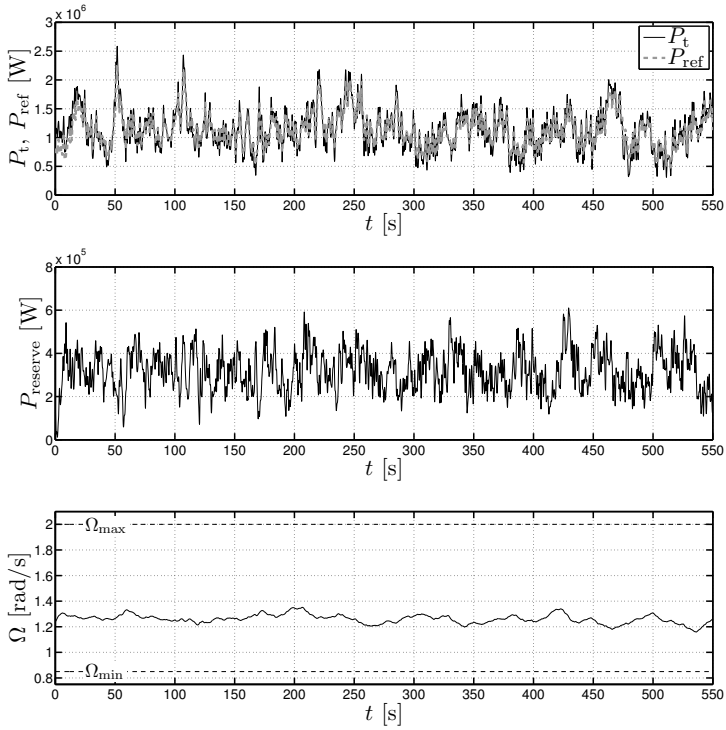

Figure 5.13: Simulation for the delta control strategy ($P_{\text{ref}} = P_{\text{delta}}$).

control tries to maintain a constant power reserve compared to the maximum power point tracking strategy, their behavior is quite similar. The linear slope control and percentage control are in between. The smoother the active power reference is, the more the rotational speed Ω fluctuates as the turbine inertia J_{wt} acts as an energy buffer. For the MPPT, on the one hand, the rotational speed Ω varies only slightly as it tries to operate in the maximum power point as much as possible. For the constant power control, on the other hand, the power output is constant, so all the variations are reflected in the rotational speed Ω. Consequently:

- Constant power control has a constant power output.
- Delta control gives the highest variations in the power output, linear slope control and percentage control are in between.

From the perspective of the BRP, constant power control is very attractive as the power output is constant for a given period of time (e.g., 15 min), which facilitates the balancing of the portfolio. However, a good wind speed

prediction is needed to use the constant power control strategy, which is a disadvantage of this control strategy. Furthermore, contrary to the other control strategies, a fairly large deloading of the wind turbine is needed to obtain a stable operation.

Concerning the active power reserves P_{reserve}, the differences are clear. With constant power control, it is possible to maintain power reserves most of the time as can be seen in Fig. 5.9. The average power reserve is 0.31 MW. However, during some time intervals there are no power reserves available. The maximum available power reserve is 1.06 MW, whereas the minimum reserve is approximately 0 MW. A possible solution is to decrease the value of the constant power reference value and use balance control, so power reserves are available at any point in time. However, this only results in a limited increase of the minimum power reserves as shown in § 5.2.4.1. Furthermore, it results in additional energy yield losses, which is undesired.

For the linear slope control strategy, the percentage control strategy and the delta control strategy, the results are quite similar, as can be seen in Figs. 5.11, 5.12 and 5.13. The average power reserve is the same as for the constant power control strategy: $P_{\text{reserve}} \approx 0.31$ MW. However, now there are power reserves available for the complete time interval. Furthermore, the amount of power reserves is much more constant: the maximum available power reserves are 0.68 MW for linear slope control, 0.67 MW for percentage control and 0.61 MW for delta control. The minimum available power reserves are 0.051 MW for linear slope control, 0.049 MW for percentage control and 0.012 MW for delta control. These periods with very low power reserves are very short and occur only rarely, which makes all three strategies suitable to provide power reserves.

In conclusion, when only a single wind turbine is considered, linear slope control, percentage control and delta control are the most suitable strategies to provide power reserves.

5.2.4.3 Comparison of the deloaded power control strategies in a wind farm

The model of the wind farm consists of N randomly positioned wind turbines. It is assumed that no wind turbine falls in the wake of another wind turbine and that each wind turbine experiences the same wind profile, but with some time delays. These delays are associated with the time needed for the wind to transverse the distance between the different wind turbines of the farm [119]. The time delays are simulated by taking a random sample of 550 s of the wind speed profile in Fig. 5.14 for each wind turbine. The same samples are used for all the different control strategies.

In Figs. 5.15, 5.16, 5.17 and 5.18, the results for wind farms of different

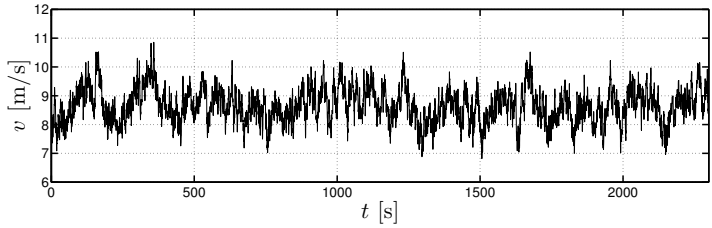

Figure 5.14: Wind speed sample in wind farm.

sizes are presented. Fig. 5.15 shows the results of the power reserve for constant power control. For each individual wind turbine, the constant power control value $P_{\text{pcst}} = P_{\text{ref,max}}$ is calculated with the presented algorithm. As every wind turbine has a slightly different wind profile, P_{pcst} will be different for every wind turbine in the wind farm. The total power reserve for the complete wind farm is obtained by summing the power reserves of the individual wind turbines. It is immediately clear that the aggregation of several wind turbines in a wind farm results in an increased ability to maintain power reserves. Already for the small wind farm ($N = 5$), power reserves are available at any point in time due to the smoothing effect of the wind farm. For the bigger wind farms ($N = 10$ and $N = 25$), the available power reserves are smoother, but there still is an important fluctuation in the amount of power reserves during the considered time frame.

Again, similar results are obtained for linear slope control and percentage control (see Figs. 5.16 and 5.17). Contrary to the constant power control strategy, the power reserves are already much smoother for the small wind farm ($N = 5$). The percentage control strategy performs slightly better than the linear slope control strategy as the fluctuations in the power reserve are smaller. The minimum power reserve is the same for both strategies: $P_{\text{reserve,min}} \approx 1.25$ MW, whereas the maximum power reserve is higher for the linear slope control:

$$P_{\text{reserve,max,lsc}} = 3.07 \text{ MW} \leftrightarrow P_{\text{reserve,max,del}} = 2.88 \text{ MW}$$

However, for bigger wind farms, no differences can be observed for both strategies. A quite constant power reserve of 9.7 MW can be maintained during the considered time interval for a wind farm consisting of 25 wind turbines. The power reserves fluctuate between 7.9 MW and 11 MW for both control strategies.

When the results for delta control are compared to the other strategies, it is immediately clear that it performs better than the other strategies as the power reserves are the most constant for this strategy (see Fig. 5.18). Al-

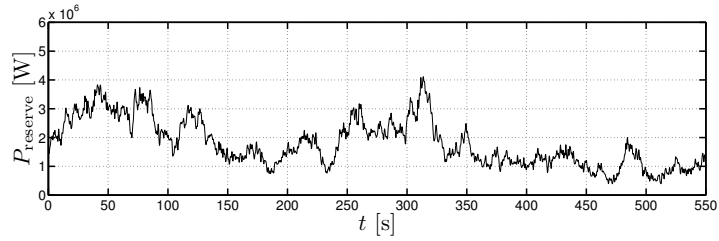

(a) $N = 5$, $P_{\text{tot}} = 7.10$ MW

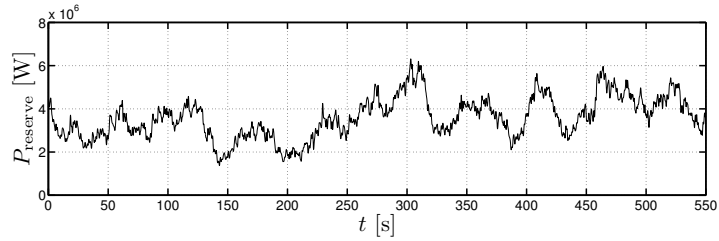

(b) $N = 10$, $P_{\text{tot}} = 14.20$ MW

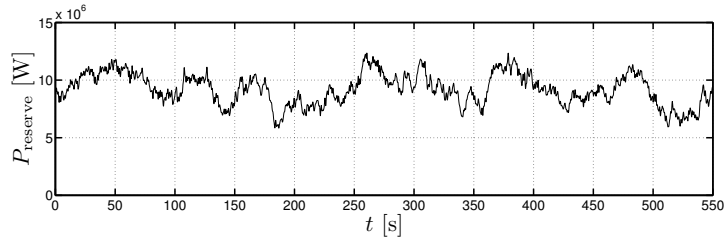

(c) $N = 25$, $P_{\text{tot}} = 34.07$ MW

Figure 5.15: Power reserves in wind farms of different size equipped with constant power control.

ready for a small wind farm consisting of only 5 wind turbines, the available power reserves are much smoother than for the other three strategies. The reserves P_{reserve} fluctuate between 1.45 MW and 2.55 MW, which is much more constant than for the other strategies. Also, for the medium ($N = 10$) and large wind farm ($N = 25$), the results are better. For 25 wind turbines, the reserves P_{reserve} fluctuate between 8.85 MW and 11 MW. However, for larger wind farms, the differences between delta control and the other control strategies become less clear due to the smoothing effect of the wind farm.

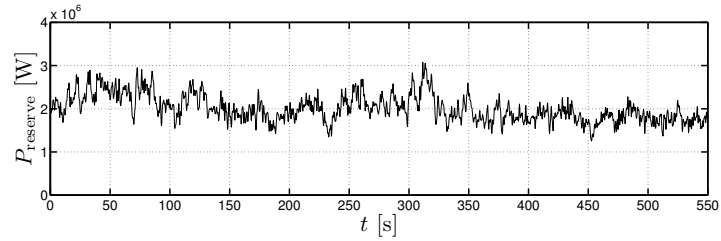

(a) $N = 5$

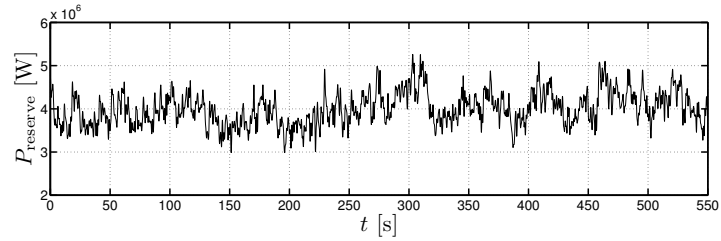

(b) $N = 10$

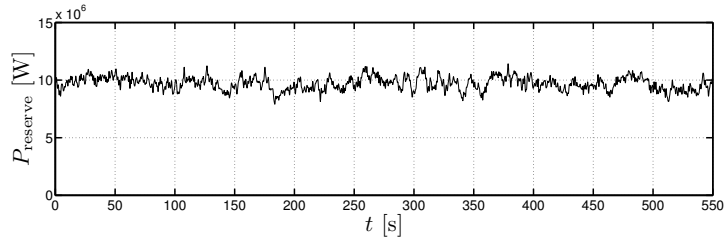

(c) $N = 25$

Figure 5.16: Power reserves in wind farms of different size equipped with linear slope control.

5.2.5 Conclusion

In this section, the provision of power reserves with wind turbines was investigated for four different control strategies.

First, the different control strategies to provide active power reserves with wind turbines were presented. An optimization algorithm to obtain the power reference for the constant power control was developed. Then, the parameters of the other control strategies were tuned to obtain the same average power reserve in order to be able to compare the performance of the different strategies.

Second, the different strategies were applied to a single wind turbine to

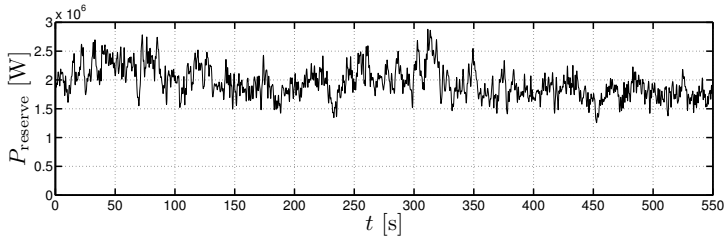

(a) $N = 5$

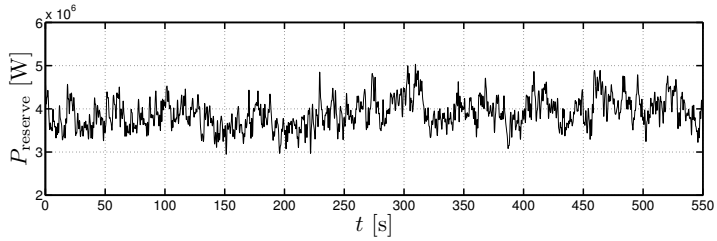

(b) $N = 10$

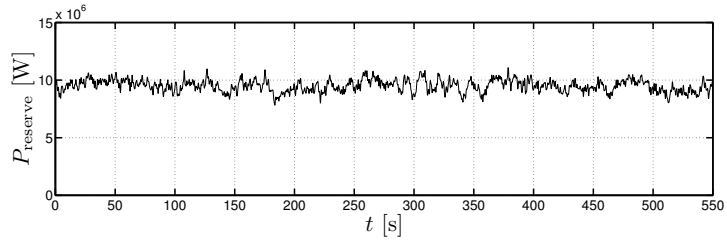

(c) $N = 25$

Figure 5.17: Power reserves in wind farms of different size equipped with percentage control.

determine their ability to maintain power reserves. It was shown that all the strategies have the ability to provide reserves. However, the constant power control strategy is not able to provide a power reserve for the complete time interval as there are periods with zero power reserves. As shown in § 5.2.4.1, lowering the constant reference value by means of balance control is an option, but this results in additional energy yield losses, which is undesired. Furthermore, it only results in a limited increase in the minimum power reserves. Therefore, balance control was not further investigated in this section. Linear slope control, percentage control and delta control give better results as they are able to always maintain a power reserve.

Third, wind farms were considered to identify the ability to provide

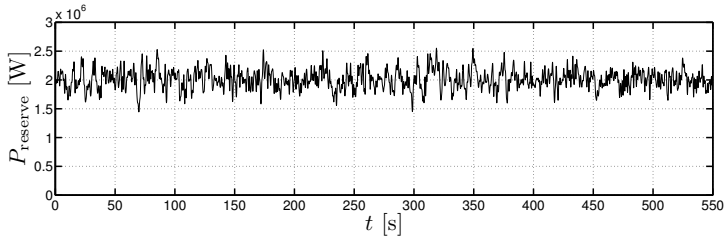

(a) $N = 5$

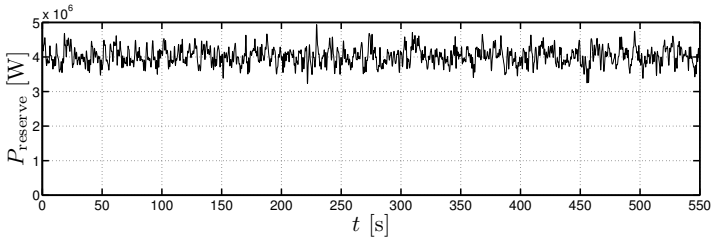

(b) $N = 10$

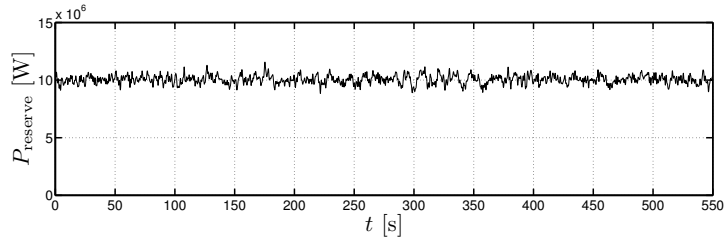

(c) $N = 25$

Figure 5.18: Power reserves in wind farms of different size equipped with delta control.

power reserves. Now, the difference between the different control strategies is less pronounced, but linear slope control, percentage control and delta control perform much better than constant power control, especially for smaller wind farms. Of these three strategies, delta control performs the best as the power reserves fluctuate the least and the minimum value for the power reserves is the highest. The difference between the strategies becomes smaller for larger wind farms.

Considering the implementation complexity of the different control strategies, there are some differences between the considered strategies. For constant power control and balance control the prediction of the wind speed is crucial. The better this prediction is, the closer the reference value can

be chosen to the maximum value. The need for an accurate wind speed prediction complicates the use of these strategies. For the linear slope control, the optimal parameters should be tuned according to the wind speed v, which is a disadvantage of this strategy. The reference power for percentage control and delta control can be calculated if the MPP-curve is known. As this curve is usually available to perform MPPT in normal operation, the implementation of these strategies is less complex than for the other strategies.

Overall, delta control is the most suitable to maintain power reserves with wind turbines as the use of this strategy result in the most constant power reserves. Percentage control is the second best option. For both delta control and percentage control, the control parameters can be derived independently of the wind speed, which is an advantage. Despite a similar power reserve behavior as the percentage control strategy, the linear slope control strategy is less suited to provide power reserves as the control parameters strongly depend on the wind speed, which is a disadvantage. Finally, considering the large fluctuations in the power reserves, constant power control can only be used for very large wind farms.

5.3 Adaptive droop control

In the previous sections, the provision of power reserves to cope with under-frequency events was explained. In this section, over-frequency events are considered. A control strategy to decrease the power output in case of an over-frequency event, i.e., adaptive droop control, is presented. Adaptive droop control allows to share the power equally between wind turbines with a different power output - contrary to the fixed droop control.

First, the control strategy is presented together with an estimation method of the maximum power point. Second, the simulation results are summarized.

5.3.1 Droop control strategies

In the following paragraphs, the two different droop control strategies of Fig. 5.19 are discussed: fixed droop control and adaptive droop control. Furthermore, the operating principle of both strategies is compared.

5.3.1.1 Fixed droop control

First, the conventional fixed droop control strategy is presented. The reference power P_{ref} of the wind turbine is given by the following expression

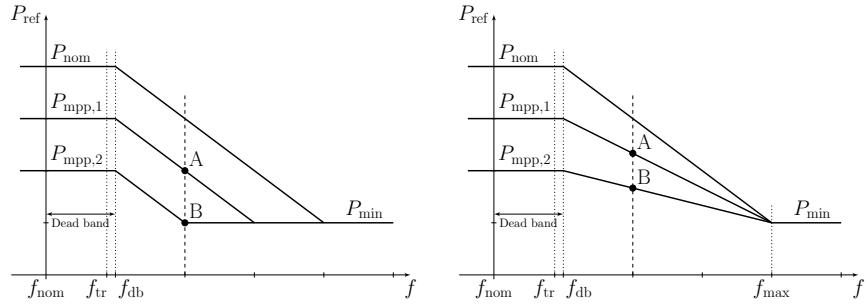

(a) Fixed droop control **(b)** Adaptive droop control

Figure 5.19: Fixed versus adaptive droop control.

(see Fig. 5.19a):

$$P_{\text{ref}} = \begin{cases} P_{\text{mppt}} & f \leq f_{\text{tr}} \\ P^*_{\text{mpp}} - \left(P^*_{\text{mpp}} - P_{\text{mppt}}\right) \frac{f_{\text{db}} - f}{f_{\text{db}} - f_{\text{tr}}} & f_{\text{tr}} < f \leq f_{\text{db}} \\ P^*_{\text{mpp}} - K_{\text{prim}} \left(f - f_{\text{db}}\right) & f_{\text{db}} < f \;\&\; P_{\text{ref}} > P_{\text{min}} \\ P_{\text{min}} & \text{else} \end{cases} \tag{5.14}$$

where P_{mppt} is the reference power determined by the maximum power point tracker (MPPT), P^*_{mpp} is the estimated maximum available power (see § 5.3.2), f is the measured grid frequency, f_{tr} is the transition frequency band and f_{db} is the frequency dead band. The power-electronic converter controls the output power of the wind turbine according to this reference power.

As long as the grid frequency f is below the transition frequency band f_{tr}, the power output is determined by the MPPT. Here, power control is used, so P_{mppt} is calculated as a function of the rotational speed Ω. Of course, the fixed droop control strategy can also be used with other MPPT strategies such as perturb and observe (P&O) or TSR control [29].

When the frequency f is between f_{tr} and f_{db}, the transition between the MPPT and the estimated power P^*_{mpp} is made. The influence of the MPPT on P_{ref} is gradually decreased while the estimated power takes over. If the estimation is not completely accurate, this transition band ensures a smooth operation of the control strategy. If the frequency f is above f_{db} and the reference power is above the minimum power output P_{min}, the reference power P_{ref} is determined by the fixed droop curve which depends on the droop constant K_{prim} and the deviation of the grid frequency from the dead band value f_{db}. When the grid frequency is so high that the

reference power would fall below $P_{\min}$, the power output remains fixed at the minimum power output value $P_{\min}$.

5.3.1.2 Adaptive droop control

Second, the mathematical formulation of the adaptive droop control strategy is provided. The reference power P_{ref} of the wind turbine is given by the following expression (see Fig. 5.19b):

$$P_{\text{ref}} = \begin{cases} P_{\text{mppt}} & f \leq f_{\text{tr}} \\ P^*_{\text{mpp}} - \left(P^*_{\text{mpp}} - P_{\text{mppt}}\right) \frac{f_{\text{db}} - f}{f_{\text{db}} - f_{\text{tr}}} & f_{\text{tr}} < f \leq f_{\text{db}} \\ P^*_{\text{mpp}} - P^*_{\text{mpp}} \frac{f - f_{\text{db}}}{f_{\max} - f_{\text{db}}} & f_{\text{db}} < f \leq f_{\max} \\ P_{\min} & f > f_{\max} \end{cases} \tag{5.15}$$

where $f_{\max}$ is the maximum grid frequency. Again, the power output of the wind turbine is controlled to this reference value by means of the power-electronic converter.

As long as the grid frequency f is below the transition frequency band f_{tr}, the power output is determined by the MPPT. When the frequency f is between f_{tr} and f_{db}, the transition between the MPPT and the estimated power P^*_{mpp} is made. The influence of the MPPT on P_{ref} is gradually decreased while the estimated power takes over. If the frequency f is between f_{db} and $f_{\max}$, the reference power P_{ref} is determined by the adaptive droop curve, as explained in section 5.3.1.3. Finally, the power output of the wind turbine reaches $P_{\min}$ when the grid frequency f exceeds its maximum value.

In order to obtain operation below the MPP, which is needed to decrease the power output of the wind turbine, speed control is used for both droop control strategies in this section.

5.3.1.3 Theoretical analysis

In Fig. 5.19a, the fixed droop control strategy is shown. The droop curve is determined by the value of the droop constant K_{prim}, which is independent of the actual power output P_{mpp} of the wind turbine. Consequently, for a certain deviation of the grid frequency Δf, the power output of the wind turbine is reduced with a fixed amount of power $K_{\text{prim}}\Delta f$, given that the power output is well above $P_{\min}$. For a high wind speed, the MPPT results in a power output $P_{\text{mpp},1}$. When the frequency increases above f_{db}, indicated by the dashed line in Fig. 5.19a, the power output of the wind turbine is decreased to point A by the fixed droop control strategy. For a low wind speed, a power output $P_{\text{mpp},2}$ is obtained, which results in operating point B for the same frequency increase. Consequently, the power output of the

wind turbine is decreased proportionally to the frequency deviation without taking into account the actual power output. Only for very low wind speeds, the decrease in power output is limited by the minimum power $P_{\min}$.

In Fig. 5.19b, the adaptive droop control strategy is presented. Here, the droop curve is determined by the actual power output P_{mpp} instead of the fixed droop constant K_{prim}. For a high wind speed v, the power output is $P_{\text{mpp},1}$. When the frequency increases above f_{db} indicated by the dashed line, the power output of the wind turbine is reduced to point B. For a lower wind speed, the power output is given by $P_{\text{mpp},2}$, which results in operating point A for the same frequency deviation. However, the power reduction is smaller for the lower wind speed than for the higher wind speed, as the droop constant K_{prim} is variable and given by:

$$K_{\text{prim,adapt}} = \frac{P^*_{\text{mpp}}}{f_{\max} - f_{\text{db}}} \tag{5.16}$$

This results in an equal percentage decrease of the power output of wind turbines with different wind speed conditions. Contrary to the fixed droop control, the adaptive droop control strategy makes it possible to establish equal power sharing between remote wind farms (with different wind speeds). In this way, wind turbines assist in the primary control according to their actual power output.

In order to be able to apply the fixed droop control strategy and the adaptive droop control strategy, knowledge of the maximum available power P_{mpp} is essential. If a wind speed measurement is available, the measured wind speed can be used to calculate P_{mpp}. However, the wind speed speed measurement is often not so accurate due to the placement of the anemometer at the top of the nacelle, behind the wind turbine rotor. Therefore, P_{mpp} can also be estimated, which is described in § 5.3.2.

5.3.2 Estimation of the maximum power point

For the droop control strategies presented in this section, knowledge of the available wind power is crucial, especially when the wind turbine is operating below the MPP. Therefore, an estimation algorithm is proposed.

First, the operating principle of the wind speed and maximum power point estimation algorithm is presented. Then, simulation results of the wind speed estimation are presented.

5.3.2.1 Estimation algorithm

In order to determine the maximum available power for every operating condition, the wind speed v has to be known. On medium and large wind

turbines, usually, an anemometer is placed on top of the nacelle to measure the wind speed. Since the wind speed is measured behind the wind turbine rotor where the wind is quite turbulent, this measurement often has limited accuracy. Short-term wind speed forecasts or LIDAR measurements could be combined with the wind speed measurements of the anemometer to enhance the accuracy. However, the higher cost associated with these methods, limits its applicability to wind turbines in a wind farm. On small wind turbines, the anemometer is sometimes omitted to reduce investment costs. Therefore, it is useful to estimate the wind speed by measuring operational parameters such as the rotational speed Ω and the power output of the wind turbine. In literature, different strategies exist to estimate the wind speed accurately [120–123]. Here, an estimation method based on measurements of the rotational speed Ω and the generator power P_g is developed. The method is simple, which is an advantage, but less accurate compared to more advanced estimation algorithms. As shown further (§ 5.3.2.2), the accuracy is sufficient to use the estimation in the adaptive P/f droop control strategy.

The rotational speed Ω can be determined by measuring the frequency f_g of the generator currents [124] or by means of an encoder or resolver. The generator power P_g is calculated by measuring the generator current I_g and line-to-neutral voltage V_g with a high sampling frequency f_s (e.g. 16 kHz). The generator power P_g is then given by

$$P_\mathrm{g} = \frac{1}{N_\mathrm{s}} \sum_{n=1}^{N_\mathrm{s}} \sum_{i=1}^{3} v_{\mathrm{g},i}(n) \cdot i_{\mathrm{g},i}(n) \tag{5.17}$$

where $v_{\mathrm{g},i}(n)$ and $i_{\mathrm{g},i}(n)$ are the sampled generator voltages and currents of the three phases and N_s is the integer number of samples in one period of the generator current:

$$N_\mathrm{s} = \left\| \frac{f_\mathrm{s}}{f_\mathrm{g}} \right\| \tag{5.18}$$

Both P_g and Ω can be measured with high accuracy.

However, in order to determine the wind speed v, the wind turbine power P_t has to be known. In steady-state, the turbine power P_t can be calculated from the generator power P_g:

$$P_\mathrm{t} = \frac{P_\mathrm{g}}{\eta_\mathrm{g}} \tag{5.19}$$

where η_g is the generator efficiency. The generator efficiency η_g depends on the generator torque T_g and the rotational speed Ω and can be determined by off-line measurements or simulations to obtain a two-dimensional efficiency map in function of T_g and Ω.

As explained in § 2.2.2, the following equation is known to be a good representation of the wind turbine power (see (2.13)):

$$P_{\mathrm{t}} = \frac{1}{2}\rho\pi r^2 v^3 \cdot C_{\mathrm{p}}(\lambda, \beta) \tag{5.20}$$

where $C_{\mathrm{p}}(\lambda, \beta)$ is determined by (2.15) and (2.16). There are also other polynomial expressions for C_{p} available which can be fitted to manufacturer data [34].

Considering (5.20), (2.14) and $C_{\mathrm{p}}(\lambda, \beta)$, the wind speed v can be calculated if the wind turbine power P_{t} and rotational speed Ω are known. The rotational speed Ω is measured and the wind turbine power P_{t} is approximated by (5.19). The calculation of P_{t} from P_{g} is only valid in steady-state operation. In order to obtain a correct value for P_{t} in varying wind conditions, the wind turbine dynamics should be taken into account when calculating the wind turbine power P_{t} from the generator power P_{g} [120–123]. However, as the focus of this section is on the comparison between the different droop control strategies, using (5.19) for the wind turbine power results in sufficient accuracy.

As the power coefficient C_{p} is often a non-linear function of λ (and thus v), it might be impossible to find a closed form analytical expression to calculate v. Therefore, an iterative procedure is used to estimate v (see Fig. 5.20). Every Δt seconds, the wind speed estimation algorithm is executed. Firstly, P_{g} and Ω are measured. Secondly, the initial speed of the algorithm v_{i} is calculated, which is an underestimation of the actual wind speed. Also, the error band $[P_{\mathrm{w,min}}, P_{\mathrm{w,max}}]$ for the power estimation is defined. Then the iterative process is started: the temporary estimation of the wind speed v_{w} and the measured rotational speed Ω are used to calculate the power coefficient C_{p} and the temporary estimation of the wind power P_{w}. Then, it is checked if P_{w} is inside the error band $[P_{\mathrm{w,min}}, P_{\mathrm{w,max}}]$. If this is the case, it means that v_{w} is a good estimation of the wind speed v^*. Otherwise, the temporary wind speed v_{w} is raised with Δv_{w} and the process is repeated until v^* is found. The choice of Δv_{w} is a trade-off between accuracy and speed: the smaller Δv_{w}, the slower the estimation process is. The parameter ΔP has to be tuned together with Δv_{w} to ensure convergence of the algorithm. The smaller Δv_{w} is chosen, the smaller ΔP should be.

When the estimated wind speed v^* is known, the maximum available wind power P^*_{mpp} can be easily calculated:

$$P^*_{\mathrm{mpp}} = \frac{1}{2}\rho\pi r^2 C_{\mathrm{p,max}} \cdot v^{*3} \tag{5.21}$$

This estimated power P^*_{mpp} can be used as P_{mpp} in the droop control strategies.

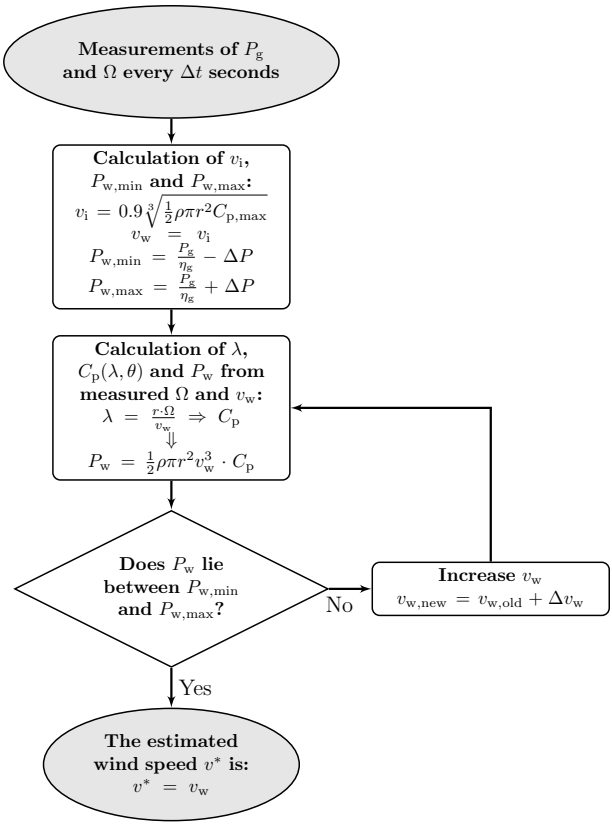

Figure 5.20: Wind speed estimation flowchart.

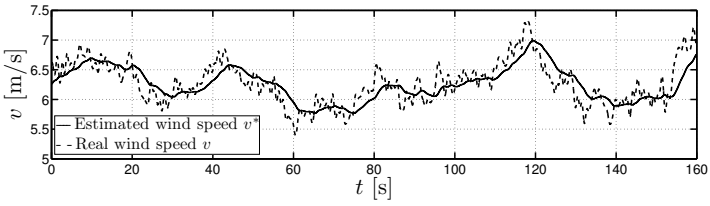

Figure 5.21: Variable wind speed pattern: wind speed estimation results.

5.3.2.2 Results of the estimation algorithm

In Fig. 5.21, the results of the wind speed estimation algorithm are shown. The parameters that are used for the simulations are given in Table 5.3.

The real wind speed v is denoted by the dashed line, whereas the estimated wind speed v^* is represented by the solid line. It can be concluded

Param.	Value	Unit	Param.	Value	Unit
P_{nom}	3.0	MW	ΔP	1000	W
r	56	m	Δv_{w}	$1 \cdot 10^{-3}$	m/s
ρ	1.225	kg/m^3	Δt	0.1	s
J_{wt}	$1.24 \cdot 10^7$	kg $\cdot$ m^2	$C_{\text{p,max}}$	0.4412	–
f_{nom}	50	Hz	f_{tr}	1.00025	pu
f_{db}	1.0003	pu	f_{max}	1.04	pu
K_{prim}	0.45	MW/Hz			

Table 5.3: Simulation parameters for the fixed droop control and adaptive droop control.

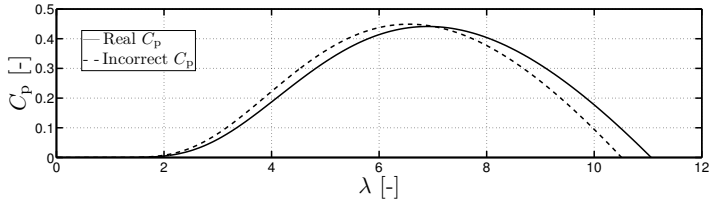

Figure 5.22: Incorrect power coefficient C_{p} for the sensitivity analysis.

that the simple estimation algorithm is able to estimate the wind speed quite accurately, but some delay between the real wind speed and the estimated wind speed can be noted.

Second, the results of the sensitivity analysis are presented. Two cases are considered and compared to the original case:

1. with an incorrect power coefficient C_{p}, shown in Fig. 5.22
2. with an incorrect efficiency η_{g} (estimated 10 % too high)

As explained in section 5.3.2.1, both C_{p} and η_{g} have an important impact on the estimation of the MPP.

In Fig. 5.23, the results are depicted. As expected, the estimation of the wind speed v is affected by the incorrect parameters. Due to the incorrect power coefficient or generator efficiency, the wind speed is underestimated. However, as the MPPT is used during normal operation, the incorrect wind speed estimation only affects the power output of the wind turbine when the droop control is activated. Due to the transition band, the transition from MPPT to droop control is smooth, so the incorrect wind speed estimation has little impact on the behavior of the droop control strategies. It will affect the decrease in power output as the maximum available power P_{mpp}

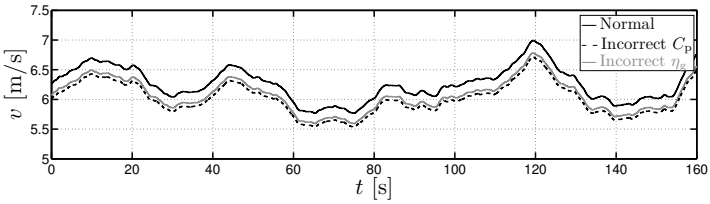

Figure 5.23: Sensitivity analysis.

is estimated incorrectly. Therefore, the actual decrease in power output might be higher or lower compared to the case with the correct estimation. Also, if some wind turbines have a correct estimation while others have not, the equal power sharing capability will be affected.

5.3.3 Simulation results

In Fig. 5.24, the simulation results for the fixed droop control and adaptive droop control are summarized. The simulation parameters are given in Table 5.3. In the power system of § 3.6.4, instead of a loss of generation of 3 GW, a load loss of 3 GW is simulated. This results in the over-frequency behavior of Fig. 5.24.

In the simulations, two wind turbines are considered: one wind turbine, operating at a wind speed of 9 m/s (WT 1) and one wind turbine operating at a higher wind speed of 10 m/s (WT 2). Considering the estimation of the wind speed v, it is clear that the algorithm is able to track the wind speed correctly with a transient immediately after the frequency rise. The tracking results for the fixed droop control and adaptive droop control are quite similar.

When the power output P_g is considered for the fixed droop control, the decrease in power output is the same for both wind turbines. This results in a different droop ratio $P_\mathrm{g}/P_\mathrm{mpp}$ for both wind turbines. The relative change in the output power is the highest for wind turbine 1, which operates under the lowest wind speed v. Consequently, for a given frequency change, the higher the power output of the wind turbine, the lower the droop ratio $P_\mathrm{g}/P_\mathrm{mpp}$ will be. This is also reflected in the change of the rotational speed Ω, which is similar for both wind turbines.

When the adaptive droop control is considered, it is clear that the power decrease depends strongly on the operating point of the wind turbine. The wind turbine with the highest power output has the highest contribution in the primary frequency control. When the droop ratio $P_\mathrm{g}/P_\mathrm{mpp}$ is compared for both wind turbines, the difference is much smaller due to the use of

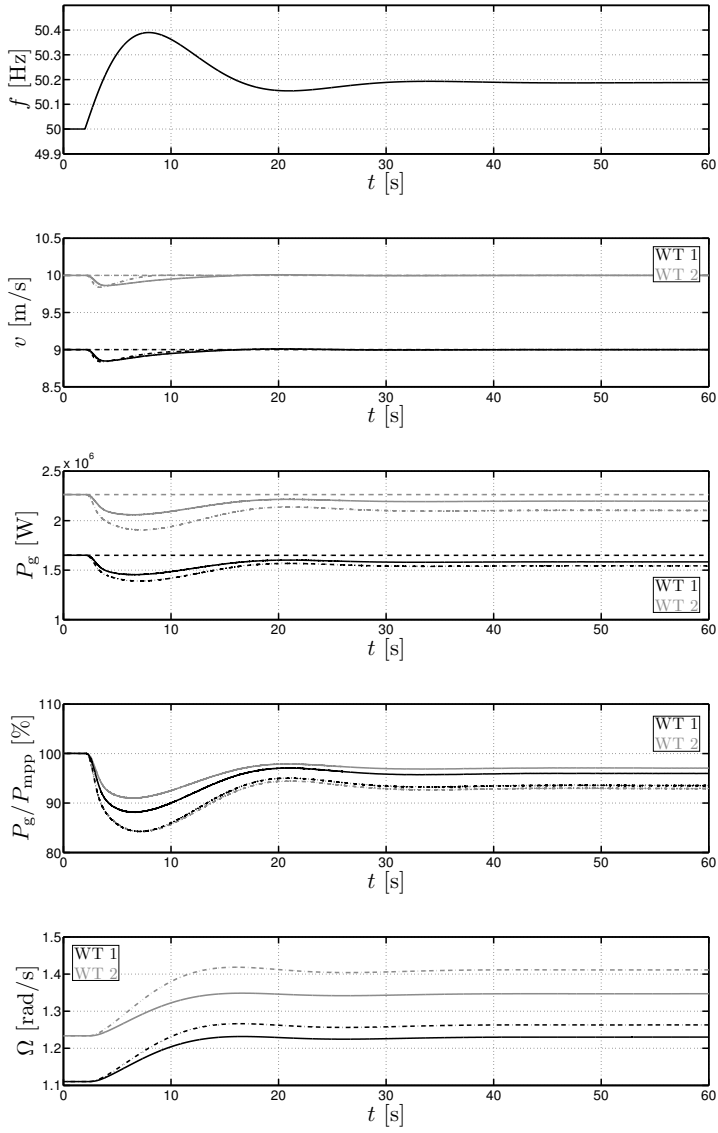

Figure 5.24: Equal power sharing results: - - = real v and maximum available P_g, — = with fixed droop control, -·- = with adaptive droop control.

adaptive droop control. The small difference in $P_\mathrm{g}/P_\mathrm{mpp}$ is due to wind speed prediction errors. Consequently, both wind turbines participate in the primary frequency control dependent on their operating point, which

results in a more equal power sharing. This is also visible in the rotational speed Ω, which changes much more for the wind turbine with the highest power output.

5.3.4 Conclusion

In this section, two droop control strategies to cope with over-frequency events were compared: fixed droop control and adaptive droop control. For both strategies, knowledge of the MPP is needed, so a simple wind speed estimation algorithm was developed. It was shown that both control strategies decrease the power output of the wind turbines after the event. For the conventional, fixed droop control, the decrease in power output is independent of the operating point. For the adaptive droop control, the droop action depends on the actual power output of the wind turbine, which results in a more equal participation of the wind turbines in the primary frequency control.

5.4 Conclusion

In this chapter, primary frequency control with wind turbines was discussed.

First, an overview of primary frequency control with wind turbines was presented. The overall control strategy was discussed and the different options to deload wind turbines were discussed. Furthermore, control strategies to allow continuous deloading of wind turbines were given.

Second, the different deloading control strategies were compared. For one of the considered strategies, i.e., constant power control, the choice of the power reference P_{ref} is crucial in order to provide active power reserves. Therefore, an optimization algorithm was developed in this work to determine the range of possible constant power references for a given time interval. It was shown that all the presented strategies are able to provide active power reserves, but there are large differences between the different strategies. Delta control gives the best results as the power reserves were the most constant for this control strategy. However, there are still some periods in time with very low power reserves. Consequently, the aggregation of several wind turbines in a wind farm was considered. Due to the smoothing effect of the wind farm, the differences between the different control strategies become less pronounced. However, delta control still results in the most constant power reserves.

Finally, a new primary frequency control strategy, called adaptive droop control was developed to cope with over-frequency events in the electrical grid. By using a variable droop constant which depends on the actual power

output of the wind turbine, it is possible to obtain more equal power sharing between wind turbines under different wind speed conditions.

6

Conclusions and further research opportunities

In this chapter, the main conclusions from this dissertation are summarized. Also, some opportunities for further research are listed.

6.1 Conclusions

The goal of this research was to investigate the possibilities to provide ancillary services with wind turbines. The different ancillary services that can be provided with wind turbines were listed, but the focus was on the provision of frequency control with wind turbines.

In chapter 2, an overview of the different ancillary services that are needed in the power system was given. Frequency control and voltage control are well known and important services as they are essential for the proper functioning of the electric grid. Furthermore, congestion management and the improvement of power quality issues enhance the reliability and availability of the power supply. Black start is a service that is only needed in case of a severe incident in the power system. Then, the different types of wind turbines are discussed together with the wind turbine model that is used during the simulations. Finally, the ancillary services that can be (partly) provided by wind turbines are discussed. As the modern wind turbines are equipped with a power-electronic converter, they are perfectly suited to provide a variety of ancillary services. It is clear that frequency

control, voltage control and the enhancement of the power quality are possible services for wind turbines.

The main topic of this research was discussed in chapter 3: emulated inertial response with variable-speed wind turbines. First, the need for sufficient inertia in the power system was clarified. A low system inertia results in a high rate of change of frequency and a low frequency nadir, which complicates the frequency control. When variable-speed wind turbines are connected to the grid, the total amount of synchronously coupled inertia decreases due to the decoupling of the rotational speed of the wind turbine and the grid frequency. Consequently, variable-speed wind turbines such as FSCs and DFIGs show almost no inertial response in case of a disturbance. For high wind power penetrations (or other converter-coupled energy sources, e.g., PV panels), this could endanger the proper functioning of the system.

To overcome this problem, wind turbines could assist in the inertial response by adding an additional control loop to the power-electronic converter. As wind turbines have a similar amount of inertia as conventional directly-coupled synchronous generators, the kinetic energy in this energy buffer could be used to increase the power output during a frequency dip. The grid frequency is continuously monitored and when a frequency disturbance occurs, the power output of the wind turbine is altered to emulate inertial response behavior. In literature, two typical control strategies are available: the synthetic inertia strategy, which mimics the behavior of a synchronous generator and the temporary power surge, which increases the power output according to a predefined reference curve.

In order to obtain the desired inertial response after a disturbance, it is important to tune the parameters of the emulated inertial response strategies. As was showed in this work, the optimal parameter selection depends strongly on the system composition. Also, the recovery strategy has a huge impact on the inertial response behavior of the temporary power surge. Furthermore, it is important not to exaggerate the additional power output. Excessive overproduction results in a longer and deeper recovery period, which could cause a second, undesired frequency dip. When the synthetic inertia strategy and temporary power surge strategy are compared, it can be concluded that synthetic inertia is the most promising as it is the most stable emulation strategy and the sensitivity for incorrect parameters is lower than for the temporary power surge.

Chapter 4 discussed the disadvantages of emulated inertial response with wind turbines. First, the energy yield losses due to emulated inertial response were calculated for optimal and non-optimal parameter selections. It can be concluded that the energy yield losses are very low for all the

considered cases. This is due to the flat shape of the power coefficient curve around the top and the limited variations in the rotational speed that are needed to obtain the optimal inertial response.

Second, the additional torque variations due to the emulated inertial response were considered. As the power output is strongly increased immediately after a disturbance is observed in the grid, a steep increase in the generator torque occurs. These fast variations may result in additional loading of the wind turbine drive-train, which is undesired. Therefore, the DC-bus voltage modulation strategy was developed in this research. This strategy reduces the heavy torque variations by using the storage capacity of the DC-link. By adapting the control strategy, it can be effectively used for both considered emulated inertial response strategies. The total inertial response obtained from the wind turbine remains unaffected, so it can be perfectly combined with the findings of chapter 3.

Consequently, it can be concluded that the negative effects of inertial response with wind turbines are either quite limited (energy yield losses) or can be effectively mitigated by using proper control strategies in the wind turbine control (torque variations). Consequently, the disadvantages associated with emulated inertial response do not outweigh the positive effect it has on the integration of variable-speed wind turbines in the power system.

In the final chapter of this dissertation, primary frequency control with wind turbines was discussed. First, an overview of the overall control strategy was given. As primary frequency control with wind turbines requires operation of the wind turbines below the maximum power point, different options to deload wind turbines were discussed. A comparison of the different deloaded power control strategies showed that a broad range of power control strategies can be used to provide power reserves. However, the delta control strategy, which aims to maintain a fixed power reserve, performs the best. If the control strategies are applied to the wind farm level, the differences between the different control strategies are almost negligible due to the smoothing effect. However, delta control still performs the best of all the control strategies.

Finally, the adaptive droop control strategy was developed to cope with over-frequency events in the electrical grid. For this control strategy, a variable droop constant dependent on the actual power output of the wind turbine is used instead of the conventional fixed droop constant. In this way, this strategy allows a much more equal power sharing between remote wind farms under different wind speed conditions.

6.2 Further research opportunities

During this research, some other interesting research paths that were out of the scope of this PhD were identified. The most important ones are summarized here.

6.2.1 Automatic optimal control parameter selection for the emulated inertial response strategies

In chapter 3, the importance of the optimal parameter selection for the emulated inertial response strategies was shown. The optimal parameter selection was performed manually, but could be automated in the future. By applying a cost function with penalties for a low frequency nadir, a high ROCOF, a double frequency dip, etc., an optimization algorithm can be used to find the optimal parameters for different system compositions.

The selection of the best suited optimization algorithm, together with the decision for on-line or off-line optimization of the control parameters could be an interesting research topic.

6.2.2 Influence of large-scale wind turbine integration on system stability

As was shown in this dissertation, large-scale integration of wind turbines in the power system results in a decrease of the synchronously-coupled inertia. Besides the influence on the inertial response behavior after a frequency disturbance, a lower system inertia also has an impact on the transient stability of the power system after a fault in the power system.

In the case of conventional directly-coupled synchronous generators, basic insights in the transient stability could be gained by using the swing-equation and the equal-area condition. However, when variable-speed wind turbines are connected to the power system, the analysis becomes much more complicated due to the presence of the power-electronic converter. Consequently, in literature, simulations are performed to investigate the influence of variable-speed wind turbines on the transient stability [125–131]. The simulations show that variable-speed wind turbines could have both a negative as a positive impact on the system stability, dependent on the type of wind turbine and the place of the connection point in the network. Therefore, it is difficult to make general statements about the influence of wind turbines on the system stability.

Furthermore, when the wind turbines are equipped with additional control loops, such as an inertial response control loop or grid voltage control

loops, this might alter the behavior in case of a system fault. Therefore, it might be interesting to study these effects in the future.

6.2.3 Impact of ancillary service provision on the lifetime of wind turbines

When wind turbines start to provide ancillary services such as emulated inertial response, frequency control, voltage control, etc., this might affect the lifetime of the wind turbines. For example, due to the additional torque variations on the wind turbine shaft due to emulated inertial response, this might result in a faster wear of the drive-train. Deloading of the wind turbines by means of speed control results in an increased rotational speed. Continuously operating at a higher rotational speed might affect the lifetime of the bearings and other components in the drive-train. When wind turbines inject reactive power in the grid to assist in the voltage control, higher currents are injected, which has an influence on the power-electronic converter.

Consequently, it is interesting to investigate the impact of the different ancillary services on the lifetime of the wind turbines. This makes it possible to estimate the costs of providing ancillary services with wind turbines. For example, in order to effectively use the DC-bus voltage modulation strategy, a larger DC-bus capacitor is needed. When the impact of the emulated inertial response on the lifetime of the different wind turbine components is known, it can be determined if it is feasible to invest in additional DC-bus capacitors to reduce the torque variations. Also, the needed amount of additional capacitors to achieve the most cost-optimal configuration could be determined.

6.2.4 Field implementation and testing of emulated inertial response and primary frequency control

In this work, it was shown theoretically and by means of simulations that wind turbines can effectively assist in the provision of ancillary services such as emulated inertial response and primary frequency control. A next step is the practical field implementation of these services in a wind farm. The frequency response of the wind turbines in case of a disturbance can be monitored to validate the participation of wind turbines in the frequency control. This way, it can be investigated if wind turbines are technically able to assist in the provision of these services.

Furthermore, a practical field trial is an ideal test case to investigate the market participation of wind turbines in the ancillary services markets. Also

the impact of the wind speed variability on the availability of ancillary services such as emulated inertial response and primary frequency control can be investigated. The possibility to use additional measurements or short-term predictions to reduce the uncertainty might be considered. Therefore, it could be interesting to study new or adapted market schemes to allow participation of wind turbines in the different ancillary services markets.

Bibliography

[1] Global Wind Energy Council, "Global wind report - annual market update 2015," p. 76, Mar. 2016, http://www.gwec.net/publications/global-wind-report-2/.

[2] T. Vandoorn, J. Van de Vyver, L. Gevaert, L. Degroote, and L. Vandevelde, "Congestion control algorithm in distribution feeders: integration in a distribution management system," *Energies*, vol. 8, no. 6, pp. 6013–6032, Jun. 2015.

[3] N. Troy, E. Denny, and M. O'Malley, "Base-load cycling on a system with significant wind penetration," *IEEE Transactions on Power Systems*, vol. 25, no. 2, pp. 1088–1097, May 2010.

[4] Union of the Electricity Industry – Eurelectric, "Ancillary services - unbundling electricity products - an emerging market," pp. 1–84, 2004, http://www.eurelectric.org.

[5] M. Braun, "Provision of ancillary services by distributed generators - technological and economic perspective," Ph.D. dissertation, University of Kassel, Dec. 2009.

[6] E. Hirst and B. Kirby, "Electric-power ancillary services," pp. 1–48, 1996, oak Ridge National Laboratory.

[7] J. Van de Vyver, T. Vandoorn, J. De Kooning, B. Meersman, and L. Vandevelde, "Provision of ancillary services with variable speed wind turbines," in *IEEE Young Researchers Symposium Proceedings*. EESA, Apr. 2014, p. 6.

[8] M. Beck and M. Scherer, "Overview of ancillary services," pp. 1–6, 2010, http://www.swissgrid.ch.

[9] ENTSO-E, "Survey on ancillary services procurement and electricity balancing market design," pp. 1–110, 2012, https://www.entsoe.eu.

[10] ENTSO-E, "Operation handbook," 2009, https://www.entsoe.eu/publications/system-operations-reports/operation-handbook/.

[11] ENTSO-E, "Operational reserve ad hoc team report," pp. 1–58, 2012, https://www.entsoe.eu.

[12] J. Zhong, "On some aspects of design of electric ancillary service markets," Ph.D. dissertation, Chalmers University of Technology, Göteborg, Sweden, 2003.

[13] ENTSO-E, "Supporting document for the network code on load-frequency control and reserves," Jun. 2013, https://www.entsoe.eu/major-projects/network-code-development/load-frequency-control-reserves/Pages/.

[14] ENTSO-E, "Network code on load-frequency control and reserves," Jun. 2013, https://www.entsoe.eu/major-projects/network-code-development/load-frequency-control-reserves/Pages/.

[15] H. Markiewicz and A. Klajn, "Voltage disturbances standard en 50160 - voltage characteristics in public distribution systems," pp. 1–16, Jul. 2004, http://admin.copperalliance.eu/docs/librariesprovider5/power-quality-and-utilisation-guide/542-standard-en-50160-voltage-characteristics-in.pdf.

[16] O. A. Mousavi and R. Cherkaoui, "Literature survey on fundamental issues of voltage and reactive power control," Jun. 2011, http://www.eeh.ee.ethz.ch/fileadmin/user_upload/eeh/MARS/Publications/Foundamental_Issues_on_Voltage_and_Reactive_Power_Control.pdf.

[17] M. H. J. Bollen and I. Y. H. Gu, *Signal Processing of Power Quality Disturbances*, ser. IEEE Press Series on Power Engineering, M. E. El-Hawary, Ed. John Wiley & Sons, Inc., 2006.

[18] M. Bollen, "What is power quality?" *Electric Power Systems Research*, vol. 66, no. 1, pp. 5–14, Jul. 2003.

[19] R. S. Vedam and M. S. Sarma, *Power Quality VAR Compensation in Power Systems*. Taylor & Francis Group, 2009.

[20] B. Meersman, "Control of 3-phase inverter-connected distributed generators regarding the improvement of the power quality," Ph.D. dissertation, Ghent University, Department of Electrical Energy, Systems and Automation, Sint-Pietersnieuwstraat 41, Ghent, Belgium, 2012.

[21] G. W. Chang and P. F. Ribeiro, *Tutorial on Harmonics Modeling and Simulation*. IEEE Power Engineering Society, 1998, ch. Harmonics Theory.

[22] J. Arrillaga, N. Watson, and S. Chen, *Power System Quality Assessment*. John Wiley & Sons, Inc., 2000.

[23] J. D. M. De Kooning, "Balancering van het middelpunt van de busspanning bij driefasige netgekoppelde invertoren met neutrale geleider," Master's thesis, Ghent University, Department of Electrical Energy, Systems and Automation, Sint-Pietersnieuwstraat 41, Ghent, Belgium, 2010.

[24] A. Larsson, "Flicker emission of wind turbines during continuous operation," *IEEE Transactions on Energy Conversion*, vol. 17, no. 1, pp. 114–118, Mar. 2002.

[25] A. Larsson, "Flicker emission of wind turbines caused by switching operations," *IEEE Transactions on Energy Conversion*, vol. 17, no. 1, pp. 119–123, Mar. 2002.

[26] B. Barahona, P. Sørensen, L. Christensen, T. Sørensen, H. K. Nielsen, and X. G. Larsén, "Validation of the standard method for assessing flicker from wind turbines," *IEEE Transactions on Energy Conversion*, vol. 26, no. 1, pp. 373–378, Mar. 2011.

[27] A. Sannino, J. Svensson, and T. Larsson, "Power-electronic solutions to power quality problems," *Electric Power Systems Research*, vol. 66, no. 1, pp. 71–82, Jul. 2003.

[28] H. Samet and M. A. Jarrahi, "A comparison between SVC and STATCOM in flicker mitigation of electric arc furnace using practical recorded data," *International Journal of Smart Electrical Engineering*, vol. 3, no. 4, pp. 209–214, Sep. 2014.

[29] Z. Chen, J. M. Guerrero, and F. Blaabjerg, "A review of the state of the art of power electronics for wind turbines," *IEEE Transactions on Power Electronics*, vol. 24, no. 8, pp. 1859–1875, Aug. 2009.

[30] J. Serrano-González and R. Lacal-Arántegui, "Technological evolution of onshore wind turbines - a market-based analysis," *Wind Energy*, Feb. 2016, online.

[31] S. Müller, M. Deicke, and R. W. De Doncker, "Doubly fed induction generator systems for wind turbines," *IEEE Industry Applications Magazine*, vol. 8, no. 3, pp. 26–33, May 2002.

[32] J. G. Slootweg, S. W. H. de Haan, H. Polinder, and W. L. Kling, "General model for representing variable speed wind turbines in power system dynamics simulations," *IEEE Transactions on Power Systems*, vol. 18, no. 1, pp. 144–151, Feb. 2003.

[33] H. Polinder, F. F. A. Van der Pijl, G.-J. de Vilder, and P. J. Tavner, "Comparison of direct-drive and geared generator concepts for wind turbines," *IEEE Transactions on Energy Conversion*, vol. 21, no. 3, pp. 725–733, Sep. 2006.

[34] L.-F. Pak and V. Dinavahi, "Real-time simulation of a wind energy system based on the doubly-fed induction generator," *IEEE Transactions on Power Systems*, vol. 24, no. 3, pp. 1301–1309, Aug. 2009.

[35] L. Mihet-Popa, F. Blaabjerg, and I. Boldea, "Wind turbine generator modeling and simulation where rotational speed is the controlled variable," *IEEE Transactions on Industry Applications*, vol. 40, no. 1, pp. 3–10, Jan. 2004.

[36] J. G. Slootweg, H. Polinder, and W. L. Kling, "Representing wind turbine electrical generating systems in fundamental frequency simulations," *IEEE Transactions on Energy Conversion*, vol. 18, no. 4, pp. 516–524, Dec. 2003.

[37] V. Agarwal, R. K. Aggarwal, P. Patidar, and C. Patki, "A novel scheme for rapid tracking of maximum power point in wind energy generation systems," *IEEE Transactions on Energy Conversion*, vol. 25, no. 1, pp. 228–236, Mar. 2010.

[38] J. R. Welty, C. E. Wicks, R. E. Wilson, and G. Rorrer, in *Grid Integration of Wind Energy: Onshore and Offshore Conversion Systems*. Wiley, 2006.

[39] J. Morren, J. Pierik, and S. W. de Haan, "Inertial response of variable speed wind turbines," *Electric Power Systems Research*, vol. 76, 2006.

[40] J. Melkebeek, *Dynamics of electrical machines and drives*. Ghent University, 2012.

[41] X. Bracke, J. D. M. De Kooning, J. Van de Vyver, and L. Vandevelde, "Effective capture of wind gusts in small wind turbines by using a full active rectifier," in *Proceedings of the 3rd IET Renewable Power Generation Conference (IET RPG)*, Sep. 2014, pp. 1–6.

[42] I. D. Margaris, S. A. Papathanassiou, N. D. Hatziargyriou, A. A. Hansen, and P. Sørensen, "Frequency control in autonomous power systems with high wind power penetration," *IEEE Transactions on Sustainable Energy*, vol. 3, no. 2, pp. 189–199, Apr. 2012.

[43] R. G. de Almeida and J. Peças Lopes, "Participation of doubly fed induction wind generators in system frequency regulation," *IEEE Transactions on Power Systems*, vol. 22, no. 3, pp. 944–950, Aug. 2007.

[44] The European Wind Energy Association, "Twenties project - final report," pp. 1–66, 2013, http://www.ewea.org/publications/reports/twenties-project/.

[45] J. Martínez, P. Kjaer, P. Rodriguez, and R. Teodorescu, "Design and analysis of a slope voltage control for a DFIG wind power plant," *IEEE Transactions on Energy Conversion*, vol. 27, no. 1, pp. 11–20, Mar. 2012.

[46] R. N. Ullah, K. Bhattacharya, and T. Torbjörn, "Wind farms as reactive power ancillary service providers - technical and economic issues," *IEEE Transactions on Energy Conversion*, vol. 24, no. 3, pp. 661–672, Sep. 2009.

[47] S. Engelhardt, I. Erlich, C. Feltes, K. Jörg, and F. Shewarega, "Reactive power capability of wind turbines based on doubly fed induction generators," *IEEE Transactions on Energy Conversion*, vol. 26, no. 1, pp. 364–372, Mar. 2011.

[48] L. Meegahapola, T. Littler, and S. Perera, "Capability curve based enhanced reactive power control strategy for stability enhancement and network voltage management," *International Journal of Electrical Power and Energy Systems*, vol. 52, no. 1, pp. 96–106, Nov. 2013.

[49] K. De Brabandere, B. Bolsens, J. Van den Keybus, A. Woyte, J. Driesen, and R. Belmans, "A voltage and frequency droop control method for parallel inverters," *IEEE Transactions on Power Electronics*, vol. 22, no. 4, pp. 1107–1115, Jul. 2007.

[50] J. De Kooning, J. Van de Vyver, J. D. M. De Kooning, T. L. Vandoorn, and L. Vandevelde, "Grid voltage control with distributed generation using online grid impedance estimation," *Sustainable Energy, Grids and Networks*, vol. 5, pp. 70–77, Mar. 2016.

[51] B. Meersman, B. Renders, L. Degroote, T. Vandoorn, and L. Vandevelde, "Three-phase inverter-connected dg-units and voltage unbalance," *Electric Power Systems Research*, vol. 81, no. 4, pp. 899–906, Apr. 2011.

[52] N. Joshi and N. Mohan, "A novel scheme to connect wind turbines to the power grid," *IEEE Transactions on Energy Conversion*, vol. 24, no. 2, pp. 504–510, Jun. 2009.

[53] V.-T. Phan and H.-H. Lee, "Control strategy for harmonic elimination in stand-alone DFIG applications with nonlinear loads," *IEEE Transactions on Power Electronics*, vol. 26, no. 9, pp. 2662–2675, Sep. 2011.

[54] T. Sun, Z. Chen, and F. Blaabjerg, "Flicker study on variable speed wind turbines with doubly fed induction generators," *IEEE Transactions on Energy Conversion*, vol. 20, no. 4, pp. 896–905, Dec. 2005.

[55] Y.-S. Kim and D.-J. Won, "Mitigation of the flicker level of a DFIG using power factor angle control," *IEEE Transactions on Power Delivery*, vol. 24, no. 4, pp. 2457–2458, Oct. 2009.

[56] W. Hu, Z. Chen, Y. Wangy, and Z. Wang, "Flicker mitigation by active power control of variable-speed wind turbines with full-scale back-to-back power converters," *IEEE Transactions on Energy Conversion*, vol. 24, no. 3, pp. 640–649, Sep. 2009.

[57] M. Bongiorno and J. Svensson, "Voltage dip mitigation using shunt-connected voltage source converter," *IEEE Transactions on Power Electronics*, vol. 22, no. 5, pp. 1867–1874, Sep. 2007.

[58] K. J. P. Macken, M. H. J. Bollen, and R. J. M. Belmans, "Mitigation of voltage dips through distributed generation systems," *IEEE Transactions on Industry Applications*, vol. 40, no. 6, pp. 1686–1693, Nov. 2004.

[59] D. Xie, Z. Xu, L. Yang, J. Ostergaard, Y. Xue, and K. P. Wong, "A comprehensive LVRT control strategy for DFIG wind turbines with enhanced reactive power support," *IEEE Transactions on Power Systems*, vol. 28, no. 3, pp. 3302–3310, Aug. 2013.

[60] L. Yang, Z. Xu, J. Ostergaard, Z. Y. Dong, and K. P. Wong, "Advanced control strategy of DFIG wind turbines for power system fault ride through," *IEEE Transactions on Power Systems*, vol. 27, no. 2, pp. 713–722, May 2012.

[61] L. Meegahapola, T. Littler, and D. Flynn, "Decoupled-DFIG fault ride-through strategy for enhanced stability performance during grid faults," *IEEE Transactions on Sustainable Energy*, vol. 1, no. 3, pp. 152–162, Oct. 2010.

[62] I. Erlich, M. Wilch, and C. Feltes, "Reactive power generation by DFIG based wind farms with AC grid connection," in *European Conference on Power Electronics and Applications, 2007*, Sep. 2007, p. 10.

[63] H. Geng, C. Liu, and G. Yang, "LVRT capability of DFIG-based WECS under asymmetrical grid fault condition," *IEEE Transactions on Industrial Electronics*, vol. 60, no. 6, pp. 2495–2509, Jun. 2013.

[64] S. Hu, X. Lin, Y. Kang, and X. Zou, "An improved low-voltage ride-through control strategy of doubly fed induction generator during grid faults," *IEEE Transactions on Power Electronics*, vol. 26, no. 12, pp. 3653–3665, Dec. 2011.

[65] M. Aktarujjaman, M. A. Kashem, M. Negnevitsky, and null, "Black start with DFIG based distributed generation after major emergencies," in *International Conference on Power Electronics, Drives and Energy Systems*, Dec. 2006, p. 6.

[66] M. Braun, "Technological control capabilities of der to provide future ancillary services," *International Journal of Distributed Energy Resources*, vol. 3, no. 3, pp. 191–206, 2007.

[67] J. Morren, S. W. de Haan, W. L. Kling, and J. Ferreira, "Wind turbines emulating inertia and supporting primary frequency control," *IEEE Transactions on Power Systems*, vol. 21, no. 1, pp. 433–434, Feb. 2006.

[68] J. Grainger and W. Stevenson, *Power System Analysis*. New York: McGraw-Hill, 1994.

[69] J. Björnstedt, "Integration of non-synchronous generation," Ph.D. dissertation, Lund University, Apr. 2012.

[70] H. Bevrani, G. Ledwich, and J. Ford, "On the use of df/dt in power system emergency control," in *IEEE/PES Power Systems Conference and Exposition, PSCE '09.*, Mar. 2009, pp. 1–6.

[71] P. Kundur, *Power System Stability and Control*, N. J. Balu and M. G. Lauby, Eds. New York: McGraw-Hill, 1994.

[72] J. M. Kennedy, B. Fox, T. Littler, and D. Flynn, "Validation of fixed speed induction generator models for inertial response using wind farm measurements," *IEEE Transactions on Power Systems*, vol. 26, no. 3, pp. 1454–1461, Aug. 2011.

[73] J. Ekanayake and N. Jenkins, "Comparison of the response of doubly fed and fixed-speed induction generator wind turbines to changes in network frequency," *IEEE Transactions on Energy Conversion*, vol. 19, no. 4, pp. 800–802, Dec. 2004.

[74] G. Lalor, A. Mullane, and M. O'Malley, "Frequency control and wind turbine technologies," *IEEE Transactions on Power Systems*, vol. 20, no. 4, pp. 1905–1913, Nov. 2005.

[75] A. Mullane and M. O'Malley, "The inertial response of induction-machine based wind turbines," *IEEE Transactions on Power Systems*, vol. 26, no. 3, pp. 1496–1503, Aug. 2005.

[76] A. Sumper, O. Gomis-Bellmunt, A. Sudria-Andreu, R. Villafafila-Robles, and J. Rull-Duran, "Response of fixed speed wind turbines to system frequency disturbances," *IEEE Transactions on Power Systems*, vol. 24, no. 1, pp. 181–192, Feb. 2009.

[77] M. Kayikçi and J. V. Milanović, "Dynamic contribution of DFIG-based wind plants to system frequency disturbances," *IEEE Transactions on Power Systems*, vol. 24, no. 2, pp. 859–867, May 2009.

[78] J. F. Conroy and R. Watson, "Frequency response capability of full converter wind turbine generators in comparison to conventional generation," *IEEE Transactions on Power Systems*, vol. 23, no. 2, pp. 649–656, May 2008.

[79] L. Ruttledge, N. W. Miller, J. O'Sullivan, and D. Flynn, "Frequency response of power systems with variable speed wind turbines," *IEEE Transactions on Sustainable Energy*, vol. 3, no. 4, pp. 683–691, Oct. 2012.

[80] X. Yingcheng and T. Nengling, "Review of contribution to frequency control through variable speed wind turbine," *Renewable Energy*, vol. 36, no. 6, pp. 1671–1677, Jun. 2011.

[81] R. Doherty, A. Mullane, G. Nolan, D. J. Burke, A. Bryson, and O. Mark, "An assessment of the impact of wind generation on system frequency control," *IEEE Transactions on Power Systems*, vol. 25, no. 1, pp. 452–460, Feb. 2010.

[82] L. Ruttledge and D. Flynn, "System-wide contribution to frequency response from variable speed wind turbines," in *IEEE Power and Energy Society General Meeting*, Jul. 2012, pp. 1–8.

[83] H. Knudsen and J. N. Nielsen, "Introduction to the modelling of wind turbines," in *Wind Power in Power Systems*, T. Ackermann, Ed. John Wiley & Sons, Ltd, Chichester, 2005, pp. 525–554.

[84] L. Ruttledge and D. Flynn, "System-wide inertial response from fixed speed and variable speed wind turbines," in *IEEE Power and Energy Society General Meeting*, Jul. 2011, pp. 1–7.

[85] J. M. Mauricio, A. Marano, A. Gomez-Exposito, and J. L. M. Ramos, "Frequency regulation contribution through variable-speed wind energy conversion systems," *IEEE Transactions on Power Systems*, vol. 24, no. 1, pp. 173–180, Feb. 2009.

[86] L. Wu and D. G. Infield, "Towards an assessment of power system frequency support from wind plant - modeling aggregate inertial response," *IEEE Transactions on Power Systems*, vol. 28, no. 3, pp. 2283–2291, Aug. 2013.

[87] J. Van de Vyver, J. D. M. De Kooning, B. Meersman, L. Vandevelde, and T. L. Vandoorn, "Droop control as an alternative inertial response strategy for the synthetic inertia on wind turbines," *IEEE Transactions on Power Systems*, vol. 31, no. 2, pp. 1129–1138, Mar. 2016.

[88] C. Luo, H. Banakar, B. Shen, and B.-T. Ooi, "Strategies to smooth wind power fluctuations of wind turbine generator," *IEEE Transactions on Energy Conversion*, vol. 22, no. 2, pp. 341–349, 2007.

[89] A. Žertek, G. Verbič, and M. Pantoš, "A novel strategy for variable-speed wind turbines' participation in primary frequency control," *IEEE Transactions on Sustainable Energy*, vol. 3, no. 4, pp. 791–799, Oct. 2012.

[90] K. Vidyanandan and N. Senroy, "Primary frequency regulation by deloaded wind turbines using variable droop," *IEEE Transactions on Power Systems*, vol. 28, no. 2, pp. 837–846, May 2013.

[91] G. C. Tarnowski, P. C. Kjær, P. E. Sørensen, and J. Østergaard, "Variable speed wind turbines capability for temporary over-production," in *IEEE Power Energy Society General Meeting*, Jul. 2009, pp. 1–7.

[92] M. Altin, R. Teodorescu, B. B. Jensen, U. Annakkage, F. Iov, and P. Kjær, "Methodology for assessment of inertial response from wind power plants," in *IEEE Power and Energy Society General Meeting*, Jul. 2012, pp. 1–8.

[93] P. K. Keung, P. Li, H. Banakar, and B. T. Ooi, "Kinetic energy of wind-turbine generators for system frequency support," *IEEE Transactions on Power Systems*, vol. 24, no. 1, pp. 279–287, Feb. 2009.

[94] M. Juelsgaard, J. Bendtsen, and R. Wisniewski, "Utilization of wind turbines for upregulation of power grids," *IEEE Transactions on Industrial Electronics*, vol. 60, no. 7, pp. 2851–2863, Jul. 2013.

[95] N. R. Ullah, T. Thiringer, and D. Karlsson, "Temporary primary frequency control support by variable speed wind turbines - potential and applications," *IEEE Transactions on Power Systems*, vol. 23, no. 2, pp. 601–612, May 2008.

[96] J. O'Sullivan, M. Power, M. Flynn, and M. O'Malley, "Modelling of frequency control in an island system," in *IEEE Power Engineering Society 1999 Winter Meeting, New York, USA*, vol. 1, Jan. 1999, pp. 574–579.

[97] N. Kakimoto and B. Kazuhiro, "Performance of gas turbine-based plants during frequency drops," *IEEE Transactions on Power Systems*, vol. 18, no. 3, pp. 1110–1115, Aug. 2003.

[98] A. Bagnasco, B. Delfino, G. Denegri, and S. Massuco, "Management and dynamic performances of combined cycle power plants during parallel and islanding operation," *IEEE Transactions on energy Conversion*, vol. 13, no. 2, pp. 194–201, Jun. 1998.

[99] J. Mantzaris and C. Vournas, "Modelling and stability of a single-shaft combined cycle power plant," *International Journal of Thermodynamics*, vol. 10, no. 2, pp. 71–78, Jun. 2007.

[100] IEEE Committee Report, "Dynamic models for steam and hydro turbines in power system studies," *IEEE Transactions on Power Apparatus and Systems*, vol. PAS-92, no. 6, pp. 1904–1915, Nov. 1973.

[101] "Hydraulic turbine and turbine control models for system dynamic studies," *IEEE Transactions on Power Systems*, vol. 7, no. 1, pp. 167–179, Feb. 1992.

[102] G. Lalor and M. O'Malley, "Frequency control on an island power system with increasing proportions of combined cycle gas turbines," in *IEEE Power Tech Conference Proceedings, 2003 Bologna*, vol. 4, Jun. 2003, p. 7.

[103] GE Energy, "WindINERTIA Control Fact Sheet," 2009, http://site.ge-energy.com/prod_serv/products/renewable_energy/en/downloads/GEA17210.pdf.

[104] ENERCON, "ENERCON wind energy converters - Technology & Service," 2012, http://www.enercon.de/p/downloads/ENERCON_TuS_en.pdf.

[105] G. Mandic, A. Nasiri, E. Muljadi, and F. Oyague, "Active torque control for gearbox load reduction in a variable-speed wind turbine," *IEEE Transactions on Industry Applications*, vol. 48, no. 6, pp. 2424–2432, Nov. 2012.

[106] J. Feller, W. Phipps, R. T. Harris, and A. G. Roberts, "Wind turbine control strategy for shaft stress reduction," in *IEEE International Conference on Industrial Technology (ICIT)*, Feb. 2013, pp. 793–798.

[107] S. Morinaga and T. Funabashi, "Torsional vibration suppression of the PMSG-based wind turbine generator using H_∞ observer," in *1st International Future Energy Electronics Conference (IFEEC)*, Nov. 2013, pp. 880–884.

[108] H. Liu, Y. Wang, Q. Tang, and X. Yuan, "Individual pitch control strategy of wind turbine to reduce load fluctuations and torque ripples," in *IET Conference Proceedings*. The Institution of Engineering & Technology, Jan. 2015.

[109] J. D. M. De Kooning, T. L. Vandoorn, J. Van de Vyver, B. Meersman, and L. Vandevelde, "Displacement of the maximum power point caused by losses in wind turbine systems," *Renawable Energy*, vol. 85, pp. 273–280, Jan. 2016.

[110] M. Shafie-khah, A. de la Nieta, J. Catalao, and E. Heydarian-Forushani, "Optimal self-scheduling of a wind power producer in energy and ancillary services markets using a multi-stage stochastic programming," in *Smart Grid Conference (SGC)*, Dec. 2014, pp. 1–5.

[111] S. Liang, Jiaqiand Grijalva and R. Harley, "Increased wind revenue and system security by trading wind power in energy and regulation reserve markets," *IEEE Transactions on Sustainable Energy*, vol. 2, no. 3, pp. 340–347, Jul. 2011.

[112] L.-R. Chang-Chien and Y.-C. Yin, "Strategies for operating wind power in a similar manner of conventional power plant," *IEEE Transactions on Energy Conversion*, vol. 24, no. 4, pp. 926–934, Dec. 2009.

[113] P. Moutis, S. A. Papathanassiou, and N. D. Hatziargyriou, "Improved load-frequency control contribution of variable speed wind variable pitch wind generators," *Renewable Energy*, vol. 48, pp. 514–523, Dec. 2012.

[114] M. E. Haque, M. Negnevitsky, and K. M. Muttaqi, "A novel control strategy for a variable-speed wind turbine with a permanent-magnet synchronous generator," *IEEE Transactions on Industry Applications*, vol. 46, no. 1, pp. 331–339, Jan. 2010.

[115] J. Van de Vyver, J. De Kooning, B. Meersman, T. Vandoorn, and L. Vandevelde, "Optimization of constant power control of wind turbines to provide power reserves," in *Proceedings of UPEC*. IEEE, Sep. 2013, p. 6.

[116] J. Matevosyan, T. Ackermann, and S. M. Bolik, "Technical regulations for the interconnection of wind farms to the power system," in *Wind Power in Power Systems*, T. Ackermann, Ed. John Wiley & Sons, Ltd, Chichester, 2005, pp. 115–142.

[117] A. D. Hansen, P. Sørensen, F. Iov, and F. Blaabjerg, "Centralised power control of wind farm with doubly fed induction generators," *Renewable Energy*, vol. 31, no. 7, pp. 935–951, Jun. 2006.

[118] J. Van de Vyver, J. D. M. De Kooning, T. L. Vandoorn, B. Meersman, and L. Vandevelde, "Comparison of wind turbine power control strategies to provide power reserves," in *Proceedings of IEEE Energycon*, Apr. 2016, p. 6.

[119] P. Li, H. Banakar, P.-K. Keung, H. G. Far, and B.-T. Ooi, "Macromodel of spatial smoothing in wind farms," *IEEE Transactions on Energy Conversion*, vol. 22, no. 1, pp. 119–128, Mar. 2007.

[120] W. Qiao, W. Zhou, J. Aller, and R. Harley, "Wind speed estimation based sensorless output maximization control for a wind turbine driving a DFIG," *IEEE Transactions on Power Electronics*, vol. 23, no. 3, pp. 1156–1169, May 2008.

[121] W. Qiao, X. Yang, and X. Gong, "Wind speed and rotor position sensorless control for direct-drive pmsg wind turbines," *IEEE Transactions on Industry Applications*, vol. 48, no. 1, pp. 3–11, Jan. 2012.

[122] G. Hafidi and J. Chauvin, "Wind speed estimation for wind turbine control," in *IEEE International Conference on Control Applications (CCA)*, Oct. 2012, pp. 1111–1117.

[123] D. Jena and S. Rajendran, "A review of estimation of effective wind speed based control of wind turbines," *Renewable and Sustainable Energy Reviews*, vol. 43, pp. 1046–1062, Mar. 2015.

[124] L. Gevaert, J. D. M. De Kooning, T. L. Vandoorn, J. Van de Vyver, and L. Vandevelde, "Evaluation of the mppt performance in small wind turbines by estimating the tip-speed ratio," in *48th International Universities' Power Engineering Conference (UPEC)*, Sep. 2013, p. 5.

[125] J. G. Slootweg, *Wind power: Modelling and impact on power system dynamics*. TU Delft, Delft University of Technology, 2003.

[126] D. Gautam, V. Vittal, and T. Harbour, "Impact of increased penetration of DFIG-based wind turbine generators on transient and small signal stability of power systems," *IEEE Transactions on Power Systems*, vol. 24, no. 3, pp. 1426–1434, Aug. 2009.

[127] M. V. A. Nunes, J. A. P. Lopes, H. H. Zurn, U. H. Bezerra, and R. G. Almeida, "Influence of the variable-speed wind generators in transient stability margin of the conventional generators integrated in electrical grids," *IEEE Transactions on Energy Conversion*, vol. 19, no. 4, pp. 692–701, Dec. 2004.

[128] E. Muljadi, C. P. Butterfield, B. Parsons, and A. Ellis, "Effect of variable speed wind turbine generator on stability of a weak grid," *IEEE Transactions on Energy Conversion*, vol. 22, no. 1, pp. 29–36, Mar. 2007.

[129] M. J. Hossain, H. R. Pota, M. A. Mahmud, and R. A. Ramos, "Investigation of the impacts of large-scale wind power penetration on the angle and voltage stability of power systems," *IEEE Systems Journal*, vol. 6, no. 1, pp. 76–84, Mar. 2012.

[130] E. Vittal, M. O'Malley, and A. Keane, "Rotor angle stability with high penetrations of wind generation," *IEEE Transactions on Power Systems*, vol. 27, no. 1, pp. 353–362, Feb. 2012.

[131] J. G. Slootweg and W. L. Kling, "Impacts of distributed generation on power system transient stability," in *IEEE Power Engineering Society Summer Meeting*, vol. 2, Jul. 2002, pp. 862–867.

Publication list of J. Van de Vyver

1. J. Van de Vyver, J. D. M. De Kooning, T. L. Vandoorn, B. Meersman, and L. Vandevelde, "Comparison of wind turbine power control strategies to provide power reserves," in *Proceedings of IEEE Energycon 2016*. IEEE, 2016, p. 6.

2. J. De Kooning, J. Van de Vyver, J. D. M. De Kooning, T. L. Vandoorn, and L. Vandevelde, "Grid voltage control with distributed generation using online grid impedance estimation," *Sustainable Energy, Grids and Networks*, vol. 5, pp. 70–77, 2016.

3. J. D. M. De Kooning, T. L. Vandoorn, J. Van de Vyver, B. Meersman, and L. Vandevelde, "Displacement of the maximum power point caused by losses in wind turbine systems," *Renewable Energy*, vol. 85, pp. 273–280, 2016.

4. J. Van de Vyver, J. D. M. De Kooning, B. Meersman, L. Vandevelde, and T. L. Vandoorn, "Droop control as an alternative inertial response strategy for the synthetic inertia on wind turbines," *IEEE Transactions on Power Systems*, vol. 31, no. 2, pp. 1129–1138, 2016.

5. L. Gevaert, T. L. Vandoorn, C. Deckmyn, J. Van de Vyver, and L. Vandevelde, "Oltc selection and switching reduction in multiple-feeder lv distribution networks," in *International Conference on Renewable Energy Research and Applications*. IEEE, 2015, pp. 562–566.

6. J. Van de Vyver, T. Feremans, T. L. Vandoorn, J. D. M. De Kooning, and L. Vandevelde, "Voltage based droop control in an islanded microgrid with wind turbines and battery storage," in *International Conference on Renewable Energy Research and Applications*. IEEE, 2015, p. 6.

7. T. L. Vandoorn, J. Van de Vyver, L. Gevaert, L. Degroote, and L. Vandevelde, "Congestion control algorithm in distribution feeders: integration in a distribution management system," *Energies*, vol. 8, no. 6, pp. 6013–6032, 2015.

8. T. L. Vandoorn, J. Van de Vyver, B. Meersman, B. Zwaenepoel, and L. Vandevelde, "Phase unbalance mitigation by three-phase damping voltage-based droop controllers in microgrids," *Electric Power Systems Research*, vol. 127, pp. 230–239, 2015.

9. J. Van de Vyver, S. Gillaerts, and L. Vandevelde, "Optiwind: grootschalige integratie van windturbines: hoe kunnen windturbines deelnemen aan de frequentieregeling in het net?" *Ecotips*, vol. 19, no. 6, pp. 32–34, 2014.

10. M. Moradzadeh, J. Van de Vyver, and L. Vandevelde, "Optimal energy storage sizing based on wind curtailment reduction," in *International Conference on Renewable Energy Research and Applications*, 2014, pp. 325–329.

11. J. De Kooning, J. Van de Vyver, J. D. M. De Kooning, T. L. Vandoorn, and L. Vandevelde, "Grid voltage control with wind turbine inverters by using grid impedance estimation," in *Proceedings of the 3rd Renewable Power Generation (RPG) Conference 2014*. IET, 2014, pp. 1–6.

12. X. Bracke, J. D. M. De Kooning, J. Van de Vyver, and L. Vandevelde, "Effective capture of wind gusts in small wind turbines by using a full active rectifier," in *Proceedings of the 3rd Renewable Power Generation Conference*. IET, 2014, pp. 1–6.

13. J. Van de Vyver, T. L. Vandoorn, J. D. M. De Kooning, B. Meersman, and L. Vandevelde, "Energy yield losses due to emulated inertial response with wind turbines," in *IEEE Power and Energy Society General Meeting PESGM*. IEEE Power and Energy Society, 2014, pp. 1–5.

14. M. Moradzadeh, B. Zwaenepoel, J. Van de Vyver, and L. Vandevelde, "Congestion-induced wind curtailment mitigation using energy storage," in *IEEE International Energy Conference*. IEEE, 2014, pp. 572–576.

15. J. Van de Vyver, T. L. Vandoorn, J. D. M. De Kooning, B. Meersman, and L. Vandevelde, "Provision of ancillary services with variable speed wind turbines," in *IEEE Young Researchers Symposium Proceedings*. EESA, Apr. 2014, pp. 1–6.

16. J. D. M. De Kooning, T. L. Vandoorn, J. Van de Vyver, B. Meersman, and L. Vandevelde, "Shaft speed ripples in wind turbines caused by tower shadow and wind shear," *IET Renewable Power Generation*, vol. 8, no. 2, pp. 195–202, 2014.

17. T. L. Vandoorn, J. D. M. De Kooning, J. Van de Vyver, and L. Vandevelde, "Three-phase primary control for unbalance sharing between distributed generation units in a microgrid," *Energies*, vol. 6, no. 12, pp. 6586–6607, 2013.

18. L. Gevaert, J. D. M. De Kooning, T. L. Vandoorn, J. Van de Vyver, and L. Vandevelde, "Evaluation of the mppt performance in small wind turbines by estimating the tip-speed ratio," in *48th International Universities' Power Engineering Conference (UPEC)*. IEEE, 2013, p. 5.

19. J. Van de Vyver, J. D. M. De Kooning, T. L. Vandoorn, B. Meersman, and L. Vandevelde, "Grid support with wind turbines by the provision of ancillary services," in *BERA Wind Workshop Abstracts*, 2013, pp. 1–2.

20. T. L. Vandoorn, W. Willems, J. D. M. De Kooning, J. Van de Vyver, and L. Vandevelde, "Contribution of a smart transformer in the local primary control of a microgrid," in *4th European Innovative Smart Grid Technologies Conference, Proceedings*. IEEE, 2013, pp. 1–5.

21. J. Van de Vyver, J. D. M. De Kooning, B. Meersman, T. L. Vandoorn, and L. Vandevelde, "Optimization of constant power control of wind turbines to provide power reserves," in *48th International Universities' Power Engineering Conference (UPEC)*. IEEE, 2013, pp. 1–6.

22. J. D. M. De Kooning, L. Gevaert, J. Van de Vyver, T. L. Vandoorn, and L. Vandevelde, "Online estimation of the power coefficient versus tip-speed ratio curve of wind turbines," in *39th Annual Conference of the IEEE Industrial Electronics Society (IECON)*. IEEE, 2013, pp. 1792–1797.

23. J. D. M. De Kooning, J. Van de Vyver, T. L. Vandoorn, B. Meersman, and L. Vandevelde, "Joule losses and torque ripple caused by current waveforms in small and medium wind turbines," in *IEEE EUROCON*. IEEE, 2013, pp. 889–895.

24. J. D. M. De Kooning, J. Van de Vyver, T. L. Vandoorn, B. Meersman, and L. Vandevelde, "Impact of speed ripple on the back-emf waveform of permanent magnet synchronous machines," *IET Electric Power Applications*, vol. 7, no. 5, pp. 400–407, 2013.

A

Power plant models

The different power plant models that are used in the simulations are briefly presented in this appendix [71, 97–102].

A.1 Steam-based generators

Parameter	Value	Unit	Parameter	Value	Unit
T_{sr}	0.1	s	T_{sm}	0.3	s
T_{ch}	0.3	s	T_{rh}	10.0	s
T_{co}	0.4	s	F_{hp}	0.3	–
F_{ip}	0.4	–	F_{lp}	0.3	–
R_{steam}	0.05	%	H_{steam}	4.2	s
$\dot{P}_{\mathrm{steam,up}}$	0.1	pu/s	$\dot{P}_{\mathrm{steam,down}}$	-0.1	pu/s
$P_{\mathrm{steam,max}}$	1	pu	$P_{\mathrm{steam,min}}$	0	pu

Table A.1: Parameters for the steam-based generator model.

A.2 Hydro generators

Parameter	Value	Unit	Parameter	Value	Unit
$K_{\mathrm{s,hydro}}$	5	–	$T_{\mathrm{p,hydro}}$	0.04	s
$T_{\mathrm{r,hydro}}$	5.0	s	δ_{hydro}	0.3	–
σ_{hydro}	0.05	–	$T_{\mathrm{g,hydro}}$	0.2	s
$T_{\mathrm{w,hydro}}$	1.4	–	A_{t}	1.0	–
H_{hydro}	4.2	s			
$\dot{P}_{\mathrm{hydro,up}}$	0.1	pu/s	$\dot{P}_{\mathrm{hydro,down}}$	−0.1	pu/s
$P_{\mathrm{hydro,max}}$	1	pu	$P_{\mathrm{hydro,min}}$	0	pu

Table A.2: Parameters for the hydro generator model.

A.3 Combined cycle gas turbines

Parameter	Value	Unit	Parameter	Value	Unit
$T_{\mathrm{g,ccgt}}$	0.05	s	$T_{\mathrm{v,ccgt}}$	0.05	s
$T_{\mathrm{f,ccgt}}$	0.4	s	$T_{\mathrm{cd,ccgt}}$	0.2	s
T_{igv}	3	s	TD_{cr}	0.01	s
TD_{te}	0.04	s	T_{r}	541	°C
T_{a}	30	°C			
R_{ccgt}	0.04	%	H_{ccgt}	4.2	s
igv_{max}	1	pu	igv_{min}	0.46	pu
$P_{\mathrm{ccgt,max}}$	1	pu	$P_{\mathrm{ccgt,min}}$	0	pu

Table A.3: Parameters for the CCGT model.

$$T = 1.3 \cdot (W_{\mathrm{f}} - 0.23) + 0.5 \cdot \left(1 - \frac{f}{f_{\mathrm{nom}}}\right) \tag{A.1}$$

$$T_{\mathrm{x}} = \left(T_{\mathrm{r}} - 390 \cdot (1 - W_{\mathrm{f}}) + 306 \cdot \left(1 - \frac{f}{f_{\mathrm{nom}}}\right) + 1.94 \cdot (igv_{\mathrm{max}} - igv)\right) \cdot \left(\frac{1}{1 + 0.005 \cdot (15 - T_{\mathrm{a}})}\right) \tag{A.2}$$

$$W_{\mathrm{x}} = \frac{f}{f_{\mathrm{nom}}} \cdot |igv|^{0.257} \cdot \frac{288}{T_{\mathrm{a}} + 273}; \tag{A.3}$$

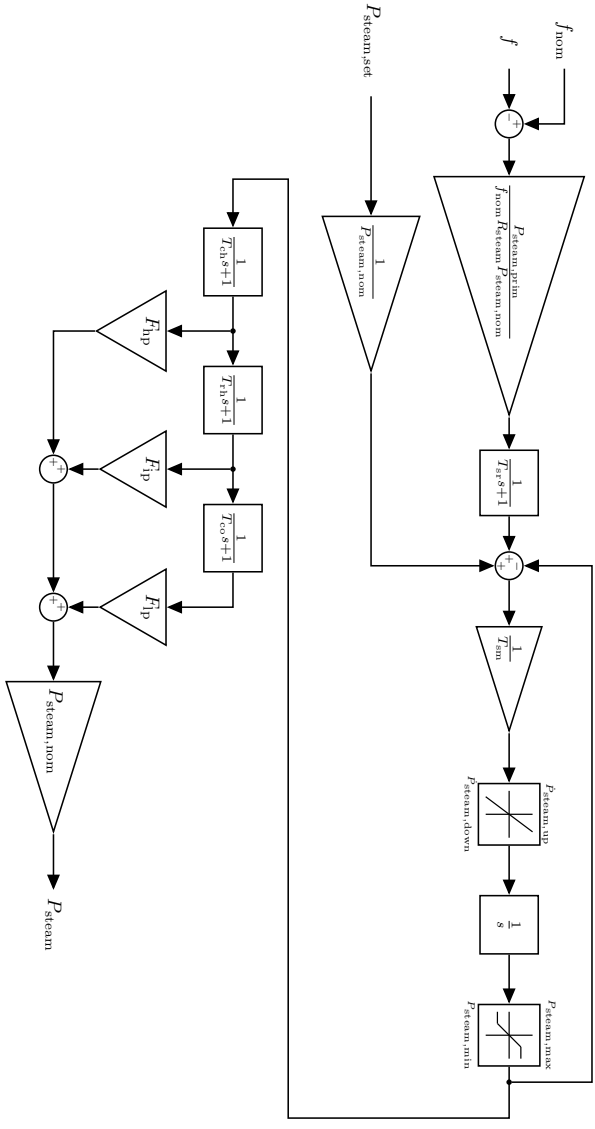

Figure A.1: Model of a steam-based generator.

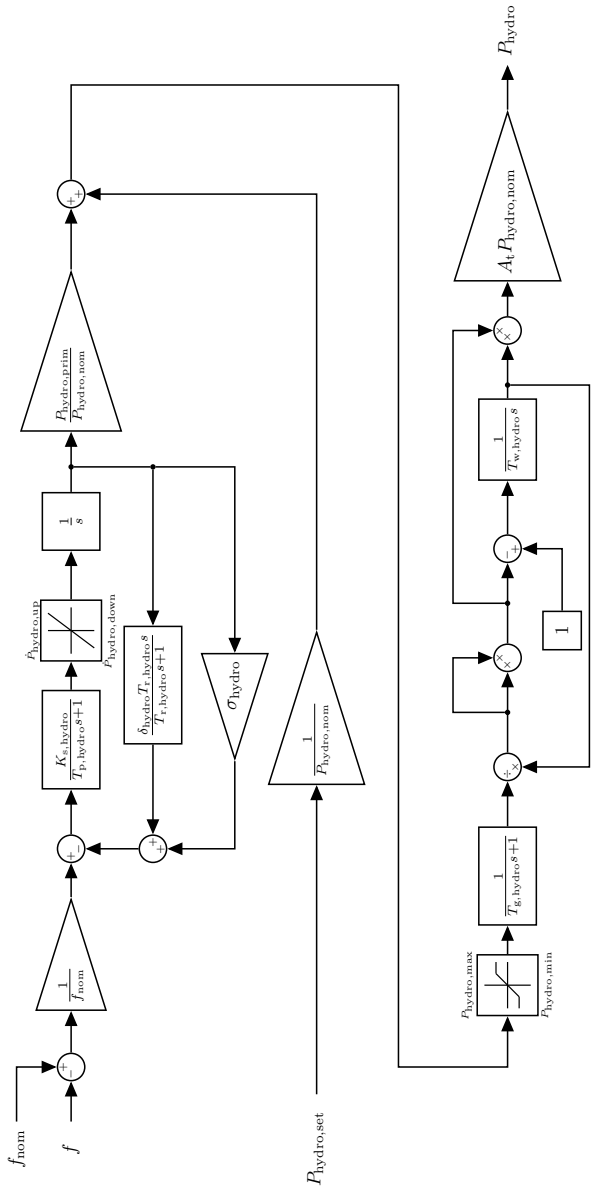

Figure A.2: Model of a hydro generator.

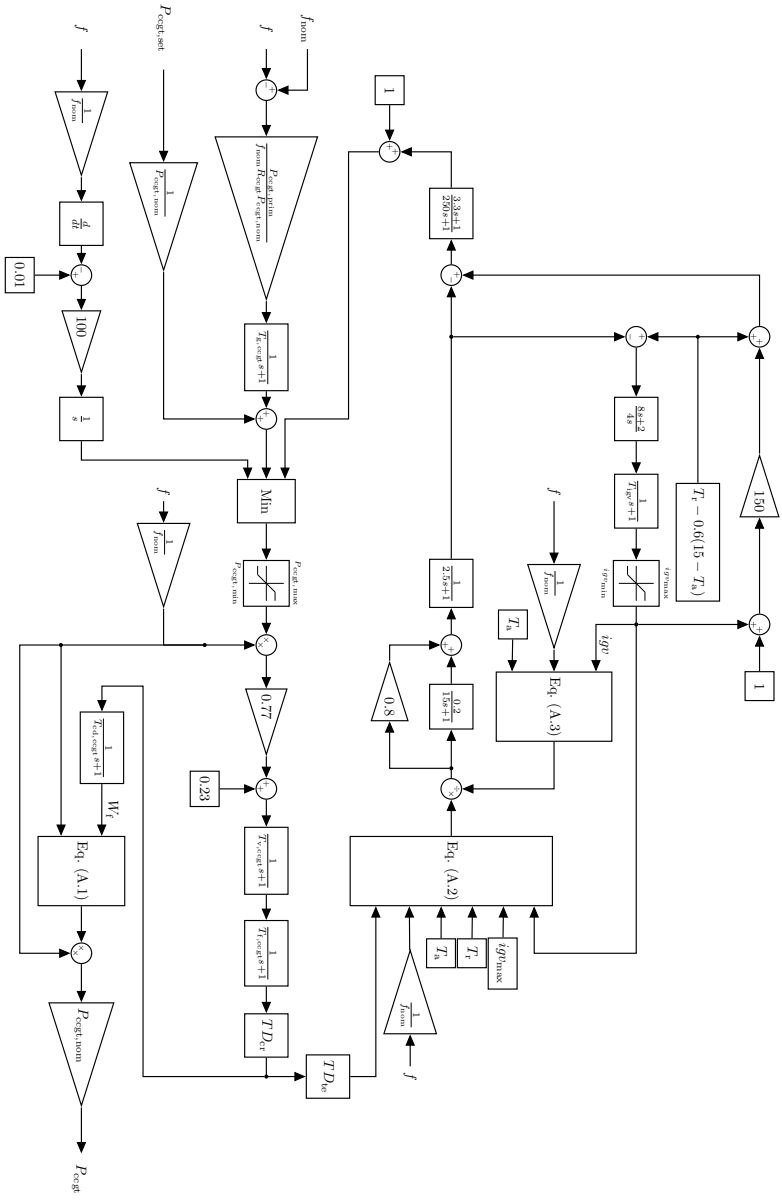

Figure A.3: Model of a CCGT.